Dissertation

zur Erlangung der Doktorwürde
an der

Gesamtfakultät für Mathematik,
Ingenieur- und Naturwissenschaften
der
Ruprecht-Karls-Universität Heidelberg

Thema:

Optimizing Human-Exoskeleton Interactions: A Comprehensive Study on Biomechanical Validation, Optimal Design, and Control of Exoskeletons

vorgelegt von:

Giorgos D. Marinou

Gutachter: Professor Dr. Katja Mombaur

Professor Dr. Daniel Häufle

Abstract

Assistive technologies and particularly wearable exoskeletons offer immense potential in aiding individuals with musculoskeletal impairments, as well as reducing the risks of occupational hazards. Despite recent technological advancements, the optimization of human-exoskeleton interactions still remains a challenge with regards to ensuring comfort, safety and transparency between the user and the device. This thesis addresses these challenges by investigating how to provide optimal biomechanical support while ensuring user acceptance and comfort. The work is anchored in two distinct yet interrelated projects: the SPEXOR project, focusing on back-support exoskeletons to prevent low back pain, and the HeiAge project, aimed at facilitating mobility in older adults through lower-limb exoskeletons.

In the context of the SPEXOR project, optimization and optimal control techniques, combined with musculoskeletal modeling, were employed to design back-support exoskeletons that minimize lumbar loads during lifting. The approach integrates human biomechanics into exoskeleton design, accounting for lumbar torque reduction and user comfort constraints. The results demonstrate that optimized torque profiles can effectively reduce cumulative and peak low back loads, improving ergonomic safety in occupational settings.

The HeiAge project extends this work by examining how users adapt to exoskeletons and by developing a mobile, modular sensory system to overcome the limitations of traditional motion capture technologies. By extending the applications of biomechanical analysis to outdoor evaluations, this system broadens the reach of exoskeleton testing and aims to provide applications for technology transfer to diverse populations such as older adults. Biomechanical metrics were used to quantify familiarization, providing insightful outcomes into early detection of adaptation and motor learning, critical for exoskeleton applications in real-world settings.

The thesis makes several key contributions, including the development of tailored torque profiles for back-support exoskeletons, the creation of a modular sensory system for real-world applications, and the quantification of familiarization and adaptation processes. These findings enhance the understanding of human-exoskeleton interactions, bringing together laboratory research and real-world applications.

This research highlights the importance of a multifold approach in designing exoskeletons, that combines biomechanical evaluation, simulation, and user adaptation studies. The combination of the SPEXOR and HeiAge projects highlights the potential of developing intuitive and effective exoskeletons, thus facilitating broader technology adaptation and improving the quality of life for a wide range of users.

Zusammenfassung

Assistive Technologien und insbesondere tragbare Exoskelette bieten ein immenses Potenzial zur Unterstützung von Personen mit Beeinträchtigungen des Bewegungsapparats und zur Verringerung der Risiken bei der Arbeit. Trotz der jüngsten technologischen Fortschritte bleibt die Optimierung der Interaktion zwischen Mensch und Exoskelett eine Herausforderung, wenn es darum geht, Komfort, Sicherheit und intuitive Steuerung zwischen Nutzer und Gerät zu gewährleisten. Die vorliegende Arbeit befasst sich mit diesen Herausforderungen, indem sie untersucht, wie eine optimale biomechanische Unterstützung bei gleichzeitiger Gewährleistung von Benutzerakzeptanz und -komfort erreicht werden kann. Die Arbeit ist in zwei unterschiedlichen, aber miteinander verbundenen Projekten verankert: dem SPEXOR-Projekt, das sich auf Exoskelette zur Unterstützung des Rückens zur Vorbeugung von Kreuzschmerzen konzentriert, und dem HeiAge-Projekt, das darauf abzielt, die Mobilität älterer Menschen durch Exoskelette für die unteren Gliedmaßen zu erleichtern.

Im Rahmen des SPEXOR-Projekts wurden Optimierungs- und optimale Kontrolltechniken in Verbindung mit Muskel-Skelett-Modellierung eingesetzt, um Exoskelette zur Unterstützung des Rückens zu entwerfen, die die Belastung der Lendenwirbelsäule beim Heben minimieren. Der Ansatz integriert die menschliche Biomechanik in das Design des Exoskeletts und berücksichtigt die Reduzierung des Drehmoments im Lendenbereich sowie die Einschränkungen des Benutzerkomforts. Die Ergebnisse zeigen, dass optimierte Drehmomentprofile die kumulative Belastung und die Spitzenbelastung der Lendenwirbelsäule wirksam reduzieren und damit die ergonomische Sicherheit am Arbeitsplatz verbessern können.

Das HeiAge-Projekt erweitert diese Arbeit, indem es untersucht, wie sich Benutzer an Exoskelette anpassen, und indem es ein mobiles, modulares Sensorsystem entwickelt, das die Grenzen herkömmlicher Bewegungserfassungstechnologien überwindet. Durch die Ausweitung des Anwendungsbereichs der biomechanischen Analyse auf Bewertungen im Freien erweitert dieses System den Technologietransfer zu weniger erreichbaren Zielgruppen, wie älteren Erwachsenen. Biomechanische Metriken wurden verwendet, um die Gewöhnung zu messen und zu analysieren, und lieferten aufschlussreiche Ergebnisse für die frühzeitige Erkennung von Anpassung und motorischem Lernen, die für Exoskelettanwendungen in der realen Welt entscheidend sind.

Die Arbeit leistet mehrere wichtige Beiträge, darunter die Entwicklung von maßgeschneiderten Drehmomentprofilen für Exoskelette zur Unterstützung des Rückens, die Entwicklung eines modularen sensorischen Systems für reale Anwendungen und die Messung sowie Analyse von Gewöhnungs- und Anpassungsprozessen. Diese Ergeb-

nisse verbessern das Verständnis der Interaktion zwischen Mensch und Exoskelett, indem sie Laborforschung und reale Anwendungen zusammenbringen.

Diese Forschung unterstreicht die Bedeutung eines vielschichtigen Ansatzes bei der Entwicklung von Exoskeletten, der biomechanische Bewertung, Simulation und Studien zur Benutzeranpassung kombiniert. Die Kombination der Projekte SPEXOR und HeiAge unterstreicht das Potenzial für die Entwicklung intuitiver und effektiver Exoskelette, die eine breitere Technologieanpassung ermöglichen und die Lebensqualität eines breiten Nutzerkreises verbessern.

Acknowledgement

I am forever grateful for the financial support of the European project "SPEXOR" (GA 687662), and the Carl Zeiss project "HeiAge", under the "Optimization, Robotics and Biomechanics" group in the Faculty of Engineering of the Institute of Computer Engineering (ZITI) at the Ruprecht-Karls-Universität Heidelberg. I extend my gratitude to the Simulation and Optimization research group of the IWR at Heidelberg University for allowing me the possibility to work with MUSCOD-II.

I would firstly like to thank my supervisor Katja Mombaur for offering me the invaluable chance of conducting research in her group and providing me with her knowledge and guidance. My gratitude and thanks to my former group and especially Luca Modenese and Erica Montefiori for infecting me with their passion for research. I thank everyone at ORB for accepting me in the group and providing a great environment for me and especially Alex for the warmest welcome to Germany, being my friend and helping me in every step of the way. I thank Lizeth for being a mentor, friend and my running motivation, Matt for being a great mentor in both science and life, Julian for being the best office mate, Peter and Kevin for the numerous coffees and nice chats, Moni for showing me the ropes to SPEXOR, Gabriel for making data collection fun, Felix Richter for the IT support, Amartya for always getting my jokes, Ibrahima and Norman for refreshing my research in my late PhD years, Thomas and Marko for sustaining our group till the end, and Sarah for her endless support. Big thanks to Jonas, Jan and Christian for sharing with me the most exciting conference in Japan.

My deepest gratitude to Thomas Thesen for always pushing me to pursue my dreams and aim higher. My most loving thanks to Pauline who has been my everything since the day I met her, as well as Andrea and Dimitra for always holding a special space for me back home. I send my deepest love and thanks to Loukia for always being my family away from home, Nikos for his loving friendship and support, Lina for always having an open ear and a warm heart, Lucas for the most unexpected and loving friendship I could have hoped for, and Flo, for all the great times we spent together. Thank you for all the trips, weekends, games and fun memories. And a special thanks to Jorge and Sarah for welcoming me to Belgium.

A massive thanks goes to my partner and home, Stijn, who has not only loved and supported me but also put up with me throughout all these years, and still stands by me in every way! My deepest appreciation to my Mom and Dad who have always supported and loved me. Big thanks to my sister, brother, Despo, and my beautiful nieces for embracing me back home in the cutest way possible every time, as well as to my wonderful dog Ice. Finally, a big thanks to Florence + the Machine, for being the voice to calm my anxiety and fuel my drive.

Contents

Introduction and Organization

> *The biophysics and the biomechanics of walking are beautifully complex and interwoven into the fabric of human evolution. Exoskeletons have the potential to restore the elegance and efficiency of natural movement to those who have lost it.*
>
> **— Hugh Herr**
> (Professor of Media Arts and Sciences, MIT,
> Yang Center for Bionics)

At a time where modern advancements extend the boundaries of human capability, the freedom of movement inherent to the human body remains subject to formidable musculoskeletal disorders. These pervasive conditions silently affect millions, challenging our healthcare systems and highlighting the need for innovative solutions. The variety and severity of musculoskeletal disorders (MSDs) depends heavily on the individual pathology, ranging from low back pain (LBP) as a consequence of a sedentary lifestyle or labor-intensive work environments, to spinal cord injury (SCI) resulting from physical trauma or degenerative conditions such as amyotrophic lateral sclerosis (ALS). In 2022, individuals living with MSDs made up approximately 20% of the global population, with LBP being the biggest contributor, amounting to roughly 570 million prevalent cases worldwide [1], with a projected increase of 36.4% of the global prevalence by 2050 [2]. Mobility impairments hindering or completely restricting gait such as SCI, multiple sclerosis, stroke and Parkinson's disease largely contribute to the majority of the rest of the cases [3].

Recent advancements in hardware and software modalities have given rise to wearable robotics and specifically exoskeletons as breakthrough devices within assistive technologies, with applications spanning lifting assistance, sit-to-stand aid, overhead work and walking support [4]. Albeit the fictional portrayal of exoskeletons through popular culture that skewed public opinion, these devices managed to gain a more pragmatic and impactful presence over the last decade via research and commercial advancements in the field. From Yang's apparatus patents for running, walking and jumping in 1889 [5], to General Electric's (Massachusets, USA) 680-kilogram power augmentation Hardiman in the late 1960s [6], these devices have laid the necessary groundwork for future powered exoskeletons to come. A few decades later, a variety of occupational exoskeletons like the Apogee and Cray X from German Bionic [7] have dominated spaces such as automotive industries, while restoration devices, for instance the Atalante X rehabilitation exoskeleton by Wandercraft [8], enable paraplegic population to walk again and in this instance Paralympian tennis player

Kévin Piette to walk carrying the Olympic Flame during the Paris 2024 Olympic Games torch relay.

Consequent of the high traction in exoskeleton development and the major breakthroughs of the last few years, is the refinement of these devices through shifting priorities towards user-acceptance while pacing technological advancement. In both physical and cognitive manner, human-exoskeleton interactions govern and define the whole wearable experience, from joint alignment and force transmission, to sensory feedback and intuitive control of such devices. It is hence imperative to thoroughly investigate human-exoskeleton interactions within a comprehensive framework, from back-support exoskeletons for injury prevention to lower-limb exoskeletons for rehabilitation. Crucial questions that are often overlooked still remain integral parts of this evolution:

1. **Comfort Limits:** What comfort limits must be adhered to, ensuring exoskeletons provide adequate support without causing discomfort or harm?
2. **Optimal Support:** How do we generate optimal support through natural movement, while adhering to the user's kinematics and comfort?
3. **User Contribution:** In which ways do users, consciously or not, adjust their own movements to maximize the efficacy of exoskeleton support and how can we quantify that?
4. **Biomechanical Evaluation:** How can we evaluate exoskeletons based on biomechanics to quantify their effects on users?
5. **Optimizing Development Time:** How can user familiarization be quantified, and what key metrics should be identified to optimize testing procedures and reduce development time?
6. **User Cues Interpretation:** How can we interpret a user's movement and support cues, ensuring the exoskeleton responds appropriately and intuitively?
7. **User Adaptation:** How can we gain insights on how able-bodied exoskeleton users adapt to such devices and familiarize themselves both physically and mentally, and use this as a framework for technology transfer to frail population groups?
8. **Optimize for the Real World:** What can we infer on motor learning and real-world applications of exoskeletons, such that we optimize the design and user-experience?

The primary motivation for this thesis is to address these questions by exploring the optimization of human-exoskeleton interactions through simulation and biomechanical evaluation. This involves focusing on two major areas of human-exoskeleton interactions: design for optimal support and optimal user experience. The first

research area falls under the scope of the research project **SPEXOR – Spinal exoskeletal robot for low back pain prevention and vocational reintegration**, and the latter under the project **HeiAge – Assistive systems and digital technologies for improving mobility in old age**. The main objectives of this thesis as part of the two research projects are detailed further in Part XX Chapter XX.

Objectives

This thesis constitutes interdisciplinary research within the scope of the two significant scientific projects, focusing on the essential aspects of optimizing human-exoskeleton interactions. Through common research areas, the first project targets low back pain prevention with means of a back-support exoskeleton, while the second project addresses function restoration in mobility impairments via a lower limb exoskeleton. Two main objectives have driven the work within this thesis:

1. **Design for Optimal Support:** A detailed investigation into how exoskeletons can be designed to provide optimal assistance while ensuring user comfort and safety. Conducted under the SPEXOR project (funded via the EU Horizon 2020 initiative), this research aims to determine the most effective ways to support users physically without causing discomfort or harm, striving to enhance the supportive capabilities of these devices in real-world applications.
2. **Optimal User Experience:** The development of advanced sensory systems and biomechanical evaluation techniques to improve the familiarization process and consequently the transparent control of exoskeletons. This project, conducted under the HeiAge project (funded via the Carl Zeiss foundation), aims to increase the overall efficacy and user-acceptance of exoskeletons by making them more intuitive and user-friendly.

These objectives were implemented cohesively across the two projects, investigating human-exoskeleton interactions under the unified scope of the thesis, and setting the main goals as follow:

Project SPEXOR: Support torque optimization of a back-support exoskeleton for preventing low back pain while lifting

The main goal of the SPEXOR project aimed to implement back-support exoskeletons in industrial environments and prevent lower back injuries without impeding user movements. To achieve this, the group at Heidelberg University examined optimal ways to complement user motions through detailed optimization of lifting tasks and parameter-optimization on the exoskeleton design, aimed to minimize lumbar spine torques. The work in this thesis related to the SPEXOR project, involves utilizing various cost functions to generate support torque profiles for exoskeleton

actuators, which inform high-level control for repetitive movements like lifting. For optimal comfort, interaction force limits are incorporated as constraints in the optimization models. With these optimal support profiles, the biomechanics of lifting are investigated, exploring how different techniques affect low back loads and torques. A comparative simulation study of improved lifting techniques versus exoskeleton support aims to identify new methods for enhancing exoskeleton efficacy in support and injury prevention.

Project HeiAge: Development of a sensory system for quantification of lower limb exoskeleton familiarization and control, via biomechanical evaluation

In effectively restoring human function and locomotion through exoskeleton assistance, the key evaluation principle is how well the device complements and supports the user, best measured through biomechanical assessment. This method quantifies the impact of hardware and software modalities on human-exoskeleton interactions, particularly in lower limb exoskeletons. A crucial yet often overlooked phase in the development cycle is the user's familiarization period. This period is essential in order for users to fully benefit from the device. By introducing a set of biomechanical metrics as familiarization indicators measured via motion capture systems, the level and timing of user adaptation to the exoskeleton can be quantified. Despite their high accuracy, traditional motion capture and laboratory-bound systems for assessing biomechanical metrics pose certain limitations such as restricted capture volume, lengthy preparation times, and high costs. These factors make it challenging to test exoskeleton performance in various everyday tasks. Recent advancements in gait analysis and motion intention detection for exoskeleton control have emerged through the last decade, however, for these technologies to be practical and impactful in daily life, a more versatile and cost-effective solution is needed. This thesis proposes the design of a new mobile and modular sensory system that can be applied to various lower limb exoskeletons. Developed in an open-source manner, this system encourages greater collaboration and enables more realistic measurements in diverse environments and outdoor terrains. Furthermore, the familiarization processes, early detection for motor learning on exoskeletons, and cognitive and physical processes are quantified through a more realistic outdoor experiment with 20 participants.

Contributions

This thesis advances the multidisciplinary field of assistive exoskeletons through innovative contributions in modeling, simulation, sensory system development, and biomechanical evaluation. The work spans two exoskeleton projects: optimization of back-support exoskeletons and facilitating adaptation to lower-limb exoskeletons during real-world use. These contributions are detailed as follows:

1. Optimizing Back-Support Exoskeleton Support

Low-back pain as an outcome of repetitive lifting and manual handling tasks remains a prevalent occupational hazard. Existing back-support exoskeletons often lack tailored torque profiles that effectively minimize lumbar spine loads while accommodating user-device interaction constraints. The early work of this thesis targets the development of human and exoskeleton models, incorporating lumbar spine mechanics, as to minimize lumbar loads and optimize the assistance from back-support exoskeletons. Using these simulations:

- Cumulative and peak low-back loads were classified, informing safe and effective exoskeleton support strategies.
- Optimal torque profiles were generated to minimize lumbar loads while respecting interaction-force constraints, setting a foundation for user-centric exoskeleton design.

These results advance active back-support exoskeleton development by aligning assistance profiles with human biomechanics, reducing injury risks in repetitive lifting scenarios. Novel to this work, is the integration of detailed lumbar spine mechanics and interaction-force constraints into human-exoskeleton models, bridging the gap between biomechanics and user-centered torque optimization in the assistive technologies field.

2. Optimization of Motion Strategies and Exoskeleton Performance

While back-support exoskeletons have taken the industrial stage in the last half-decade, it remains unclear whether exoskeleton assistance or improved lifting techniques alone can sufficiently reduce lumbar spine loads, particularly for cumulative versus peak load scenarios. A detail simulation-driven evaluation took place, comparing various functions of improved lifting techniques based on targeted biomchanical metrics, with exoskeleton assistance. The key findings include:

- Quantification of the trade-off between improved technique and exoskeleton assistance.
- Identification of optimal motion strategies for reducing both cumulative and peak low-back loads in repetitive lifting tasks.

This study provides evidence for the necessity of exoskeletons in occupational settings, while offering actionable insights for training users in safer lifting techniques. Unlike previous studies, this research uniquely quantifies the trade-offs between optimized lifting techniques and exoskeleton assistance, proving the necessity of exoskeletons and providing a tailored framework for reducing lumbar loads under real-world conditions.

3. Development of Modular and Open-Source Sensory Systems

Existing sensory systems for exoskeleton evaluation are often costly, limited to controlled laboratory settings, or lack modularity for diverse applications. A modular, open-source, cost-effective and wireless sensor system was developed to enable seamless collection of motion and force data, outside of laboratory confinement. This system is able to:

- Support biomechanical evaluation within both laboratory and outdoor environments.
- Integrate a high-level, 'plug-and-play' control framework for compatibility with a wide range of lower-limb exoskeleton devices.

The system democratizes access to robust biomechanical data collection, facilitating more versatile and scalable exoskeleton evaluations. It is novel in its ability to function seamlessly across laboratory and outdoor environments while offering open-source modularity, and the simultaneous possibility for control, a capability not currently available in exoskeleton evaluation systems.

4. Benchmarking Lower-Limb Exoskeleton Familiarization and Long-Distance Adaptation

Long-term adaptation to lower-limb exoskeletons during real-world use remains poorly understood, with limited benchmarks for user familiarization. Spanning two studies on familiarization, this thesis developed and validated biomechanical indicators to quantify user familiarization with lower-limb exoskeletons, including:

- Longitudinal tracking of gait metrics such as stride duration, gait velocity, and double support time during overground walking.
- A comprehensive framework for benchmarking exoskeleton performance in outdoor environments, accounting for cognitive-motor interference and user adaptation.

These findings provide critical insights into user adaptation processes, paving the way for improved exoskeleton training protocols and real-world deployment strategies. This work introduces the first comprehensive benchmarking framework for lower-limb exoskeleton familiarization, combining biomechanical indicators and cognitive-motor interference analysis in overground, real-world conditions.

Summary and Organization

This thesis entails three main parts that delve into, and detail novel research work in optimizing human and exoskeleton interactions, through the multidisciplinary

areas of assistive exoskeletons, biomechanics, modeling and motion analysis, optimal control, and electrical, computer and mechanical engineering.

The following thesis entails three main parts that delve into the definition and introduction of assistive exoskeletons as state-of-the-art technologies, defining biomechanics, modeling and motion analysis as evaluation frameworks, and defining the classification of human-exoskeleton interactions through research literature.

Part I - Preliminaries

Part 1 of the thesis establishes a comprehensive framework for understanding and applying biomechanical principles to the study and optimization of human-exoskeleton interactions. This first part not only addresses the technical aspects of biomechanical evaluation but also sets the foundation for subsequent parts of the thesis, which build upon these initial concepts to explore advanced applications and real-world implementations of exoskeletons.

Chapter 1 introduces the foundational concepts of biomechanics and the role of exoskeletons in enhancing human movement. It discusses the need for biomechanical analysis in various fields such as sports, rehabilitation, and robotics. The chapter sets the stage by defining key terms and outlining the scope of research, particularly focusing on the integration of biomechanical tools to optimize the design and functionality of exoskeletons.

Chapter 2 explores the various technologies used for biomechanical evaluation, including motion capture systems, force plates, and sensorized insoles. Each technology is discussed in detail, providing insights into their principles, applications, and limitations. This chapter emphasizes the critical role these technologies play in accurately assessing human movement and the biomechanical impact of exoskeletons. It also covers the integration of these technologies to provide a comprehensive toolkit for researchers and practitioners in the field.

Chapter 3 focuses on the modeling and simulation of human movement in interaction with exoskeletons. It elaborates on the creation of accurate biomechanical models and discusses both forward and inverse kinematics and dynamics. The chapter dives deep into optimal control, illustrating how it can be applied to biomechanics to optimize human-exoskeleton interaction. It provides a thorough explanation of motion reconstruction and optimization techniques, utilizing case studies and theoretical frameworks to highlight the benefits of these methods in designing better assistive devices.

Part II - Computational Evaluation and Optimization of a Back-Support Exoskeleton

Part 2 of the thesis delves into the advanced optimization of exoskeleton-assisted lifting techniques to mitigate lower back load, a critical factor in preventing lumbar injuries during manual handling tasks. This part builds upon the foundational models and preliminary analyses presented in Part 1, exploring deeper into the dynamics and potential of exoskeleton technology to enhance human biomechanics under lifting conditions. This part contributes significantly to the understanding of how exoskeletons can be optimized to improve human performance and safety. The findings propose practical guidelines for the deployment of exoskeletons in the workplace and suggest directions for future technological enhancements.

Chapter 4 develops detailed models of human-exoskeleton interaction during lifting tasks, building on prior work in the SPinal EXOskeletal Robot (SPEXOR) project. This chapter extends earlier efforts by incorporating advanced dynamics, optimizing actuation strategies, and improving biomechanical accuracy to minimize lumbar torques. The human model is a sagittal-plane multibody system with an articulated, coupled lumbar spine for realistic bending mechanics. Joint torques are applied directly with scaling and damping to approximate muscle properties efficiently. The exoskeleton model integrates passive flexible beams, modeled with cubic splines, and an active hydraulic actuator, considering torque-angle relationships, piston velocities, and mechanical impedance. Human-exoskeleton coupling is analyzed through three pelvis interaction cases with kinematic constraints and interaction forces derived from experiments. The lifting problem is modeled as a three-phase optimal control problem (OCP), incorporating ground contact dynamics, box impact, and loop constraints for accurate simulation.

Chapter 5 focuses on optimizing exoskeleton support to minimize lumbar torques during lifting, using recorded human motions as inputs. Motion-capture data from three participants performing stoop and free lifts were segmented into three phases: reaching, force buildup, and lifting. Human motions were accurately reconstructed using inverse kinematics and least-squares optimal control, forming the basis for optimization. Six configurations were tested, varying pelvis interface dynamics (free, torsional spring, fixed) and actuator velocities (high, low). Results showed that a free pelvis interface with high piston velocity achieved the greatest reductions in cumulative (23.1%) and peak (16.0%) low back loads without exceeding comfort limits. Introducing an additional cost function term for torque reduction and kinematic preservation further optimized results, with a medium weight coefficient achieving 25.9% reductions in cumulative low back load (CLBL) and 18.1% in peak low back load (PLBL), while maintaining natural joint movements. This demonstrates the effectiveness of exoskeleton assistance in reducing lumbar stress.

Chapter 6 compares the benefits of improved lifting techniques with active exoskeleton support in reducing lumbar torques. An optimal control framework was developed to synthesize lifting motions that minimize CLBL, PLBL, and combined low-back loads. Both human-only and human-with-exoskeleton scenarios were evaluated and compared to reconstructed motions from recorded data. Optimized lifting techniques alone reduced CLBLs by 35.4% and PLBLs by 22.2%, while exoskeleton assistance achieved greater reductions of 46.9% and 38.4%, respectively. The hybrid cost function balanced both metrics effectively, showing that while improved techniques reduce cumulative loads, peak load management—key for preventing acute injuries—requires exoskeleton support. These findings highlight the exoskeleton's potential to enhance ergonomic safety during demanding tasks.

Part III - Experimental Evaluation and Optimization of a Lower-Limb Exoskeleton

Part 3 comprises the research conducted under the HeiAge project and builds upon gold standard methodologies for biomechanical evaluation of lower-limb exoskeletons discussed in Part 1, as well as investigating novel practices that push the boundaries of exoskeleton assessment even further. This part investigates the fundamental concepts of user-exoskeleton adaptation as means of optimizing evaluation, testing and development with the aim of supporting a wide range of user populations. The final part of this thesis makes critical contributions to better understanding human-exoskeleton interactions through both physical and mental frameworks, while setting the groundwork for benchmarking exoskeleton performance, detecting early markers for motor learning, and using these findings to promote a more user-intuitive control platform for exoskeletons.

Chapter 7 investigates familiarization with lower-limb exoskeletons (LLEs) as a critical factor for optimizing human-exoskeleton interactions and improving biomechanical evaluation. Familiarization is defined as the process of users adapting to exoskeleton-assisted walking, quantified here through four biomechanical metrics: stride duration, mediolateral deviation, polygon of support area, and upper- and lower-body muscle effort. Using the TWIN exoskeleton, five young able-bodied participants performed repeated walking bouts in both manual and automatic control modes, while motion capture and electromyography (EMG) data were collected. Results showed significant reductions in stride duration, mediolateral deviation from a straight path, and polygon of support area, indicating familiarization occurred after 25 to 30 strides. These findings suggest that familiarization is a time-dependent process, occurring more effectively in intuitive, user-driven modes. This study establishes promising metrics for quantifying familiarization, paving the way for more efficient exoskeleton testing and improved user adaptation strategies.

Chapter 8 presents the development and evaluation of a modular, open-source, and mobile sensory system designed to address the limitations of traditional biomechanical assessment technologies in lower-limb exoskeleton (LLE) research. The system comprises flexible 3D-printed pressure-sensing insoles and instrumented force-sensing crutches integrated with inertial measurement units (IMUs), enabling the collection of critical metrics such as ground reaction forces, center of pressure (CoP), and gait phases in a cost-effective and real-world-capable manner. Validated against gold-standard motion capture and force plate technologies through exoskeleton-assisted walking experiments with three participants, the system demonstrated high accuracy, with Pearson correlation coefficients exceeding 0.90 and low root mean square errors (RMSE) for CoP (17.2 mm), crutch forces (15.3 N), and heel strike detection (29.1 ms). A fuzzy logic algorithm was implemented to estimate gait phases, offering computational efficiency and robustness in motion intention detection. The chapter further explores system applications, including advanced biomechanical evaluation and proposed high-level control strategies, such as safety assurance and adaptive support controllers, aimed at enhancing user safety, transparency, and adaptability of exoskeleton systems. By bridging the gap between laboratory-based assessments and real-world evaluations, this modular system not only promotes collaboration and innovation through its open-source design but also lays the groundwork for future research involving larger, more diverse populations and real-time exoskeleton control strategies for frail and older individuals.

Chapter 9 presents a large-scale, outdoor experimental study to advance the understanding of human-exoskeleton interaction by evaluating the familiarization process, cognitive performance, and motor learning during assisted walking with a lower-limb exoskeleton (lower-limb exoskeleton (LLE)). Building on concepts introduced in previous chapters, this study uniquely combines biomechanical and cognitive analyses to address limitations of laboratory-based evaluations and explore user adaptation in real-world settings. Twenty-one able-bodied participants walked over 150 meters, alternating between single- and dual-task conditions, while biomechanical data (e.g., gait velocity, stride duration, ground reaction forces) and cognitive performance (correct response rate during a subtraction task) were quantified. Results demonstrate concurrent familiarization across all biomechanical metrics, with significant reductions in variability and improvements in performance, underscoring familiarization as an early marker for motor learning. Notably, cognitive interference during dual-task conditions improved gait consistency and velocity, suggesting that external focus can expedite adaptation in exoskeleton-assisted walking. These findings have profound implications for optimizing exoskeleton training protocols, particularly for older adults and frail populations, by informing strategies for skill attainment, retention, and transfer. The chapter highlights the importance of integrating cognitive and physical assessments to better understand human-exoskeleton

interaction dynamics, laying the groundwork for user-centric design and technology transfer to real-world mobility applications.

Part I

Preliminaries

Musculoskeletal and Neuromuscular Disorders

1

Modern-day humans, or homo sapiens, have inhabited the earth for about 300,000 years [9], inheriting bipedal locomotion from our early ancestors, a function honed through an evolutionary track of about six to seven million years [10]. Despite significant evolutionary milestones and optimized features such as bipedalism, this is but a brief period of time compared to the grand scope of evolution and life on earth. It is hence consequent, that our musculoskeletal system is still subject to complications, many of which still affect the lives of individuals to this day [11].

MSDs can arise from a diverse range of factors, including environmental and occupational influences, injuries, idiopathic conditions, and genetic inheritance. Occupational hazards such as repetitive motions, poor ergonomics, heavy lifting, and prolonged sedentary behavior are well-known contributors to MSDs, often leading to conditions like chronic lower back pain. Traumatic injuries, such as blows to the spinal cord can result in long-term musculoskeletal issues, evolving into chronic conditions that lead to loss of function, sensation and movement. Idiopathic pathologies, where the cause is unknown, and genetic inheritance can also bring upon significant impacts to the musculoskeletal system [12].

This chapter explains the underlying mechanisms of two major symptoms of musculoskeletal and neuromuscular disorders: low back and gait impairments, emphasizing the importance of prevention and rehabilitation. Section 1.1 details basic demographics of LBP and provides brief descriptions of the mechanics of the spine and the contributions of the musculoskeletal system to lifting, as well as the pathologies that can arise from it. Section 1.2.1 reports the prevalence of lower limb disorders and explains the physiological attributes of the lower limb and its contributions to walking.

1.1 Low Back Pain

LBP is one of the most prevalent disorders and the main contributor to years lived with disability (YLDs) globally. By the year 2050, it is projected that global prevalence of LBP will reach over 800 million cases based on data recorded from 1990 to 2020 [13]. According to the European Agency for Safety and Health at Work, work-related back pain is a leading cause of worker absenteeism in Europe, costing employers billions of euros annually [14]. Addressing these issues through preventive

measures and ergonomic interventions can significantly reduce their impact on worker productivity and decrease the economic burden on businesses and the healthcare sector. In order to successfully tackle this issue however, we have to first understand the basic functions of the spine and the underlying mechanisms leading to LBP.

1.1.1 Anatomy of the Spine

The human spine is a complex biomechanical structure, consisting of 33 vertebrae coupled together to form a central supporting column for the torso (Figure 1.1). The vertebrae are small bony structures, surrounding the spinal cord and stacked on top of each other, separated by the intervertebral discs. These discs act as shock absorbers, dealing with a considerable portion of intervertebral joint torques thanks to their gel-like centres, maintaining the integrity of the vertebrae. The spinal vertebrae are arranged into five regions: cervical (7 vertebrae), thoracic (12 vertebrae), lumbar (5 vertebrae), sacral (5 fused vertebrae), and coccygeal (4 fused vertebrae). The natural curvature of the spine follows an S-shaped path, with two lordodic curves at the cervival and lumbar, and two kyphotic curves at thoracic and sacral regions.

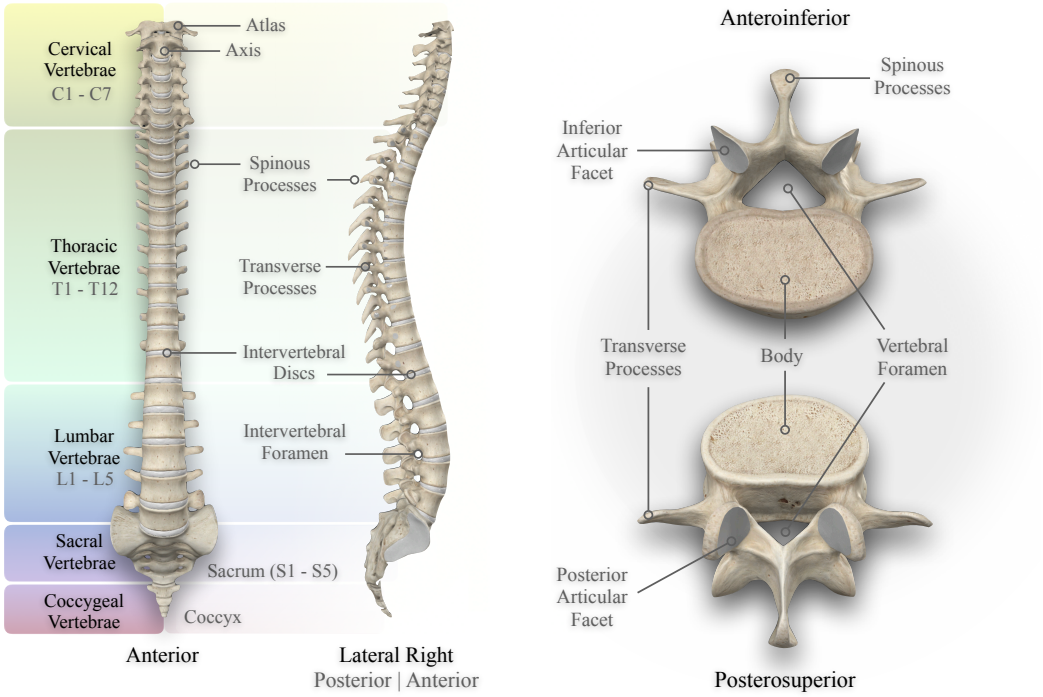

Figure 1.1: Overview of the vertebral column. **(a)** The human spine with its five regions: cervical, thoracic, lumbar, sacral and coccygeal, along with anatomical landmark annotations. **(b)** The anatomical features of a lumbar vertebra with annotations. Images partially created with Complete Anatomy 2023 (3D4Medical, Elsevier).

Vertebrae

The shape and size of each vertebra determine its function and range of motion (ROM). The vertebrae names are categorized accoding to the first letter of the spinal region they fall under, followed by a number from top to bottom. For example, the lowest lyumbar vertebra above the sacrum is called 'L5', while the topmost sacral vertebra is named 'S1'. The disc and joint, therefore, formed between this two vertebrae is described as the 'L5/S1'. Cervical vertebrae allow for extensive head movements; thoracic vertebrae are designed for stability and protection, with limited mobility; lumbar vertebrae provide the strength necessary for supporting the body's weight while allowing for bending and lifting motions. Each vertebra is composed of a **vertebral body** (anterior), a **vertebral arch** (posterior) and several **processes** (spinous, transverse, articular) that provide necessary attachment points for muscles and ligaments. The **vertebral foramen** is the central hole in each vertebra which allows for the spinal cord to pass through. **Facet joints** facilitate the articulation processes amongst adjacent vertebrae, forming synovial joints. Facet joints guide and limit the movements of the spine, helping to control the direction of spinal motion while also contributing to its stability.

Intervertebral Discs

These shock absorbers are arranged in a way as to both facilitate the joints between adjacent vertebrae but also act as fibrocartilaginous cushions between them. Each disc consists of the **nucleus pulposus**: a gel-like core that distributes pressure evenly across the disc when the spine is subjected to compression, and the **annulus fibrosus**: a tough and layered ring surrounding the nucleus, which provides structural integrity. The health and longevity of the intervertebral discs is of high importance to both the skeleton and the musculature of the back, as degeneration can lead to conditions such as herniated discs which commonly affect the lumbar region.

Muscles of the Spine

The spinal column is supported and mobilized by a complex network of muscles that can be categorized into extrinsic and intrinsic groups, each contributing to posture, movement, and the protection of the spinal cord. The extrinsic muscles include the trapezius, latissimus dorsi, rhomboids, and levator scapulae. These muscles, while primarily involved in movements of the shoulder and upper limbs, also play a crucial role in stabilizing the spine. For instance, the trapezius extends from the occipital bone to the thoracic vertebrae and scapula, facilitating scapular movement and neck extension. The latissimus dorsi, originating from the lower thoracic and lumbar regions, is pivotal in shoulder adduction and extension, indirectly influencing spinal stability.

The intrinsic muscles (Figure 1.2), directly responsible for spinal movements, are organized into three layers. The superficial layer comprises the splenius capitis and splenius cervicis, which are key in extending, rotating, and laterally flexing the head and neck. The intermediate layer includes the erector spinae group—iliocostalis, longissimus, and spinalis—muscles that run longitudinally along the spine and are essential for spinal extension and lateral flexion. The deep layer, consisting of the transversospinalis group (semispinalis, multifidus, and rotatores), plays a critical role in stabilizing the spine and facilitating fine rotational movements.

Additionally, the quadratus lumborum and psoas major are crucial muscles in the lumbar region. The quadratus lumborum, extending from the iliac crest of the pelvis to the lumbar vertebrae and the 12th rib, is vital for lateral flexion and pelvic stability during ambulation. The psoas major, originating from the lumbar vertebrae and inserting into the femur, is primarily involved in hip flexion but also contributes significantly to lumbar spine stability.

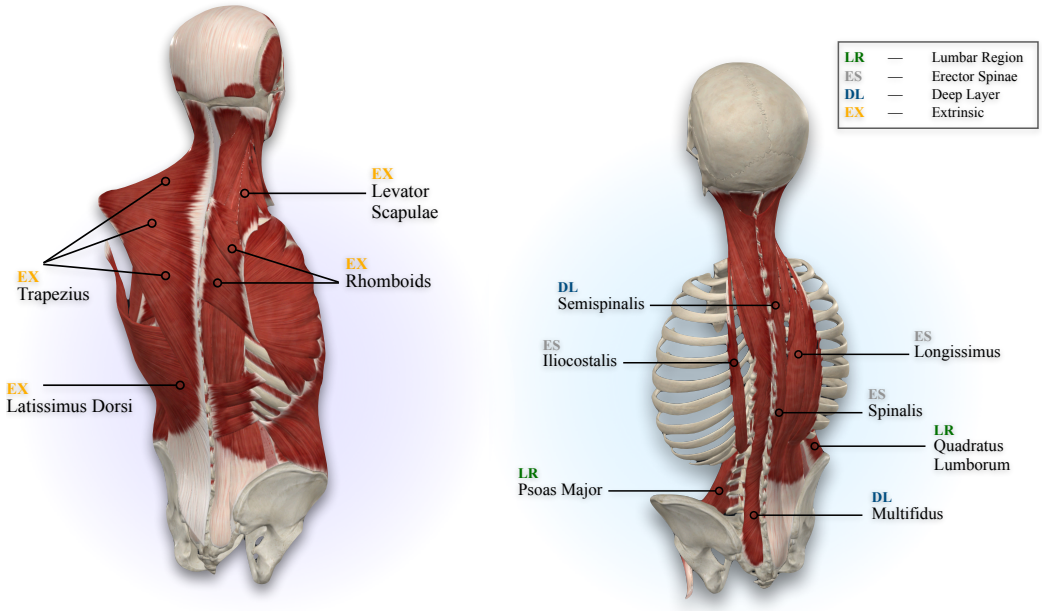

(a) (b)

Figure 1.2: Overview of major back muscles. **(a)** The extrinsic and **(b)** the intrinsic muscles influencing the vertebral column, categorized into three groups: lumbar region, erector spinae, and deep layer. Images partially created with Complete Anatomy 2023 (3D4Medical, Elsevier).

Collectively, these muscles not only support and stabilize the spinal column but also enable a wide range of movements, ensuring the functional integrity of the vertebral column and protecting the spinal cord. Their coordinated activity is fundamental to maintaining posture, executing complex movements, and preventing spinal injuries.

1.1.2 The Toll of Lifting

A number of various pathologies can affect the spinal column, with a majority of them affecting the lumbar region. Many of these pathologies are the product of mechanical loading of the spine, caused by factors such as repetitive or heavy lifting. The most common disorder that affects the intervertebral discs is **disc herniation**, where the disc's nucleus pupolsus may protrude through the annulus fibrosus, forming a bulge which could potentially compress nearby nerves. This could lead to symptoms such as **sciatica**, where the S1 nerve is pressed leading to radiating pains from the lower back to the foot, or muscle tightness and degeneration of the lumbar stabilising muscles, both leading to discomfort and chronic pain [15]. Another condition affecting the discs is the **degenerative disc disease**, where repetitive stress and micro-tears can accumulate over time and cause wear and tear [16]. In the same way, **spondylosis** affects the joints leading to osteoarthritis, leading to pain and stiffness. **Spondylolisthesis** can also occur, affecting the vertebrae via stress fractures from mechanical loading, causing a vertebra to 'slip' over the one below.

LBP often arises from a combination of factors, making it difficult to pinpoint a specific physical cause and directly address the underlying mechanisms responsible for it. Heavy lifting and prolonged sitting are proven to exacerbate the symptoms of LBP, and have been studied extensively with the aim of identifying the exact path to spine complications [17, 18]. Prolonged sitting, especially with poor posture, is a well-documented contributor to LBP. In occupational settings, whole-body vibrations — common among crane operators and truck drivers — compound these risks, particularly when combined with awkward postures and prolonged spinal flexion [19]. The risks associated with lifting are influenced by the duration, frequency, technique, and weight of the object being lifted, with improper lifting practices significantly increasing the likelihood of injury [20].

Table 1.1: Quantified cumulative spinal loads during sitting, standing, and lifting compared to standing upright.

Study	Posture / Activity	Quantified Load*
Nachemson (1981) [21]	Sitting with flexed posture	1.4
Wilke et al. (1999) [22]	Lifting (19.8 kg)	4.6
Sato et al. (1999) [23]	Standing in flexion (40 degrees)	2.7
Wilke et al. (2001) [24]	Lifting with flexed knees (20 kg)	2.3
Rohlmann et al. (2014) [25]	Lifting (10.8 kg)	3.3
Schäfer et al. (2023) [26]	Lifting in flexion (10 kg)	4.6

** All values represent the ratio of intradiscal pressure compared to standing upright. Loads for lifting depend on the sagittal distance of the load from the spine.*

A meta-analysis study by Roman-Liu et al. in 2023 [27] revealed that sitting without support increased intradiscal pressure by about 30%, compared to standing. Table 1.1 lists a number of studies and compares the quantified load of sitting and lifting as measured on specific locations on the lumbar spine, to the intradiscal pressure of standing upright. The results suggest that both sitting, and especially lifting weighted objects increase the pressure up to a factor of 4.6 times the standing load. While the direct link between poor posture, lifting, and LBP is complex and not entirely straightforward, evidence from the above studies suggests that certain occupational behaviors can indeed contribute to the deterioration and wear of lumbar vertebrae and discs. Especially for the tasks of sitting and lifting, where the spine is bent forwards, compressive foces on the lumbar and intervertebral shear loads are directly proportional to values of intradiscal pressure in Table 1.1. This wear can lead to conditions that either cause or exacerbate pain in the lumbar region. To better understand optimal prevention and rehabilitation strategies for LBP, it is essential to closely examine the mechanics of lifting. In this thesis, the lumbosacral joint (L5/S1) is used as a reference point for focusing on the lumbar region and describing relevant quantities.

The definition of low back load can vary from the shear forces active when flexing the spine, to the compressive forces pushing successive vertebrae together, to pressure within the discs themselves (Table 1.1). In this thesis, low back loads are defined as the product of all forces acting on the vertebrae; dynamic quantity that is the moment (M_L in Figure 1.1.4), or torque, experienced about the lowest lumbar joint: the L5-S1 lumbosacral joint. In order to better understand and offer targeted interventions for low back problems caused by repetitive lifting, these torques are classified according to their time-dependency.

1.1.3 Low Back Loads Classification

Repetitive lifting has been a focus of extensive research for many decades due to the significant concerns it raises, affecting thousands of individuals each year. Its negative impact not only poses health risks to workers but also leads to substantial economic losses for industries [28, 29]. Repetitive lifting causes the accumulation of microdamage to the tissue through cumulative low-back load (CLBL) [30]. Apart from CLBL, instantaneous damage can be caused to the lower back by peak low-back load (PLBL). Both of these quantities are typically highest at the L5/S1 lumbosacral joint [31]. Risk factors based on the L5/S1 extension moment (such as CLBL and PLBL) are both easy to calculate and capture the risk associated with many different specific injuries because the loads applied to the ligaments, disks, vertebrae, and muscles of the back scale with the L5/S1 extension moment [32]. In order to mitigate these loads and alleviate the lower back, we need to first understand how the various forces come in play and contribute to forming these loads.

1.1.4 Mechanics of Lifting

LBP remains a leading cause of disability worldwide, with occupational lifting often cited as a significant risk factor. However, the relationship between lifting and LBP is complex and multifaceted, involving both biomedical and biopsychosocial factors. When investigating the biomechanical factors, isolating the lifting movement aids the understanding of the underlying principles negatively affecting the lumbar region. In the instance of lifting a weight above the ground with a flexed spine, several forces act on the lumbar vertebra, achieving a static equilibrium, represented in Figure 1.3. While active muscle forces contribute largely to the initial compression of the vertebrae, passive muscle forces, especially at the bottom of a lift where long muscles such as the erector spinae are stretched beyond their resting length, accumulate equally large forces on the vertebrae.

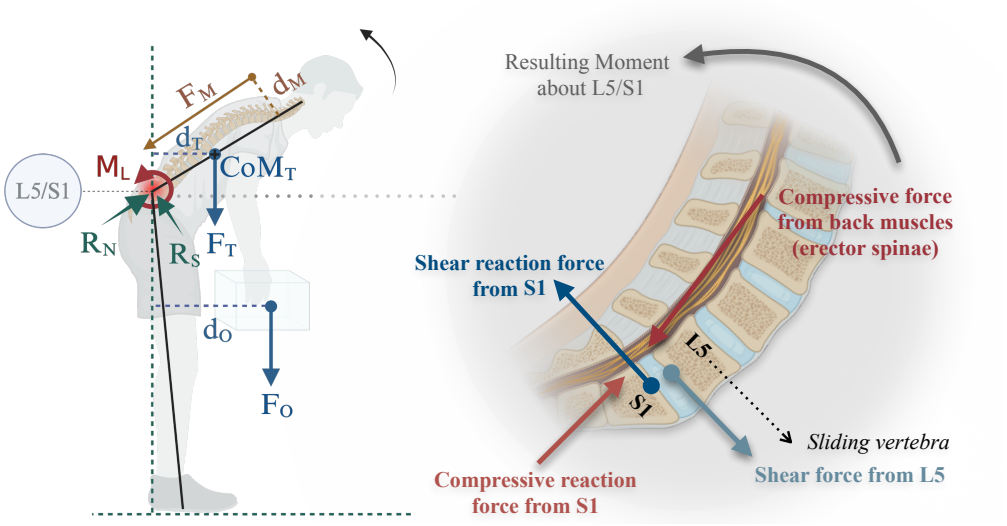

Figure 1.3: A simplified model describing force and moment distribution during lifting, about the L5/S1 joint. The inset describes the intervertebral compressive and shear forces taking place between L5 and S1. Created with BioRender.com.

Force Distribution During Lifting

While bending forward, the projected centre of mass of the torso CoM_T results to a vertical downward force F_T at a perpendicular distance (or lever) d_T from the lumbar. The object being lifted applies an additional force F_O from a distance d_O. A moment M_L is generated about the L5/S1 joint by the compressive force F_M produced by the back muscles and majorly the erector spinae muscles to counteract the downwards forces,

$$M_L = F_M D_M = F_O D_O + F_U D_U \tag{1.1}$$

and bring the lumbar to a static equilibrium. As the weighted torso bends forward, due to the curve of the spine the upper vertebrae experience a slight shift forward

relative to the lower ones. In the case of the lumbosacral joint, the L5 vertebra shifts to the front with respect to the S1, consequently creating an anterior shear force due to the components of F_T and F_O, triggering a posterior reaction shear force R_S from the S1, resulting to a considerable amount of stress for the intervertebral disc. Similarly, a reaction force R_N normal to the direction of the sliding vertebra is generated to counteract the compressive force of the back muscles,

$$R_S = sin(\alpha)(F_T + F_O) \tag{1.2}$$

$$R_N = F_M + cos(\alpha)(F_T + F_O) \tag{1.3}$$

and balance the force distribution acting on the lumbar.

Based on the simplified mechanical model presented, it is evident that lever arms significantly influence intervertebral forces and moments. Reducing the risk associated with lifting can be achieved by positioning the object closer to the body and maintaining a more extended or neutral spine, thereby decreasing the distance between the torso and the lumbar region. Considering the kinematic chain involved in and around the lumbar, several more ways can be employed in order to potentially alleviate stress on the L5/S1 region.

Kinematic Chain

The kinematic chain is the culmination of all joints and bones involved in the process of executing a specific movement. In the context of lifting, it begins at the **feet** and **ankles** which influence the balance of the whole body and provide an initial force when lifting. Subsequently, the **knees** extend to help raise the body, while the **hips** hinge to allow for the forward bending and subsequent extension of the spine. The **pelvis** serves as the connection between the lower limbs and the **spine**, transmitting forces generated by the legs to the upper body. The spine, particularly the lumbar region, acts as a lever, where forces are concentrated during lifting. Finally, the shoulders stabilize the arms, which then transfer the lifting force to the object. The movement of these joints and bones is dependent on muscular activity and how much force is exerted from the surrounding muscles.

Dynamic Chain

The dynamic, or muscular chain, is essentially the collection of muscles surrounding the kinematic chain, providing force for the movement, working in unison and influencing each other.The primary muscles involved in lifting are crucial for stabilizing the spine and providing the necessary force to lift an object [33], and are mainly around the central point of the kinematic chain (the pelvis):
Erector Spinae: A group of muscles running along the spine that are primarily responsible for extending the vertebral column. During lifting, these muscles are

heavily engaged to maintain spinal extension and resist the flexion forces acting on the spine.

Quadratus Lumborum: Located on either side of the lumbar spine, this muscle plays a critical role in stabilizing the pelvis and the lumbar spine. It helps in maintaining an upright posture and supports the spine during lateral flexion and extension movements.

Rectus Abdominis: This muscle runs vertically along the front of the abdomen. It works to flex the lumbar spine and stabilize the core, counteracting the extension forces generated by the erector spinae during lifting.

Obliques (Internal and External): These muscles are located on the sides of the abdomen. They are involved in trunk rotation, lateral flexion, and stabilizing the core during lifting. The obliques help in maintaining balance and posture, especially when lifting objects asymmetrically.

Gluteus Maximus: The largest muscle in the buttocks, which is the primary extensor of the hip. During lifting, especially in squat lifting, the gluteus maximus is responsible for extending the hips and aiding in the upward movement.

Quadriceps: The muscles located in the front of the thigh are crucial for extending the knee. In lifting, particularly during a squat, the quadriceps engage to extend the knee and lift the body upward. These muscles work in concert to maintain posture, balance, and force production during lifting. Proper coordination among them is essential to distribute the load effectively across the body and minimize the strain on the lumbar spine. The erector spinae and quadratus lumborum stabilize the spine, while the rectus abdominis and obliques provide core stability. The gluteus maximus and quadriceps generate the primary lifting force. Depending on the lifting technique, these muscles have different contributions and activation patterns during a lifting motion.

1.1.5 Lifting Techniques

This study focuses on two of the most common symmetric lifting techniques: the stoop lift and the squat lift [34]. During a stoop lift, the legs are minimally used as the spine is more engaged, leading to high spine flexion angles and compressive forces. During a squat, the legs are active contributors to the lift and require more energy, and the spine maintains a closer-to-neutral position, with lower compressive loads. Figure 1.4 illustrates a classic sequence of both lifts, from idle standing to reaching for the object and lifting it back to a straight posture. For a stoop lift, the process of standing to reaching the box starts with initial lumbar and hip flexion, introducing increasing lumbar and thoracic flexion and minimal knee flexion. For standing back up, hip, lumbar and thoracic spines slowly extend until they return to the neutral posture. When squatting down to reach the object on the other hand, the spine maintains a neutral posture while hip and knee joints flex deeply, along with ankles as to allow for balance. Depending on the distance of the object from the

person, the spine flexes as well in order to enable reaching the object at the lowest point of the lift. As the object is being lifted, the spine, hips, knees and ankles start to slowly extend until they reach the standing positions.

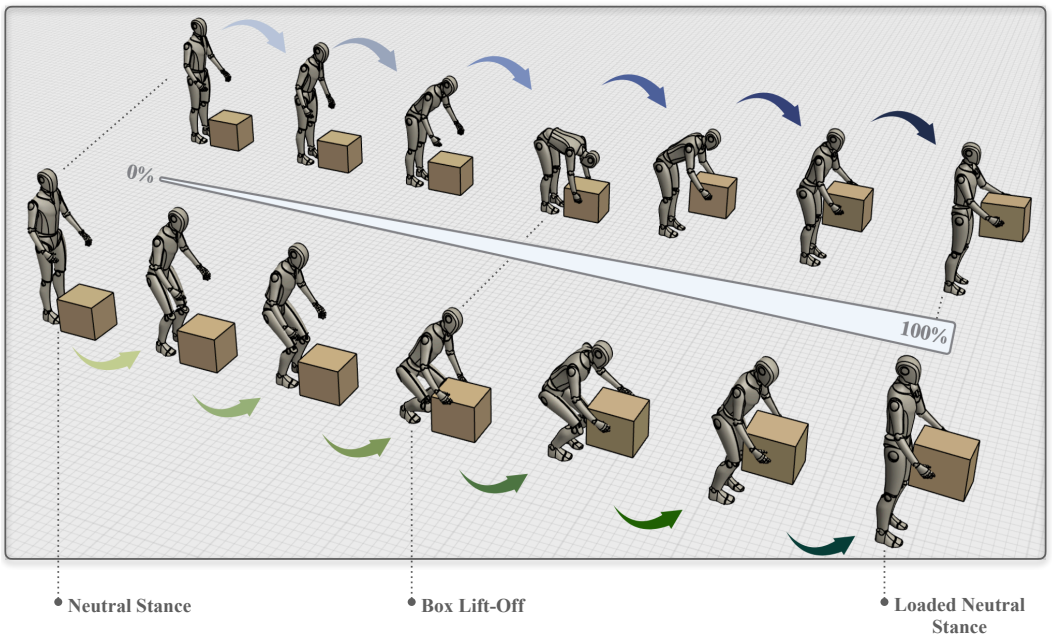

Figure 1.4: The two most common lifting techniques: **(Top)** a stoop lift with higher flexion in the spine and minimal work in the legs, versus, **(Bottom)** a squat lift with high energy requirements from the legs and lower spine flexion.

Various professionals have explored the impact of training on specific lifting techniques, but the findings have been inconsistent and inconclusive regarding the role of training in preventing low back pain [35]. As a result, a direct causal link between lifting techniques and low back pain cannot be definitively established. Notably, randomized studies involving 17,720 participants [36] also failed to draw clear conclusions about the effectiveness of improved lifting techniques for individuals engaged in repetitive lifting and handling tasks. This ambiguity could stem from several factors, including the tendency for individuals to deviate from optimal lifting techniques, such as the squat, as fatigue sets in over the course of the day, often resulting in a hybrid squat-stoop lift, which is commonly observed. Another common observation is the over-extension of the lumbar spine as means of compensation, which results in compressive loads and shear forces in the opposite direction while lifting, especially at the lowest point of the lift (position four in Figure 1.4).

1.1.6 Low Back Pain Prevention

Training in proper lifting techniques has long been considered a key approach to preventing low back pain, particularly for those engaged in repetitive manual tasks. However, emerging technologies are increasingly being explored as complementary or alternative solutions to address this persistent issue. Among these, back-support

exoskeleton (BSE)s and lifting assistance devices are gaining attention for their potential to reduce the load on the lower back, specifically targeting the lumbar region and the L5/S1 intervertebral disc, which is often the site of significant strain. Ongoing research is focused on evaluating the effectiveness of these technologies in mitigating lumbar stress, and they are rapidly becoming a topic of great interest within the field. BSEs are wearable devices designed to assist the user by providing mechanical support to the lower back during lifting tasks. They work by redistributing the load from the lumbar spine to other parts of the body, such as the hips and legs, through a combination of passive and active components. This support can help reduce the strain on the lower back muscles and spine, potentially lowering the risk of injury and fatigue during repetitive lifting activities.

Within the scope of this thesis, and under the framework of the European Project SPEXOR, an active BSE is investigated through multibody modeling and optimal control techniques. The aim is to explore the effects of training and lifting assistance on the user, and to determine how to optimally complement the user's movements by providing tailored support profiles. This research seeks to enhance our understanding of how such exoskeletons can be used to reduce the physical strain on the lower back, particularly in repetitive lifting tasks, while optimizing their effectiveness in real-world applications.

1.2 Gait Impairments

Gait abnormality refers to gait deviation from normal walking, usually due to a motor dysfunction but also commonly due to sensory complications. Neurological conditions, MSDs, systemic disorders and injuries often lead to conditions that impact the mobility of individuals and negatively affect their independence and quality of life, leading to increased risk of falls and injuries [37]. The prevalence of gait impairments increases with age, affecting over a quarter of individuals aged 70 to 74, and rising to nearly 60% among those aged 80 to 84 [38]. Globally, the aging population is expected to grow significantly, with projections suggesting that by 2050, the number of elderly people will reach 1.5 billion [39]. In Europe, gait impairments are a leading cause of reduced mobility in older adults, contributing to significant healthcare costs and resource utilization .

Addressing gait impairments through preventive meisasures, rehabilitation, and technological interventions, such as gait training and assistive devices, is crucial for enhancing mobility and reducing the long-term burden on healthcare systems. To effectively address this challenge, a comprehensive understanding of the biomechanics of gait and the underlying causes of gait impairments is essential. The next subsections offer a brief introduction into the anatomy of the lower limb.

1.2.1 Lower Limb Anatomy

The lower limb is essential for human movement, supporting body weight, enabling locomotion, and providing stability during activities like lifting. At the top, the pelvic girdle—composed of the ilium, ischium, and pubis—connects the lower limbs to the spine via the sacroiliac joint (Figure 1.5). It transmits forces during walking, standing, and lifting, while also maintaining posture through its tilt angle. The femur, the body's longest and strongest bone, connects to the pelvis at the hip joint, a ball-and-socket structure where the femoral head fits into the acetabulum. The lower leg comprises the tibia and fibula, which connect to the femur at the knee joint. The tibia bears most of the weight, while the fibula provides muscle attachments and stability. The patella (kneecap), embedded in the quadriceps tendon, protects the knee joint and improves quadriceps leverage. The foot, divided into hindfoot, midfoot, and forefoot, facilitates mobility. The hindfoot includes the calcaneus and tarsal, forming the ankle joint with the tibia and fibula, enabling dorsiflexion and plantar flexion. The midfoot's five bones—navicular, cuboid, and three cuneiforms—form low-mobility joints, while the forefoot contains the metatarsals, phalanges, and sesamoids, supporting toe movement.

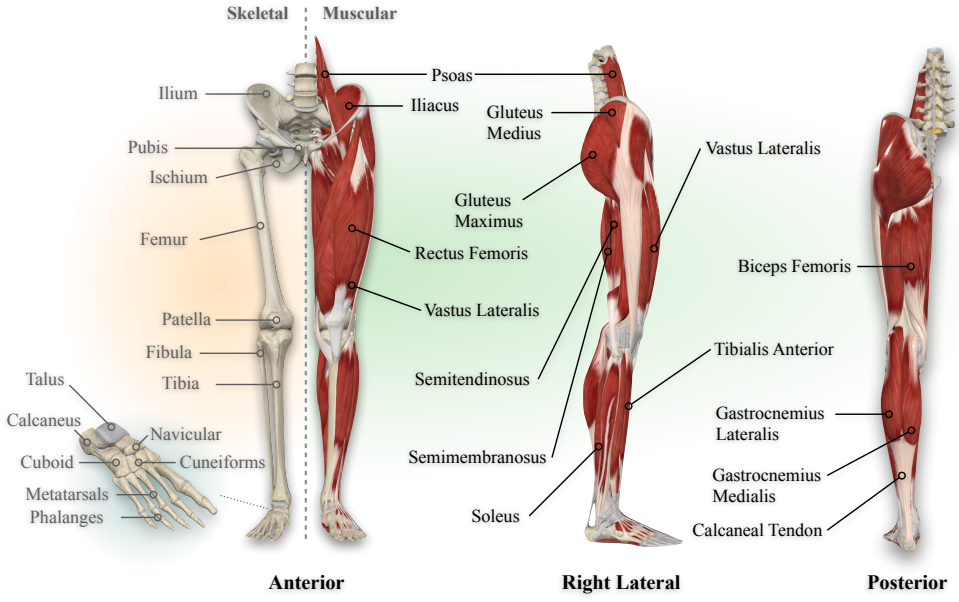

Figure 1.5: The musculoskeletal system of the lower limb. **(Left)** anterior view of the lower limb split into the skeletal system on the left, and muscular system on the right. The inset labels the foot bones in further detail. **(Middle)** right lateral view of the lower body with the muscular system. **(Right)** posterior view of the lower limb with the muscular system. Only major muscles contributing to gait are labelled. Images partially created with Complete Anatomy 2023 (3D4Medical, Elsevier).

Muscles of the Lower Limb

The lower limb's functional anatomy relies on a complex muscle system (Figure 1.5) that enables movement, maintains posture, and ensures stability. At the hip

and pelvis, muscles like the **gluteus maximus**, **gluteus medius**, **gluteus minimus**, and **iliopsoas** play key roles. The gluteus maximus drives hip extension, while the medius and minimus stabilize the pelvis and perform abduction. The iliopsoas, a primary hip flexor, initiates leg movement during walking and running. In the thigh, muscles are divided into three compartments. The anterior compartment houses the quadriceps femoris (**vastus lateralis**, **intermedius**, **medialis**, and **rectus femoris**), which extend the knee for activities like standing and climbing. The posterior compartment contains the hamstrings (**semitendinosus**, **semimembranosus**, and **biceps femoris**), responsible for knee flexion and hip extension. The medial compartment includes the adductor muscles, which stabilize the thigh through adduction.

The lower leg muscles control foot and ankle movement. The **gastrocnemius** and **soleus**, inserting into the calcaneus via the Achilles tendon, drive plantarflexion for push-off, acting as the propulsion muscle during walking and running. The **tibialis anterior**, in the anterior leg, manages dorsiflexion and inversion, ensuring proper foot placement during locomotion, acting as the breaking muscle during walking and running. Smaller intrinsic foot muscles support the arches and fine-tune toe movements, essential for balance and adapting to uneven surfaces. Together, these muscle groups provide the stability, mobility, and weight-bearing capacity needed for efficient locomotion and maintaining posture.

1.2.2 Mechanics of Walking

Walking is the most fundamental form of human locomotion, crucial for maintaining mobility and independence in one's life. It involves complex interactions within the musculoskeletal system, providing propulsion, support and stability. Understanding the mechanics of walking is essential in optimizing performance, as well as preventing and rehabilitating injuries and pathologies that result in gait abnormalities. This subsection delves into the intricate processes that take place during a typical gait cycle, as demonstrated in Figure 1.6, highlighting the coordinated actions of muscles that make walking possible.

Force Distribution During Walking

During a typical gait cycle, the distribution of forces and torques across the body plays a critical role in maintaining balance, propulsion, and overall movement efficiency. Forces generated actively by muscles produce **active torques**, which control joint motion and contribute to forward propulsion. These muscle-generated forces interact with external forces, producing ground reaction forces (GRFs)-forces exerted by the ground on the body in response to weight-bearing and movement, including frictional components.

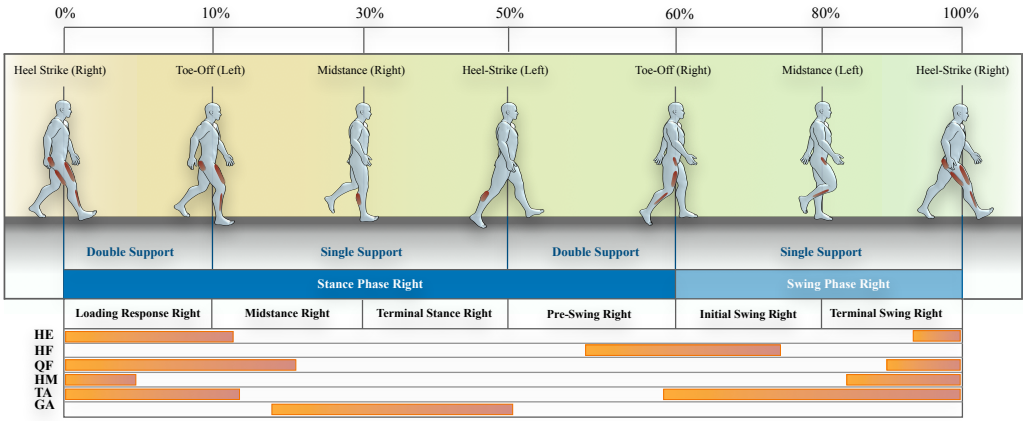

Figure 1.6: A typical gait cycle, with gait phase and sub-phase indications, highlighting the active muscle contributions per phase. Approximate muscle durations are indicated [40] for the right leg, next to their corresponding acronyms: HE = Hip Extensors, HF = Hip Flexors, QF = Quadriceps Femoris, HM = Hamstrings, TA = Tibialis Anterior, GA = Gastrocnemius.

As the GRFs propagate through the body, they are absorbed and transmitted via the foot, ankle, knee, and hip joints, resulting in joint reaction forces (JRFs)—internal forces acting between adjacent joints. Simultaneously, the interaction of these forces with passive structures, such as ligaments, tendons, and joint capsules, generates **passive torques** that resist deformation and stabilize the joints without active muscle input. Both active and passive torques vary significantly across the phases and sub-phases of the gait cycle and understanding the interplay between these forces, torques, and joint reactions is crucial for analyzing gait biomechanics, diagnosing abnormalities, and developing targeted interventions to enhance movement efficiency.

Loading Response: Upon heel strike, the initial impact generates a superoposterior peak in GRFs, which is then progressively absorbed by the body as it decelerates. This force is transmitted through the foot and up the kinetic chain, primarily affecting the ankle and knee joints. The quadriceps contract eccentrically to control knee flexion and absorb shock, while the tibialis anterior activates to prevent foot slap and ensure a smooth transition from heel strike to foot flat (mid-stance).

Mid-Stance: As the body transitions into mid-stance, GRFs decreases slightly but remains significant as the entire body weight is supported by the stance leg. The force vector shifts to a more anterior position relative to the foot, influencing joint mechanics in the ankle, knee, and hip. The gluteus medius and minimus stabilize the pelvis, preventing it from dropping on the opposite side. The gastrocnemius and soleus begin to engage, preparing for the push-off phase.

Terminal Stance: During terminal stance, GRFs peak again as the foot pushes off the ground, propelling the body forward. This phase requires coordinated action between the foot and ankle to efficiently transfer forces, primarily affecting the

hip and knee joints. The gastrocnemius and soleus muscles generate powerful plantarflexion, propelling the body forward. The hamstrings also contribute by flexing the knee and controlling the deceleration of the leg.

Swing Phases: The iliopsoas and rectus femoris initiate hip flexion in pre-swing, while the hamstrings flex the knee to lift the foot off the ground. The tibialis anterior remains active during the swing phases to maintain dorsiflexion, ensuring toe clearance and preventing tripping. In terminal swing, the quadriceps extend the knee, and the hamstrings decelerate the leg, preparing for the next heel strike.

These muscle forces work in harmony with the GRFs and JRFs to create a smooth, efficient, and coordinated walking pattern. Proper muscle function and timing are essential for maintaining balance, preventing injury, and ensuring effective energy transfer throughout the gait cycle [41, 42]. However, various pathologies result in different frailty levels for individuals, which can moderatelty or severely impact their gait and ability to walk, including performing simple everyday tasks.

1.2.3 Walking Frailty and Impairment

Frailty can be described as the diminished physiological capacity and the increased susceptibility to illness and other stressors [43], usually associated with older adults but also impaired individuals. The evaluation of frailty and impairment in walking is of high importance as it impacts mobility and independence, and can substantially lower the quality of life of older adults and those suffering from chronic conditions. Variability in specific gait parameters such as walking speed, step length and double support duration, can therefore give evidence towards frailty and impairment, when compared to typical gait.

According to the 7-point Clinical Frailty Scale [44], the four frailty levels for older adults that impact but do not completely disable mobility are levels (3): managing well, (4): vulnerable, (5): mildly frail and (6): moderately frail. Through levels three and four, individuals show altered gait traits such as decreased speed and stride length due to muscle weakness and imbalance, with levels five and six showing exacerbation of these symptoms and increased need for external assistance and walking aids. These frailties typically arise due to muscle weakness and atrophy, reducing the ability to generate adequate forces to sustain typical gait, affecting GRFs and impacting joint loading, primarily at the knee and hip levels.

Comparatively, gait impairments arising from MSDs negatively impact individuals through similar mechanisms. Conditions such as osteoarthritis, cerebral palsy and limb deformities disrupt the normal biomechanics of walking, leading to altered force distribution and increased joint loading. MSDs often lead to compensatory gait patterns that can exacerbate the condition over time. The combined effects of frailty

and musculoskeletal impairments highlight the importance of early intervention and targeted rehabilitation.

More severe conditions such as strokes and SCI can permanently affect the ability of an individual to walk, leading to the need of more impactful technological interventions. The use of assistive devices and orthotics can aid in redistributing forces more evenly across the joints, reducing pain and restoring or enhancing overall mobility. To adequately assess the level of impairment and determine the appropriate interventions, it is essential to thoroughly study the individual's gait, allowing us to pinpoint where and by how much support is needed.

Whether addressing the gradual decline associated with aging or the acute impairments resulting from injury, a comprehensive approach to gait analysis and intervention can significantly enhance the quality of life for affected individuals. Understanding the nuanced characteristics of frailty and impairment can be detrimental in effectively designing assistive and rehabilitating technologies.

1.2.4 Gait Rehabilitation

Physical therapy aims to rehabilitate patients suffering from various mobility impairments, targeting the underlying mechanisms of the specific pathologies. In cases of post-stroke rehabilitation, therapists re-train patients by manipulating their gait patterns as to regain the motor coordination [45], or provide techniques aiming to reduce the burden of impairments arising from degenerative conditions or injuries.

In the case of irreversible or severe impairments and high frailty, assistive technologies help restore mobility in various ways, depending on the impairment, by utilizing devices such as walking canes, rollators, wheelchairs, or orthotics. For individuals with profound gait impairments where traditional assistive devices are insufficient, LLEs offer an advanced solution. These wearable robotic systems are designed to provide support, enhance strength, and improve the gait mechanics of individuals with severe motor deficiencies, such as those resulting from spinal cord injuries or advanced neuromuscular conditions [46]. By integrating sophisticated sensors and actuators, exoskeletons facilitate natural walking movements, allowing users to regain a level of independence that would otherwise be unattainable with conventional mobility aids.

As technology continues to advance, LLEs are becoming increasingly viable as part of comprehensive rehabilitation programs, not only for their physical benefits but also for the psychological boost they offer by enabling users to engage more fully in daily activities. These devices represent a significant leap forward in the effort to restore mobility and improve the quality of life for individuals with severe gait impairments and frailty.

The latter part of this study investigates the use of a LLE and evaluates its ability in restoring mobility, providing support and assisting the task of walking. Within the scope of the HeiAge project funded by the Carl Zeiss foundation, the LLE TWIN [47] is used in order to investigate the familiarization process of such devices and their effects on walking. Gait analysis is used in order to quantify the effects of assistance through familiarization, and a modular sensor-based device for collecting biomechanical metrics and providing control feedback is developed and validated. This study aims to enhance exoskelton validation through gait analysis in various environments as to enhance the design process of these devices in order to meet individual patients needs.

Exoskeletons for Rehabilitation, Assistance and Prevention

2

Assistive technologies and specifically wearable robotics and exoskeletons have seen an unprecedented development over the past decades, emerging as powerful tools in enhancing mobility and preventing injuries [48]. As previously discussed, various individuals can be aided by correctly applying these wearable technologies either in industrial work settings or for rehabilitation purposes. Initially limited by bulky designs and rudimentary functions, effective integration of state-of-the-art sensor and actuator technologies has advanced these devices, making them increasingly accessible and effective in complementing human movement.

Exoskeletons are utilized across a wide range of fields, including sports, personal mobility, industrial work, military applications, and healthcare. Each sector leverages exoskeleton technology to enhance human capabilities, whether by improving performance, providing physical support, or augmenting strength. However, in this thesis, the focus is specifically on assistive and rehabilitation exoskeletons. These devices play a critical role in injury prevention and the restoration of mobility function, particularly for individuals recovering from musculoskeletal disorders or coping with physical impairments. The research herein is centered on exploring how these exoskeletons can support users in daily activities, promote rehabilitation, and prevent injuries, ultimately improving quality of life. To better understand how these devices aid in prevention and rehabilitation, classifying them based on their applications and functionalities can shed light on their intrinsic properties.

2.1 Classification of Exoskeletons

The main streams of assistive and rehabilitation exoskeleton development focus on the back, upper, and lower limbs. **BSEs** such as Ottobock's SuitX IX Back and IX Back Air (Figure 2.1A and 2.1B) by Ottobock SE & Co. KGaAare (Duderstadt, Germany), are primarily designed to alleviate the strain on the lower back during activities such as lifting and bending. By reducing the load on the lumbar spine, these exoskeletons help prevent injuries in physically demanding jobs and support rehabilitation for those with existing back conditions. They are particularly valuable in occupational settings where heavy lifting or prolonged standing is required, offering a proactive solution to one of the most common sources of workplace injuries [49].

Upper limb exoskeletons, on the other hand, provide support for the arms and shoulders, assisting with tasks that require repetitive motion or strength, such as lifting, reaching, or rehabilitation following an injury [50]. These devices, like Ottobock's SuitX IX Back Air (Figure 2.1C) are often used in industrial settings to reduce muscle fatigue and the risk of injury, as well as in clinical environments to help patients regain function and independence.

Lower limb exoskeletons like Ekso Bionic's (San Rafael, CA, USA) Indego (Figure 2.1D), focus on enhancing mobility for individuals with impaired walking ability due to conditions such as spinal cord injuries, stroke, or age-related decline [51]. These exoskeletons support the hips, knees, and ankles, enabling users to walk with greater stability and less effort. Advances in robotics and control systems have made lower limb exoskeletons increasingly effective, allowing for more natural gait patterns and improving the user's overall quality of life by restoring a significant degree of independence.

Figure 2.1: Types of exoskeletons. The occupational Ottobock SuitX exoskeletons: **(A)** the active back-support 'IX Back' for heavy lifting tasks, **(B)** the passive back-support 'IX Back Air' supporting lifting up to 20kg and **(C)** the passive upper-limb 'IX Shoulder Air' for supporting overhead work, and **(D)** the Indego lower-limb exoskeleton for rehabilitation. License for images acquired from SuitX by Ottobock.

Apart from the body area of attachment, the classification of exoskeletons also depends on the form of support they provide, through passive or active elements. The material structure of these devices further categorizes them, primarily between soft and rigid exoskeletons.

Passive Exoskeletons: These devices rely on providing force generated from passive structures via elastic elements such as springs, often incorporating damping elements as well. Depending on the position of the body segment they enclose, these elastic elements store energy during specific movements and provide back support when the movement is reversed. Although they are lightweight and generally comfortable to wear, passive exoskeletons can sometimes hinder users by resisting movements they are not designed to accommodate. *Quasi-Passive Exoskeletons* exist that include clutch-like mechanisms that disable their use when not reacquired, as to provide ease of movement in carrying out other activities.

Active Exoskeletons: Exoskeletons often incorporate active elements in the form of motors, hydraulic or pneumatic actuators, able to generate forces and torques that provide support to the body. In order to provide task-specific or personalised support, these devices offer control units where inputs can be selected or detected, as to instruct the actuators on the amount and timing of support needed. Hence, active exoskeletons are equipped with various arrays of sensors, in order to interpret user movements and provide feedback to the system. The added instrumentation, however, yields a higher weight and thus an increased effort from the wearer, which is often compensated in some extend through the additional support these active elements can provide. Rigorous testing is necessary in order to prevent injuries and ensure safety of moving parts able to exert great forces.

Rigid Exoskeletons: Constructed with solid materials like metals or hard plastics, they create a durable frame that provides structural support to the body, designed to augment strength and stability by rigidly linking the user's limbs and joints with the external structure. They offer significant mechanical support in heavy lifting or movement rehabilitation and they offer precise motion control in applications where strength and support are crucial. Though able to withstand greater loads, these exoskeletons increase considerably the weight the user has to carry, for example in BSEs. However, lower limb exoskeletons are responsible for transmitting the user's and their own weight to the ground.

Soft Exoskeletons: Primarily made from textiles and soft fabrics, they rely on pneumatic or cable-driven actuators embedded in flexible materials to assist with movement. Soft exoskeletons, or exosuits, are highly adaptable to the wearer's body, allowing natural movement and being comfortable for prolonged use. They are particularly suitable for lightweight tasks and rehabilitation. These devices are often much lighter and less bulky than rigid designs, which makes them ideal for everyday use or for patients recovering from injury. Because of their soft structure, these exoskeletons provide less mechanical support and strength, making them unsuitable for heavy lifting or highly demanding tasks. Achieving precise control in soft exoskeletons can be more challenging due to the variability in material elasticity and flexibility.

Flexible Exoskeletons: These exoskeletons exist in the interface of soft and rigid exoskeletons, as they combine rigid structures with elastic materials, allowing for more movement adaptability while still offering support. While maintaining structural integrity, they offer flexibility in joints, making them ideal for tasks where both flexibility and support is reacquired. They often employ flexible materials such as beams and springs in order to produce passive torques while bending.

In this thesis, the focus is on two specific types of exoskeletons: back-support and lower-limb exoskeletons. Sections 2.2 and 2.3 provide a detailed classification of these devices and explore examples of current solutions in each category. Additionally, subsections 2.2.2 and 2.3.3 introduce the two exoskeletons central to the methodology of this research.

2.2 Back-Support Exoskeletons

In response to the rise of LBP cases worldwide (Section 1.1), the advent of BSEs represents a significant innovation in both the prevention of low back injuries and the reintegration of affected workers. These wearable devices are designed to alleviate the physical burden placed on the lumbar region during strenuous tasks, thereby reducing the risk of injury and aiding in the recovery process. By providing mechanical assistance and distributing loads more effectively, BSEs are emerging as a critical tool in occupational health, offering a proactive solution that aligns with modern industry needs for safety and efficiency [52].

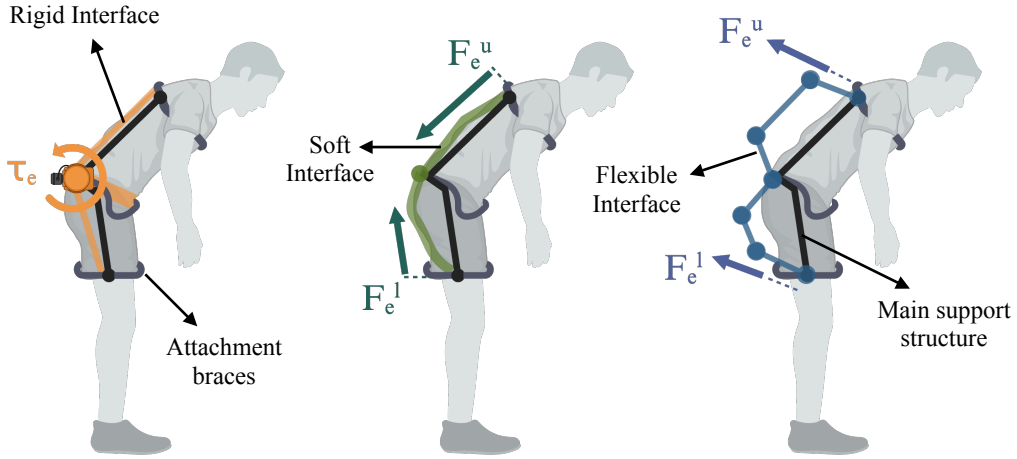

Figure 2.2: Differences in structural design and support application of three exoskeleton design scenarios. **(Left)** An ideal exoskeleton that provides direct joint torque on the lumbar, with an actuator, without introducing additional compression forces. Active exoskeletons are typically rigid structures. **(Middle)** Parallel force support via a soft exoskeleton introducing forces acting parallel to muscle compression forces on the spine. **(Right)** An exoskeleton that generates forces perpendicular to the spine, via the use of both rigid and elastic elements, constituting a flexible structure. τ_e denotes torque generated from the exoskeleton's actuator, whereas F_e denotes forces produced by the soft and flexible exoskeletons. Created with BioRender.com.

A typical BSEs transfers forces to the human body via attachment points, or braces, at the thighs, pelvis and upper back. Mechanical assistance from BSEs comes in three main forms: **direct joint torque**, **parallel force support** and **perpendicular force support** (Figure 2.2). A direct torque applied to the lumbar would be the ideal scenario, however there are numerous mechanical design, joint alignment and comfort implications that make this approach hard to realize. Instead, common active exoskeletons targeting the lumbar region apply torques at hips and transfer loads from the back to the thighs. Forces acting parallel to the spine can be achieved using soft exoskeletons with elastic materials such as springs, in order to help lower and lift the torso. Though these forces add to the compression of the lumbar spine, if the lever arms exceed the length of the back muscles such as the erector spinae, the exoskeleton forces are lower than the muscle forces; hence, in addition with partial disengagement of these muscles, the compressive forces of the spine are still lower in comparison to lifting without such exoskeletons [52]. Lastly, assistance provided by forces perpendicular to the spine aid with assisting the torso without imposing additional compressive forces and offloading the lumbar. Active rigid exoskeletons, as well as flexible exoskeletons can provide this kind of assistance to the wearer.

Apart from providing mechanical assistance and handling load redistribution, BSEs offer postural benefits and control to the wearer. Due to their design and structure, they are able to prevent excessive bending and hyper-flexion of the lumbar region which typically increases the bending moment experienced at the lumbar. Additionally, they offer lumbar support by braces wrapping around the waist, helping with lumbar stabilization. It is however important to note that prolonged use of such orthosis-type braces must be cautious, as long-term use is associated with atrophy of the lumbar region muscles [53]. Conclusively, these devices manage to successfully decrease CLBL in applications reacquiring prolonged static postures [54] as well as repetitive lifting of moderately heavy loads [55]. The following subsection provides a detailed outline on recent state-of-the-art back-support devices and their potential applications in preventing LBP.

2.2.1 Overview of Back-Support Exoskeletons

The most common areas of application of these devices include industrial work such as package lifting, baggage handling at airports, or crane operation, healthcare providers assisting limited-mobility patients, and various applications including first responders and military. Most of these exoskeletons aim to reduce biomechanical metrics that affect the spine such as mean and peak lumbar erector spinae (LES) muscle activations, lumbar compression forces (LCF), cumulative and peak lumbar loads and overall lumbar moments. In this subsection, the potential of exoskeletons tailored towards prevention of LBP in occupational settings is investigated, summarizing their main contributions.

Table 2.1: Comparison of Exoskeletons based on support[1], structure[2], experimental validation task[3], and resulting reduction metrics.

Exoskeleton	Support			Structure			Task			Reduction Metric
	P	Q	A	S	F	R	L	B	H	
PLAD										LCF (23-29%)
Smart Suit Lite										Mean LES activity (24.4%)
WAD										Mean LES activity (23.2%)
IX Back Air										Peak LES activity (9-20%)
Happy Back										Mean LES activity (23%)
VT-Lowe's										Mean LES activity (31.5%)
SPEXOR										LCF (18 - 26%)
Leave Bosch										Back muscle stress (40%)
BNDR										LCF (13%)
WMRD										Mean LES activity (54%)
APEX										LES fatigue (19-85%)
Passive Spine										Mean LES activity (24%)
BackX (Paexo)										Mean LES activity (56%)
WSAD										Mean LES activity (47%)
Soft Power Suit										Mean LES activity (54%)
Muscle Suit										Torso muscle power (37%)
Cray X										Mean LES activity (50%)
HAL Lumbar										LCF (14-18%)
H-WEX										Mean LES activity (23.5%)
Robomate										Mean LES activity (50%)

[1] *P = Passive, Q = Quasi-passive, A = Active*

[2] *S = Soft, F = Flexible, R = Rigid*

[3] *L = Lifting, B = Bending, H = Holding*

A brief overview of 20 BSEs is provided, highlighting their key features, properties, and applications. Table 2.1 offers a visual comparison of the fundamental attributes of both current and past solutions in back-exoskeleton technology, summarizing their contributions to reducing biomechanical metrics. Additionally, the following list outlines the experimental validation procedures and key findings for each device, where available:

- The **Personal Lift Augmentation Device (PLAD)** is a passive exoskeleton designed to reduce the load on lower back muscles during repetitive lifting. Using elastic elements (Thera-band® latex bands), PLAD stores energy during trunk flexion and releases it during lifting. In a study with loads of 5, 15, and 25 kg, PLAD reduced lumbar erector spinae activation by 14.4% and thoracic erector spinae by 27.6% [56]. Another study using a box weighing 10% of participants' maximum back strength found an 8.4% reduction in thoracic erector spinae activation during lowering and a 14% reduction in biceps femoris activation during lifting, with no significant change in oxygen consumption [57]. These findings suggest PLAD reduces muscle strain but does not lower overall energy expenditure, making it effective for reducing fatigue but not for improving task efficiency.
- The **Smart Suit Lite (SSL)** is a passive exoskeleton designed to provide trunk stabilization and reduce lumbar muscle strain during physical activities. SSL uses elastic materials that stretch as the user bends, generating forces that assist in extending the lumbar and hip joints. The resulting tension increases compression around the lumbar region, functioning similarly to a corset. One study demonstrated that the SSL increased body pressure around the pelvis by 34.6% when bending at 45°, compared to an upright posture [58]. Additionally, previous experiments showed an average 24.4% reduction in lumbar muscle activation during nursing care tasks. The device also enhanced postural stability by increasing lumbar joint stiffness, leading to a decrease in body sway, which further supports its role in trunk stabilization. These results suggest that SSL is effective at reducing muscle strain and improving postural stability through passive means, making it suitable for tasks that require lumbar support without the need for active assistance.
- The **Wearable Assistive Device (WAD)** is a passive exoskeleton designed to reduce muscle strain in the lumbar region during static holding tasks. It uses elastic bands that connect the upper and lower parts of the body, providing support by stretching during forward flexion. These elastic elements store energy, which is then released during extension, reducing the external moment on the lumbar spine and muscle activity. Biomechanical modeling showed that WAD reduced lumbar moments by 20% to 43%, depending on flexion angle and load. electromyography (EMG) results revealed reductions of 23.2% in

lumbar erector spinae, 30% in thoracic erector spinae, and 27.8% in latissimus dorsi at 60° trunk flexion with a 15 kg load [59]. WAD effectively lowers lumbar muscle activity and external moments, making it suitable for tasks requiring static load holding while reducing fatigue.

- The **IX Back Air** by *SUITX* (now part of Ottobock SE & Co. KGaA, Duderstadt, Germamny) is a passive exoskeleton designed to alleviate lower back strain during repetitive tasks such as bending and lifting. Weighing less than 3 kg, the IX Back Air is one of the lightest BSEs available, providing users with flexibility and comfort. It utilizes an AIR-Drive system, harnessing the body's movement to redistribute forces and reduce lumbar loads by 56-75% without adding spinal compression [60]. Studies show that the device can improve endurance by 52%, enabling users to perform physically demanding tasks for longer periods with less fatigue [61]. Additionally, the exoskeleton is easy to use, requiring less than 20 seconds to put on or remove, and is designed to fit all body types [62]. Its lightweight, ergonomic design makes it ideal for dynamic work environments, including logistics and warehouse operations, where workers perform frequent lifting and bending tasks.
- The **Happy Back Exoskeleton** is a passive weight transfer device designed to reduce lumbar loads during agricultural stoop labor. The exoskeleton works by transferring the weight from the upper body to the legs, reducing the strain on the lower back. In an early study comparing four exoskeleton devices [63], the Happy Back Exoskeleton demonstrated a reduction in both lumbar disc compression and erector spinae muscle activation, key contributors to lower back pain in agricultural workers. The results suggest that it effectively mitigates the biomechanical load on the lumbar region, making it suitable for use in labor-intensive tasks where forward flexion is common.
- The **VT-Lowe's Exoskeleton** is a passive, BSE designed to reduce the strain on the lower back during repetitive lifting tasks. The exoskeleton uses a number of flexible mechanical beams to redistribute loads away from the spine, particularly targeting the erector spinae muscles [64]. In a study by Simon et al. (2021), the exoskeleton demonstrated a 29% reduction in erector spinae muscle activation during lifting, while also improving ankle dorsiflexion and reducing knee flexion [65]. Additionally, metabolic cost modeling by Alemi et al. (2022) revealed that the exoskeleton led to a significant reduction in oxygen consumption, lowering it by 9% for an empty box and 8% for a box with 20% of body weight. The findings suggest that the exoskeleton effectively reduces both muscular and metabolic loads, making it suitable for tasks involving repetitive lifting [66].
- The **Laevo Bosch Exoskeleton** is a passive exoskeleton designed to reduce strain on the lower back during forward bending tasks, such as assembly work.

The exoskeleton uses spring-like elements and pads positioned on the chest, back, and upper legs to redistribute forces away from the lower back. In a study evaluating its performance, the Laevo exoskeleton reduced erector spinae muscle activity by 35-38% during assembly tasks and by 44% during static holding tasks. Additionally, it significantly increased endurance time in the static task from 3.2 minutes to 9.7 minutes [67]. However, the study also noted increased discomfort in the chest region due to the exoskeleton's pressure on the chest pads during prolonged use.

- The **Bending Non-Demand Return (BNDR)** is a passive weight transfer device designed to reduce the physical demands on the lower back during stooped posture tasks. The BNDR uses torsional springs and curved bars to redistribute the load from the lower back to the legs. In a study, the BNDR reduced lumbar erector spinae muscle activity by 26% in subjects who did not exhibit the flexion-relaxation phenomenon. It also decreased biceps femoris activity by 17%, offloading strain to the legs. The device limited total torso flexion by 16.7% and lumbar flexion by 9%, making it a useful intervention to help prevent low back disorders in workers frequently adopting the stooped posture [68].
- The **Wearable Restoring Moment Device (WMRD)** is a passive exoskeleton designed to reduce forces on the lower back during squat lifting tasks. It generates a restoring moment at the hips using a spring-cable system, reducing the need for erector spinae muscle force. In a study, the device demonstrated a 54% reduction in erector spinae muscle activity during squat lifting of a 133.5 N (30 lb) package, and reduced spinal compression forces by approximately 1300 N [69]. The exoskeleton's ground connection eliminates high contact stress on the lower extremities, making it an effective solution for reducing back strain during manual material handling tasks.
- The **APEX Exoskeleton** by HeroWear is a passive exoskeleton designed to reduce lower back strain during lifting and repetitive tasks. It uses elastic bands that stretch during bending and provide assistive force during extension movements [70]. This reduces the load on the lumbar muscles, allowing for greater comfort and reduced fatigue. In a study by Lamers et al. (2018), the exoskeleton reduced erector spinae muscle activity by 23–43% during leaning tasks and 14–16% during lifting tasks [71]. These reductions suggest the APEX is effective in mitigating muscle strain and helping prevent injury during manual labor.
- The **Passive Spine Exoskeleton** is designed to assist spinal flexion and extension using a push-pull strategy, where a pulling force is applied to the thoracic region and a pushing force to the lumbar region. These forces reduce the load on the lower back and decrease intervertebral bending moments.

In experimental tests, the exoskeleton reduced thoracic erector spinae (TES) muscle activity by 54% and lumbar erector spinae (LES) activity by 24%, with a corresponding reduction in intervertebral bending moment of 36 Nm and muscle force by 479 N [72].

- The **BackX Exoskeleton** by SuitX (Ottobock SE & Co. KGaA) is a passive, trunk-supporting exoskeleton designed to reduce lower back strain during repetitive bending and lifting tasks. It employs gas spring-based torque generators that activate during forward bending to reduce the load on the spine. BackX is capable of reducing thoracic erector spinae muscle activity by 75% and lumbar erector spinae activity by 56% during static bending tasks [73]. This exoskeleton also lowered bending moments at L5/S1, effectively decreasing the risk of lower back injuries for workers performing repetitive tasks. BackX was shown to allow users to perform a wide range of tasks, including walking, squatting, and climbing stairs, without impeding motion due to its integrated clutch-based mechanism.
- The **Wearable Stooping-Assist Device (WSAD)** is a passive exoskeleton designed to reduce the physical demands of prolonged stooped postures common in agricultural and construction work. The WSAD uses tension bands to assist trunk flexion by redistributing the load from the lower back to the legs and upper body. In EMG experiments, the WSAD reduced thoracic erector spinae (TES) muscle activity by 42%, LES activity by 47%, and latissimus dorsi activity by 28% during 90° forward bending [74]. By lowering muscle activation, the WSAD effectively reduces the physical strain on the back, decreasing the risk of low back disorders during stooped work.
- The **Soft Power Suit** is a soft exoskeleton designed to assist the lower back during dynamic lifting and static forward bending tasks. It uses twisted string actuators (TSA) attached to a back brace to generate tensile forces that mimic muscle function, thereby reducing strain on the erector spinae muscles. Weighing only 2.4 kg without the battery, the suit offers a lightweight and flexible solution for back support. In a preliminary study, the suit reduced erector spinae muscle activity by 50.2–54.0% during static bending tasks and by TSA during dynamic lifting [75].
- The **Muscle Suit**, developed by Tokyo University of Science, is a soft, active exoskeleton designed to assist manual laborers by reducing muscle strain during lifting and repetitive tasks. The suit utilizes McKibben artificial muscles, which are pneumatic actuators that provide mechanical assistance by generating tensile force during trunk flexion and extension. Weighing 9.2 kg, the suit is equipped with a compressor to power the actuators. In a study, the Muscle Suit reduced muscle activation by 85% in the elbow and shoulder and 50% in the lower back (sacroiliac region) during lifting tasks [76].

- The **Cray X Exoskeleton** (now Apogee) by German Bionic (Augsburg, Germany) is an active, AI-powered exoskeleton designed to assist industrial and logistics workers by providing up to 30 kg (66 lbs) of support per lift. It combines AI-driven technology with real-time ergonomic monitoring to reduce the strain on the lower back and legs during both lifting and walking tasks [77]. This exoskeleton is ideal for applications in logistics, warehousing, and manufacturing, enhancing worker productivity and safety by reducing the risk of overexertion.
- The **HAL Lumbar Type for Labor Support** by Cyberdyne Inc. (Tsukuba, Ibaraki, Japan) is an active, powered exoskeleton designed to assist workers in reducing lower back strain during physically demanding tasks. The device utilizes bio-electrical Signals to detect the wearer's muscle activity, particularly in the erector spinae and gluteus maximus, and applies torque to the hip joints to reduce lumbar strain. Weighing 3.1 kg, the exoskeleton provides up to 4.5 hours of continuous operation per charge. It reduces stress on the lower back during lifting and carrying tasks, significantly lowering lumbar and intervertebral disk loads [78].
- The **Hyundai Waist Exoskeleton (H-WEX)** is an active exoskeleton by Hyunday Motor Company (Seoul, South Korea) designed to assist industrial workers by reducing back strain and muscle fatigue during repetitive tasks such as bending and lifting. Developed by Hyundai Motor Company, the H-WEX uses a singular actuation mechanism with a differential gear to drive both legs using one motor, offering natural movement during walking with minimal resistance. Weighing 4.5 kg, the exoskeleton provides up to 90 Nm of assistive torque. In a study, the H-WEX reduced erector spinae muscle activity by 23.5% in the semi-squat posture and 10.5% in the stoop posture [79].
- The **Robo-Mate Exoskeleton** is an active, torque-controlled BSE designed to reduce spinal loads during manual handling tasks. Developed under the Robo-Mate project [80], it utilizes a parallel-elastic actuator (PEA) to combine the energy efficiency of springs with the torque-control benefits of motors. The PEA configuration helps reduce motor torque requirements, while providing up to 50 Nm of assistive torque, reducing strain on the user's lower back during lifting tasks. In trials, Robo-Mate reduced spinal loads by assisting with up to 50% of the required joint torque during lifting [81].

The SPEXOR exoskeleton is described in the following section and in detail later in this thesis. While the current range of exoskeleton technologies is impressive, offering significant advancements in reducing back strain and enhancing worker safety, many of the technological breakthroughs required to effectively integrate these devices into the workforce have emerged only in the late last decade. The BSE research in this thesis, conducted as part of the **SPEXOR** project, aimed to

address the prevention of low back pain and support vocational reintegration at a time when lumbar assistance in repetitive lifting was critically needed yet underdeveloped. When the project began, research into BSEs was in its infancy, lacking both the empirical evidence and technological sophistication seen in today's solutions. SPEXOR's primary objectives were to provide optimal mechanical assistance while ensuring user comfort, laying the groundwork for significant advancements in the field. The following section introduces the aims and objectives of the project, with a particular focus on the contributions made in this thesis, detailing the development stages of the SPEXOR exoskeleton.

2.2.2 The SPEXOR Project

The SPEXOR project aimed to produce a back-support exoskeleton for low-back pain prevention and vocational reintegration and was funded by the European Union's Horizon 2020 research and innovation program under grant agreement No. 687662. The project was directed by Jan Babič of the Jožef Stefan Institute (Ljubljana, Slovenia) and involved multiple academic and commercial partners across the European Union. The project's primary goal was to create a spinal exoskeleton that could effectively reduce lumbar strain while ensuring comfort and long-term wearability. SPEXOR focused on developing passive and active systems to generate optimal torque profiles, monitoring musculoskeletal stress and enhancing the user experience by adjusting support based on movement patterns and task-specific biomechanical needs.

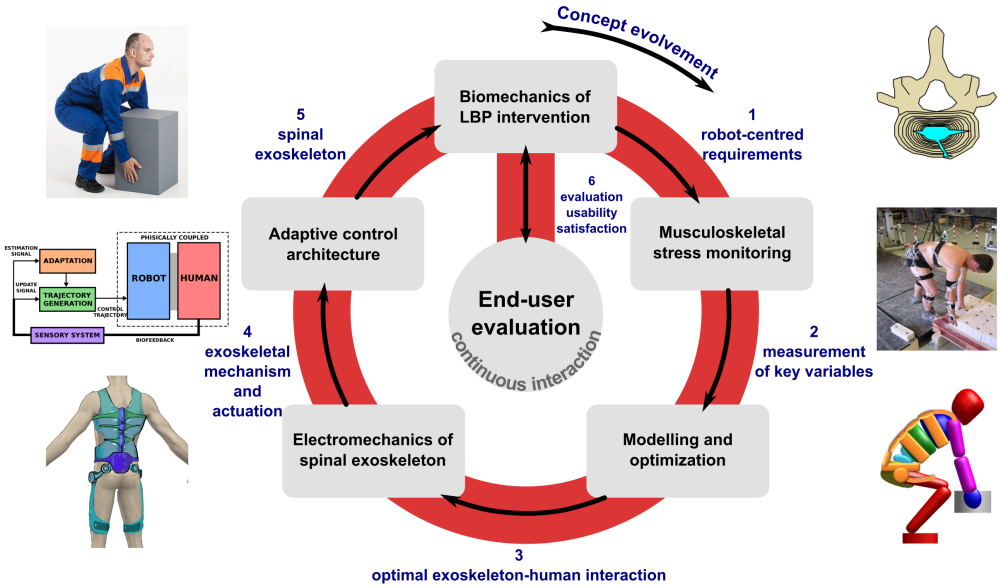

Figure 2.3: Concept development and objectives for project SPEXOR. Gray boxes represent development stages including work packages shared amongst the consortium members. Figure taken from `www.spexor.eu` [82].

The various objectives of the SPEXOR project were distributed across the consortium partners, each responsible for realizing and developing the work packages shown in Figure 2.3. The first task focused on the *biomechanics of LBP intervention*, where risk factors for low-back pain were identified through biomechanical experiments. This research informed the design requirements for the exoskeleton. Additionally, various feedback strategies, such as monitoring torso flexion and joint moments, were tested to determine how they influenced user behavior. This work package was led by the MOVE Research Institute at Vrije Universiteit Amsterdam (Amsterdam, The Netherlands).

The *musculoskeletal stress monitoring* task developed a system to measure user positions and provide feedback using indicators from the biomechanics research. This task was managed by Ottobock SE & Co. KGaA (Duderstadt, Germany). The *modeling and optimization* team worked on modeling human and exoskeleton interactions as rigid multibody systems, optimizing both the passive elements and motor actuation patterns. The goal was to ensure comfortable and effective use of the exoskeleton. This task was handled by the Optimization, Robotics and Biomechanics (ORB) at Heidelberg University (Heidelberg, Germany) and the work of this thesis lies therein.

In the task dedicated to *electromechanics*, the mechanical design of the exoskeleton was developed, including its structural concept, joint design, and selection of actuators and passive elements. This was undertaken by the Robotics and MultiBody Mechanics Research Group at Vrije Universiteit Brussel (Brussels, Belgium), while Otto Bock Healthcare Products (Vienna, Austria) developed a lightweight and efficient hydraulic actuation system. The *adaptive control architecture* work package focused on creating a control system that could distinguish between different user motions based on sensor data, such as torso inclination and hip flexion. This also involved developing the exoskeleton's electronic system. This task was coordinated by the Department of Automation, Biocybernetics and Robotics at the Jožef Stefan Institute (Ljubljana, Slovenia), which also oversaw the entire project.

Finally, the *end-user evaluation* task involved developing a protocol to assess the functional performance and user acceptance of the exoskeleton. This task was a collaborative effort involving Science2Practice (S2P) (Ljubljana, Slovenia), the Faculty of Health Sciences at the University of Primorska (UP), and the Rehabilitation Center Heliomare (Wijk aan Zee, The Netherlands).

SPEXOR Foundations and Evolution of Prototypes

Prior to this thesis work, a number of prototypes were designed and produced evaluating various aspects of assistance and support, while utilizing both passive and active elements in a flexible prototype framework. The mechanical design of the exoskeleton prototypes has been informed by parameter optimization and based on

musculoskeletal modeling and biomechanical evaluation, three primary prototypes were developed throughout the course of the project.

SPEXOR Passive Prototype (Figure 2.4)
Early work brought about the development of a passive and flexible exoskeleton [83]. The exoskeleton consists of three interfaces attaching to the wearer at the level of the thigh using straps, on the pelvis using a belt with integrated carbon plates and shoulder straps that wrap around the thorax, overall weighing 6 kg. This exoskeleton utilizes three to five (subject to desired level of support and anthropometric features) flexible carbon fibre beams (4.7 mm in diameter, with a Young's modulus of 166 GPa) to enhance the ROM while providing passive torque support to the lumbar spine. The beams bend with the user's trunk, storing energy during flexion, which is released during extension, providing passive support, allowing for up to a 25% increase in ROM compared to rigid designs.

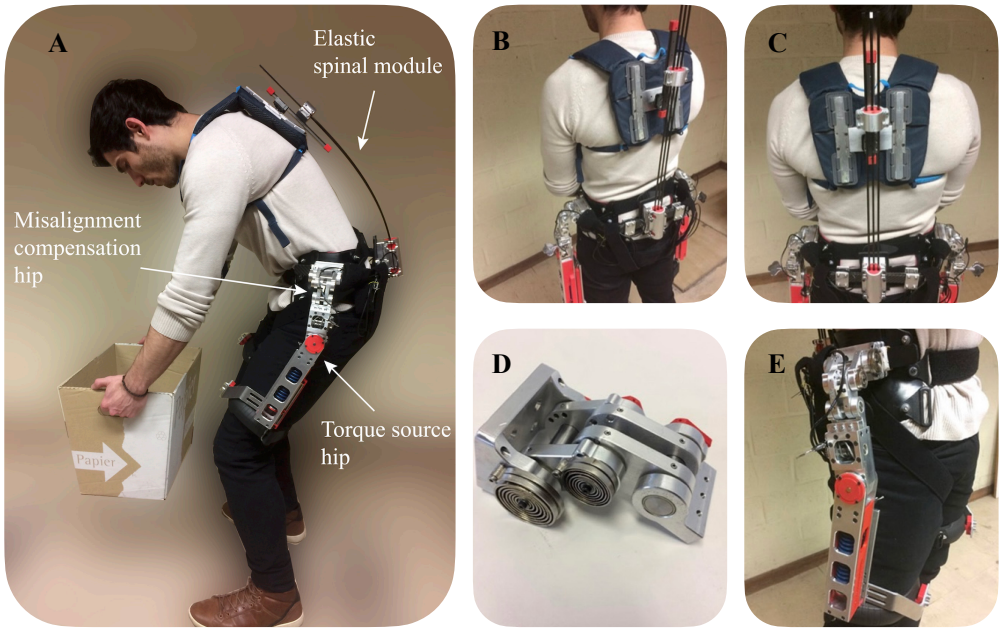

Figure 2.4: The SPEXOR passive prototype and main frame. **(A)** sagittal view highlighting main exoskeleton components. **(B)** A posterior view of the exoskeleton. **(C)** A posterior view of the top interface of the exoskeleton showcasing the flexible beams. **(D)** The three-joint misalignment compensation mechanism. **(E)** Anterio-sagittal view of the lower part of the exoskeleton showcasing the misalignment compensation mechanism attached to the passive adjustable actuator. Figures taken from `www.spexor.eu` [82].

For generating support at each side of the hips, a passive spring-based and adjustable compliant actuator is used [84] that produces a nonlinear deflection-torque profile, the mechanical properties of which can be adjusted prior to use. The exoskeleton generates a maximum torque of 25 Nm at the lower back and 22 Nm at each hip, and misalignment compensation mechanism further enhances comfort and reduces parasitic forces during movement. This mechanism allows the exoskeleton to follow

natural spine and hip motion, reducing unwanted forces and improving comfort. Tests show it significantly reduces back loading while maintaining flexibility, making it less restrictive than designs like Laevo.

SPEXOR Quasi-Passive Prototype (Figure reffig:EXOs:spexorall)
Through the evolution of the project, a quasi-passive prototype was developed, introducing an adaptive control framework with a built-in clutch mechanism [85]. The structure and passive elements of the exoskeletons remained the same, but the addition of the clutch mechanism enabled users to either manually engage or disengage the assistance, or rely on the automatic mode where using a high lever controller assistance was activated with a servo motor at the beginning of a forward bend. To inform the automatic mode of clutch engagement and disengagement an encoder was fitted at each hip to measure the hip angle and an inertial measurement unit (IMU) was fitted on the chest to measure trunk inclination. The addition of the clutch mechanism brings the overall weight of the exoskeleton to 6.7 kg.

SPEXOR Active Prototype (Figure 2.5)
Two different prototype versions were investigated for the active SPEXOR exoskeleton, influencing the design and incorporating a new element for each version; a hydraulic actuator and an electric motor. The hydraulic actuator provided by Otto Bock Healthcare Products (Vienna, Austria) was attached on the existing misalignment compensation mechanism, effectively replacing the passive compliant actuators and is able to provide a maximum output torque of 25 Nm.
The electric version of the active prototype closely followed the quasi-passive approach, where the passive compliant actuators remain at the hips, with the addition of a servo motor able to control the pretension of the springs, offering a dynamically variable stiffness through the lift. Apart from the passive elements, two electric motors are introduced to the hips as well able of providing an additional variable torque source.

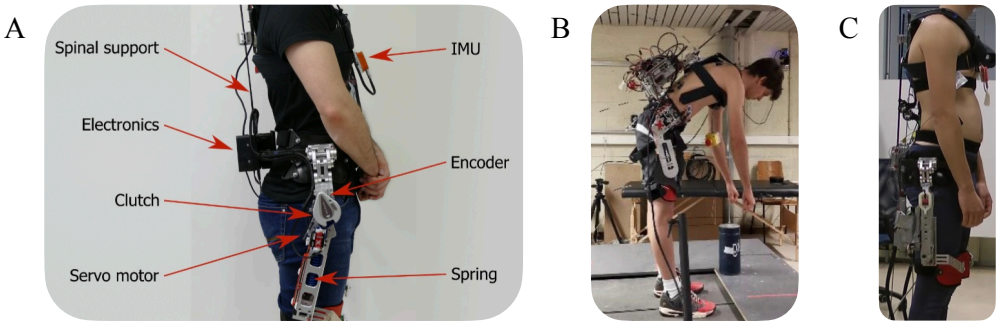

Figure 2.5: The three evolutions of the SPEXOR passive prototype and main frame. **(A)** The quasi-passive prototype featuring a clutch mechanism. **(B)** The electromechanical prototype with electrical motors atatched on the back, driving the hips. **(C)** The hydraulically actuated prototype with the hydraulic actuator replacing the spring element on the hips.

SPEXOR Monitoring System

A monitoring system was developed to be used along with the exoskeleton, responsible for integrating data from inertial measurement units (IMUs) and force-sensitive insoles in order to perform a comprehensive biomechanical and ergonomic assessment of the user's posture [86]. The system can detect unergonomic movements in real-time and provides immediate feedback to the user, enabling them to correct their posture or avoid improper movements in the future. This feedback mechanism helps improve ergonomics and reduces the risk of injury by promoting healthier movement patterns. As the SPEXOR project evolved, the focus shifted toward developing an active exoskeleton capable of delivering personalized support through optimal torque control. This transition led to the creation of active prototypes and emphasized the generation of optimal torque profiles using advanced modeling and simulation techniques.

This thesis specifically focuses on applying optimal control to the hydraulically actuated exoskeleton, generating torque profiles designed to maximize user assistance while ensuring comfort in human-exoskeleton interaction. The research also explores how external assistance affects cumulative and peak low back loads, and compares the effectiveness of the exoskeleton with traditional training approaches. Ultimately, this work on BSEs aims in optimizing human-exoskeleton interactions in terms of adeqaute support at optimal comfort levels. Chapters 4, 5, and 6 present the foundational methodology, detailed results, and a thorough analysis of the outcomes, and ultimately concluding the SPEXOR project's contributions.

2.3 Lower-Limb Exoskeletons

Related to the rise of global population, musculoskeletal disorders and pathologies related to old age have respectively increased over the last few decades. As to effectively aid frail population in battling everyday challenges, lower limb exoskeletons have emerged as a powerful solution to assist rehabilitation and restore mobility. These exoskeletons aim to reduce the physical burden on the lower limbs by providing mechanical assistance, facilitating improved gait patterns, and supporting physical therapy. By enhancing both rehabilitation outcomes and assisting in daily activities, lower limb exoskeletons represent a crucial technological advancement in addressing the challenges posed by aging, musculoskeletal mobility impairments and other neuromuscular conditions [51].

Lower limb exoskeletons function by assisting the various phases of gait, particularly during stance and swing phases. These devices provide mechanical support to users with impaired or weakened lower limb function, facilitating foot clearance during swing and aiding in weight-bearing during stance. By using advanced sensors, such as IMUs, force sensors, and encoders, exoskeletons can accurately track

user movements and deliver tailored assistance in real-time. They are designed to complement natural human movement, synchronizing with the user's gait pattern to enhance walking performance and aid their low-mobility regions.

In terms of structural features, lower limb exoskeletons typically include rigid frames, often made of lightweight materials like aluminum or carbon fiber, and are powered by electric actuators or hydraulic systems, usually aligned at the human joint. These actuators provide assistance through either position control, which ensures that the joints follow a predefined trajectory, or force control, where the exoskeleton applies forces in response to user interaction. Meanwhile, impedance control modulates resistance in response to user movement, and admittance control adjusts the exoskeleton's position based on applied forces. These control strategies are crucial in maintaining stable and adaptive assistance while minimizing resistance to voluntary movement [87]. In order to maintain balance and control over the device and movement path, almost all LLEs are assisted by the use of crutches.

Another form of assistance exists in exosuits, which, as opposed to rigid exoskeletons, are typically soft, flexible devices that assist specific joints, most commonly the hip or knee. These suits are designed to provide targeted support, often helping with either hip extension or knee flexion, depending on the intended application. They use motors placed at the back, to minimize bulk at the joints, often providing support in under-actuated systems. These motors drive cable-based actuation systems, transmitting forces through cables to assist joint movements. This design allows for a lightweight and unobtrusive structure, making exosuits ideal for reducing muscle effort while preserving a wide range of motion for the user, in cases where lower levels of support are needed, in less frail or more mobile populations [88].

The classification of LLEs mainly lies within five categories:

- **Rehabilitation exoskeletons**, helping people with movement disorders overcome walking impairments caused by SCIs and strokes, like the EksoNR from Ekso Bionics (Ekso Bionics Holdings, Inc, Richmond, California, USA) [89],
- **Assistive mobility exoskeletons** designed to aid people with limited mobility due to muscle weakness or paralysis, an example of which is the ReWalk exoskeleton robot by ReWalk Robotics Ltd. (Marlborough, Massachusetts, USA) [90],
- **Personal mobility exoskeletons** which also fall under assistive mobility, but cater towards people with lesser mobility impairments and are more mobile in nature, while aiding the user in everyday tasks including standing and walking, like the soft exosuit from the Wyss Institute of Harvard University (Boston, Massachusetts, USA),

- **Power augmentation exoskeletons** such as the HAL-5 exoskeleton from the University of Tsukuba (Ibaraki, Japan) [91] aimed at enhancing and upgrading human capabilities, and
- **Sports and functional exoskeletons** which are being developed to functionally assist the wearer in sports performance or improving endurance, for example in activities such as hiking, which the newly developed MO/GO exoskeleton pants by Skip Innovations (Mountain View, California, USA) cater to [92].

In this work the focus is given on rehabilitation and assistive mobility exoskeletons (Figure 2.6), and their impact on biomechanical functionality of the individuals they cater to.

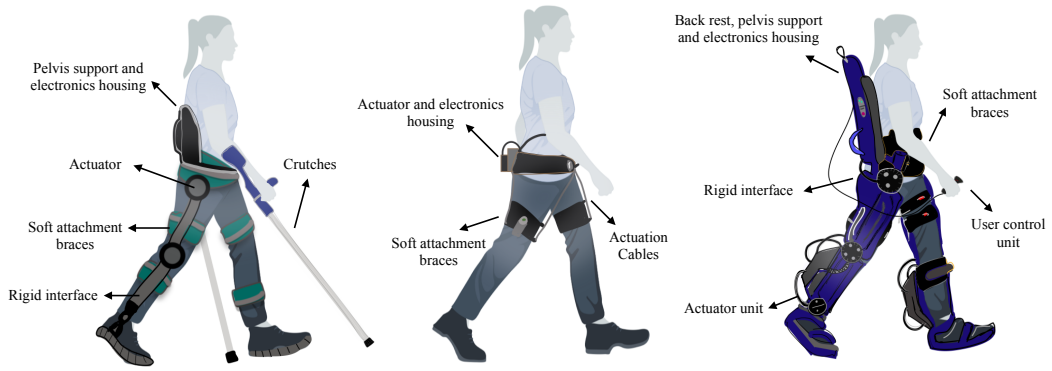

Figure 2.6: Three types of LLEs. **(Left)** A rigid exoskeleton indented for rehabilitation of mobility impaired patients using crutches. **(Middle)** A soft exosuit for personal mobility purposes, catering to individuals with partial mobility issues. **(Right)** A rigid self-balancing exoskeleton robot that restores mobility to severely impaired or paraplegic patients, enabling them to stand and walk without limitations.

LLEs are predominantly actuated robots as they typically need to provide substantial forces in order to carry their own, and the user's weight. This in turn requires an array of actuators and sensors, paired with a complex software and control architecture framework, in order to successfully identify kinematic and dynamic queues from the paired human and exoskeleton couple, and respond to biomechanical parameters. The user interface depends heavily on the type of exoskeleton at hand, as well as the specific user requirements. A number of exoskeletons collect muscle activity feedback via EMG, limb orientations and accelerations via IMUs, joint angles via encoders and interaction forces via pressure and force sensors in order to inform the control system and thereafter the actuation [93]. By combining actuators with data from these sensors, LLEs can dynamically adapt to the user's movements, ensuring responsive and precise mechanical assistance. The following subsection details the mechanics of exoskeleton assistance of the lower limb, providing a simplistic explanation of the main function these devices share.

2.3.1 Lower-Limb Exoskeleton Mechanics

To effectively assist the lower limb and optimize the design and control of exoskeletons, it is crucial to analyze the intrinsic relationships between the human body and the exoskeleton as two coupled multibody systems. By modeling the interactions through mechanics equations, the system can be approached as a multi-body problem, allowing for the calculation of both kinematic and dynamic properties. The coupled human-exoskeleton dynamics can then be simulated to inform design decisions. This section presents a generalised and simplified model of a two degree of freedom (DoF) system in the sagittal plane, with one actuated DoF per joint (hip and knee). In this model, we assume perfect coupling between the leg and exoskeleton, with the shank and foot treated as a single rigid body. Figure 2.7 visualises the problem and denotes the variables expressed in Equations 2.1 to 2.7.

The dynamics of the two-DoF exoskeleton in the two-dimensional coordinate system (x and y) can be derived using Lagrange's equation,

$$L = EK - EP \tag{2.1}$$

where EK is the kinetic energy and EP is the potential energy of the system. We can hence solve the Lagrangian equation using partial differential equations (PDEs),

$$\frac{d}{dt}\left(\frac{\partial L}{\partial \dot{\theta}_i}\right) - \frac{\partial L}{\partial \theta_i} = \tau_j \tag{2.2}$$

where θ_i represents the generalized coordinates for the hip and knee joints, $\dot{\theta}_i$ is the angular velocity, and τ_j is the joint torque. The joint torque governs the link motion and is a result of the kinetic and potential energy terms,

$$EK = \frac{1}{2}\sum_{i=1}^{n} m_i(\dot{x_i}^2 + \dot{y_i}^2) + \frac{1}{2}\sum_{i=1}^{n} I_i\dot{\theta_i}^2 \tag{2.3}$$

$$EP = \sum_{i=1}^{n} m_i g y_i \tag{2.4}$$

with m_i corresponding to the mass of each link, I_i being the rotational inertia, and g the gravitational acceleration. The global position of the center of mass (x_i, y_i) of each link can be derived based on the link's orientation,

$$x_i = \sum_{j=1}^{i-1} L_j \sin(\theta_j) + d_i \sin(\theta_i) \tag{2.5}$$

$$y_i = \sum_{j=1}^{i-1} L_j \cos(\theta_j) + d_i \cos(\theta_i) \tag{2.6}$$

where d_i is the distance from the joint to the center of mass, and L_j is the length of the corresponding link. By hence applying the Lagrangian equations we can obtain the dynamic equations of motion for the system,

$$M(\theta)\ddot{\theta} + C(\theta, \dot{\theta})\dot{\theta} + G(\theta) = \tau_j \tag{2.7}$$

where $M(\theta)$ is the mass matrix, $C(\theta, \dot{\theta})$ represents centripetal and Coriolis forces, and $G(\theta)$ is the gravitational force vector. The torque dynamics can further be analyzed in order to account for motor impedance and current-to-torque relationships.

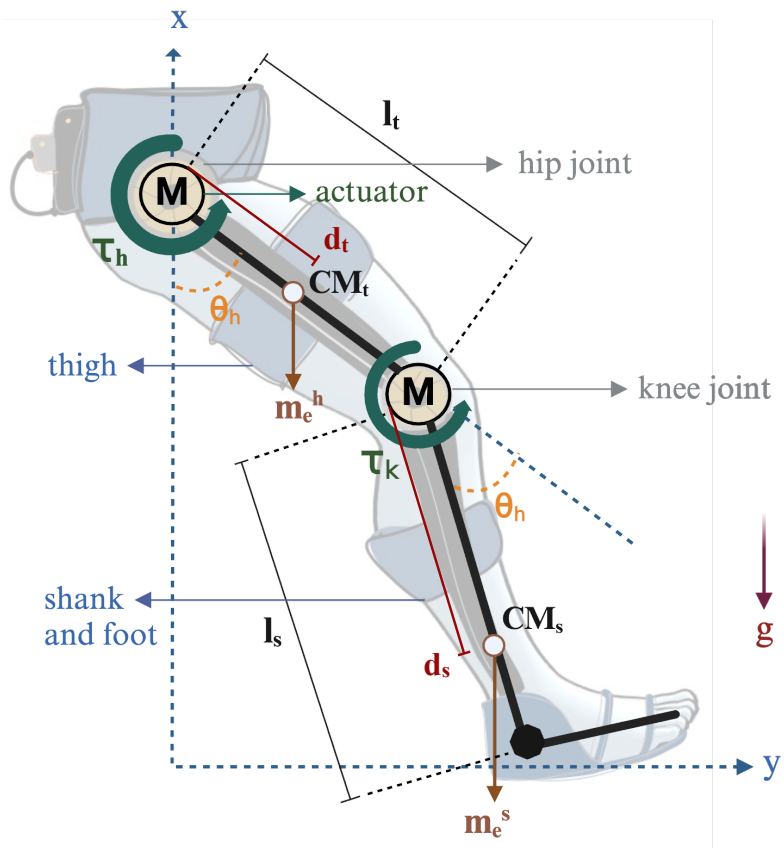

Figure 2.7: A simplified two-DoF sagittal model of a LLE. The hip and knee joints are actuated, the shank forms one rigid body with the foot, and the human is assumed to be perfectly couple to the exoskeleton.

In a real-life system, interaction forces arise in a numerous ways due to the coupling of the human and exoskeleton; these forces are experienced through the joints – a direct product of the torque applied at the joint and the distance to the centre of mass – and between the contact braces where the exoskeleton applies pressure to the human limbs where normal and trasnversial forces to the orientation of the limb arise. In summary, the interaction forces between the human and exoskeleton, including joint reaction forces, muscle-generated forces, and contact pressures, play a pivotal role in ensuring effective assistance and comfort. These forces must be carefully managed through advanced control strategies and ergonomic design to enhance user

performance while minimizing resistance and discomfort. The following subsection delves into current lower-limb exoskeleton technologies, examining their diverse properties, control mechanisms, and applications across various domains.

2.3.2 Overview of Lower-Limb Exoskeletons

Lower-limb exoskeletons are designed to assist in mobility and rehabilitation by providing mechanical support to the lower limbs, particularly during gait, standing, and weight-bearing activities. These devices target individuals with conditions such as spinal cord injuries, stroke, and other neuromuscular impairments, helping to restore or enhance walking capabilities. Lower-limb exoskeletons operate by complementing natural human movement, offering dynamic assistance during key phases of gait such as the stance and swing phases, and are increasingly used in clinical rehabilitation, assistive mobility, and industrial applications. Over the last decade, advancements in actuation mechanisms, control strategies, and materials have led to a variety of exoskeleton designs aimed at improving joint kinematics, reducing muscle effort, and promoting long-term rehabilitation. This section reviews the extensive research on lower-limb exoskeletons, analyzing their biomechanical benefits, the control strategies they employ, and their impact on gait and joint dynamics.

With the main focus in rehabilitation and assistive mobility devices, 18 exoskeletons are presented, highlighting their function, applications and mechanical makeup, as well as their contributions in clinical and assistive circumstances. Table 2.2 provides a comprehensive visual comparison on their attributes and main biomechanical outcomes for each exoskeleton are reported. The following list details further their main features:

- **EksoNR**, developed by Ekso Bionics [89], is a lower-limb exoskeleton designed to provide powered assistance to the hip and knee joints for gait rehabilitation. It is actuated by electric motors that control flexion and extension at both joints, utilizing a combination of IMUs, force sensors, and encoders for real-time tracking and feedback during walking. The control system offers three modes: FirstStep, ProStep, and ProStep Plus, which allow varied levels of user-initiated control through torso tilt and weight shifting. In clinical trials, EksoNR demonstrated substantial improvements in gait function among stroke patients, particularly in metrics like the Timed Up and Go (TUG) test, with reductions in time from 48.79 to 38.47 seconds, and significant increases in walking time and steps [94].

Table 2.2: Comparison of Exoskeletons based on function[1], actuated joints[2], actuation method[3], sensors[4], control method[5], experimental task[6], and resulting reduction metrics.

Exoskeleton	Function						Actuated Joints				Actuation Method			Sensors					Control Method			Task				Notable Outcomes
	RH	AM	PM	SE	SF	PA	H	K	A	P	EM	PAc	HA	IMU	FS	EN	EMG	EEG	TB	BS	SS	OW	WB	S-S	TW	
EksoNR																										increase in average walking time (16.55 to 29.57 minutes)
ReWalk																										reduced step length and walking speed
Indego																										increased distance (+15.5 m) and walking speed (from 0.31 m/s to 0.37 m/s)
HAL																										increased walking speed (+61.5%) and distance (+49%)
LOPES-II[7]							2	1		2[7]																high correlation to natural gait (0.84 - 1.0) in severely impaired patients
ExoMotus X2																										volitional adjustment of step length for impaired users
X1																										decoding EEG and EMG signals from walking
TWIN																										natural gait control for SCI patients
Walk Assist																										improvement on hip flexion angles in stroke patients
REX[9]							2	1	2																	higher GRFs indicated higher balance and stability
Atalante[9]							3	1	2																	walking without external aids at an average speed of 0.13 m/s
Phoenix								.																		slower speeds (0.11 m/s) but much lower weight than other exoskeletons
XoMotion Beta 2[9]							3	1	2																	successful adaptation to various ground surfaces and users
Keeogo																										improvement in walking ability and distance (+27.9 m)
HAL-5																										efficient walking in severely impaired patients and reduced muscle activity
BLEEX							2	1	1																	able to transfer human, exoskeleton and payload weights to the ground
Soft Exosuit																										average reduction in metabolic cost of 22.8%
MO/GO Pants																										designed for hiking, provides up to 40% assistance in knee flexion
Forge by Roam																										designed for improving strength and endurance while minimising strain,

[1]*RH = Rehabilitation, AM = Assistive Mobility, PM = Personal Mobility, SE = Soft Exosuit, SF = Sports and Functional, PA = Power Augmentation*
[2]*H = Hip, K = Knee, A = Ankle, P = Pelvis*
[3]*EM = Electric Motor, PAc = Pneumatic Actuator, HA = Hydraulic Actuator* [4]*IMU = Inertial Measurement unit, FS = Force Sensor, EN = Encoder, EMG = Electromyography, EEG = Electroencephalography* [5]*TB = Trajectory-Based, BS = Bio-Signals, SS= Sensor-Signals* [6]*OW = Overground Walking, Weight Bearing, S-S = Sit-to-Stand, TW = Treadmill Walking*
[7]*Stationary Exoskeleton* [8]*Numbers denote DoFs actuated, when higher than 1* [9]*Self-balancing exoskeleton (no crutches needed*

- **ReWalk**, by ReWalk Robotics, is another notable lower-limb exoskeleton designed primarily for individuals with SCI. This device actuates the hip and knee joints using electric motors, relying on IMUs and foot force sensors to monitor the user's posture and foot placement. The control system is driven by torso inclination, allowing users to initiate walking by leaning forward, triggering motor-assisted steps. Clinical evaluations on overground walking with SCI patients revealed significant improvements in joint kinematics and gait parameters [95]. Despite reduced walking speed and shorter step lengths compared to able-bodied individuals, the system proved highly effective in enabling upright ambulation.
- **Indego**, developed by Parker Hannifin, is a modular exoskeleton that provides assistance to the hip and knee joints using **electric motors**. It uses IMUs and force sensors to monitor user posture and detect movement, adjusting support dynamically. The control system is centered on the user's centre of pressure (CoP) and can provide support during both stance and swing phases of gait. In experimental tests with stroke patients, Indego demonstrated significant improvements in walking speed and endurance, with participants increasing their walking speed from 0.31 to 0.37 m/s after 8 weeks of training [96].
- The **hybrid assistive exoskeleton (HAL)** exoskeleton, developed by Cyberdyne, is a powered lower-limb device designed to assist in hip and knee joint movements. It operates using electric motors that control flexion and extension, responding to voluntary muscle signals from the user. The system is driven by surface EMG sensors, which detect bioelectrical signals from the user's muscles, allowing HAL to provide neurologically controlled assistance. This enables HAL to amplify weak bioelectric signals, enhancing the user's movement during walking tasks. Gait initiation occurs when the EMG sensors detect muscle activation, signaling the exoskeleton to begin the walking motion. In clinical trials with SCI patients, HAL has been used in overground walking, treadmill-based gait training, and functional assessments, including the 10-meter walk test (10MWT), 6-minute walk test (6MWT), and the Timed Up and Go (TUG) test. Results from these studies reported significant improvements in walking speed (by 61.5%) and endurance (49% improvement in distance walked during the 6MWT). Additionally, users showed enhanced functional mobility, with reduced reliance on assistive devices [97].
- The **LOPES-II** exoskeleton, developed by the University of Twente, is a robotic gait trainer designed for neurorehabilitation. It features 8 actuated DoFs, providing assistance at the hip flexion/extension, hip abduction/adduction, and knee flexion/extension joints, along with pelvis motion in forward/backward and side-to-side directions. The exoskeleton is powered by electric motors and controlled using an admittance-based control system, which allows for real-time adjustment of resistance and support based on the user's input. The

system incorporates IMUs and force sensors to measure interaction forces and ensure a precise control of joint movements. The gait is initiated through the exoskeleton's responsive control system, which tracks the user's movements during treadmill-based walking sessions. In experimental trials with stroke survivors, LOPES-II was tested for tasks such as overground walking, pelvic perturbation training, and gait rehabilitation. Results showed significant improvements in gait patterns, including enhanced joint angle control and reduced interaction forces during the swing phase of walking, with high correlations to natural human gait. Additionally, the exoskeleton demonstrated a reduction in user dependency on external aids [98, 99].

- The **ExoMotus X2**, developed by ExoAtlet, is a lower-limb exoskeleton designed for rehabilitation of patients with SCI. It assists the hip and knee joints using powered actuation for flexion and extension. The exoskeleton is driven by electric motors, which provide targeted assistance to support the user's gait. The system uses a combination of surface EMG sensors to monitor muscle activity and force sensors to measure interaction forces during walking. The control is primarily based on a predefined trajectory, initiated through a button press on a handheld or crutch-mounted interface. In clinical trials, ExoMotus X2 was tested with both able-bodied participants and individuals with SCI, focusing on user volitional control over step length during gait tasks. The results demonstrated that users could adjust their step length voluntarily, even within the constraints of a predefined trajectory, showing the exoskeleton's ability to assist individuals with reduced or no voluntary muscle control. Furthermore, muscle activation was minimized, especially in able-bodied participants instructed to avoid leg muscle use, indicating the exoskeleton's efficacy in supporting lower-limb movement [100].
- The **X1 exoskeleton**, developed by NASA and the Florida Institute for Human and Machine Cognition, is a lower-limb exoskeleton designed for both space exploration and terrestrial rehabilitation. The exoskeleton features 4 powered DoFs at the hip and knee joints, assisting with flexion and extension movements. The actuation is provided by electric motors connected via a series elastic actuator (SEA) system, which enables precise control over joint movements. The X1 integrates a suite of sensors, including EMG and goniometers, allowing it to monitor muscle activity and joint angles. The control system is based on a combination of dynamic position trajectory generators and a passive mode that mimics natural joint movement. In experimental trials, the X1 was tested in rehabilitation scenarios with stroke survivors, focusing on tasks such as overground walking and treadmill-based gait training. Results demonstrated the device's ability to accurately track joint angles with a high correlation ($r \approx 0.9$) and successfully decode muscle activation patterns. The X1 showed

potential as a rehabilitation tool, aiding in lower-limb mobility and muscle reactivation through real-time biofeedback [101].

- The **TWIN**, a novel modular lower limb exoskeleton for personal use of SCI subjects. This system was designed according to a set of user requirements (lightweight and autonomous portability, quick and autonomous donning and setup, stability when standing/walking, cost effectiveness, long battery life, comfort, safety) which emerged during participatory investigations that organically involved patients, engineers, designers, physiatrists, and physical therapists from two major rehabilitation centers in Italy. As a result of this user-centered process, TWIN's design is based on a variety of small mechatronic modules which are meant to be easily assembled and donned on or off by the user in full autonomy [47].
- The **Honda Walking Assist Device (HWAD)**, developed by Honda Motor Co., is a lightweight exoskeleton designed to assist individuals with gait impairments, particularly those with neurological conditions such as stroke. The device provides powered assistance at the hip joint, aiding in flexion and extension during walking. Actuation is driven by electric motors, with integrated IMUs and pressure sensors that monitor walking patterns and adjust assistance dynamically. The control system uses a predefined trajectory based on the user's walking pattern, enabling real-time adjustments to assist with balance and coordination. Gait initiation is handled by the Stride Management Assist (SMA®) system, which detects the user's movement through the sensors and provides automatic assistance without manual intervention. In clinical trials, HWAD has shown positive effects in improving hip flexion angles and reducing asymmetry during gait in hemiplegic stroke patients. Although immediate gains in walking speed were minimal, users reported improved endurance and stability after repeated training sessions [102].
- The **REX exoskeleton**, developed by Rex Bionics, is a statically balanced, self-supporting lower-limb exoskeleton designed for individuals with severe mobility impairments, including those with SCI. Unlike most exoskeletons, REX is equipped with five actuated DoFs per leg, covering the hip, knee, and ankle joints. These joints are powered by brushed DC motors, enabling precise control of flexion, extension, and rotation. REX uses a combination of gyroscopes, accelerometers, and force sensors to maintain balance and support user movement without requiring external aids, such as crutches. The exoskeleton is controlled through a joystick interface that allows the user to navigate, walk, and perform transitions such as sitting and standing. Experimental trials conducted on a treadmill showed that REX achieves a statically balanced gait with high joint extensor moments and slower walking speeds compared to natural gait. This exoskeleton is particularly suitable for

individuals with severe mobility impairments, offering increased independence in everyday tasks like walking and turning [103].

- The **Atalante exoskeleton**, developed by Wandercraft, is a dynamically self-balancing lower-limb exoskeleton designed for patients with SCI and neurological conditions. Atalante features 12 actuated DoFs, providing powered assistance at the hip, knee, and ankle joints. Its electric motors enable a wide range of movements, including walking, standing, and turning, without the need for crutches. The exoskeleton uses a combination of force sensors, gyroscopes, and IMUs for real-time control and balance. The system is powered by an advanced Hybrid Zero Dynamics (HZD) control system, which ensures smooth, dynamic walking by controlling joint torques. In clinical trials with SCI patients, Atalante successfully enabled hands-free walking and transitions between movements. In the 10-meter walk test (10MWT), patients achieved an average walking speed of 0.13 m/s after 12 training sessions. The exoskeleton has demonstrated effectiveness in rehabilitation by improving walking function and enabling greater independence without external aids [8].
- The **Phoenix exoskeleton**, developed by SuitX, is a lightweight and modular device designed for individuals with SCI and other mobility impairments. It features electric motors that power the hip joints, while the knee joints operate with a semi-passive locking mechanism, reducing the need for additional actuators and keeping the system lightweight. The exoskeleton is controlled via a handheld interface, typically mounted on crutches, allowing users to initiate movements such as walking, standing, and sitting. The Phoenix employs force sensors and a basic feedback system to ensure the correct timing of joint movements during gait. In clinical trials, Phoenix demonstrated an average walking speed of 0.11 m/s and significant improvements in functional independence, including enhanced scores on the Functional Independence Measure (FIM). The exoskeleton's modular design and affordability make it an attractive option for personal and clinical use [104].
- The **XoMotion Beta 2** exoskeleton, developed by Human in Motion Robotics, is a next-generation lower-limb exoskeleton with 12 DoFs, powered by electric motors that assist movements at the hip, knee, and ankle joints. This exoskeleton is equipped with advanced sensors, including force sensors, IMUs, and encoders, to provide real-time feedback on joint positions, velocities, and ground reaction forces. XoMotion Beta 2 utilizes a model-predictive control (MPC) system paired with admittance control, allowing the device to adapt dynamically to different terrains and user movements. The system also employs Bayesian Optimization for adaptive control, enabling it to fine-tune its performance based on the user's gait and environmental variations. In experimental trials, XoMotion Beta 2 demonstrated effective adaptation to diverse surfaces such as soft, solid, and uneven terrains, significantly improving veloc-

ity tracking and stability. The exoskeleton's capability to quickly adjust to the user and environment underscores its potential for use in both rehabilitation and mobility enhancement applications [105].

- The **Keeogo** exoskeleton, developed by B-Temia, is a powered device designed to assist with knee flexion and extension, making it ideal for individuals with mobility impairments caused by conditions such as multiple sclerosis and osteoarthritis. Keeogo is powered by electric motors at the knee joints, and it uses an array of force sensors, motion sensors, and encoders to detect user movement and provide adaptive assistance. The control system adjusts the level of assistance dynamically based on the user's movement, without following a predefined trajectory. Gait initiation is user-driven, as Keeogo provides support during activities such as walking, stair climbing, sitting, and standing. In clinical trials with participants with multiple sclerosis, Keeogo showed significant improvements in endurance and unassisted walking ability. After two weeks of using Keeogo at home, participants demonstrated an average improvement of 27.9 meters in the 6-minute walk test (6MWT), highlighting the device's potential for rehabilitation and mobility enhancement [106].
- The **HAL-5** exoskeleton, developed by Cyberdyne, is a full-body, powered exoskeleton designed to assist with both lower and upper limb movements, targeting individuals with mobility impairments such as SCI or other neuromuscular disorders. HAL-5 uses electric motors to power the hip, knee, and ankle joints, providing support for walking and other physical activities. What sets HAL-5 apart is its integration of surface EMG sensors, which detect the user's muscle activity and translate these signals into movement. The exoskeleton's Cybernic Voluntary Control system allows it to amplify weak bioelectric signals, enabling the user to control the device based on their own muscle activations. Additionally, HAL-5 features an Autonomous Control mode that can assist the user even when voluntary control is limited or absent. In experimental tests with patients suffering from SCI, HAL-5 has demonstrated significant improvements in walking speed, endurance, and functional mobility, making it an effective tool for rehabilitation and mobility support [91].
- The **Berkeley Lower Extremity Exoskeleton (BLEEX)**, developed at the University of California, Berkeley, is one of the earliest powered exoskeletons designed for load-bearing and mobility assistance. BLEEX is equipped with seven DoFs per leg, with powered joints at the hip flexion/extension, hip abduction/adduction, knee flexion/extension, and ankle flexion/extension. The system uses hydraulic actuators, providing high power-to-weight ratio and enabling the user to carry heavy loads with minimal effort. BLEEX relies on a dynamic control system that allows the exoskeleton to move in harmony with the user, without the need for direct force sensors to measure human-

exoskeleton interaction. The system includes a suite of sensors, including force sensors, foot switches, and inclinometers, to monitor the user's movements and adjust the exoskeleton's support dynamically. In experimental tests, BLEEX was able to transfer the load of up to 75 kg from the user to the ground, significantly reducing the metabolic cost of walking while maintaining a natural gait. The device demonstrated robust performance in carrying heavy loads while walking and climbing stairs, with power consumption measured at approximately 1143 W during walking tasks [107].

- The **Soft Exosuit**, developed by the Wyss Institute at Harvard, is a flexible, textile-based exoskeleton designed to provide targeted assistance at the ankle joint for plantarflexion. Unlike rigid exoskeletons, the soft exosuit utilizes Bowden cables driven by electric motors located off-board, which apply forces through the soft fabric to assist joint movement. The system's lightweight structure ensures that the exosuit remains unobtrusive, allowing for a wide range of motion. The exosuit is equipped with load cells, gyroscopes, and motor encoders to monitor cable tension and foot movement, adjusting the assistance provided during each step in real time. The control strategy is force-based and adjusts assistance according to the user's gait cycle, providing support during the stance phase of walking. In clinical trials, the soft exosuit was shown to reduce metabolic cost by up to 22.83% in healthy users walking on a treadmill at 1.5 m/s, demonstrating its efficacy in reducing muscle strain during gait without restricting movement [108].
- The **Mo/Go exoskeleton**, developed by Skip Innovations, is designed for outdoor activities such as hiking, offering enhanced physical performance by providing assistance to the knee joints. Powered by compact electric motors, the Mo/Go exoskeleton provides support during knee flexion and extension, helping users tackle uphill climbs by boosting leg strength by up to 40%. The exoskeleton also reduces knee strain during downhill walking by absorbing impact forces. The system features a lightweight, modular design that integrates seamlessly with the user's movements. It is equipped with an intuitive control interface, allowing users to adjust the level of assistance with just three buttons—on/off, more assistance, and less assistance. The motors and battery pack are integrated into the pants, making the exoskeleton comfortable and flexible for prolonged use. In field tests, the Mo/Go exoskeleton has shown significant benefits in reducing muscle fatigue and improving endurance during extended hikes, with users reporting feeling up to 30 pounds lighter during uphill climbs [92].
- The **Forge exoskeleton**, developed by Roam Robotics, is a lightweight, pneumatically powered exoskeleton designed for military applications and emergency responders. Forge provides targeted assistance to the knee joints, enhancing physical endurance, speed, and strength while reducing the physical

strain on the wearer. The exoskeleton uses pneumatic actuators, powered by compressed air, to deliver torque to the knees, providing up to a 50% reduction in g-forces during high-impact activities like running or jumping. Equipped with an AI-guided control system, Forge dynamically adjusts the level of assistance based on real-time sensor data, ensuring the exoskeleton adapts to user movement and terrain. In field trials, Forge demonstrated its effectiveness in reducing muscle fatigue and increasing load-carrying capacity, allowing soldiers to move heavy objects with greater efficiency. Its lightweight design, combined with the flexibility of pneumatic actuation, makes Forge ideal for use in extreme conditions, offering enhanced mobility without compromising freedom of movement [109].

The collection of lower-limb exoskeletons reviewed here demonstrates significant technological advancements over the past decade. With the integration of cutting-edge sensor and actuation solutions, these devices have revolutionized mobility assistance, particularly for individuals with near-zero mobility, such as those with SCI. However, while these devices have proven to be life-changing for SCI patients, there is immense potential to extend their use to a broader spectrum of MSDs. By promoting technology transfer within the field, we can leverage these innovations to serve a wider population, adapting the existing technologies for various applications. It is crucial that, as the hardware and software modalities evolve, we do not overlook the biomechanical evaluation of human-exoskeleton interaction. To ensure optimal assistance and safety, a unified framework for control, assessment, and biomechanical evaluation is necessary, one that tracks and evaluates the entire development process from prototype to clinical or personal deployment. Such a framework will have the potential to enhance the effectiveness and applicability of these technologies across a range of physical conditions and environments.

2.3.3 The HeiAge Project

LLEs, through the combination of mechanical assistance, adaptive control, and real-time feedback, represent a pivotal technological advancement in improving quality of life for individuals with mobility impairments. As these technologies continue to evolve, their role in rehabilitation and daily assistance will expand, offering greater independence and improved physical outcomes. Although assistive technologies have made significant progress in addressing the needs of individuals with severe mobility impairments and highly frail older adults, there remains a pressing need for further development in technologies assisting less frail individuals. The growing demand to enhance these solutions highlights the importance of expanding their capabilities to serve a broader population, particularly individuals with varying levels of mobility challenges and musculoskeletal disorders.

Through a consortium established via various functions of Heidelberg University (Heidelberg, Germany) and under the umbrella of the HeiAge [110] project funded by the Carl Zeiss foundation, various sub-projects delved into the research and development of assistive systems and digital technologies for improving mobility in old age but also a wide spectrum of mobility impairments of various frailty levels. As shown in Figure 2.8, this ranges from more able older adults requiring some assistance in performing sports activities, to more frail older adults that are dependent on high levels of assistance in order to perform everyday tasks. The research undertaken by the HeiAge project ranges from basic understanding of biomechanics of everyday life, mathematical simulations of the contributions of external assistance, the development of new assistive technologies and psychological insights into the acceptance of these technologies. Finally, the project additionally deals with ethical, legal and social considerations in terms of the usability and development of these devices.

The project's work program is structured into three distinct methodological components:

1. **Fundamentals (A):** This section focuses on the foundational knowledge necessary for developing intelligent systems. It includes the creation of key algorithms required for advanced digital technologies.
2. **Application (B):** This part is dedicated to the development and evaluation of concrete digital technologies and assistive systems. These systems are specifically designed for various groups of older adults, and their effectiveness is rigorously tested in real-world scenarios.
3. **Overlapping Topics (Q):** This interdisciplinary section addresses the validation and societal acceptance of digital and robotic systems. It encompasses a broad spectrum of considerations, including psychological, ethical, legal, social, nursing, and political factors to ensure widespread adoption and public use.

Within the *Fundamentals*, sub-project **A1** focuses on understanding the movement abilities of older adults via conducting multiple biomechanical studies to analyze the coordination between different body segments during tasks such as walking and standing up from a chair. Part **A2** builds on the insights from A1, by developing as to enable users to interact effectively with digital technologies, including assistive robots and virtual reality systems. Sub-project **A3** explores how assistive devices can best be used to achieve desired goals as mobility not only involves motor functions but also decision-making and planning. While young individuals perform this automatically, for older adults, it requires active effort.

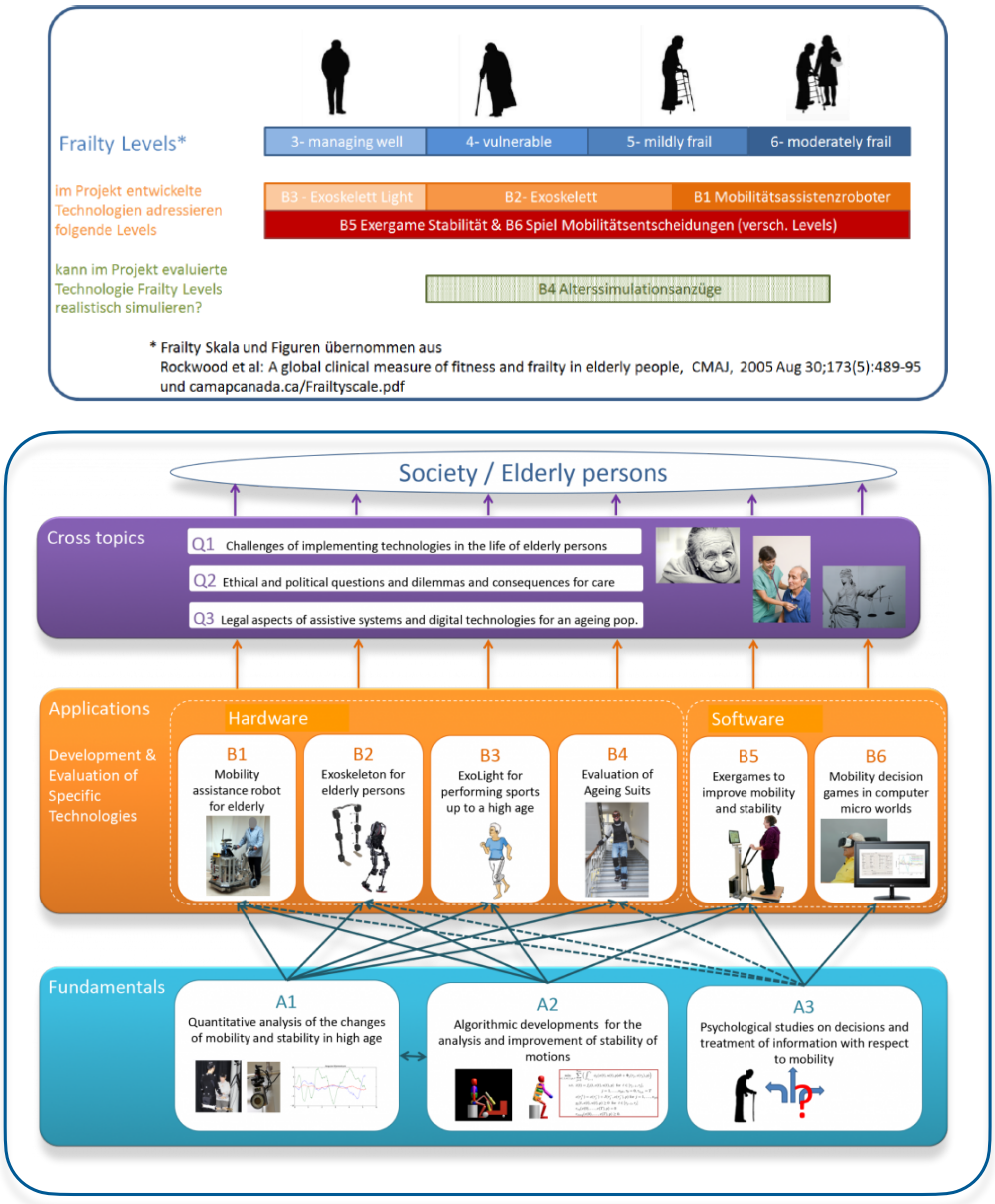

Figure 2.8: Project HeiAge of Heidelberg University. **(Top)** The frailty scale and respective sub-projects developing technologies that target these groups. Scale and figure taken from Rockwood et al. [44]. **(Bottom)** The dissemination of sub-projects and inter-collaborations between them. Figure taken from [110].

In the *Applications* section, **B1** aims to develop a mobility robot—a robot rollator—for older adults. This device will consist of a rolling platform with a structure that users can hold onto for support. Sub-project **B2** acquires an existing exoskeleton with the aim of exploring fine-tuning methods to enhance the user's strength and stability, helping prevent falls and meet the needs of older adults. Part **B3** sets on to create a light exosuit, allowing active older adults (Frailty Level 3) to continue engaging in sports. In part **B4** the impact of age-simulation suits is investigated, with regards to movement and perceptions of aging. While interest in these suits is growing, more research is needed to understand their limitations and potential. Sub-project

B5 focuses on developing exergames to improve cognitive and functional abilities in older adults, aiding in the maintenance or enhancement of mobility. Lastly, **B6** assesses individual diagnoses and the effects of training, where measurement devices that track decision-making in mobility contexts are needed. Virtual environments will be used to evaluate user decisions effectively.

Finally, within *Overlapping Topics*, **Q1** emphasizes feasibility and testing of mobility-supporting technologies like smart rollators and exoskeletons. By using a user-centered design (UCD) approach, potential end-users directly influence the development, increasing acceptance and applicability. In **Q2** the ethical implications of introducing technology that makes decisions for users are explored, addressing the moral considerations. Part **Q3** delves into the legal perspective, and deals with two key issues: (1) identifying what data is needed from users and how it can be obtained, and (2) determining legal responsibility in the event of an accident involving autonomous assistive systems.

Sub-Project B2: Lower-Limb Exoskeleton

The research presented in this thesis aligns with the objectives of sub-project B2, focusing on the human-exoskeleton interactions of a lower limb device. It investigates biomechanical evaluation procedures to assess the effects of LLEs and implements various methodologies aimed at improving the interaction and usability of exoskeletons. These enhancements are designed to accommodate a broader range of frailty levels, ensuring that the technology serves a wider population effectively. To this end, the TWIN exoskeleton was acquired by the INAIL group [111] of the Italian Institute of Technology (IIT) and this section introduces its main features and functionalities.

The TWIN exoskeleton [47] is a modular lower-limb device designed to enhance mobility and autonomy for individuals with SCI. Its structure features nine small mechatronic modules, including actuators for the hip and knee, structural links, and adjustable braces, all made from lightweight Al7075 T6 aluminum alloy. The device's modular design allows users to assemble and disassemble it autonomously, facilitated by a lateral quick-release system that prioritizes ease of donning and transportability. The exoskeleton is powered by Maxon EC90 brushless motors with Harmonic Drive gearboxes at the hip and knee, providing stable and controlled motion for users weighing up to 110 kg. The TWIN can reach walking speeds up to 1.4 km/h, it weighs 25 kg and can accommodate users between 155 and 190 cm height.

The TWIN uses a position control system based on IMU triggers, which detect torso inclination to initiate each step. Users can customize gait parameters such as step length, height, and speed through a mobile-based graphical user interface (GUI). Notably, the exoskeleton's interchangeable thigh and shank braces, along with

passive elastic ankle joints, ensure a tailored fit and support natural foot movements. With a battery life of up to three hours, the device can sustain 1-2 continuous walking sessions. Early trials demonstrated the TWIN's high usability, offering SCI patients a promising solution for improving their mobility and independence.

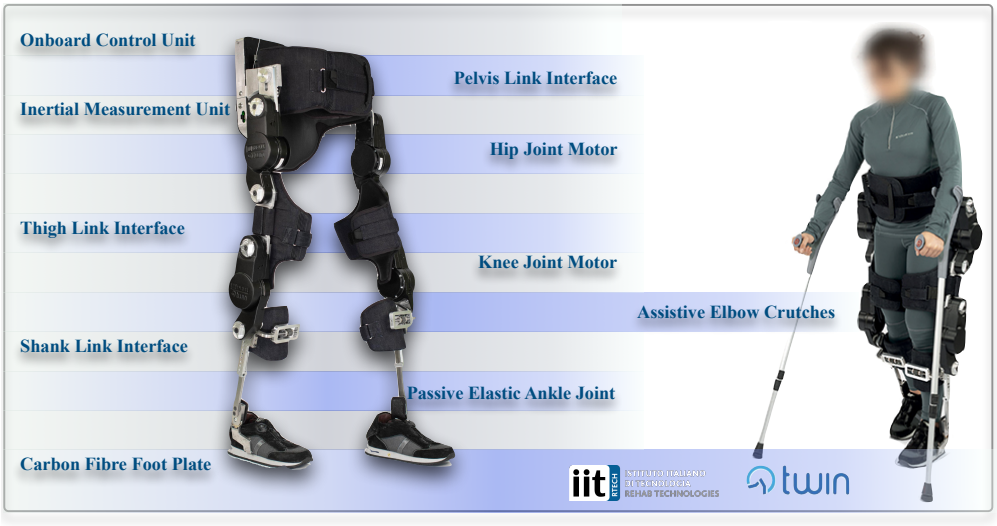

Figure 2.9: The TWIN Exoskeleton by INAIL group at IIT. **(Left)** The exoskeleton with labels of its various parts. **(Right)** A person using the exoskeleton with the assistive crutches.

This thesis investigates the optimization of human-exoskeleton interactions within the domain of rehabilitation and assistive mobility exoskeletons. While the initial aim was to adapt a lower-limb exoskeleton (LLE) to meet the needs of elderly users, the Covid-19 pandemic restricted early recruitment of elderly participants for biomechanical testing, prompting a shift in project focus. The research pivoted toward exploring user familiarization with exoskeletons through biomechanical evaluation, with the objective of establishing standardized practices for assessing exoskeleton effectiveness, facilitating technology transfer, and designing tailored training protocols for frail populations without requiring direct testing. To enable this, a modular sensory system was developed and validated for biomechanical assessments beyond laboratory settings, which was then deployed in a large-scale outdoor study. Building on these findings, a more intuitive control framework for LLEs was proposed using minimal, low-cost components. Chapters 7, 8, and 9 outline the methodologies for evaluating LLE biomechanics, advancing human-exoskeleton interfaces, and summarizing the key outcomes and conclusions of the HeiAge project.

Biomechanical Evaluation, Modeling and Optimal Control

3

Motion analysis and biomechanical evaluation technologies play a crucial role in understanding human movement; from game design and film production to clinical applications and monitoring physical progress or deterioration, these systems offer valuable insights into how the body moves [112]. They also have wide-spread applications in sports and performance enhancement, helping athletes optimize their movements and reduce injury risks. The field of robotics also benefits from motion analysis and modeling by recreating natural movement patterns and applying them to devices such as robotic snakes, birds, humanoid robots, and more. In the field of assistive technologies, such as exoskeletons, these tools allow for precise assessment of their biomechanical impact, translating complex movements into quantifiable metrics.

This chapter explores the most prominent biomechanical evaluation methodologies and technologies, providing insight into their purpose and applications in relation to exoskeletons and assistive devices. Section 3.1 outlines key commercial products and demonstrates how they are used to gather critical biomechanical data. In Section 3.2, the focus shifts to how the collected data can be used to identify important movement principles and parameters through modeling, while Section 3.3 describes how the outcomes modeling and optimal control can be used to inform the design and control of wearable devices via simulation.

3.1 Motion Capture Techniques

These technologies rely on a combination of sensors and motion capture systems to collect data on joint kinematics, muscle activation, and external forces. By translating complex human motion into quantifiable metrics, these tools allow researchers to evaluate the biomechanical impact of assistive technologies on the body. This section delves into the various motion capture techniques used to gather and analyze human movement and vitals, offering insights into how biomechanical data is harnessed to assess the functional outcomes of assistive devices.

3.1.1 Camera-Based Capture Systems

Camera-based capture systems have been a cornerstone of motion analysis for several decades, offering precise kinematic data for gait analysis and other biomechanical

evaluations. These systems can be broadly categorized into marker-based and marker-less approaches, both of which play a crucial role in understanding human movement patterns [113].

Marker-based systems involve the use of reflective markers placed on key anatomical landmarks, the 3D trajectories of which are tracked by multiple cameras to calculate joint angles, velocities, and other movement metrics. Some widely used examples are the Vicon system [114] from Vicon Motion Systems [114] (Oxford, United Kingdom) and Qualisys system [115] by Qualisys AB (Gothenburg, Sweden). These marker-based camera systems high precision and set the gold standard for clinical and sports biomechanics motion capture and gait analysis. While based on the same principle of tracking markers, two different types of systems exist, due to marker functionality: active and passive.

- **Passive marker-based systems:** Markers are coated in infrared light reflecting material, while multiple infrared cameras encircling the capture volume emit infrared light that bounces off the markers on the subject. Each camera captures the reflected light and records the 2D position of the markers, which is later translated into the 3D global coordinate via the camera system's software, based on the multiple camera angles the marker has been captured from, at each timeframe.
- **Active marker-based systems:** The markers are usually equipped with LEDs, like the OptoTrak marker system [116] by Northern Digital Inc. (Waterloo, Ontario, Canada), generating their own unique signal which is then recorded by a collection of cameras around the capture volume. Since the markers emit their own light, this can reduce interference problems which are more common in passive markers. The processing of the marker positions thereafter follows a similar principle to the passive markers.

In contrast to marker-based systems, **marker-less systems** rely on advanced algorithms such as human pose estimation technologies, often supported by machine learning, to detect and track human movement without the need for physical markers. These systems, such as the Theia3d [117] by Theia Markerless, Inc (Kingston, Ontario, Canada), or open-source project OpenPose [118] by the Carnegie Mellon Perceptual Computing Lab (Pittsburgh, Pennsylvania, USA) that can work with standard cameras, are growing in popularity due to their ease of setup and application in less controlled environments, although they may sacrifice some accuracy compared to marker-based alternatives [119].

Marker-less motion capture systems operate by using standard cameras or depth-sensing devices to capture images or videos of a subject in motion. Instead of relying on physical markers, these systems employ advanced computer vision algorithms, often powered by machine learning, to recognize and detect key body landmarks,

such as joints and limbs, directly from the visual data. The system then extracts 2D or 3D key points based on the images, enabling accurate tracking of body movement. For 3D motion capture, depth-sensing cameras or multiple angles are used to estimate the depth of the subject. Once key points are identified, they are connected to form a skeletal structure that allows for detailed analysis of movements, including joint angles and gait. This technology enables real-time motion analysis without the need for wearable equipment, making it more practical for diverse environments and applications.

Both types of systems offer valuable insights into gait kinematics, joint mechanics, and overall movement patterns, making them essential tools in fields ranging from rehabilitation to robotics. While offering higher accuracy, marker-based capture systems are bound within laboratory settings, consisting of expensive equipment, ranging from $50,000 to $100,000 and require a pre-calibrated capture volume where the subjects can move within. Marker-less capture systems provide more freedom to the users as they can easily be placed outside and require less equipment and set-up time than traditional marker-based camera systems, though they also are bound to the capture volume the cameras can record. Therefore, for activities requiring a larger setup, like running or testing exoskeletons over uninterrupted long distances, both of these systems pose limitations.

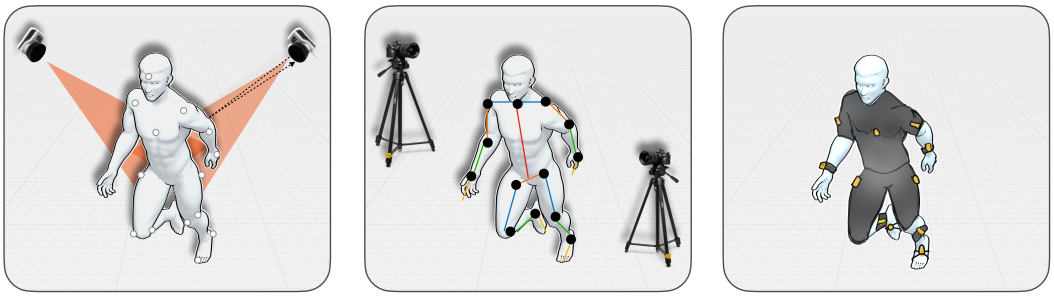

Figure 3.1: Current technologies in motion analysis. **Left:** Gold standard marker-based camera system with infrared light reflective markers tracking 3D trajectories of markers. **Middle:** Markerless motion capture with standard camera equipment and algorithmic construction of skeletal system. **Right:** IMU-based sensorised suit for motion analysis by tracking limb orientations and accelerations.

3.1.2 Inertial Measurement Units

Inertial Measurement Units (IMUs) are compact devices that consist of multiple sensors, typically including an accelerometer, a gyroscope and a magnetometer. These sensors work together to measure the orientation, velocity, and acceleration of a body segment in real time, providing comprehensive motion data. The accelerometer tracks linear acceleration, while the gyroscope measures angular velocity, and the magnetometer can help with orientation relative to the Earth's magnetic field.

IMUs are widely used in wearable motion capture suits, where multiple units are placed on various body segments to track the movement of the entire body. These suits are capable of recording data in real-world environments without the need for external cameras or tracking systems, making them highly versatile. The collected data is processed using algorithms that convert raw sensor signals into joint angles and body positions, allowing for a detailed analysis of human motion. They are not bound to a specific capture volume like camera-based systems, though they are only limited by the maximum distance the receiver and sensor units (peripherals and central) allow.

In biomechanical applications, IMU-based suits are commonly used in gait analysis, sports performance monitoring, and rehabilitation, offering a portable and non-invasive alternative to traditional camera-based systems [120]. Much like marker-based systems however, the calibration of an IMU suit is a critical step to ensure accurate motion tracking. This process typically involves aligning the sensors with a reference coordinate system by having the subject stand in a known pose, such as a T-pose, and performing specific movements to calibrate sensor orientation. For systems that include magnetometers, additional calibration is required to correct for local magnetic interference. The calibration ensures that joint angles and body segment movements are tracked correctly during use, but even with proper calibration, IMU systems face several limitations.

A primary challenge is sensor drift, where small errors in accelerometer and gyroscope data accumulate over time, causing inaccuracies in position and orientation estimates. Without external reference points, this drift can degrade motion tracking, especially during long-duration use. Additionally, IMUs that rely on magnetometers can be affected by magnetic interference in the environment, further reducing accuracy. While these issues can be managed with periodic re-calibration and noise filtering, they underscore the need for careful handling of IMU systems in complex environments. A prominent advantage of IMUs as opposed to other systems is the sensor integration in the control architecture of wearable robotics, by gathering feedback on the state of the human and the device.

3.1.3 Force Plate Technologies

In addition to camera-based and inertial measurement systems, force plates play a crucial role in biomechanical analysis and dynamics modeling by capturing the GRFs exerted by the body during movement. These devices are commonly used in combination with other motion capture systems to provide comprehensive insights into a subject's biomechanics. Devices such as the Kistler force plates [121] by Kistler Instrumente AG (Winterthur, Switzerland), measure forces in multiple directions (vertical, horizontal, and lateral), as well as moments and calculate the CoP. These

measurements are essential for tasks such as gait analysis, balance assessment, and the evaluation of joint loading during dynamic movements.

Force plates are typically integrated into the floor or embedded in a walkway, allowing subjects to perform activities such as walking or jumping over the plates. By combining the GRFs data with joint kinematics captured from systems like Vicon or Qualisys, we can better understand how forces are distributed throughout the body and joints during movement. The data also aids in evaluating the effectiveness of assistive devices such as exoskeletons and prosthetics, as it helps determine how external assistance alters the forces acting on the body. These type of insoles can also be included in an exoskeleton's controle environment as foot switches, by informing the robot of feet and ground contacts in order to apply a sequence of successive steps and identidy certain gait phases through the gait cycle [122, 123].

The major limitation of force plates is that their measurements are restricted to the area of the plate, requiring careful positioning or multiple plates for continuous motion analysis. Though mobile solutions exist, the recording area per plate is still limited, and both of these devices can pose high costs. Despite this, they remain a gold standard in biomechanics research due to their precision and ability to measure forces that directly impact joint health and overall movement quality.

3.1.4 Sensorised Insoles

Sensorised insoles, equipped with either pressure or force sensors, offer a mobile and cost-effective alternative to capturing ground dynamics during movement, though they tend to be less accurate compared to gold-standard force plate technologies. These insoles are particularly useful in situations where portability and ease of use are prioritized, such as field-based studies or long-duration gait assessments outside of lab environments. They allow for continuous monitoring of pressure distribution and forces exerted on the foot during activities like walking, running and sit-to-stand.

One example is the Moticon insole by Moticon ReGo AG (Munich, Germany), which features wireless pressure sensors embedded within a slim, flexible design. The Moticon insole [124] provides real-time data on pressure distribution across the foot, enabling researchers to track gait patterns and detect asymmetries in ground contact. It has applications in sports performance analysis, injury prevention, and rehabilitation, offering an unobtrusive way to monitor the user's movement over time. Similarly, Novel insoles [125] by Novel GmbH (Munich, Germany) incorporate multiple pressure sensors to capture detailed data on foot mechanics, often used in clinical and research settings to assess gait, balance, and footwear performance.

Although sensorised insoles may not provide the same level of precision as force plates, their ability to collect data in real-world conditions and over extended periods makes them highly valuable in research on gait dynamics, sports performance, and rehabilitation. They allow for natural movement outside the constraints of a lab environment, offering insights that are often difficult to capture using stationary systems.

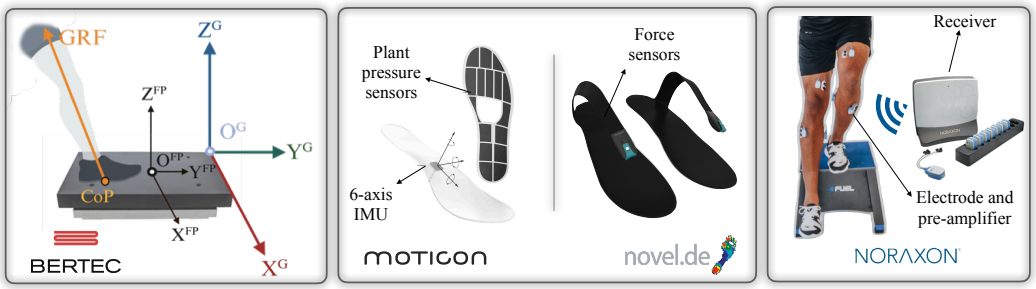

Figure 3.2: Commercial products in kinematic data collection. **Left:** Gold standard force plate system by Bertec Corporation (Columbus, Ohio, USA) [126], with illustration of global and force plate reference systems, CoP of foot in contact with the plate and force vector generated. **Middle:** Plantar pressure-sensing insoles from Moticon with IMU integration and force-sensing insoles from Novel. **Right:** EMG sensors consisting of electrodes and pre-amplifies along with the receiver unit from Noraxon.

3.1.5 Electromyography

Electromyography (EMG) is a technique used to measure the electrical activity produced by muscles during contraction. It works by detecting the small electrical signals generated when muscle fibers contract, providing valuable insight into muscle activation patterns. These signals are captured using electrodes that can either be placed on the surface of the skin (non-invasive) such as the system by Noraxon USA Inc. [127] (Scottsdale, Arizona, USA), or inserted directly into the muscle tissue (invasive) [128]. Surface EMG is the most commonly used in biomechanics and rehabilitation, as it involves placing electrodes on the skin above the muscle of interest.

To interpret EMG signals meaningfully, maximum voluntary contraction (MVC) trials are typically performed, where the person is asked to contract the specific muscle as forcefully as possible, generating a baseline reference. The EMG signals recorded during subsequent tasks can then be normalized against this maximum value, allowing for comparisons between different muscle activation levels. This standardization gives context to the voltage signals obtained from EMG, making it easier to assess the intensity of muscle activation during various activities.

In the field of exoskeleton research, EMG is often used to assess the impact of assistive devices, especially in back-support exoskeletons used during lifting tasks. By

comparing muscle activity with and without the exoskeleton, researchers can quantify how much the device reduces the strain on key muscles like the erector spinae. Lower EMG values in assisted tasks suggest that the exoskeleton is successfully offloading muscle work, reducing fatigue and the risk of injury.

Beyond evaluation, EMG can also play a crucial part as a control mechanism, especially in LLEs. By capturing muscle activity in real-time, EMG sensors can provide feedback to the exoskeleton, allowing it to proportionally adjust the level of support based on the user's effort. This approach, known as myoelectric control, enables more intuitive interaction between the user and the exoskeleton, enhancing the effectiveness of the assistance provided and increasing the transparency during activities such as walking or standing up. However, surface EMG requires proper skin preparation, such as shaving and cleaning, to ensure signal accuracy. It is also sensitive to perspiration, which can degrade signal quality, making it less reliable during prolonged or intense activities.

Whether collecting data for analyzing kinematics and dynamics of movement, evaluating assistance levels and reductions in specific metrics due to the assistance of exoskeletons, navigating the design and informing the control of wearable devices, or simply monitoring movement, biomechanical evaluation is a crucial part of optimizing human-exoskeleton interaction. By integrating technologies like motion capture systems, force plates, sensorized insoles, and electromyography, researchers can gain deep insights into how these devices impact muscle activity, joint loading, and overall movement efficiency, guiding the development of more effective and user-friendly assistive technologies. Part III presents a closer insight in how this thesis work investigates the optimization of human-exoskelton interactions via utilizing biomechanical evaluation and developing versatile technologies able to assess motion feedback and interpret user intentions.

3.2 Modeling and Simulation

Modeling and simulating human movement, particularly in conjunction with exoskeletons, is essential for understanding and optimizing human-exoskeleton interaction. By representing the human body and exoskeleton as a multibody system, we can simulate movements, forces, and interactions that provide critical insights into the mechanics of both the human body and assistive devices. This section will outline the mechanics of multibody systems, and explain the fundamental concepts of forward and inverse kinematics (IK) and dynamics, both of which are vital to biomechanical modeling. Lastly, optimal control problem formulations are explained as means of reconstructing motion based on collected kinematic and dynamic data, as well as motion optimization for the minimzation of biomechanical parameters and the generation of support from exoskeletons.

3.2.1 Defining a Model

A biomechanical model of the human body, particularly when integrated with an exoskeleton, is typically represented as a multibody system (Subsection 2.3.1). This system consists of a series of rigid body segments that are interconnected by joints, with each segment representing an anatomical part of the body (e.g., thigh, shank, foot) or a component of the exoskeleton. Defining the model accurately is essential for capturing the mechanics of the system, including joint movements, segment interactions, and external forces.

The first step in defining a model is identifying the segments of the body or exoskeleton. Each segment is characterized by properties such as mass, centre of mass (CoM), and moment of inertia, which describe how the segment will behave under dynamic conditions. The inertia of each segment quantifies its resistance to changes in motion and is critical when calculating joint torques or forces during movement. A kinematic joint tree is then established, and each joint is assigned an individual reference system, defining the connections between segments and governing how they move relative to one another. Common joint types include revolute joints (which allow rotation, such as the knee or elbow) and prismatic joints (which allow linear motion). Each joint is assigned DoFs, which determine the number of independent ways the joint can move. For example, a revolute joint has one degree of rotation, while a ball-and-socket joint, like the hip, has three rotational DoFs. The total number of DoFs in a model reflects the complexity and range of motion of the system. A higher number of DoFs allows for more detailed and accurate simulations of complex movements but increases the computational complexity of the model. Depending on the level of detail, purpose and application of the modeling or simulation task, simplifications and assumptions can be made as to decrease the computational expense of the model. For example, when dealing with locomotion only in the sagittal plane, hip joints can be approximated to a one DoF joints that allow for flexion and extensions, or when analyzing symmetrical movements, the model can be split in half. Figure 3.3 shows a possible division of segments of a generic model of a human [129] and assignment of joints, as well as the joint tree resulting from this model.

In order to build an actual representation of the kinematic and dynamic properties of each segment and joint, several pipelines exist in generic or subject-specific modeling. A simplified and popular way is specifying mass and inertial properties, as well as segment lengths and using this information to scale a generic model to the subject either by measuring segment lengths and height, or using marker locations when collecting data with marker-based motion capture techniques [130]. The joint centre locations are determined in a similar fashion and their DoFs can be adjusted depending on the application of the modeling task. The pelvis is considered as a

floating base of six DoFs, being the origin of the body and relating to the global reference system, subject to kinematic and dynamic constraints.

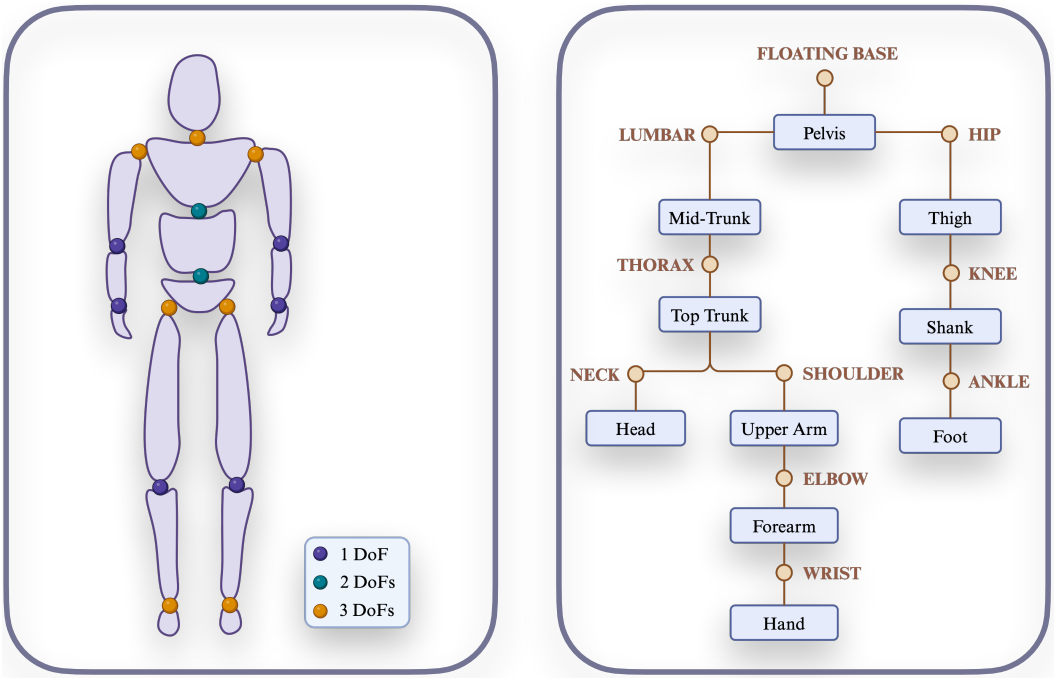

Figure 3.3: A typical definition of a human model. **Left:** Representation of a simple segment division of human limbs with their corresponding joints represented by coloured spheres: blue corresponds to 1 DoF at the elbows, wrists and knees, green to 2 DoFs for the thorax and lumbar spine joints, and orange to 3 DoFs for the neck, shoulders, hips and ankles. **Right:** Kinematic joint tree starting from the root segment pelvis which is considered as the floating based of 6 DoFs. Rectangular boxes denote the segments while circles name the joints connecting them together.

3.2.2 Kinematics and Dynamics

This section presents a general description of multibody systems, focusing on the kinematic and dynamic equations that govern their motion, along with an introduction to contact modeling.

Multibody Systems

A multibody system is a collection of rigid bodies connected by joints, forming an interconnected structure. The motion of these bodies is described by kinematic and dynamic equations that govern their behavior based on their configuration, velocities, and accelerations. The system's state is typically described by the position, velocity, and acceleration vectors $\mathbf{q}$, $\dot{\mathbf{q}}$, and $\ddot{\mathbf{q}}$, that can be assigned to each segment.

Kinematics

Kinematics deals with the motion of a system without reference to the forces that cause it. In particular, there are two problems to address: forward kinematics and IK.

Forward Kinematics: This problem involves calculating the position, velocity, and acceleration of the system based on known joint angles $\mathbf{q}$, velocities $\dot{\mathbf{q}}$, and accelerations $\ddot{\mathbf{q}}$,

$$\mathbf{x} = f(\mathbf{q}), \tag{3.1}$$

$$\dot{\mathbf{x}} = G(\mathbf{q})\dot{\mathbf{q}}, \tag{3.2}$$

$$\ddot{\mathbf{x}} = G(\mathbf{q})\ddot{\mathbf{q}} + \dot{G}(\mathbf{q}, \dot{\mathbf{q}})\dot{\mathbf{q}} \tag{3.3}$$

where $\mathbf{x}$ is the position of the end-effector, $G(\mathbf{q})$ is the Jacobian matrix, which relates joint velocities to end-effector velocities, and $\dot{G}(\mathbf{q}, \dot{\mathbf{q}})$ is the time derivative of the Jacobian matrix, which accounts for changes in joint velocities and positions over time.

Inverse Kinematics: IK involves determining the joint coordinates $\mathbf{q}$, velocities $\dot{\mathbf{q}}$, and accelerations $\ddot{\mathbf{q}}$ that produce a given end-effector position $\mathbf{x}$, velocity $\dot{\mathbf{x}}$, and acceleration $\ddot{\mathbf{x}}$,

$$\mathbf{q} = f^{-1}(\mathbf{x}), \tag{3.4}$$

$$\dot{\mathbf{q}} = G^{-1}(\mathbf{q})\dot{\mathbf{x}}, \tag{3.5}$$

$$\ddot{\mathbf{q}} = G^{-1}(\mathbf{q})\left(\ddot{\mathbf{x}} - \dot{G}(\mathbf{q}, \dot{\mathbf{q}})\dot{\mathbf{q}}\right) \tag{3.6}$$

where $\mathbf{q}$ is the vector of joint angles, $\dot{\mathbf{q}}$ is the vector of joint velocities, and $\ddot{\mathbf{q}}$ is the vector of joint accelerations.

Note that solving the IK problem often requires numerical methods, particularly if the Jacobian matrix $G(\mathbf{q})$ is non-invertible (i.e., singular) or if there are multiple solutions to the IK problem.

Dynamics

Dynamics involves the relationship between motion and the forces causing it. As with kinematics, there are two main problems: forward dynamics and inverse dynamics.

Forward Dynamics: Forward dynamics calculates the system's accelerations $\ddot{\mathbf{q}}$ based on known forces τ. The general equation of motion for a multibody system can be written as:

$$\tau = \mathbf{H}(\mathbf{q})\ddot{\mathbf{q}} + \mathbf{C}(\mathbf{q}\dot{\mathbf{q}}), \tag{3.7}$$

where $\mathbf{H}(\mathbf{q})$ is the system's inertia matrix and $\mathbf{C}(\mathbf{q}, \dot{\mathbf{q}})$ includes the Coriolis, centrifugal, and gravitational forces. Solving this equation for $\ddot{\mathbf{q}}$ involves inverting the inertia matrix $\mathbf{H}$, which can be computationally expensive depending on the system size.

Inverse Dynamics: In inverse dynamics, the forces τ required to achieve a known acceleration $\ddot{\mathbf{q}}$ are computed. For example, the inverse dynamics problem for a closed-loop system is expressed as:

$$\tau = \mathbf{H}\ddot{\mathbf{q}} + \mathbf{C} - \mathbf{K}^T\lambda \tag{3.8}$$

where λ represents the constraint forces due to closed-loop kinematic constraints.

Contact Modeling

Contact modeling describes how forces and constraints affect the motion of a system when bodies come into contact. Featherstone's approach distinguishes between rigid and compliant contact models, with compliant contact being easier to implement but introducing high-frequency dynamics. Contact modeling includes three key aspects: forces, constraints, and impacts. In this part we investigate the first two functions.

Forces: In a compliant contact model, the contact force f_c between two surfaces, for example a foot on the ground, is modeled as a function of position and velocity, and the generalised equation of motion accommodates the external forces, such that

$$\tau + \tau_c = \mathbf{H}(\mathbf{q})\ddot{\mathbf{q}} + \mathbf{C}(\mathbf{q}, \dot{\mathbf{q}}) \tag{3.9}$$

where τ_c represents the distribution of the contact forces and can be written as

$$\tau_c = \mathbf{G}(\mathbf{q})_c^T\lambda \tag{3.10}$$

where $\mathbf{G}_c$ is the Jacobian matrix associated with the contact constraints andλ is the vector of Lagrange multipliers representing the contact forces.

Constraints: When bodies are in contact, geometric constraints must be respected. For rigid bodies, constraints can be described using complementarity conditions, ensuring that bodies do not interpenetrate.

Contact forces, τ_c, are integrated into the overall system dynamics, ensuring that the constraints imposed by contact are respected. The Lagrange multipliers λ can be solved using constraint equations that respect physical boundaries,

$$\mathbf{G}(\mathbf{q})_c\ddot{\mathbf{q}} + \dot{\mathbf{G}(\mathbf{q})}_c\dot{\mathbf{q}} = 0, \tag{3.11}$$

which ensures that the acceleration at the contact points remains zero, maintaining the constraint throughout the motion. By adding a non-slipping contact constraint

to Equation 3.9, the generalised system dynamics equation satisfying non-slipping constraints can be constructed,

$$\begin{bmatrix} \mathbf{H}(\mathbf{q}) & \mathbf{G}(\mathbf{q})^T \\ \mathbf{G}(\mathbf{q}) & 0 \end{bmatrix} \begin{bmatrix} \ddot{\mathbf{q}} \\ -\lambda \end{bmatrix} = \begin{bmatrix} \tau - \mathbf{C}(\mathbf{q}, \dot{\mathbf{q}}) \\ -\gamma(\mathbf{q}, \dot{\mathbf{q}}) \end{bmatrix} \tag{3.12}$$

where,

$$\gamma(\mathbf{q}, \dot{\mathbf{q}}) = \mathbf{G}(\mathbf{q})_c \ddot{\mathbf{q}} + \dot{\mathbf{G}(\mathbf{q})}_c \dot{\mathbf{q}}. \tag{3.13}$$

The principles of forward and IK, along with the dynamic equations governing multibody systems, form the foundational tools for understanding the motion and behavior of complex mechanical systems such as exoskeletons and robotic systems. By determining the relationships between joint angles, velocities, accelerations, and forces, these kinematic and dynamic models provide crucial insights into the system's performance and potential for control.

In the next section, these principles are extended to the formulation of optimal control problems, focusing on motion reconstruction and motion optimization. These techniques allow for precise prediction of system behavior, while also providing solutions that maximize performance or minimize energy expenditure. By leveraging both kinematic and dynamic models, we can optimize motions for tasks such as walking and lifting, while ensuring the system behaves in a desired manner within predefined constraints.

3.3 Optimal Control in Biomechanics

Optimal control applies mathematical optimization within dynamical systems as to determine a control over a period of time so that it minimizes specific variables by optimizing a given objective function. In the case of a biomechanical system such as the human body, forces or joint torques can be used as controls so that a particular objective such as muscle activation or joint stress is minimized, subject to the dynamic and physical constraints of the human body. Optimal control has been extensively used in biomechanics to analyze and optimize human motion [131, 132, 133]. This can apply in various cases, such as optimizing movement patterns or exoskeleton assistance to achieve the most efficient or least damaging outcome during activities like walking, running, or lifting [134].

By formulating human movement as an optimal control problem (OCP), we can investigate how specific movements can be performed efficiently, minimizing joint forces, torques, and other biomechanical parameters. This approach not only helps

to understand the mechanics of human movement but also informs exoskeletons about the level of support they need to provide. Additionally, optimal control allows for the enforcement of interaction force limits, ensuring the safe and comfortable use of assistive devices. In the context of biomechanics alone, optimal control is often used in two primary contexts: motion reconstruction and motion optimization.

Motion Reconstruction

Motion reconstruction refers to the process of determining the underlying kinematics such as joint trajectories, and dynamics such as joint torques, and muscle forces that are responsible for producing movement. This is typically done by minimizing the error between measured kinematic data - for example physical and virtual motion capture markers - and simulated movement [135]. After describing the model's kinematic and dynamic properties, a least-squares quadratic (LSQ) problem can be formulated to perform IK and map the motion capture frames to the model for every marker,

$$\min_{\mathbf{q}_i} R(\mathbf{q}_i) = \frac{1}{2}\mathbf{r}(\mathbf{q}_i)^T \mathbf{W}\mathbf{r}(\mathbf{q}_i) \tag{3.14}$$

where $\mathbf{m}_{i,j}^D$ denotes marker data with $i = 1, ..., n_F$ and $j = 1, ..., n_M$ referring to the motion capture frames and number of markers respectively, and p^c, p^m stand for joint centers and virtual marker locations, making up the model parameters. with

$$\mathbf{r}(\mathbf{q}_i) = \begin{bmatrix} \mathbf{m}_{i,1}^D - \mathbf{r}^M(1, \mathbf{q}_i, \mathbf{p}^c, \mathbf{p}^m) \\ \vdots \\ \mathbf{m}_{i,n_M}^D - \mathbf{r}^M(n_M, \mathbf{q}_i, \mathbf{p}^c, \mathbf{p}^m) \end{bmatrix} \in \mathbb{R}^{3n_M} \tag{3.15}$$

constituting the error between the virtual and real markers for the current pose q_i, where $\mathbf{r}^M(1, \mathbf{q}_i, \mathbf{p}^c, \mathbf{p}^m) \in \mathbb{R}^3$ describes the forward kinematics function which computes the global coordinates of marker j.

In order to solve Equation 3.14, an OCP problem is formulated as to fit the dynamics of the model to the kinematic motion obtained from the motion mapping. A general dynamics reconstruction problem can be defined as:

$$\min_{x(\cdot),u(\cdot)} \sum_{j=0}^{M_i} \left\| \mathbf{q}^D(t_j) - \mathbf{q}(t_j) \right\|_2^2 \tag{3.16a}$$

subject to:

$$\dot{\mathbf{x}}(t) = f_i(t, \mathbf{x}(t), \mathbf{u}(t), \mathbf{p}) \tag{3.16b}$$

$$\mathbf{x}(t_i^+) = c_i(\mathbf{x}(t_i^-), \mathbf{p}) \tag{3.16c}$$

$$\mathbf{g}(t, \mathbf{x}(t), \mathbf{u}(t), \mathbf{p}) \geq 0 \tag{3.16d}$$

$$\mathbf{r}^{eq}(\mathbf{x}(\mathbf{0}), \ldots, \mathbf{x}(t_f), \mathbf{p}) = 0 \tag{3.16e}$$

$$\mathbf{r}^{ineq}(\mathbf{x}(\mathbf{0}), \ldots, \mathbf{x}(t_f), \mathbf{p}) \geq 0 \tag{3.16f}$$

The objective function (3.16a) minimizes the sum of squared errors of the joint angles of the model (derived from virtual markers markers) in relation to the joint angles from the motion captures (derived from motion markers). The dynamics of the model are described by the ordinary differential equation (ODE) (3.16b) where $\mathbf{x}(t)$ represents the time dependent states of the system, and $\mathbf{p}$ are the free parameters that are fixed in time. The optimization results in the necessary controls $\mathbf{u}(t)$ that satisfy the minimization of state trajectories.

For formulating a more complicated problem, where multiple contacts are present, for example when a foot strikes the ground or a hand grasps to lift a box, the OCP can be split into multiple phases of any given duration. Phase transition functions such as $\mathbf{c}_i(\mathbf{x}(t_i))$ help describe the changes in state. The dynamics of the system are then bound to a set of constraints describing the limits of the model; continuous inequality constraints are described by Equation 3.16d and pose lower and upper bounds to all variables and point-wise equality and inequality constraints are given by Equations 3.16e and 3.16f respectively, such as boundary, phase-switching and periodicity constraints. This approach typically an inverse OCP where the objective functions or controls are calculated given the state of the model.

Motion Optimization

In contrast to motion reconstruction, motion optimization involves the formulation of a forward OCP formulation, predicting the best movement pattern to achieve a specific goal, such as minimizing joint forces or maximizing energy efficiency, with no or limited initial data on the states of the system. In this case, the OCP is formulated to generate an ideal motion trajectory by considering various biomechanical constraints and objectives. For example, minimizing joint torques or forces can help optimize lifting patterns in BSEs, reducing the strain on joints and improving the comfort and safety of the user. These OCP formulations often include cost functions related to minimizing effort or joint loading, while ensuring that movement constraints - such as joint limits or ground reaction forces - are respected.

A general multi-phase OCP formulation can take up on one of the two, or both of the following functions [136]:

$$\min_{\mathbf{x},\mathbf{u},\mathbf{p},T} \sum_{i=0}^{n_{ph}-1} \int_{t_{i-1}}^{t_i} \phi_{L_i}(t, \mathbf{x}(t), \mathbf{u}(t), \mathbf{p})dt + \sum_{i=0}^{n_{ph}-1} \phi_{M_i}(t_i, \mathbf{x}(t_i), \mathbf{p}), \tag{3.17}$$

where the first part describes the integral objective function ϕ_{L_i} of the Lagrange type that can dynamically minimize states and controls, and the second part denotes the Mayer type objective functions ϕ_{M_i} that depend solely on the end points.

The OCPs mentioned in this section can be solved in various ways including direct and indirect methods, as well as dynamic programming. In the work presented in this thesis through Chapters 5 to 6, a direct multiple shooting method is used, within the software MUSCOD-II [137, 138], as to discretise the controls and states, resulting to a Nonlinear Program (NLP) which is solved using Sequential Quadratic Programming (SQP).

Control Discretization

In optimal control problems, continuous-time control and state variables must often be discretized in order to be solved numerically. This is typically achieved using the multiple shooting method, which divides the time horizon into several sub-intervals. The goal is to obtain a piecewise representation of the control and state trajectories, allowing the problem to be formulated as a finite-dimensional nonlinear program (NLP).

The continuous control input $u(t)$ is discretized over the time horizon $[t_0, t_f]$, which is split into sub-intervals $I_j = [t_j, t_{j+1}]$, $j = 0, \ldots, m-1$. On each sub-interval I_j, the control is approximated by a parameterized base function $\phi_j(t, q_j)$, where $q_j \in \mathbb{R}^{k_j}$ represents the control parameters. This leads to a piecewise representation of the control input:

$$\mathbf{u}(t) := \phi_j(t, \mathbf{q}_j), \quad t \in I_j, \quad \mathbf{q}_j \in \mathbb{R}^{k_j}. \tag{3.18}$$

For simple cases, the controls can be approximated using piecewise constant functions:

$$\phi_j(t, \mathbf{q}_j) = \mathbf{q}_j, \quad \mathbf{q}_j \in \mathbb{R}^k. \tag{3.19}$$

Alternatively, for a more accurate representation, piecewise linear functions can be used, that subsequently increase the complexity of the problem as well. This discretization reduces the continuous-time control problem into a parameterized optimization problem where the parameters q_j are determined.

State Parameterization

Similarly, the state trajectory $x(t)$ is discretized using the multiple shooting method. The time horizon is divided into the same sub-intervals I_j, and the system dynamics are solved independently over each interval:

$$\dot{\mathbf{x}}(t) = \mathbf{f}(t, \mathbf{x}(t), \mathbf{u}(t), \mathbf{p}), \quad \mathbf{x}(t_j) = s_j, \tag{3.20}$$

where s_j are the states at the interval boundaries and p represents the system parameters. To ensure the continuity of the state trajectory across the sub-intervals, the following constraints are enforced:

$$\mathbf{x}(t_{j+1}, \mathbf{q}_j) - \phi_{j+1}(t_{j+1}, \mathbf{q}_{j+1}) = 0, \quad j = 0, \ldots, m-2. \tag{3.21}$$

These continuity constraints guarantee that the state trajectory remains consistent over the entire time horizon.

Sequential Quadratic Programming

Once the controls and states have been discretized, the original continuous-time optimal control problem is transformed into a finite-dimensional NLP. SQP is a widely used method for solving such NLPs. In SQP, the nonlinear objective function is approximated by a quadratic model, and the constraints are linearized at each iteration.

At each iteration k, the following quadratic program is solved:

$$\min_p \nabla F(x_k)^T p + \frac{1}{2} p^T \nabla^2 F(x_k) p, \tag{3.22}$$

subject to:

$$g(x_k) + \nabla g(x_k)^T p = 0, \tag{3.23}$$

$$h(x_k) + \nabla h(x_k)^T p \geq 0, \tag{3.24}$$

where $F(x)$ is the objective function, $g(x)$ represents the equality constraints, and $h(x)$ represents the inequality constraints. The solution to the QP provides the search direction p, which is used to update the state and control variables:

$$x_{k+1} = x_k + \alpha_k p, \tag{3.25}$$

where α_k is the step size, often determined through a line search procedure. The Lagrange multipliers λ are also updated at each iteration to ensure the satisfaction of the Karush-Kuhn-Tucker (KKT) conditions.

For the multiple shooting method, additional constraints are introduced to ensure continuity between sub-intervals and satisfy the boundary conditions. These constraints are incorporated into the NLP, resulting in the following system of equations:

$$h(y) = \begin{pmatrix} x(t_1; s_0, q_0) - s_1 \\ \vdots \\ x(t_{m-1}; s_{m-2}, q_{m-2}) - s_{m-1} \\ x(t_f; s_{m-1}, q_{m-1}) - s_m \\ r_0(x(t_0), p) + r_f(x(t_f), p) \end{pmatrix} = 0. \tag{3.26}$$

This ensures that the trajectory is continuous and satisfies the initial and final boundary conditions. The complete objective function for the discretized optimal control problem is:

$$\min_{x,u,p,T} \sum_{i=0}^{n_{ph}-1} \int_{t_{i-1}}^{t_i} \phi_{L_i}(t, x(t), u(t), p)\, dt + \sum_{i=0}^{n_{ph}-1} \phi_{M_i}(t_i, x(t_i), p), \tag{3.27}$$

subject to the constraints outlined above.

The multiple shooting method, combined with SQP, provides a powerful framework for solving optimal control problems by discretizing continuous-time control and state variables. Through control discretization, state parameterization, and iterative optimization using SQP, the method ensures accurate solutions while maintaining system continuity and satisfying all constraints.

In exoskeleton design, optimal control can be used to inform the device's control strategies by determining the appropriate level of assistance at each joint. Furthermore, interaction force limits can be integrated into the control system to prevent excessive forces that could cause discomfort or injury. By optimizing the exoskeleton's support, the system can dynamically adjust its assistance based on the user's biomechanical needs during activities like walking, standing, or lifting. The following part delves deeper into the use and application of these methods and presents the work done in this thesis in optimizing human-exoskeleton interactions via means of optimal control, to generate optimal support and minimize the toll on the lower back.

Part II

Computational Evaluation and Optimization of a Back-Support Exoskeleton

Modeling Assisted Lifting Motions

4

Credit and Publication Statement
The research work in Chapters 4, 5 and 6 constitute an advancement of early work from Manish Sreenivasa, Matthew Millard and Monika Harant, during their time at Heidelberg University. Giorgos Marinou built upon the concept and methodology, carried out all the computational, simulation and modeling work, designed the concept of these chapters, and conducted the investigation and analysis of the data. Matthew Millard aided in undertaking the research, analysis and the preparation of written work in Chapter 6. Nejc Šarabon performed all experimental recordings mentioned. Katja Mombaur conceived of the research idea and plan, obtained funding for the project, and assisted in the work. Chapters 4 to 6 are based on content from published work [139] with Giorgos Marinou the first author. Partial portions of the text, figures, and analysis have been adapted and extended here with acknowledgment of the original publication.

Within the scope of this research work, the back-support exoskeleton SPEXOR (Section 2.2.2) was investigated with the aim of optimizing the human-exoskeleton interactions by (1) *optimizing the level of actuation and support provided* and (2) *predicting human movement while maintaining adequate comfort levels*, using modeling and simulation in the context of optimal control. Previous work in the SPEXOR project set the groundwork on collecting motion data of lifting motions, developing the passive SPEXOR prototype and generating human and exoskeleton models and OCP formulations. The modeling and simulation in this and the following chapters using the SPEXOR exoskeleton, focuses on the motion of humans reaching forward and lifting a weighted box. The movement sequence follows a model of a human reaching forward from an idle standing position, to pick up a box and lifting it to return to a standing position while holding the box.

Models of the human body and the exoskeleton were implemented in LUA [140], a light scripting language that enables assigning kinematic trees and dynamic properties to the models, which can be embedded into existing applications for computing kinematics and dynamics; the Rigid Body Dynamics Library (RBDL) [141] was used for this purpose. It is a high-performance library for computing forward and inverse dynamics, kinematics, Jacobians, and contact constraints for kinematic chains and branched models, featuring algorithms like Recursive Newton Euler Algorithm

(RNEA), Composite Rigid Body Algorithm (CRBA), and Articulated Body Algorithm (ABA), with support for Lua and URDF model loading, and optimized with Eigen3 math library for enhanced efficiency. The OCP is built in C++ language using RBDL and LUA, to solve the modeling parameters and inform the multiple-shooting algorithm MUSCOD-II which in turn minimizes the objective function.

This chapter summarizes the groundwork on modeling and optimization of the human and SPEXOR models this work is based on and extends this research further as to more accurately describe the dynamics and optimize the exoskeleton's output. Modeling approaches are presented regarding the human, exoskeleton and box involved in the lifting problem scenario, along with dynamics formulations of the human-exoskeleton interaction. The modeling methodologies employed are detailed in this chapter, while Chapter 5 delves into the OCP formulation for reconstructing the movement from motion capture experiments and optimizing the exoskeleton's actuation, and 6 describes the synthesis of optimal lifting motions and compares this approach to the assistance provided from the SPEXOR exoskeleton.

4.1 Modeling the Human

Various approaches for modeling the human body exist in the literature, differing in the number of DoFs, articulation, and body segments represented. To simplify the computational process and OCP formulation, the human body in this work is modeled as a two-dimensional multibody system in the sagittal plane. This simplification is supported by the kinematic analysis of initial lifting experiments [142] conducted at the start of the SPEXOR project, which showed that the motion of a human lifting a box can be approximated as symmetrical, thereby justifying a simplified modeling framework.

As a result, the human body is represented as an 11-segment model with 13 DoFs in the sagittal plane: ten internal actuated DoFs and three for the floating base of the pelvis (Figure 4.4). The head and wrists are fixed to the upper torso and forearms, respectively, preventing any movement or rotation relative to their parent segments. In preliminary experiments, participants lifted a box with straight wrists and minimal head movement, justifying the assumption of fixing the hand to the forearm and preventing irregular extremity movements during optimization. The segment geometry, masses, and inertias in the model are scaled using linear regression equations and anthropometric data from de Leva's tables [129], which require the subject's height and weight as inputs to calculate segment lengths, masses, and inertias. These dynamic properties are further adjusted to each subject by scaling them according to the measured segment lengths obtained during the experiments.

All human models developed in this thesis adhere to this approach. Joint actuation is achieved through torques applied to the modeled DOFs, excluding the three DOFs of the floating pelvis base. To accurately model lumbar spine mechanics and investigate the intrinsic properties of the lumbar vertebrae, a more complex spine model is used, accounting for the coupling properties of vertebral joints.

4.1.1 Lumbar Spine Model

The work of modeling the spine has been carried out with the help of Matthew Millard (University of Stuttgart).

While previous work has modeled the human using a dual-trunk interface with one joint connecting to the pelvis at the level of the L5/S1 and one joint connecting the middle trunk to the upper torso at the L1/T12, this thesis work explores the more intrinsic modeling of the human spine. An articulated and coupled model of the lumbar spine, similar to the one described by Christophy et al. [143], is created to ensure the accuracy of the bending movements. The lumbar spine is modeled as five vertebrae connected in series using revolute joints (Figures 4.1 and 4.4. These revolute joints are positioned at the average center-of-rotation for each vertebra, as reported by Pearcy and Bogduk [144]. The data from Pearcy and Bogduk [144] have been fit to the high-resolution vertebral meshes of Mitsuhashi et al. [145] and scaled to fit the participant.

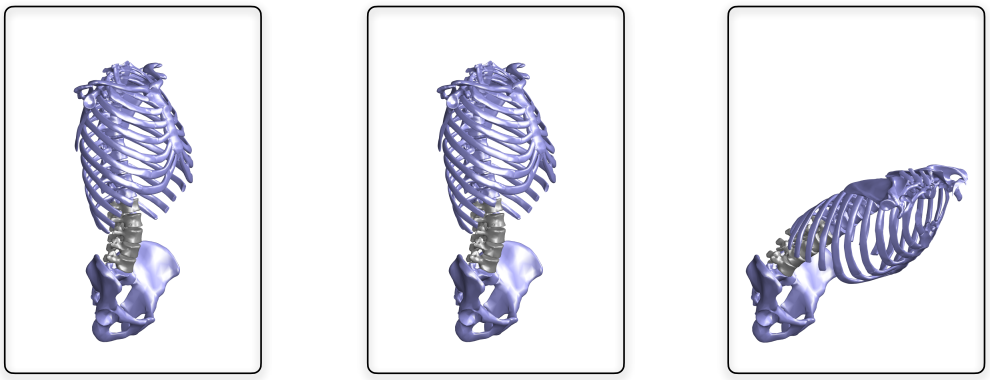

Figure 4.1: The model of the lumbar spine. **(Left)** Neutral posture of the spine. **(Middle)** Maximum extension angle achieved with the model (20°). **(Right)** Maximum flexion angle achieved with the model (70°).

Although the lumbar spine consists of five joints, these joints are coupled using four constraint equations, resulting in a lumbar spine with only one degree of freedom in the sagittal plane. The constraint equations are formulated to ensure that the coordinated motion is consistent with the coordinated bending of the lower back, as measured by Wong et al. [146]. According to Wong et al. [146], the flexion of

each joint, α_i, scales linearly with the total lumbar flexion angle, $\alpha_L = \sum_1^{i=5} \alpha_i$, such that $\alpha_i = \mathrm{n}i\alpha\mathrm{L}$, where α_5 represents the angle from the S1 to L5 and α_4 represents the angle from L5 to L4, and so on. The coefficients $\mathrm{n}5, \ldots, \mathrm{n}1$ that best fit the 30 participants in Wong et al.'s [146] study are 0.255, 0.231, 0.204, 0.185, and 0.125. As in the model of Christophy et al. [143], this linear relationship between α_i and $\alpha\mathrm{L}$ is used to form the velocity-level constraint

$$ci : \frac{\dot{\alpha}i}{\mathrm{n}i} - \frac{\dot{\alpha}i+1}{\mathrm{n}i+1} = 0 \tag{4.1}$$

between neighboring pairs of joints (Fig. 4.4). Prior to simulation, each lumbar joint angle is biased so that a lumbar flexion angle of zero, $\alpha_{\mathrm{L}} = 0$, positions the lumbar spine to match the participant's resting posture (shown in Figure 4.4) from Mitsuhashi et al. [145]. In this configuration, the bias angles are $2.1°$, $8.8°$, $10.6°$, $12.9°$, and $11.3°$ of extension for the joints from the L5/S1 joint to the L1/L2 joint, respectively. As with other kinematic constraints in the model, index reduction is applied to transform the original set of differential algebraic equations of index 3 into a system of differential algebraic equations of index 1. During the simulation, the constraint error is minimized using Baumgarte stabilization [147] (see Section 4.4.2).

4.1.2 Simplified Muscle Modeling

Neuromuscular models, which simulate the interplay of neural signals, muscle activation dynamics, and musculoskeletal interactions, offer a detailed representation of human motor control. However, these models introduce significant computational complexity due to nonlinear activation dynamics, time delays, and feedback loops, making them less practical for tasks requiring efficiency, such as solving large-scale OCPs. This thesis focuses on optimizing the interaction dynamics between the human and the SPEXOR back-support exoskeleton during repetitive lifting motions. These tasks, characterized by predictable and symmetrical joint dynamics in the sagittal plane, do not heavily rely on real-time neuromuscular feedback, rendering a simpler modeling approach both appropriate and efficient.

A significant body of research has focused on neuromuscular modeling using Hill-type muscle models, which describe muscle behavior through force-length, force-velocity, and passive elasticity relationships. The simple Hill-type model represents muscle force generation as a combination of contractile and elastic elements, while extended Hill-type models incorporate more detailed activation-contraction dynamics and tendon compliance. Studies have laid the foundation for these models, highlighting their ability to simulate physiological properties such as muscle activation and relaxation [148]. Later advancements introduced reflex-based control and stabilization

mechanisms for dynamic tasks, emphasizing the role of elastic tendon elements [149].

Refinements in Hill-type models include activation-contraction coupling, making them suitable for tasks requiring precise muscle coordination [150]. While these models are critical for studying dynamic locomotion tasks like walking and running, their computational cost remains a significant challenge, particularly in OCP formulations. For instance, neuromuscular models have successfully reproduced human walking dynamics and muscle activities, highlighting the importance of muscle-reflex interactions in legged mechanics [151]. In the context of repetitive lifting tasks however, muscle dynamics are relatively consistent and less influenced by rapid neuromuscular adjustments, making simplified modeling approaches more feasible without significant loss of accuracy.

Contraction dynamics, describing the transition from neural activation to muscle force production and able to convey processes such as excitation-contaction coupling and accurately capture the force-velocity relationship of muscles, are essential for accurtely modeling muscle behaviour. However, this detailed modeling could potentially introduce additional complexity due to inherent time delays and nonlinearities. Research has shown that incorporating detailed contraction dynamics is crucial for simulating rapid movements and reflexive responses, as they significantly influence the timing and magnitude of muscle forces. For instance, studies have shown that muscle dynamics play a vital role in stabilizing movements and reducing the control effort required by the nervous system [152].

When concerning repetitive lifting tasks however, the impact of muscle dynamics is less pronounced, which in turn allows for the use of more simplified approached in muscle modeling and torque generation, while maintaining a relatively high level of accuracy in dynamics representation.

4.1.3 Joint Torque Generation

In biomechanical models, Muscle Torque Generators (MTGs) are often used to represent the muscle forces responsible for moving a joint in various degrees of freedom (e.g., flexion, extension, abduction, and rotation) [153, 142]. MTGs reduce the complexity involved in simulating numerous muscles by summarizing their contribution at a single joint level, effectively simplifying the overall model without compromising the accuracy of muscle actuation properties.

Implementing MTGs requires accounting for passive muscle forces and nonlinear relationships between muscle length, velocity, and activation, which can be computationally expensive. This becomes particularly problematic when performing optimal control tasks that need efficiency and stability. The use of MTGss is proven rather

effective in generating accurate results for joint-level muscle torques [142, 154], however, it introduces significant computational overhead due to nonlinear torque computations.

For these reasons, direct joint torques were chosen in this thesis, simplifying the computational cost while still incorporating essential muscle properties [155]. Instead of modeling the muscle dynamics through MTGs, scaling factors and damping coefficients are applied directly to the joint torques to approximate the characteristics of muscle force generation [148]. This approach preserves the influence of muscle properties, such as torque-angle and torque-velocity dependencies, without the need for complex MTG equations. The torque generated at the joint τ_i^{HUMAN}, which combines both muscle flexion and extension contributions, is given by:

$$\tau_i^{\text{HUMAN}} = \alpha_i \cdot \tau_{\max}(q_i) - \beta_i \cdot \dot{q}_i \tag{4.2}$$

where α_i is the scaling factor applied to approximate muscle activation, $\tau_{\max}(q_i)$ represents the maximum possible torque for the joint angle q_i, and $\beta_i \cdot \dot{q}_i$ introduces damping proportional to the angular velocity of the joint $\dot{q}_i$. This torque relationship can be seen as an adaptation of the muscle torque generator framework, which also incorporates joint damping. The equation used in this model aligns with the core principles of MTGs, which calculate the torque for both flexion and extension as:

$$\tau_i^{\text{MTG}} = \tau_0^{\text{MTG}} \left[\alpha f^A(\theta) f^V(\omega) + s^P f^P(\theta - \theta_0^P) \left(1 - \beta^P \frac{\omega}{\omega_{\max}^{\text{MTG}}} \right) \right] \tag{4.3}$$

where f^A and f^V represent the force-activation and force-velocity curves, and the terms s^P and θ_0^P describe the passive muscle force contribution. This equation captures the nonlinear muscle force characteristics, which are omitted in the direct joint torque model. However, through the use of appropriate scaling factors α_i and damping terms β_i, this approach retains the key dynamics necessary for accurate actuation, while ensuring computational efficiency.

To this end, direct joint torques were employed in place of MTGs or neuromuscular models. This approach uses scaling factors and damping elements to approximate key muscle properties, such as torque-angle and torque-velocity relationships, while avoiding the computational overhead associated with force-sharing and activation dynamics. Preliminary comparisons of MTGs and direct torque models showed close agreement in joint torque profiles, with peak differences remaining within $\pm 0.4 Nmkg^{-1}$ across the studied joints (Figure 4.2.

While neuromuscular models might be indispensable for tasks involving dynamic balance recovery or perturbation responses, their omission in this work ensures computational feasibility without compromising biomechanical accuracy for the lifting tasks analyzed. Future research could expand on this framework by integrating

neuromuscular dynamics to explore applications involving more complex movements or adaptive feedback requirements.

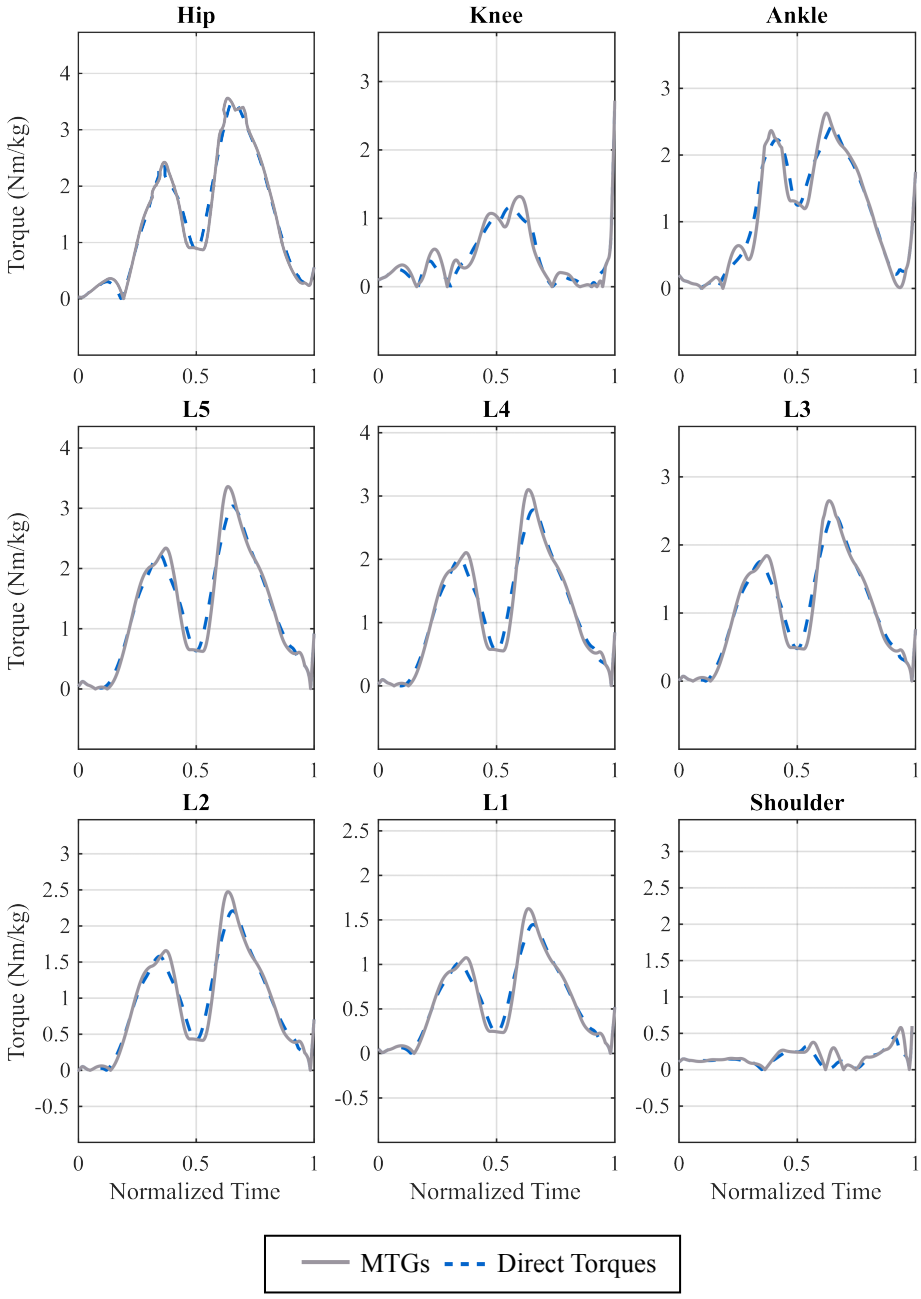

Figure 4.2: Comparison of mass-normalized MTGs torque vs. direct joint torque for the OCP controls of hip, knee, ankle, lumbar vertebrae and shoulder joints. The solid lines represent torques generated using MTG, while the dashed lines represent direct joint torques.

4.2 Modeling the SPEXOR Exoskeleton

For the aims of the SPEXOR project, this thesis focuses on the optimization of the actuated hydraulic prototype described in Section 4.2.2, resulting to a six segment

and eight DoF exoskeleton model (Figure 4.4). This exoskeleton prototype includes two main support elements: three passive carbon fibre beams ($4.7mm$ in diameter and $43.6cm$ in length with a Young's Modulus of $166GPa$) producing counter torques at the lumbar back and a hydraulic actuator (with a maximum output torque of $25Nm$) at each of the hips. The exoskeleton model further includes a pelvis and trunk module which are connected by the carbon fibre beams, and a thigh module that is connected to the pelvis module via a rigid metal rod. The carbon fibre beams are rigidly attached to the pelvis interface and can slide through the trunk module through a series of rollers. These connections impart corresponding boundary conditions on the beam that describe the beam kinematics at its two attachment points. The dynamic parameters, mass, CoM and inertia properties of each segment were derived from 3D CAD models of the existing prototype, and the masses were corrected for additional components (such as screws and nuts) to more accurately represent the weight of the exoskeleton, which amounts to $9.12kg$. In order to simulate the behavior of the passive and active elements of the exoskeleton, mathematical models are implemented and described here.

4.2.1 Exoskeleton Passive Element Modeling

The SPEXOR exoskeleton maintains passive beam support throughout all its prototypes as a way of delivering counter-torques at the lumbar region, aiding with flexion and extension during lifting. As stated above, three parallel beams are fixed at the pelvis and allowed to travel through rollers on the upper torso interface. In the simulation, each beam is modeled using the same cubic spline approach described below, ensuring consistency in beam behavior across the exoskeleton.

As has been shown by Holladay [156] a cubic spline traces a path that minimizes total curvature, which is the same path traced by a slender elastic beam. At every instant in time a cubic spline $w(u)$ is fitted to match the end conditions imposed by the rigid pelvis mount and the rollers (Figure 4.4). The spline is described in normalized coordinates

$$u = \frac{z}{L} \tag{4.4}$$

along the undeformed path of the beam, and by deflections

$$w(u) = \mathrm{A} + \mathrm{B}u + \mathrm{C}u^2 + \mathrm{D}u^3 \tag{4.5}$$

perpendicular to u. Here L is the distance between the pelvis mount and the rollers projected onto the beam's axis that is fixed to the pelvis module. The coefficients in Eqn. 4.5 are evaluated using the boundary conditions imposed by the rigid pelvis mount

$$w(0) = \frac{d\,w(0)}{d\,u} = 0 \tag{4.6}$$

and the boundary conditions imposed by the rollers on the torso module where the beam must deflect by Δ

$$w(1) = \Delta, \tag{4.7}$$

and

$$\frac{d^2\, w(1)}{d\, u^2} = 0 \tag{4.8}$$

since the rollers cannot apply a reaction moment. The moments and shear forces the slender bent beam applies to the pelvis ($z = 0$) and torso ($z = L$) modules are evaluated using the spline $w(u)$ and an Euler-Bernoulli beam model where

$$M(u) = -EI \frac{d^2\, w(u)}{d\, u^2} \left(\frac{d\, u}{d\, z}\right)^2 \tag{4.9}$$

and

$$S(u) = -EI \frac{d^3\, w(u)}{d\, u^3} \left(\frac{d\, u}{d\, z}\right)^3. \tag{4.10}$$

Comparison to Experimental Data

Parameter identification for modeling the beam was carried out by Monika Harant of the Heidelberg University, including extensive work on varied results and modeling methodologies which can be found in her doctorate manuscript [157]. The work here builds upon these outcomes and simplifies the approach in order to achieve a high accuracy beam modeling at a low computational cost.

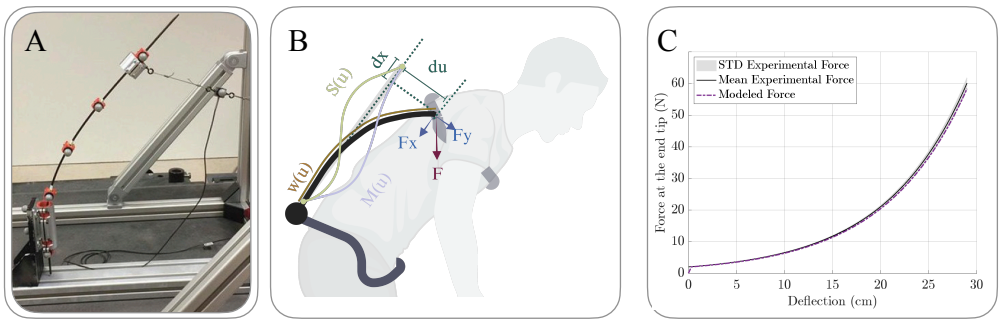

Figure 4.3: Comparison of measured and modeled beam force - deflection relationship. **(A)** Experimental setup at VUB, taken from [83], **(B)** Modeled beam dynamics with indicated shear force $S(u)$ and moment $M(u)$ curvatures and **(C)** Experimental results for force-displacement relationship plotted against modeled values used in exoskeleton modeling.

In order to confirm that the beam model described here can accurately represent the three-beam configuration of the SPEXOR exoskeleton, the force-deflection relationship is compared between the modeled beam and experimental data of the beam. The experimental data was collected by the SPEXOR partner at VUB where the one end of the beam was fixed on a custom-made test bed, and the free end was being pulled and slowly deflected by a cable connected to a load cell (Futek LSB200) as shown in Figure 4.3. Motion capture markers along the length of the beam captured

the curvature of the beam, aiding in computing deflections and heights along the motion. The experiment was repeated several times.

The plotted results (Figure 4.3C) suggest a close correlation between the modeled and measured force at the end tip of the beam values, at the given deflection intervals. As the values for smaller deflections, that are expected to take place in a real application scenario, have less error, the model is deemed adequate in representing the physical beam properties in the simulations using optimal control. A boundary value problem was was setup [157] in order to investigate the force deviation of the beam modeling reporting a maximum deviation of $0.86N$ and mean deviation of $0.04 \pm 0.1N$ to the experimentally measured force between deflection angles of 60 to $90\,\mathrm{deg}$.

4.2.2 Exoskeleton Active Element Modeling

The hydraulic actuator included in the active SPEXOR prototype was assembled and provided by the project partner Otto Bock HealthCare Products GmbH (Vienna, Austria). Due to the commercialized use of this product, the exact dynamic properties and functions of the actuator can not be provided in this thesis, however some details of the torque-angle relationships are disclosed. The hydraulic actuator presents various modes of operation, including a passive element, able to store energy while the user is bending forward. It is able to provide an active force when the user is lifting a weight and support the movement at the hip.

The placement of the actuator on the exoskeleton, along with its dynamic movement while the wearer is bending forwards and backwards was optimized via a collaboration between Heidelberg University (Monika Harant) and Otto Bock HealthCare Products GmbH. The misalignment compensation mechanism remained on the exoskeleton, with the hydraulic actuator replacing the MACCEPA quasi-passive element [84]. The level of the torque provided by the hydraulic actuator varies with the magnitude of the hip angle and is able to reach its maximum output when the user is approaching a higher hip angle, towards the end point of reaching forward and initiating the lift. It is modelled as a spring of known stiffness in parallel to a motor and pump system, both of which essentially exert pressure on the hydraulic piston which consequently actuates the hip joint.

The hydraulic actuator can offer various levels of support and in this work it has been modeled to work for three modes of operation: (1) *Compliant Mode* where the actuator can remain idle without impeding the movement of the user, (2) *Energy Storing Mode* where the actuator harnesses energy from the user while they move and stores it in its passive element, and (3) *Support Mode* where the actuator provides torque to the user via its piston, from combined efforts of the active (pump) and passive elements. The dynamics equations of the actuator (that cannot be

disclosed here) take into account its position along the thigh of the user and the force transmission via the misalignment compensation mechanism. The dynamic equations applied for describing the actuator ensure that the following constraints are followed: (1) torque-angle limits, (2) maximum extension velocity of the piston (54 mm/s) and (3) valve dynamics (50 - 100 ms from close to open).

While theoretically the hydraulic actuator can provide a maximum ideal torque output of $27.5Nm$, due to mechanical impedance present in the actuator itself as well as the exoskeleton structure, such as the misalignment compensation mechanism, the maximum achievable torque output the exoskeleton can successfully provide directly at the hip joint amounts to $25Nm$. To reflect this limitation a scaling factor has been applied linearly through the modeling equations of the hydraulic actuator.

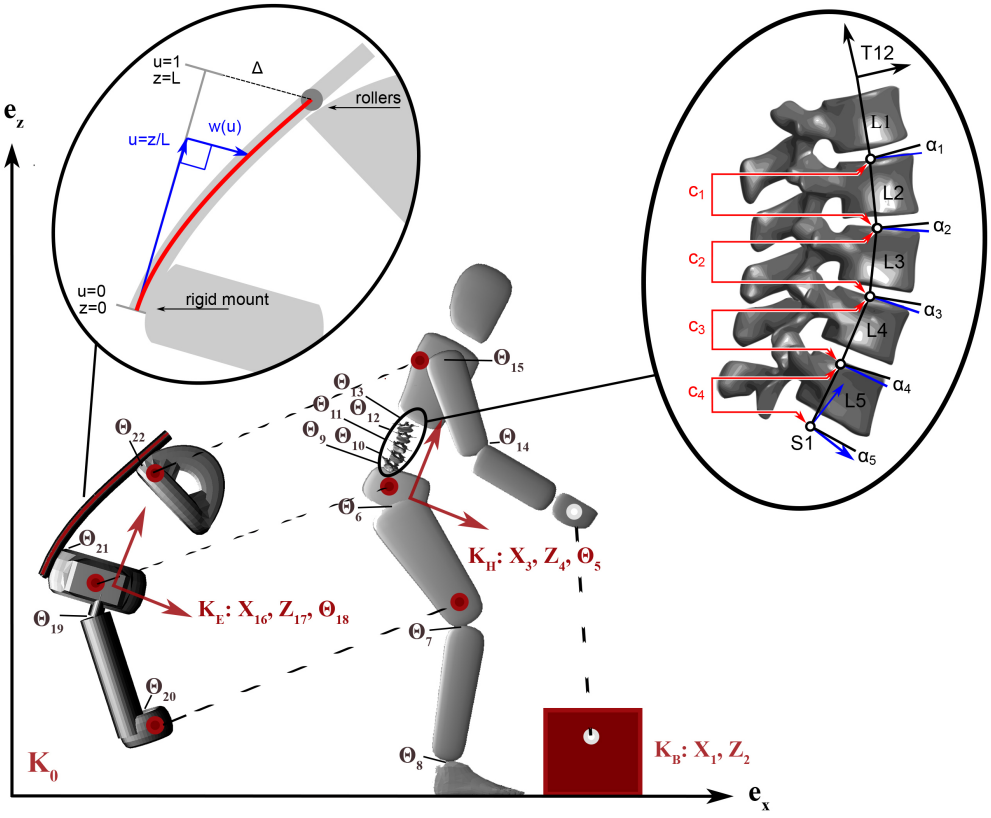

Figure 4.4: The human as an 11-segment, 13-DoF model and the attachment points to the 6-segment, 8-DoF exoskeleton. Dashed lines indicate the kinematic constraints between the exoskeleton and the human, as well as the human and the box (see Section 4.5.3. The feet are constrained to the ground throughout the motion whereas the box is constrained to the ground until lifted by the human.The letter K denotes a coordinate system where the subscripts B, H, E and 0 correspond to the coordinate systems of the box, human, exoskeleton and global reference frames, respectively. The planar positions are indicated with x and z and angles by Θ. A close-up of the lumbar spine model depicts the L1 to L5 lumbar vertebrae and the four constraint equations that couple the movements of the joints.

Another key factor influencing the dynamic torque generation of the hydraulic actuator, and consequently playing a critical role in optimizing torque profiles for high-level control, is the piston velocity. The mathematical model of the actuator dynamics, which is integrated into the optimization framework to minimize torques at the L5/S1 joint, incorporates piston velocity to accurately capture the relationship between lumbar flexion angles and actuator-generated hip torque support. To investigate this, two distinct cases of piston velocity are considered:

1. **Case 1:** A high piston velocity, where the piston reaches 90% of its full length in 51 ms.
2. **Case 2:** A low piston velocity, where the piston reaches 90% of its full length in 100 ms.

These two cases are evaluated using a LSQ OCP formulation to compare the resulting reductions in lumbar torque. The outcomes and corresponding analysis are discussed in detail in Section 5.3.

4.3 Combining Human and Exoskeleton Models

In a simulation scenario, modeling the coupling of the exoskeleton and human models is of utmost importance in order to accurately represent the kinematic and dynamic properties of the combined motions. Before proceeding in solving forward or IK and dynamics, a correct description of the relationships is realized through constraining and coupling the bodies together.

Preliminary motion capture experiments, where a subject performed repetitive lifting motions, indicated that while the exoskeleton's thigh and upper trunk interfaces are firmly attached on the body, the pelvis interface has some rotational flexibility in relation to the human pelvis. In these experiments, the exoskeleton pelvis interface indicated posterior and anterior tilt differences with respect to the human pelvis, which directly influence the application of torque both from the hydraulic actuator at the hip, as well as the flexible beams on the lumbar. Though determining the relative angle between the human and exoskeleton pelvis interface was not possible, based on the findings of these experiments, a more representative modeling approximation has been implemented, through studying three different cases of coupling the exoskeleton pelvis onto the human pelvis:

Case 1: Constraint-Based with Prescribed Angle Limits

In this case, the exoskeleton pelvis interface is free to rotate relative to the human pelvis but is subject to rotational limits deduced from experimental observations. These limits enforce a range of permitted motion, ensuring the interface stays within realistic bounds while still capturing its flexibility. The resulting torque τ^{EP} reflects

the interaction at the extremes of these rotational limits, and the relationship is modeled through kinematic constraints rather than dynamic forces.

Case 2: Force-Based with Rotational Spring Dynamics

Here, the coupling between the exoskeleton pelvis interface and the human pelvis is modeled as a rotational spring. The torque τ^{EP} generated at the interface is described by $\tau^{EP} = -k\theta^{EHP}$, where k is the rotational spring constant, and θ^{EHP} is the relative anteroposterior angle between the exoskeleton and human pelvis. This approach captures the dynamic relationship between the two segments, allowing for continuous torque generation proportional to the angular displacement.

Case 3: Constraint-Based with Fixed Interface

In this case, the exoskeleton pelvis interface is rigidly fixed to the human pelvis, with no relative motion allowed between the two. This relationship is modeled using constraints that enforce identical positions and orientations, resulting in zero torque at the interface ($\tau^{EP} = 0$). This case represents a highly restrictive scenario where the interface behaves as a single rigid segment.

A kinematic comparison was thus implemented in order to match as closely as possible the anteroposterior rotations of the modeled exoskeleton pelvis interface to the ones of the motion capture experiments. IK were solved based on markers placed on the exoskeleton's pelvis interface and the resulting motion was compared to the simulated one as a result of optimization. The results of this comparison along with the selection of the most optimal case of modeling the human-exoskeleton pelvis interface interactions are reported in Section 5.3, where the LSQ OCP is presented.

4.4 Human and Exoskeleton Dynamics

After completing models of the human and exoskeleton with descriptions of their dynamic properties and torque generation patterns, the dynamics connecting the human, exoskeleton and the box need to be formulated. By adopting the general equation of motion with contact forces from Equations 3.9 and 3.10, we obtain

$$\mathbf{H}(\mathbf{q})\ddot{\mathbf{q}} + \mathbf{C}(\mathbf{q}, \dot{\mathbf{q}}) = \tau + \mathbf{G}(\mathbf{q})_c^T \lambda \tag{4.11}$$

$$g(q) = 0 \tag{4.12}$$

where matrix H contains the mass and inertia properties of the human, exoskeleton and box and similarly τ contains the generalized forces for the three models. The box is modeled as a two translation DoFs with no rotational movement, as observed in the preliminary lifting experiments. λ includes the constraint forces that describe the predefined contacts of the system. These include maintaining the contact of the user to the ground, coupling the exoskeleton to the user and fixing the contact of the

user to the box. The constraint Jacobian G varies depending on the nature of the constraint, affecting the generalized positions q, velocities $\dot{q}$ and accelerations $\ddot{q}$.

4.4.1 Ground Contact Modeling

In the lifting scenario, both the human and the box initially make contact with the ground. The human maintains contact throughout, while the box is allowed to lift off when the human picks it up. Ground contact dynamics are modeled by Equation 4.17:

$$\begin{bmatrix} \mathbf{H}(\mathbf{q}) & \mathbf{G}(\mathbf{q})^T \\ \mathbf{G}(\mathbf{q}) & 0 \end{bmatrix} \begin{bmatrix} \ddot{\mathbf{q}} \\ -\lambda \end{bmatrix} = \begin{bmatrix} \tau - \mathbf{C}(\mathbf{q}, \dot{\mathbf{q}}) \\ -\gamma(\mathbf{q}, \dot{\mathbf{q}}) \end{bmatrix} \tag{4.13}$$

At the moment of contact, the invariants of the constraint set must be satisfied, which requires the following conditions:

$$g(\mathbf{q}) = 0 \tag{4.14}$$

$$\mathbf{G}(\mathbf{q})\dot{\mathbf{q}} = 0 \tag{4.15}$$

These conditions enforce that both velocity and acceleration at the contact points are initially zero, meaning that no relative motion or force is introduced at the contact interface at the start of the simulation. Before solving Equation 4.13, both the human's foot and the box can be constrained to have zero deviation in position, velocity, and acceleration relative to the ground. This ensures that the human's foot remains in place and that the box remains grounded until lifted, maintaining the physical realism of the scenario.

4.4.2 Loop Constraints of Exoskeleton, Box and Lumbar

In biomechanical modeling, two primary approaches are commonly used to simulate motion and interaction: constraint-based modeling and force-based modeling. Constraint-based modeling relies on kinematic constraints to enforce specific positional and velocity relationships between connected segments. In contrast, force-based modeling uses forces and torques to regulate movement by directly modeling the interactions between segments, such as joint forces, muscle activations, or contact forces.

Constraint-based modeling is particularly advantageous in systems with rigid attachments or predefined motion paths, where enforcing exact geometric relationships is essential. This approach simplifies computations by replacing force equations with constraint equations, which can be solved algebraically or integrated into the dynamics of the system. In the human-exoskeleton system, kinematic loop constraints ensure that the motion of the exoskeleton aligns with the human's natural

movement while maintaining the mechanical interaction between both systems. These constraints are applied to the joints where the exoskeleton is attached to the human body, enforcing zero relative motion between connected segments. These constraints reduce the complexity of force computations while accurately capturing the coupled motion dynamics.

For instance, the exoskeleton's attachment points at the pelvis, upper torso, and legs form kinematic loops that link the exoskeleton's rigid segments to corresponding human body segments. These constraints are also used when kinematically looping the lumbar vertebrae together. These loops impose positional and velocity constraints to prevent excessive relative movement, ensuring that the exoskeleton follows the human motion while providing the intended support. Additionally, they prevent over-constraining the system by allowing certain degrees of freedom, such as rotational or translational motions, where necessary to accommodate natural movement patterns.

By introducing the additional active kinematic loop forces τ_a to the system of Equation 3.9,

$$\tau + \tau_c + \tau_a = \mathbf{H}(\mathbf{q})\ddot{\mathbf{q}} + \mathbf{C}(\mathbf{q}, \dot{\mathbf{q}}) \tag{4.16}$$

we can solve the multibody system with kinematic loops for the joint accelerations $\ddot{q}$ and forces λ by

$$\begin{bmatrix} \mathbf{H}(\mathbf{q}) & \mathbf{G}(\mathbf{q})^T \\ \mathbf{G}(\mathbf{q}) & 0 \end{bmatrix} \begin{bmatrix} \ddot{\mathbf{q}} \\ -\lambda \end{bmatrix} = \begin{bmatrix} \tau - \mathbf{C}(\mathbf{q}, \dot{\mathbf{q}}) + \tau_a \\ -\gamma(\mathbf{q}, \dot{\mathbf{q}}). \end{bmatrix} \tag{4.17}$$

The addition of the loop-constrained forces and in general positional constraints which are handled as accelerations can introduce numerical drift during the integration process, leading to errors in maintaining the closed-loop position constraint, where the position error $\mathbf{e}$ can drift over time, causing deviations from the desired motion. To address this issue, a Baumgarte stabilization term is introduced [147]. This method helps stabilize the kinematic loop constraints by correcting both the position and velocity errors within the closed loop, ensuring the system adheres to the desired kinematic relationships over time. The Baumgarte stabilization term adds proportional and derivative corrections to the constraint equation to manage the drift. Specifically, it augments the constraint violation $\mathbf{e}$ and its time derivative $\dot{\mathbf{e}}$ with feedback terms to produce a controlled correction:

$$\gamma(\mathbf{q}, \dot{\mathbf{q}}) = \ddot{\mathbf{e}} + 2\alpha\dot{\mathbf{e}} + \beta^2\mathbf{e}, \tag{4.18}$$

where α and β are positive stabilization parameters. These parameters are tuned to balance stability and responsiveness. The term $2\alpha\dot{\mathbf{e}}$ introduces damping to reduce

oscillations, while $\beta^2\mathbf{e}$ corrects positional errors by pulling the system back toward the desired constraint configuration. This stabilization ensures that small deviations in the loop constraints, both in position and velocity, are corrected over time, preventing the propagation of errors and ensuring smooth motion for the system.

4.4.3 Impact Modeling of Human and Box

In the context of this lifting scenario, we model the impact that occurs when the user grabs the box as a perfectly inelastic collision. A perfectly inelastic impact implies that there is no rebound, and the box and hand remain in contact, moving as a single system post-impact. The impact results in a discontinuity in the velocities, shifting from a negative velocity $\dot{q}^-$ before the impact to a positive velocity $\dot{q}^+$ after the impact.

To represent this mathematically, we use the impulse-momentum equation:

$$\mathbf{H}(\mathbf{q})\Delta\dot{\mathbf{q}} = \mathbf{G}^T\Lambda, \tag{4.19}$$

where $\mathbf{H}(\mathbf{q})$ is the system's generalized inertia matrix, $\Delta\dot{\mathbf{q}}$ is the change in velocity due to the impact, $\mathbf{J}$ is the Jacobian matrix relating the system's coordinates to the contact point, and Λ represents the impact forces (impulses). The change in velocity is calculated as:

$$\Delta\dot{\mathbf{q}} = \dot{\mathbf{q}}^+ - \dot{\mathbf{q}}^-, \tag{4.20}$$

where $\dot{\mathbf{q}}^+$ and $\dot{\mathbf{q}}^-$ denote the velocities after and before the impact, respectively.

Substituting these conditions into the momentum equation, we solve for the impact forces Λ and post-impact velocities $\dot{\mathbf{q}}^+$, which can be summarized in the system of equations,

$$\begin{bmatrix} \mathbf{H}(\mathbf{q}) & \mathbf{G}(\mathbf{q})^T \\ \mathbf{G}(\mathbf{q}) & 0 \end{bmatrix} \begin{bmatrix} \dot{\mathbf{q}}^+ \\ -\Lambda \end{bmatrix} = \begin{bmatrix} \mathbf{H}(\mathbf{q})\dot{\mathbf{q}}^- \\ 0 \end{bmatrix} \tag{4.21}$$

This ensures that the box is effectively "grasped" by the user, transitioning from its independent motion to a common velocity shared with the human hand, marking the start of the lifting motion. The resulting system of dynamic equations can be solved either by using inverse or forward dynamics, depending on the necessities of each scenario.

4.4.4 Limiting Interaction Forces

In addition to modeling the relationships between the two systems, interaction forces must also be considered, as they play a pivotal role in the overall dynamics and directly impact the user experience. These forces not only influence the physical

coupling between the human and exoskeleton but are also critical in determining how effectively the exoskeleton supports the user during lifting tasks. Properly accounting for interaction forces ensures a more accurate representation of the biomechanical and actuator-based support, ultimately improving comfort, safety, and performance. While exoskeletons - and specifically active exoskeletons - can provide high torque outputs in order to assist with lifting movements, the comfort of the user comes into play when considering ideal torque generation. According to findings based on the SPEXOR exoskeleton's attachment points, pressure tolerance experiments through qualitative studies on participants [158] carried out by project partners, managed to quantify the following limits on interaction forces:

Table 4.1: Interaction forces limits based on experimental results from Kozinc et al. [158].

	Torso Interface	Pelvis Interface	Thigh Interface
Normal Force (N)	230	162	333
Shear Force (N)	138	97	200

4.5 General Formulation of the Lifting Problem

As previously explained, optimal control is used to analyze lifting motions in two ways: (1) reconstruct lifting problems from motion capture experiments and (2) synthesize optimal lifting motions. Both of these approaches are used in this thesis to respectively optimize (1) the support from the exoskeleton actuation elements and (2) the lifting movement with the aim of minimizing lumbar torques, specifically at the level of the L5/S1 joint. This subsection provides the general formulation of the optimal control lifting scenario which is applied across all computational formats.

Table 4.2: Summary of the three phases involved in the lifting process, indicating the start and end conditions of each phase.

Phase	**Phase Name**	**Start Condition**	**End Condition**
1	Downward Reach	Idle Upright Standing	Box Contact ($\dot{q}^-$)
2	Force Buildup	Box Contact ($\dot{q}^+$)	Box Lift-off
3	Lifting	Box Lift-off	Standing with Box

The OCPs are formulated both with and without the use of the SPEXOR exoskeleton. The various phases of the lift are broken down and explained, along with the

applied constraints for each phase, offering a detailed explanation of the variables and parameters involved in the optimization problem and cost functions. This work builds upon previous optimization research conducted within the grounds of the SPEXOR project, introducing new insights on actuation optimization and the limitation of interaction forces as to maintain comfortable limits.

4.5.1 The Box Lifting Problem

The human lifting a box problem follows a simple approach which has been maintained both throughout the experimental protocol, as well as the simulations in this study. The human stands at an idle upright position at the start of this motion, then they reach downward, grasping for the box which is set at a given height and of a given weight, building up force for lifting it and ultimately lifting the box to come back to a standing position while holding it.

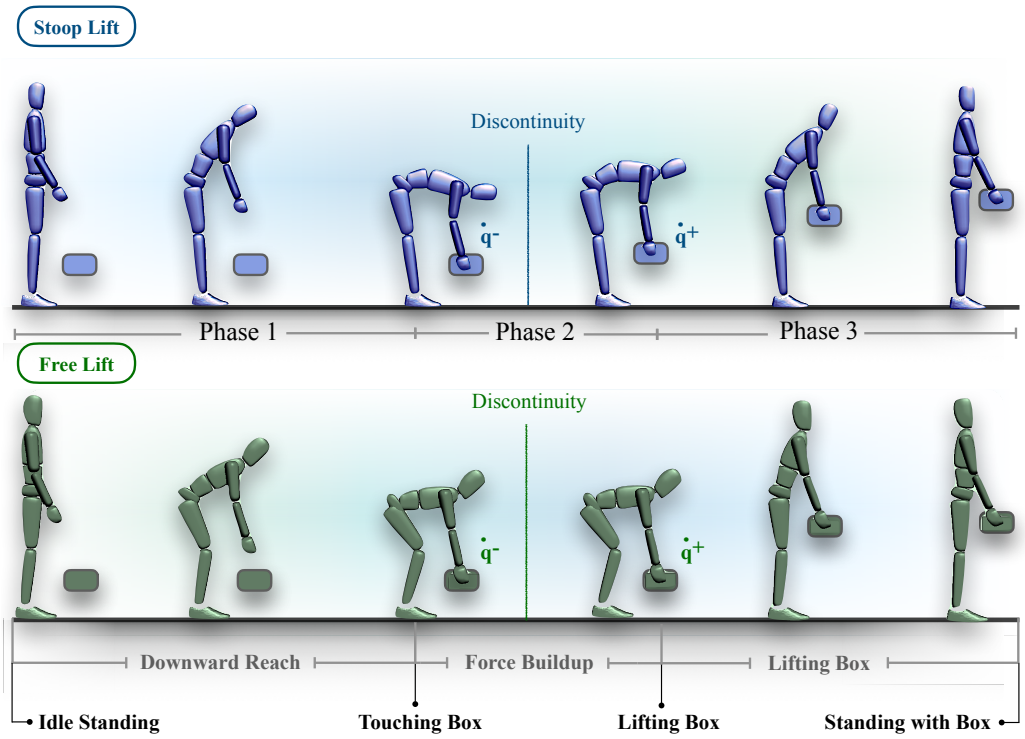

Figure 4.5: The three phases of the lifting problem with the start and end conditions. **Top:** A demonstration of the stoop lift where there is minimal knee, and high lumbar flexion. **Bottom:** A squat lift with high knee, and low lumbar flexion. The box in both cases is placed on a platform above the ground. Phase numbers and descriptions are indicated, as well as the discontinuity caused by the inelastic impact of the hand and the box at phase 2.

Based on the discontinuities of the contacts with the box as described in Subsection 4.4.3, this problem is split into a three-phase OCP, outlined in Table 4.2 and visualized in Figure 4.5. The sequence of motions applies both to problems solved with, and without exoskeleton support. The constraint sets involved in each or all

phases are explained in Subsection 4.5.3 providing details on their formulation and conditions.

4.5.2 Lifting Techniques

Both the experimental setup and the simulation procedures analyze two distinct lifting techniques: the stoop and the free lifts. In a stoop lift, the legs remain straight or only slightly bent at the knees, resulting in a more pronounced bend in the lower back, which reduces the natural lumbar lordosis. In contrast, the free lift, partly resembles that of a squat, since it involves deeper knee flexion while maintaining a straight or lordotic lower back, preserving the natural curvature of the lumbar spine. The difference of these lifts can be observed in Figure 4.5 along with the phases of the lifting problem.

Table 4.3: Summary of all virtual points used in the human, exoskeleton and box models as to facilitate constraint equations.

Point Name	Location
Points on the human model	
p^{HP}	*on the posterior side of the human pelvis*
p^{HT}	*on the posterior side of the human upper torso*
p^{HL}	*on the anterior side of the human thigh, above the knee joint*
p^{HH}	*on the middle of the human hand, in the palm*
p^{HFH}	*on the posterior point of the sole of the foot, at the heel*
p^{HFT}	*on the anterior point of the sole of the foot, at the toe*
Points on the exoskeleton model	
p^{EP}	*on the posterior side of the exoskeleton pelvis interface*
p^{ET}	*on the lower posterior side of the exoskeleton upper torso interface*
p^{EL}	*on the lower anterior inner side of the exoskeleton thigh interface*
Points on the box model	
p^{BH}	*on the vertical and horizontal centre of the box where the handle is*
p^{BB}	*on the bottom of the box in the horizontal centre*

4.5.3 Phase-Dependent Constraints

In OCP formulations, constraints ensure that solutions are feasible and adhere to the described model limitations. Path constraints apply continuously over the entire trajectory, restricting state or control variables at all times, like imposing upper and lower bounds on velocity or joint angles. Point constraints (or boundary constraints) apply at specific time points, such as initial or final conditions (e.g., start and end positions in a phase). These constraints can be coupled, involving multiple variables jointly, like the case of the exoskeleton being attached onto the human and enforcing periodicity in the solution, or decoupled, applying independently to individual variables (e.g., separate bounds on velocity and acceleration). Throughout the whole lifting motion, these sets of constraints are in place that characterize the physical boundaries of the multi-phase problem.

In order to accurately define coupled or loop constraints, between the various physical models within the problem, a set of virtual points is used as to defined the contacts made within the system; attaching the exoskeleton to the human, the human to the ground, and depending on the phase the box to the ground and the box to the human. Table 4.3 outlines the list of points used in the models and their descriptions.

Throughout the work in optimizing lifting motions, two main cases are explored: unassisted lifting without the exoskeleton and assisted lifting with the exoskeleton. Both cases share the same conditions regarding the constraints defined between the human, box and ground, whereas in the second case additional constraints apply to define the relationships between the human and the exoskeleton. The key path and point constraints that define the lifting motion and physical interactions between the models are outlined here.

Detailed interactions of a more dynamic nature involving the models of human and exoskeleton (described in Sections 4.3 and 4.4 are part of the modeling pipeline and the mathematical descriptions used to solve these interactions are contained within the optimal control code, both for the case of the LSQ fit to motion capture data, and the motion synthesis based on optimally minimizing lumbar torques.

Starting Conditions of the Lift

The starting conditions are a set of constraints for initializing the lifting motion, that set the posture of the human and defined the relationships between all the models. Lumbar joints orientations are set to their predefined lordotic path (see Section 4.1.1). The pelvis location is defined from the lower body segment lengths and its orientation is set according to recorded data. All other human joints (ankle, knee, shoulder, elbow) orientations are set to zero, ensuring a neutral starting posture.

All human joint velocities are set to zero, with the human starting from a resting position. The foot is set flat on the ground,

$$\mathbf{pos}(p^{HFH})_t z = 0, \quad \mathbf{pos}(p^{HFT})_t z = 0, \tag{4.22}$$

with zero starting velocities,

$$\mathbf{vel}(p^{HFH})_{tx,tz} = 0, \quad \mathbf{vel}(p^{HFT})_t z = 0. \tag{4.23}$$

The box is set at a sagittal distance d^{BH} from the human and vertical height d^{BG} from the ground, as recorded from the initial experiments,

$$\mathbf{pos}(p^{BB})_t x = d^{BH}, \quad \mathbf{pos}(p^{BB})_t z = d^{BG}, \tag{4.24}$$

with zero velocity in a resting state

$$\mathbf{vel}(p^{BB})_t x = 0, \quad \mathbf{vel}(p^{BB})_t z = 0. \tag{4.25}$$

The exoskeleton is fixed onto the human based on a set of translational coordinates on the predefined points of the exoskeleton and the respective points on the human,

$$\mathbf{pos}(p^{EP})_{tx,tz} = \mathbf{pos}(p^{HP})_{tx,tz}, \tag{4.26}$$

$$\mathbf{pos}(p^{ET})_{tx,tz} = \mathbf{pos}(p^{HT})_{tx,tz}, \tag{4.27}$$

$$\mathbf{pos}(p^{EL})_{tx,tz} = \mathbf{pos}(p^{HL})_{tx,tz}. \tag{4.28}$$

The orientations of the exoskeleton and human contact points need to align as well, which is realised through equating the dot product of the exoskeleton points' x vector to the human points' z vector for the trunk and lower thigh interface,

$$\mathbf{ori}(p^{ET})^T_{cx} \cdot \mathbf{ori}(p^{HT})^T_{cz} = 0, \tag{4.29}$$

$$\mathbf{ori}(p^{EL})^T_{cx} \cdot \mathbf{ori}(p^{HL})^T_{cz} = 0. \tag{4.30}$$

Initial experiments yielded a linear relationship between the exoskeleton's pelvis module and the human pelvis, at various lumbar angles, hence the exoskeleton pelvis interface is subject to the three cases mentioned in Section 4.3, related to its rotation about the human pelvis about the mediolateral axis. The rotational velocity about the same axis is not constrained, while the rest of the translational velocities including all the velocities of the other two interfaces, are set to match the corresponding ones of the human,

$$\mathbf{vel}(p^{EP})^T_{tx,tz} = \mathbf{vel}(p^{HP})^T_{tx,tz} = 0, \tag{4.31}$$

$$\mathbf{vel}(p^{ET})^T_{tx,tz,ry} = \mathbf{vel}(p^{HT})^T_{tx,tz,ry} = 0, \tag{4.32}$$

$$\mathbf{vel}(p^{EL})^{T}_{tx,tz,ry} = \mathbf{vel}(p^{HL})^{T}_{tx,tz,ry} = 0. \tag{4.33}$$

Constraints for All Phases

Some constraints are required to be imposed throughout the whole lifting motion, and are set on each phase. These are inequality constraints that make sure that positive ground reaction forces exist on the foot,

$$\mathbf{force}(p^{HFH}_{tz}) \geq 0, \tag{4.34}$$

$$\mathbf{force}(p^{HFT}_{tz}) \geq 0, \tag{4.35}$$

and maintain the horizontal forces on the foot within the friction cone,

$$\mathbf{force}(p^{HFH}_{tx}) \leq c_o f^{FG}(\mathbf{force}(p^{HFH}_{tz}) + \mathbf{force}(p^{HFT}_{tz}), \tag{4.36}$$

with $c_o f^{FG} = 0.8$ defining the coefficient of friction between the foot (shoe) and the ground. For the contacts between the human and the exoskeleton, limits are placed on the interaction forces, as explained in the following Section (4.4.4), for the trunk, pelvis and lower thigh points,

$$\mathbf{force}(p^{H}_{tx,tz,ry}) \leq F^{H}_{tx,tz,ry}, \tag{4.37}$$

by limiting forces that can be experienced on the points allocated on the human model.

First Phase Constraints

In addition to the constraints of the starting conditions and the constraints that apply through all phases, a positive ground reaction force is set in place on the box to ensure it rests on the ground,

$$\mathbf{force}(p^{BB}_{tz}) \geq 0. \tag{4.38}$$

Second Phase Constraints

The second phase starts by realising the connection between the point on the hand of the human to the point on the handle of the box,

$$\mathbf{pos}(p^{HH}_{tx,tz}) = \mathbf{pos}(p^{BH}_{tx,tz}), \tag{4.39}$$

while bringing the hand to a rest by zeroing the velocities,

$$\mathbf{vel}(p^{HH}_{tx,tz}) = 0. \tag{4.40}$$

Consequently, the horizontal interaction forces of the hand and the box are limited within the friction cone formed,

$$\mathbf{force}(p_{tz}^{BH}) \leq c_o f^{HB} \mathbf{force}(p_{tx}^{BH}), \tag{4.41}$$

with $c_o f^{FG} = 0.6$ defining the coefficient of friction between the hand and the box (handle). Finally, the net vertical force on the box is set to be positive in order to avoid the human resting on the box,

$$\mathbf{force}(p_{tz}^{BB}) \geq 0. \tag{4.42}$$

In the end of the second phase, the hand velocities are released, leading to the final phase.

Third Phase Constraints

The final phase of the problem starts with the box leaving the ground, and applies the end conditions of the lifting motion. The joint positions (state vector entries) are set to a standing posture like the starting conditions, and the velocities are brought to a rest along with the velocity of the box. The final phase ensures that the human returns to an idle standing position, at rest, while holding the box close to the body.

4.6 General Optimal Control Problem Formulation

Within this optimal control framework, the aim is to identify control functions that minimize a specified cost function, while satisfying a collection of constraints that involve differential-algebraic equations. This formulation leads to an optimization problem of infinite dimension. The general structure of a multi-phase optimal control problem, spanning a time interval $I = [t_0, t_M] \subset \mathbb{R}$, and governed by differential-algebraic equations, can be expressed as follows:

$$\min_{x,z,u,p} \Psi[x, z, u, p] := \Phi_{M_i}(x(t_M), z(t_M), p) + \sum_{i=0}^{M-1} \int_{t_i}^{t_{i+1}} \Phi_{L_i}(x(t), z(t), u(t), p) dt \tag{4.43}$$

subject to:

$$\dot{x}(t) = f_i(x(t), z(t), u(t), p), \tag{4.44}$$

$$x(t_i^+) = h_i(x(t_i^-), z(t_i^-), p), \tag{4.45}$$

$$a_i(x(t), z(t), u(t), p) = 0, \tag{4.46}$$

$$h_i(x(t), z(t), u(t), p) = 0, \tag{4.47}$$

$$g_i(x(t), z(t), u(t), p) \geq 0, \quad t \in [t_i, t_{i+1}], \quad i = 0, \ldots, M-1, \tag{4.48}$$

$$r_{eq}(x(t_0), z(t_0), u(t_0), \ldots) = 0, \tag{4.49}$$

$$r_{ineq}(x(t_0), z(t_0), u(t_0), \ldots) \geq 0. \tag{4.50}$$

In this formulation, the cost function Ψ (Equation 4.43) is dependent on the state variables $x : I \to \mathbb{R}^n$, the algebraic variables $z : I \to \mathbb{R}^m$, the control variables $u : I \to \mathbb{R}^a$, and a set of parameters $p \in \mathbb{R}^p$. If both Φ_M and Φ_L are active in the optimization framework, the cost function is called a Bolza problem, where $\Phi : \mathbb{R}^n \times \mathbb{R}^m \times \mathbb{R}^p \to \mathbb{R}$ represents the terminal cost (Lagrange term), and $\Psi : \mathbb{R}^n \times \mathbb{R}^m \times \mathbb{R}^a \times \mathbb{R}^p \to \mathbb{R}$ represents the Mayer term. Within the context of optimizing the SPEXOR exoskeleton, the Lagrange cost function is used.

The dynamic behavior of the system is captured by the differential equations in Equation 4.44, where the function f_i differs between phases. Phase changes are handled using the algebraic conditions described in Equation 4.45. Additional algebraic constraints are included in Equations 4.46 and 4.47, representing the equality conditions, while inequality constraints are captured in Equation 4.48, which typically enforce limits on the state and control variables.

Boundary conditions and other pointwise constraints are described in Equations 4.49 and 4.50 , which enforce conditions at specific time points t_i, including the initial and terminal times. Box constraints are imposed to bound the state and control variables,

$$x(t) \leq \bar{x}(t), \quad u(t) \leq \bar{u}(t). \tag{4.51}$$

The optimal control problem can take on various forms depending on the specific application and the variables to be optimized. In the context of the SPEXOR project, two primary formulations are considered: one focused on motion reconstruction using a LSQ approach, and the other centered on generating synthetic motion by minimizing variables such as the lumbar torque control at the L5/S1 joint. These formulations are instrumental in studying the biomechanics of lifting tasks and optimizing human-exoskeleton interaction. Reference motions, derived from empirical data, provide critical insight into both understanding human movement and guiding the optimization of control strategies in exoskeleton-assisted motions. With this in mind, accurately capturing and analyzing lifting motions becomes a crucial step in informing and validating optimal control formulations.

In summary, this chapter laid the foundation for modeling assisted lifting motions, focusing on the dynamics of human-exoskeleton interactions, the mechanical properties of both systems, and the physical constraints that govern these interactions. By accurately describing the human body, the SPEXOR exoskeleton, and the envi-

ronment in which the lifting task occurs, the groundwork has been established for investigating how these models can be optimized for effective assistance. Finally, the fundamental formulation of an OCP is described, subject to constraints.

Chapter 5 delves into applying optimal control via a LSQ approach to reconstruct recorded liftingm otions and generate optimal support provided by the exoskeleton. The LSQ problem is solved both for unassisted human, and exoskeleton-assisted human with the aim of minimizing lumbar torques while closely following the recorded motion of the unassisted human experiments. In addition, it also addresses parameter identification for the dynamic models discussed here, and evaluates the actuator's torque dynamics in real-world conditions.

Optimizing Exoskeleton Support Based on Recorded Motions

5

The main aim of the SPEXOR project involved the manufacturing of a BSE that can optimally and comfortably provide support to a user performing a lifting task, while minimizing torques about the lumbosacral joint. The first step in deducing the dynamic properties of the support required - when and by how much - includes investigating how humans tackle the task of lifting a box from a given height, via motion-capture experiments. This chapter delves into the processes of collecting kinematic and dynamic data and reconstructing the lifts, modeling and simulation as to provide important insights on the human biomechanics involved in this process, and optimal control in order to investigate and fine-tune the contributions of the SPEXOR exoskeleton when applied to a reference lifting motion. The next section outlines the process of recording these motions, which serves as the foundation for refining the exoskeleton's support and enhancing its interaction with human biomechanics.

5.1 Recording Lifting Motions

Motion capture experiments were carried out in the early stages of the project by the SPEXOR project partner Science2Practice (Ljubljana, Slovenia). Three male participants ($1.69 \pm 0.005m, 72.4 \pm 3.27kg$) were recruited to perform a study of lifting a 10 kg box from an elevated position, by executing once a stoop lift, and once a 'free' lift resembling more that of a squat. For the first lift, participants were given clear instructions on maintaining their lower limb as straight as possible while flexing with their back to bend forward. For the second lift they were instructed to perform what felt better for them while encouraged to flex their legs as well and keep a straight back. Kinematics of the body segments and the box were recorded by recording the position of markers on the participant and the box, using an OptoTrack system (Northern Digital Inc., Canada). Ground reaction forces were collected using Kistler force plates (model 9260AA6 from Kistler, Winterthur, Switzerland). The experiment was conducted at the University of Primorska in Slovenia and approved by the national medical ethics committee of the Republic of Slovenia (0120-199/2016-2, KME 93/04/16) with written and informed consent from the participants. The data was collected for the humans alone, without the aid of the exoskeleton, as shown in Figure 5.1. The recorded lifting motion was categorized into the three lifting phases and the durations of each phase were recorded and given as input in the OCP formulation.

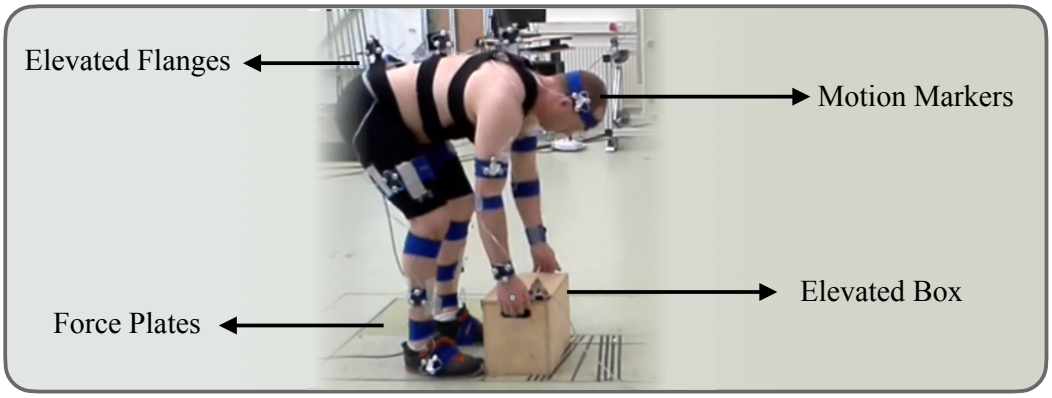

Figure 5.1: Motion capture experiments carried out by SPEXOR project partner Science2Practice (Ljubljana, Slovenia). One participant performing a squat lift during the experiment rounds for capturing reference lifting motions.

The participants performed the lifts in a randomized order and their kinematics were captured. Marker clusters were formed in the shape of a triangle and attached on rigid plates before being fitted on the participants, making every cluster able to determine the location and orientation of a given segment. Three clusters were placed along the spine (lumbar, thoracic and cervical), one cluster was placed on each of the shoes, upper and lower leg, hip, head, and upper and lower arm. Two clusters were placed on the sides of the box and one marker was placed on the outside of the hand. The marker clusters on the lower, middle and upper back were placed on elevated flanges as to enhance visibility and not obstruct the participants from the lifting motion. Cameras recorded the markers at a frequency of 44 Hz and ground reaction forces of the feet were recorded via the force plates at a rate of 1 kHz. Marker and force plate data were filtered using a second-order bidirectional Butterworth filter with a cutoff frequency of 5 Hz. A kinematic fitting of the physical markers translated the motion into virtual markers, yielding accurate joint angles for solving IK.

The reference motions from recorded experiments involving three participants, form the foundation of this work, serving as a crucial input across the following two chapters. These reference motions are applied in several key areas:

1. **Reconstructing reference lifting motions** of the unassisted human and applying the SPEXOR exoskeleton to optimize the torque profile generation of the hydraulic actuator, with an evaluation of the exoskeleton's impact.
2. Using the reference motion as a basis for **synthesizing optimal lifting motions**, both with and without the SPEXOR exoskeleton, and comparing the effects of the exoskeleton as opposed to optimally executed lifting motions.

Within this chapter, the first case is investigated by applying a LSQ optimization algorithm to reconstruct the recorded motion of the human, and to apply the

exoskeleton on the human model as to optimally minimize lumbar torques. For solving both of the above cases, a general optimal control problem formulation is applied. In Chapter 6, attention shifts toward the latter application and the biomechanical advantages offered by a back-support exoskeleton, addressing the critical question of how much external support is truly necessary, and whether optimal lifting techniques alone can mitigate excessive lumbar torques.

5.2 Reconstructing Human Lifting Motions

Accurately reconstructing human motion is critical to the success of the optimization process, as the precision of the derived kinematics and dynamics directly influences the validity of the results. In the context of the SPEXOR project, the reconstruction of lifting motions plays a pivotal role in both assessing the interaction between the human and exoskeleton and refining the exoskeleton's support strategy. This section outlines the methods employed to reconstruct human lifting motions, beginning with a kinematic fitting procedure used to extract joint angles from experimental marker data, followed by the formulation of the LSQ optimal control problem to optimize the exoskeleton's support during lifting tasks.

5.2.1 Kinematic Fitting

In previous work conducted within the SPEXOR project, a kinematic fitting procedure was employed to extract joint angles from marker data [157]. Building upon earlier work [135], this approach defined virtual markers on subject-specific models. The virtual markers were based on a static trial and their exact placement was carefully determined using subject photos. Since small deviations between the virtual and recorded marker clusters could lead to large errors in the calculated joint angles, the approach was extended to account for both position and orientation discrepancies.

This method minimized the deviation in both the position and orientation of the virtual markers relative to the motion capture markers. The optimization was performed for each captured frame, minimizing the sum of weighted errors in marker position and orientation. The fitting was executed using the IK solver from the RBDL library [141], leveraging the Levenberg-Marquardt algorithm for greater accuracy in the fitting process. The IK procedure yielded results in terms of joint angles which are used throughout the rest of this study as input and reference comparison to the optimization reconstruction and synthesis results.

5.2.2 Least-Squares Optimal Control Problem

For the support optimization of the exoskeleton, the stoop lifts were investigated within the motion reconstruction framework. The modeling pipeline incorporates

the human and exoskeleton models described in Chapter 4, Sections 4.1 to 4.3. Two LSQ OCPs are solved: one with the unassisted human lifting motions which is reconstructed from the recorded reference data, and one with assisted-human which integrates the exoskeleton model on the prior OCP. The multiphase lifting problem described in Section 4.5 is applied where the human starts from an idle standing position, reaches forward to grab the box, builds up force while in contact with the box and ends the lift by coming back to an upright position with the box, as shown in Figure 5.2, with the SPEXOR exoskeleton.

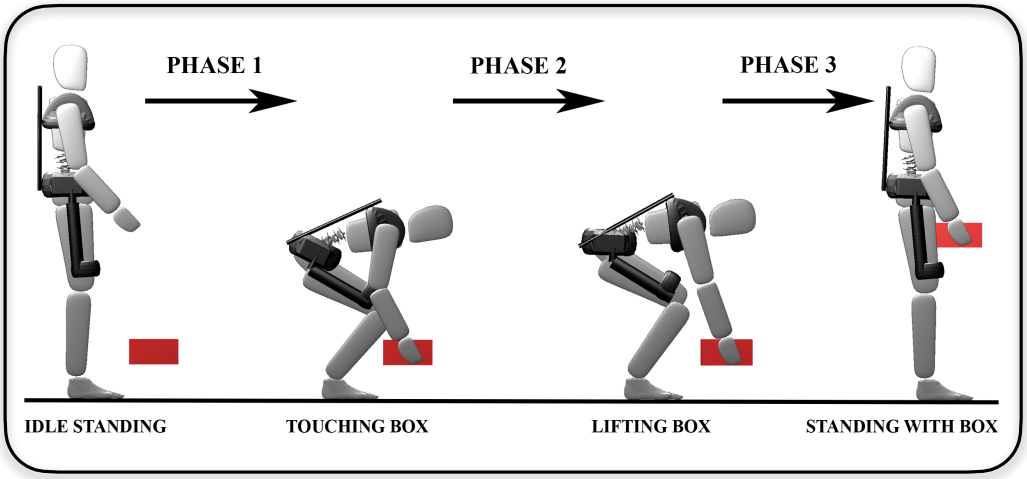

Figure 5.2: The lifting motion is formulated as a three phase problem with and without the exoskeleton: **Phase 1:** Reaching the box from idle standing to touching the box, **Phase 2:** Force buildup, from touching the box to starting to lift, and **Phase 3:** Lifting the box to come to a standing position with the box. Image sequence taken from the LSQ-OCP with the exoskeleton.

The following LSQ problems of the unassisted-human and assisted-human serve as a reference comparison for joint angles and torques, and an exoskeleton actuator optimization method respectively. The first OCP formulation describes the minimization of physical motion capture and virtual model markers,

$$\Phi_i(\mathbf{x}, \mathbf{u}, \mathbf{p}) := \sum_{i=0}^{M-1} \left\| \mathbf{q}^H(t_{im}) - \mathbf{q}^{\text{REF}}(t_{im}) \right\|_2^2 \tag{5.1}$$

along with a small regularization term on the human joints,

$$w_1 \int_{t_i}^{t_{i+1}} \left\| \bar{\mathbf{u}}^{\mathbf{ALL}} \right\|_2^2 dt \tag{5.2}$$

as to minimize redundancy in the optimization problem. In this multiple shooting problem, the number of nodes is given by M_i where i is the current phase, and the sum of the shooting nodes is denoted by M. The vectors $\mathbf{q}^H$ and $\mathbf{q}^{\text{REF}}$ denote the computed and tracked positional coordinates respectively, the distance of which

is minimized in Equation 5.1. The time for each phase is fixed and is prescribed according to the experimental times recorded (Table 5.1. The control vector $\bar{\mathbf{u}}^{\mathbf{ALL}}$ is the normalized human joint torques vector which takes a weight $w_1 = 0.000001$ in the LSQ problem. The weight for the regularization term holds a small value as to maximize the tracking accuracy of the solution while balancing the overall human generated torques and imposing a smoothing effect on the controls of the OCP.

Table 5.1: Phase durations for the recorded 'free' lift of the three participants, without assistance.

	Phase 1 (s)	Phase 2 (s)	Phase 3 (s)	Total (s)
P1	1.34	0.12	1.42	2.88
P2	1.14	0.14	1.20	2.48
P3	1.24	0.14	1.18	2.56

5.2.3 Fitting Accuracy Results of the LSQ

The accuracy of the least-squares fitting plays a crucial role in the motion reconstruction process, as it ensures that the optimized motion closely aligns with the recorded reference data. In this section, the results of the inverse kinematic fitting and the least-squares optimal control problem LSQ-OCP are presented, focusing on the precision of the kinematic fit between the reconstructed human motion and the original motion capture data. This comparison is vital for validating both the human-only optimization and the assisted human-exoskeleton lifting motions, as described in the preceding section. The quality of the fitting directly impacts the overall success of the motion reconstruction and support optimization, making it a key factor in assessing the exoskeleton's performance during stoop lifts.

Throughout the optimization process the weight of the regularization term has been adjusted and a trade-off between accuracy and smoothness of the solution has been selected. The results report a close agreement between the inverse kinematic and the LSQ solution. Figure 5.3 presents an example of the fitting comparison for one of the participants, for the pelvis location (floating base) and rotation, as well as the hip, knee, shoulder and elbow rotations, while Figure illustrates the collective deviations of distances and angles between the two solutions for all three participants.

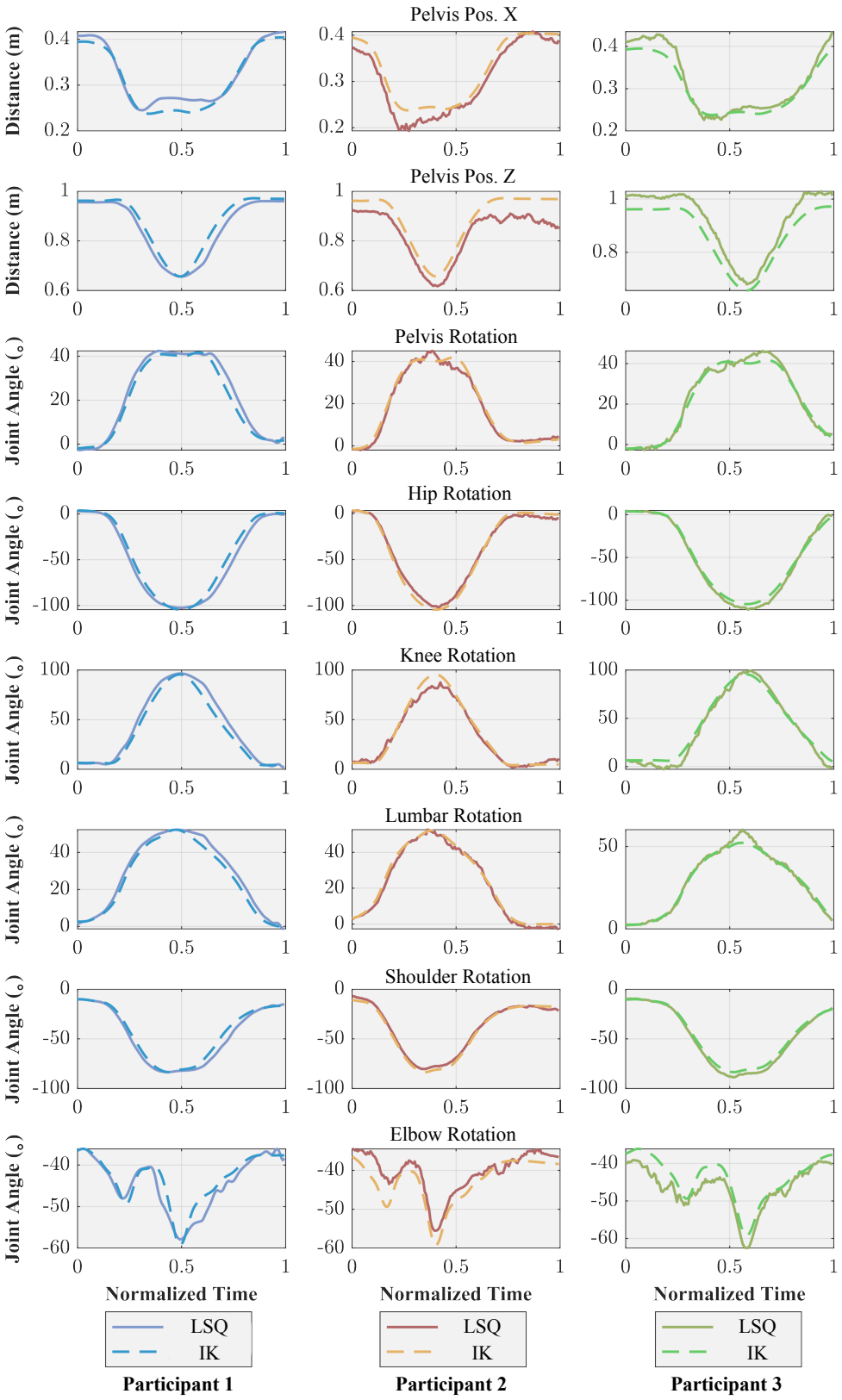

Figure 5.3: Comparison of the inverse kinematic and LSQ fitting accuracy based on the experimental data for all three participants. The horizontal and vertical locations of the pelvis as the floating base are presented in the first two subplots, while the rest of the subplots depict the correlation between joint angles at the pelvis, hip, knee, lumbar, shoulder and elbow. The dashed lines present the IK solution and the continuous lines the LSQ result. Left to right: participant one to three.

All participants' motions were computed using the same cost-functions and weights for the regularization term. Table 5.2 reports all results for mean angle and position errors, including the mean angle error of each joint as a percentage of its maximum ROM. The pelvis horizontal (sagittal plane) and vertical positions track the accuracy of the fit in the Cartesian coordinate space and present with low error ($0.0118 - 0.0401m$) compared to the IK solution. The mean angle errors for the joint tracking of the pelvis, hip, knee, lumbar, shoulder and elbow joints present a close fit to the kinematic solution as well, with a mean error of $2.21[3.08]°$ across all joints and participants. A comparison of the mean angle error as percentage of the maximum ROM during the lifting motion yields an error of 2.54% across all joints and all participants, which is a moderately low value for the kinematic fit of the LSQ solution. As the floating base of the model, the pelvis accumulates errors from all connected joints, making its vertical position particularly sensitive to deviations in hip and lumbar motions. This central role amplifies the impact of joint-level fitting errors, contributing to the slightly higher Z-position error observed.

Table 5.2: Mean and standard deviation angle and position errors for the kinematic fit of the LSQ solution compared to the IK solution.

Variable	Participant 1		Participant 2		Participant 3		Mean of Participants		% ROM[1]
	Mean	STD	Mean	STD	Mean	STD	Mean	STD	
Pelvis X (m)	0.00973	0.0120	0.0153	0.0135	0.0103	0.00669	0.0118	0.0107	–
Pelvis Z (m)	0.0236	0.0185	0.0484	0.0158	0.0482	0.0183	0.0401	0.0175	–
Pelvis θ (°)	1.86	2.21	0.252	1.60	0.222	1.40	0.778	1.74	2.39
Hip θ (°)	4.56	4.53	0.898	4.56	3.49	5.66	2.98	4.92	2.36
Knee θ (°)	4.72	4.49	2.61	3.62	2.35	4.12	3.23	4.08	2.90
Lumbar θ (°)	2.40	1.76	1.11	1.63	1.79	1.75	1.77	1.72	2.57
Shoulder θ (°)	3.21	3.32	3.94	4.91	1.18	4.82	2.78	4.35	2.46
Elbow θ (°)	1.05	1.96	1.89	1.59	2.27	1.36	1.74	1.64	2.55
						Mean (Rotations)	2.21	3.08	2.54

[1] *The mean angle error as a percentage of the maximum range of motion of the specific motion throughout the lifting problem.*

Following the validation of the least-squares solution for the human lifting a box across all three participants, the methodology and simulation results are used in the subsequent sections to optimize the support provided by the hydraulic actuator in the exoskeleton-assisted OCP. These results will also serve as a basis for comparing the kinematics and dynamics of the assisted motion, as the simulation aligns the exoskeleton with the reference motions reconstructed for each participant. Section 5.3 details the optimal control formulations used for optimizing the exoskeleton and

reports the results on lumbar torque minimization of various cases used including different pelvis interface configurations and hydraulic piston velocities.

5.3 Optimizing Human-Exoskeleton Interactions

The LSQ problem is extended by fitting the exoskeleton model on the human model based on the modeling dynamics and constraints described in Sections 4.3 and 4.4 respectively. A new least-squares OCP is formulated which still tracks the kinematics of the recorded motions of the three participants while complementing their efforts with the SPEXOR exoskeleton. To this aim, the general formulation of the kinematic tracking OCP incorporates a new term which is added to the cost function Equations 5.1 and 5.3,

$$w_2 \int_{t_i}^{t_{i+1}} (u^{pump})^2 dt \tag{5.3}$$

serving as a regularization term on the exoskeleton's actuator torque, ensuring that the exoskeleton is not used unnecessarily. u^{pump} denotes the already normalized control signal of the hydraulic actuator's pump and takes a small weight within the cost function of $w_2 = 1x10^{-9}$. The small value of w_2 is chosen to ensure that kinematic tracking remains the primary objective and avoid over-constraining the optimization, while allowing for natural variation in actuator usage based on the lifting task dynamics.

Even though the main goal of fitting the exoskeleton onto the human is to reduce the lumbar torques, the first stage of the exoskeleton optimization procedure remains purely a LSQ problem. This will serve later as a comparison and reference. While solving for optimal exoskeleton torque profiles based on minimal lumbar torques, the following objectives are investigated:

1. Imposing interaction force limits between exoskeleton interfaces and human (Subsection 4.4.4).
2. Comparing the two cases of low and high piston velocity and their effect on lumbar torque (Subsection 4.2.2).
3. Comparing the three cases of the exoskeleton pelvis interface and human pelvis coupling dynamics (Section 4.3).

5.3.1 Comparative Dynamic Interactions Analysis

When solving the assisted LSQ problem the general formulation is a combination of cost functions 5.1, 5.2 and 5.3 in which the exoskeleton dynamics are incorporated in the problem and the OCP employs the exoskeleton's torque as support to the human model. In this formulation, the six different cases stated in Table 5.3 of the combined system dynamics are tested, as described in Sections 4.3 and 4.2.2.

In order to assess the efficacy of each of these cases in lowering lumbar moments about the L5/S1 joint, two biomechanical metrics contributing to low back pain (Subsection 1.1.3) are evaluated: CLBL and PLBL. The first metric concerns the integrated lumbar moment throughout the whole lifting motion, while the latter denotes the peak lumbar moment experienced during the lifting motion.

Table 5.3: The six cases investigated in the dynamic interactions analysis. The relationship between the exoskeleton pelvis interface and the human pelvis, as well as the hydraulic actuator's piston velocity are examined in all possible combinations.

Case	Pelvis Interface Model	Piston Velocity
1	Constraint-based with prescribed angle limits	Fast (51 ms to 90% extension)
2	Constraint-based with prescribed angle limits	Slow (100 ms to 90% extension)
3	Force-based with rotational spring dynamics	Fast (51 ms to 90% extension)
4	Force-based with rotational spring dynamics	Slow (100 ms to 90% extension)
5	Constraint-based with fixed interface	Fast (51 ms to 90% extension)
6	Constraint-based with fixed interface	Slow (100 ms to 90% extension)

5.3.2 Results of Comparative Dynamic Interactions Analysis

The exoskeleton model was fitted onto the human model in the LSQ reconstruction of the recorded reference motions of the three participants performing a stoop lift, as to compare and incorporate optimized dynamics relationships between the exoskeleton pelvis interface and the human pelvis, as well as to deduce the optimal piston speed for the hydraulic actuator. The cost function comprised only of the least-squares fit, and two regularization terms on the controls of the human and exoskeleton.

The results of the simulations are summarized in Table 5.4, reporting the reductions of CLBL and PLBL for all six cases of human-exoskeleton dynamic interactions, compared to the LSQ solution of the unassisted human. The cumulative torques corresponded to the integrated lumabar moment (area under the curve) whereas the peak torques correspond to the maximum achieved moment throughout the lift. Regarding the minimization of lumbar moments, all cases performed relatively well, even without a cost function specifically targeting the minimization of lumbar torques. As it is evident from Figure 5.4, there is a noticeable reduction both in cumulative and peak low back loads. The lumbar moment figures show the comparison of the peak torques from literature where participants performed lifting motions of a 10.5 kg box [159].

Table 5.4: Reduction of cumulative low back loads (CLBL) and peak low back loads (PLBL) for each of the six cases.

Case No.	Reduction of CLBL (%)			Mean	Reduction of PLBL (%)			Mean
	P1	P2	P3		P1	P2	P3	
1	26.3	18.4	24.5	23.1	18.2	14.6	15.2	16.0
2	24.8	17.1	23.0	21.6	19.1	15.3	15.9	16.8
3	23.4	16.9	22.2	20.8	16.3	12.8	14.3	14.5
4	21.9	14.3	19.7	18.6	17.2	13.4	15.3	15.3
5	21.5	14.6	20.9	19.0	15.1	11.4	12.6	13.0
6	20.2	13.5	18.8	17.5	15.8	12.3	13.2	13.8

Comparing the results in Table 5.4 it is clear that the free pelvis interface produces the most desirable outcome in the context of combined lumbar torques (Reductions of 23.1% in CLBL and 16.0% in PLBL), as it successfully manages to provide support from the hip joint actuator to the lumbar, thus alleviating it from high torques. To this end, and judging from the results of the simulations, it is also speculated that the hydraulic actuator helps in increasing the support from the back beams as well, since it can help counter-rotate the pelvis and increase the bending moment created from the beams.

A close look at the actuator and beam profiles in Figure 5.4 shows that the actuator is engaged throughout the motion, affecting the behavior of the beams as well, especially in the middle phase of the lift, where the hip angle is at its highest. It is also clear that the actuator does not violate its physical limits, and is able to provide around 50 Nm of support on both hips. Additionally, when comparing piston speeds, we can see that the two extremes behave rather similarly, with the slow piston speed being more successful in decreasing peak torques, whereas the faster piston speed manages to decrease more the cumulative torques.

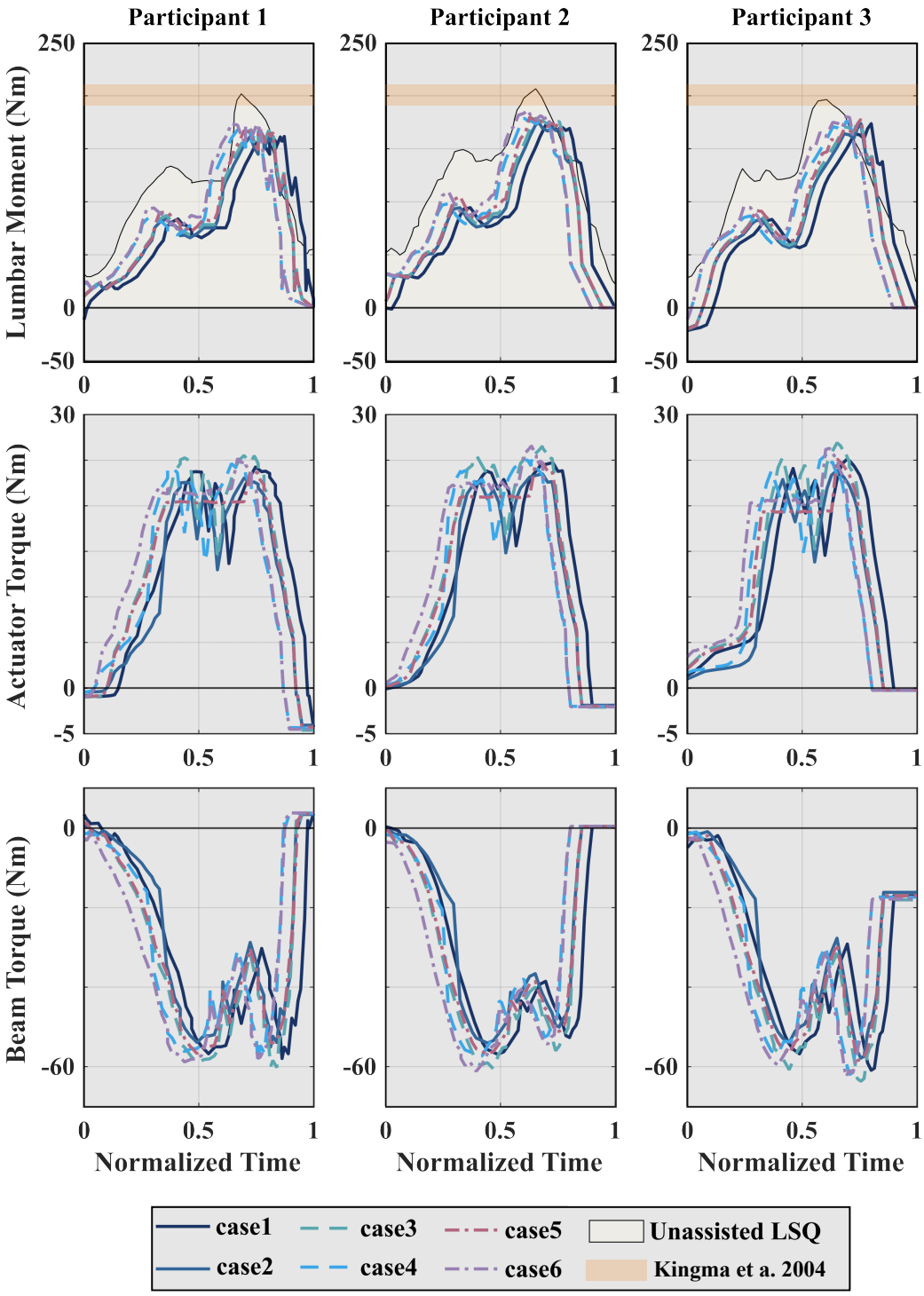

Figure 5.4: Comparison of the performance on reducing lumbar torques, for the six different cases of human-exoskeleton dynamic interactions. Lumbar moments (row 1), actuator torques (row 2) and beam torques (row 3) are presented for all three participants (columns 1 to 3) performing the assisted lift. Shaded region represents literature values for lumbar moments from Kingma et al. [159].

5.3.3 Validation of Interaction Force Limits

Force limits are imposed as part of modeling the dynamic human-exoskeleton interactions in the simulation regime (see Section 4.4.4). Figure 5.5 illustrates the resulting contact forces between the exoskeleton model's interfaces and the human model for Case 1, showing that for all contact points the limits [158] on the interaction forces are respected within the optimization framework.

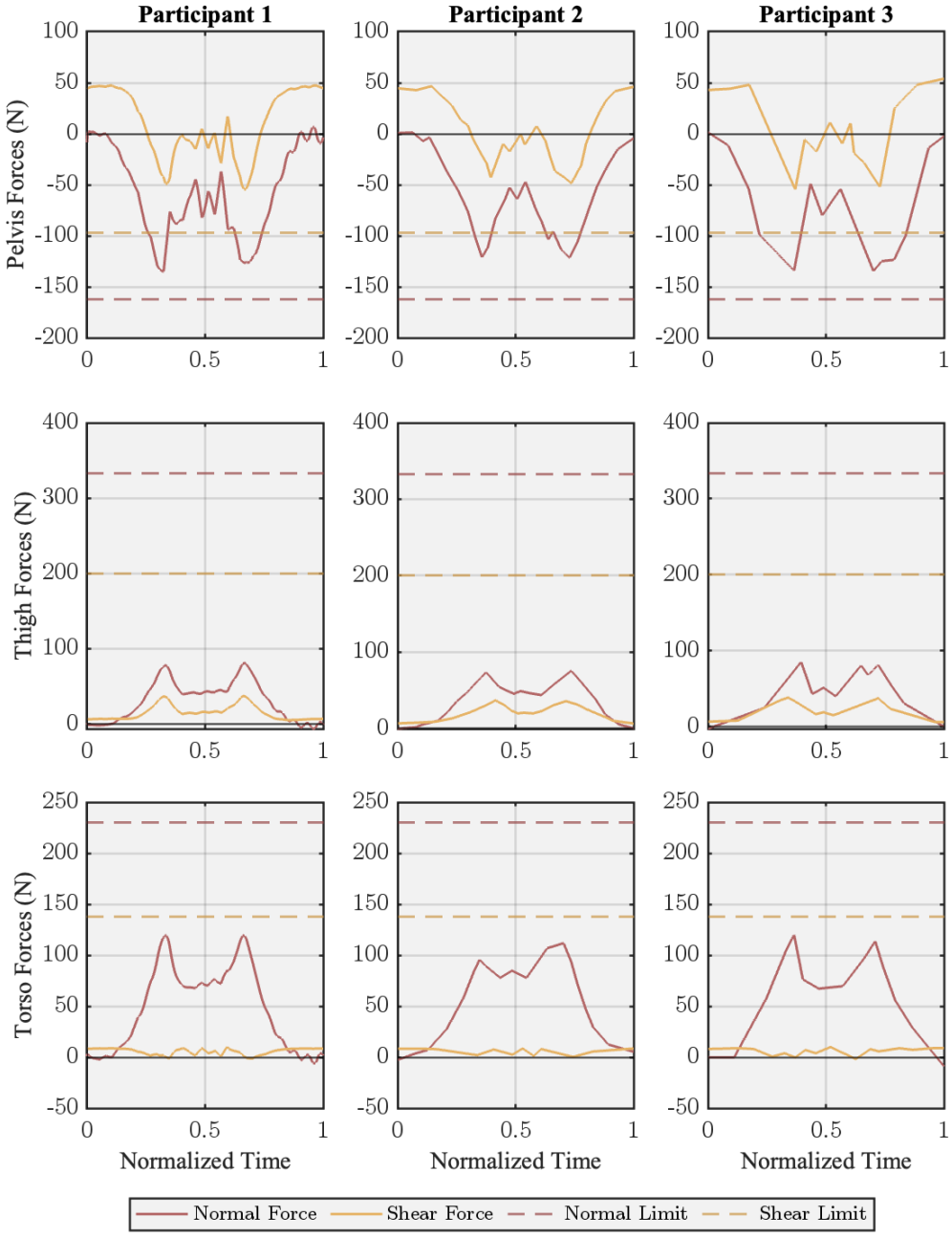

Figure 5.5: Results on interaction force limits imposed on the optimization algorithm as constraints, for Case 1. Left to right: Participants 1 to 3. Top to bottom: Pelvis, thigh and torso interfaces. Results include both shear and normal forces as well as the respective limits of each.

As seen in the plots, both the normal and shear forces are consistently below the imposed thresholds, maintaining values within the bounds of 162 N and 97 N for the pelvis, 333 N and 200 N for the thigh, and 230 N and 138 N for the torso interface, respectively. These limits, derived from pressure tolerance experiments, were crucial in ensuring the user's comfort and safety during the simulated lifting tasks. By staying within these predefined force limits, the exoskeleton provides adequate support without overloading any contact points, validating the effectiveness of the force-limiting approach outlined in the thesis. These findings reinforce the importance of considering interaction forces not only for mechanical efficiency but also for improving the user's experience by reducing discomfort and preventing excessive pressure at attachment points.

5.3.4 Conclusion of Dynamic Interactions Analysis

The analysis confirmed that the constraint-based pelvis interface with angle limits resulted in the highest reductions in lumbar torques, aligning with initial expectations. The particular case also presents the most realistic representation of the real-world problem, as it respects actual angle limits derived from empirical data without introducing additional dynamics relationships that are not well defined.Consequently, the exoskeleton design was finalized with this configuration, allowing free rotation, within bounds, about the y-axis between the exoskeleton and human pelvis. This configuration remains unchanged in the subsequent computations, where the pelvis interface remains unconstrained in the optimal control formulations.

Regarding piston velocity, the results indicate that a non-linear optimal velocity profile may be beneficial. Specifically, a high piston velocity was effective in reducing CLBLs, while a slower velocity reduced PLBLs. Thus, a strategy that lowers piston velocity during the middle phase of the lift, when the hip angle and PLBLs are at their maximum, could be advantageous. However, since the difference between the velocity profiles was not substantial, the high piston velocity was selected for future computations, prioritizing CLBLs reduction due to its potentially greater impact on mitigating low back pain risks. Hence, dynamic human-exoskeleton interactions from here on after, are described using the definitions of *case 1*. Lastly, the interaction force limits imposed in the algorithm to ensure user comfort have been validated, confirming their effectiveness in maintaining a safe and comfortable user experience.

5.3.5 Minimizing Lumbar Loads of Recorded Lifting Motions with Exoskeleton Support

The work in this chapter so far dealt with optimizing the dynamic human-exoskeleton relationships, as well as the behavior of the passive and active elements of the

SPEXOR exoskeleton based on realistic outcomes and maximum support to the human, without violating comfort limits. Within the groups of optimizing support, while still following the recorded lifting motions of the three participants, another study took place, introducing a term within the LSQ function as to specifically target lumbar load minimization. It is important to note however, that an appropriate weight should be assigned to such a term, in order to give it an appropriate role within the objective function that does not affect the result of the least-squares term. This begs the question of the best trade-off: a weight that manages to further reduce lumbar loads while still following the kinematics of the recorded motion.

Appendix A includes the detailed methodology for conducting this exploratory study, assessing the dependency of the solution on the cost function weights. The results of the comparison of three distinct weights for the lumbar minimization term and their effect on both lumbar moments and kinematics are reported. Conclusively, the medium weight (0.001) on the lumbar torque minimization term produced the best balance between reducing lumbar loads and preserving recorded kinematics, achieving a 25.9% reduction in CLBL and 18.1% in PLBL, with moderate kinematic deviations (RMSE = 2.19° for L5, 14.6° for hip). These findings emphasize the importance of balancing load reduction with kinematic preservation for safer and more compliant lifting strategies, where the exoskeleton follows the natural movement of the user. It is interesting to question however, whether the lifting patter of an untrained user is indeed the most ergonomic way, or whether the exoskeleton should instead adjust the kinematics of the user.

5.4 Intermediate Conclusions

The studies outlined in this chapter confirm the effectiveness of reconstructing lifting motions via OCP formulations, which align closely with IK solutions. This validates the precision of the motion reconstruction and forms the foundation for optimizing the interaction between the human and the exoskeleton. Additionally, optimizing human-exoskeleton dynamic interactions revealed that the free pelvis interface configuration and high piston velocity (Case 1) offer the best reductions in lumbar moments. These findings suggest that the dynamic interaction between the human and exoskeleton is crucial for achieving optimal support during lifting tasks.

These findings highlight the importance of refining both human-exoskeleton dynamic interactions and the exoskeleton's torque contributions for minimizing lumbar stress. This sets the stage for further investigation, where motion prediction through optimal control is explored to evaluate whether improvements in lifting technique or exoskeleton assistance provide the greatest benefits in reducing both CLBLs and PLBLs.

Optimizing Lifting Technique vs. Exoskeleton Assistance

6

This chapter introduces the investigation into a more synthetic approach of lifting motions, where the exoskeleton's active support elements are optimized in parallel to optimized lifting techniques. Based on the findings and outcomes of Chapter 5, the main focus of this chapter is to explore the concepts of minimizing lumbar torques via a pure optimal control approach, with reference motions been used suggestively as to set the starting states of each multiple shooting node, and inform the duration of each phase of the lifting problem accordingly. Within this framework, three different cost functions are explored that target CLBLs, PLBLs and a combination of the two, while comparing their effects to the least-squares (LSQ) solutions of unassisted and assisted motions. Finally, the importance of optimal technique and training is assessed, compared as an alternative to external support provided by BSEs, in the aims of verifying the effectiveness and necessity of these devices.

The work on this chapter reflects our previously published work on optimizing the SPEXOR exoskeleton [139] and extends the impact of the study by reproducing the results for more participants, thus contributing important insights and outcomes on the optimal support of lifting motions. Section 6.1 outlines the new OCP formulation for motion synthesis and explains the main changes to the LSQ approach, both for optimizing the lifting technique, and exoskeleton assistance, for all three participants. Section 6.2 describes the cost-function generation based on the quantity minimized in each case described in Section 6.1, reports the results on the comparison study including the reference LSQ motion results and discusses their significance. Finally, Section 6.3 concludes the main outcomes of this chapter and summarizes the overall contributions of Part II in relation to the SPEXOR Project.

6.1 Optimal Control Problem Formulation for Motion Synthesis

This section outlines the procedure of formulating an optimal control framework as explained above, in order to incorporate a minimization term on the lumbar torques of the human model. The goal of this minimization is to fully engage the passive and active elements of the exoskeleton as to successfully minimize lumbar loads. The

general optimal control framework remains the same as described in Section 4.6, aiming to only minimize the Lagrangian cost function (part two of Equation 4.43),

$$\min_{x,z,u,p,t} \sum_{i=0}^{M-1} \int_{t_i}^{t_{i+1}} \Phi_{L_i}(x(t), z(t), u(t), p)dt \tag{6.1}$$

containing the appropriate lumbar torque minimization terms depending on the case. The OCP remains subject to predefined constraints as before,

$$\dot{x}(t) = f_i(x(t), z(t), u(t), p), \tag{6.2}$$

$$x(t_i^+) = h_i(x(t_i^-), z(t_i^-), p), \tag{6.3}$$

$$a_i(x(t), z(t), u(t), p) = 0, \tag{6.4}$$

$$h_i(x(t), z(t), u(t), p) = 0, \tag{6.5}$$

$$g_i(x(t), z(t), u(t), p) \geq 0, \quad t \in [t_i, t_{i+1}], \quad i = 0, \ldots, M-1, \tag{6.6}$$

$$r_{eq}(x(t_0), z(t_0), u(t_0), \ldots) = 0, \tag{6.7}$$

$$r_{ineq}(x(t_0), z(t_0), u(t_0), \ldots) \geq 0. \tag{6.8}$$

that include constraint sets imposed at each phase, throughout the whole duration of motion, and boundary constraints such as the values of the states at the multiple-shooting node intervals, where in this case take the values from the recorded reference motions of the three participants.

The general formulation reported here applies both to the human and the human with the exoskeleton OCPs, with varying cost function combinations. The models describing the human and the exoskeleton remain the same as the LSQ formulation, including the dynamic relationships of the interactions between the two models, deduced in Chapter 5. A comparison framework is set up for this study, shown in Figure 6.1, where the recorded motions of the human, along with the LSQ result of the exoskeleton-assisted lifting motions, are compared to the results from evaluating a number of cost functions that synthesize optimal motions, which aim to minimize lumbar loads.

6.1.1 Minimizing Lumbar Loads

When analyzing experimental data of low back loads, the CLBL is calculated as the integral of the lumbar torques at the L5/S1 joint, assuming the whole area under the moment curve [160]. Although this approach is perfectly suited for analysis, it is rather ill-suited as a cost function for an optimal control problem because it is signed: it is possible for the model to produce a flexion torque and thus reducing the CLBL after lifting. While using the absolute value would prove adequate, integrating

the torque of the lumbar squared manages to penalize even larger torque values. This new term,

$$\int_{t_i}^{t_{i+1}} \bar{\mathbf{u}}^{\mathbf{lumbar}} dt \tag{6.9}$$

is responsible for minimizing the controls of the lumbar torques of the human model for the custom spine model joints $\bar{\mathbf{u}}^{\mathbf{lumbar}}$ T12/L1, L1/L2, L2/L3, L3/L4, and L5/S1, according to the dynamic chain described in Subsection 4.1.1. The entries of $\bar{\mathbf{u}}^{\mathbf{lumbar}}$ are normalized according to the maximum possible torque values of the respective lumbar joints.

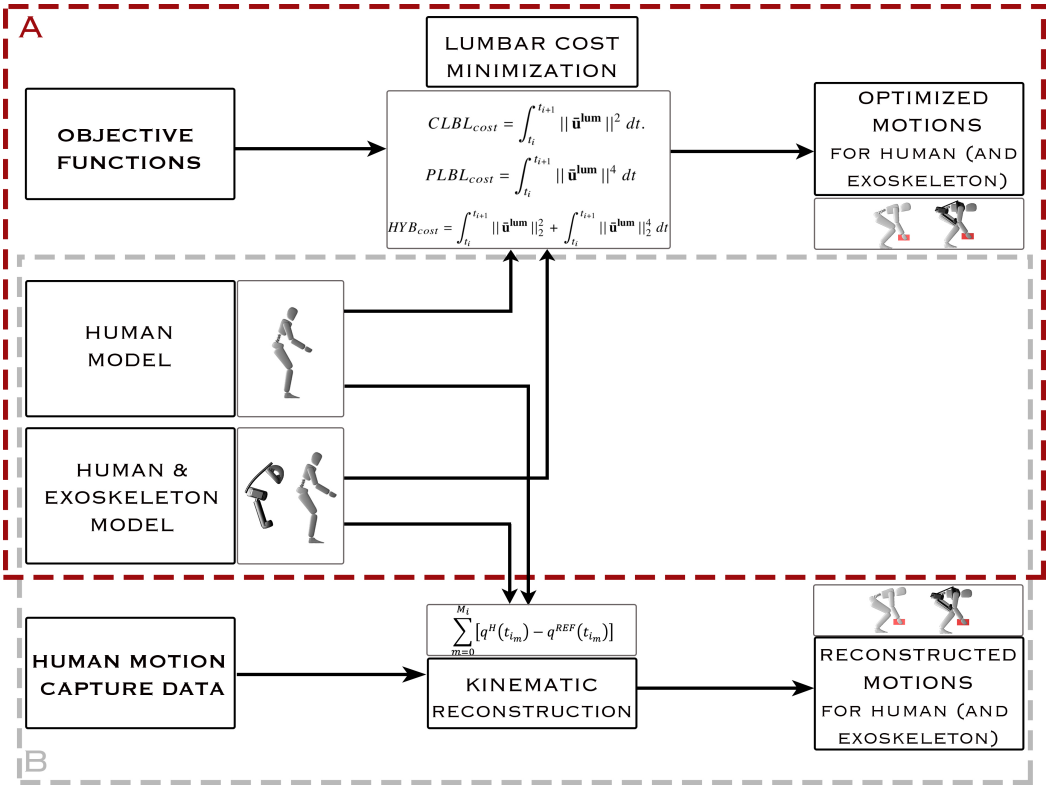

Figure 6.1: A comparative framework comprising of two optimization approaches: (A) a prediction through optimization of human-only and human-with-exoskeleton lifts, and (B) a dynamic reconstruction of human-recorded free-squat lifts for both human-only and human-with-exoskeleton lifting motions, based only on human capture data.

6.2 Cost Function Evaluation for Assisted and Unassisted Lifting Motions

This section outlines the comparative approach between reconstructed least-squares and optimally synthesized motions for both human-only and human-with-exoskeleton lifting tasks. In the human-only case, recorded motions are compared against synthesized motions generated by minimizing various cost functions. Similarly, in

the human-with-exoskeleton case, the reconstructed exoskeleton-assisted motions are evaluated against synthesized ones. Three distinct cost functions—$CLBL_{cost}$, $PLBL_{cost}$, and HYB_{cost}—are employed to investigate their effectiveness in minimizing cumulative low-back loads (CLBLs) and peak low-back loads (PLBLs). These comparisons aim to assess the impact of optimal control strategies on reducing lumbar loads and improving lifting techniques, both with and without the assistance of an exoskeleton.

The risk of low-back injury can be reduced by improving lifting technique and by using an exoskeleton [49]. Two of the biomechanic metrics that have been associated with the risk of injury to the lower back are CLBL and PLBL. In this study, simulation is used to examine how effective training, and an exoskeleton, are at reducing the cumulative and peak low back loads during a lift of a 10 kg box. The contributions of the improved technique alone, and those with the exoskeleton assistance, are then compared to the human-only reference motion reconstructed from motion capture data, as well as between themselves. The cost functions we use do not only change the motion of the human in order to decrease the risk of injury, but they affect the way the exoskeleton supports the human as well, in order to help decrease the risk of injury.

6.2.1 Cumulative and Peak Low Back Loads

A few studies exist in literature aiming to investigate how various loading conditions can affect the lower back and increase the risk of low back pain. Coenen et al. [31] report that repetitive lifting and bending tasks contribute most to LBP [160], as it causes the accumulation of microdamage to the tissue through CLBLs [30]. Apart from CLBLs, instantaneous damage can be caused to the lower back by PLBLs. Both of these quantities are typically highest at the L5/S1 lumbosacral joint [31], the origin of the range of motion of the spinal column. Risk factors based on the L5/S1 extension moment (such as CLBL and PLBL) are both easy to calculate and capture the risk associated with many different specific injuries because the loads applied to the ligaments, disks, vertebrae, and muscles of the back scale with the L5/S1 extension moment [32].

Even though there has been a lot of modeling and simulation work done to learn more about back injury [143, 161, 162], much of this work is based on inverse-dynamics data taken from real people lifting, and therefore cannot predict how someone might use a novel exoskeleton. The few optimal control studies that have been done to predict new lifting motions [163], do not combine human and exoskeleton models. The limited amount of work that includes an exoskeleton [153, 164], however, does not consider the effects of training, nor risk factors related to low-back injury. Additionally, no simulation work has been found that examines the effect of lifting technique on the risk of low-back injury.

Within the framework of this thesis work and the grounds of the SPEXOR project, this chapter explores the risk of low-back injury in a comparative approach: lifting using experimentally measured technique vs. lifting with optimal lifting technique; and lifting without any aids vs. lifting with the assistance of an exoskeleton. Hence, three different optimal lifting techniques are evaluated, that minimize three different risk factors of lifting: (a) CLBLs, (b) PLBLs, and a weighted sum of both CLBLs and PLBLs (a hybrid approach). Additionally, the effects of assistance are evaluated by simulting the lift using two differently system models: (1) a model of the human participants, and (2) a model of the human participants wearing the SPEXOR exoskeleton.

6.2.2 Cost Functions for Optimizing Technique

When investigating the unassisted human lifting motions, the aim is to find appropriate cost functions that manage to produce lifting motions that minimize lumbar torques without the aif of an exoskeleton. In order to minimize the cumulative loads of the L5/S1 joint, the term used in Equation 6.9 within the LSQ is called again, where the lumbar torques are squared, in order to apply more emphasis on the CLBL result on higher loads. This term including the normalized lumbar vertebrae torque values is considered as the cost value of the CLBL,

$$CLBL_{cost} = \int_{t_i}^{t_{i+1}} \left\| \bar{\mathbf{u}}^{\mathbf{lumbar}} \right\|_2^2 dt. \tag{6.10}$$

Since the motion of the 5 vertebrae is coupled by 4 constraint equations, it is possible to drive the lumbar spine using only a subset of the joints, but this is physiologically unrealistic. By summing across the moments developed by each joint, we ensure that the final load distribution does not favor one vertebra at the expense of the other joints.

When analyzing experimental data, the PLBL is evaluated as the maximum, or peak value, of the torque vector of the L5/S1 joint, over a time duration of interest [165]. Two studies by Coenen et al. [165] and Jäger et al. [166], suggested instead to evaluate the risk of PLBLs by assessing its cost as the integral of the L5/S1 moment, much like the CLBL cost, but raised to a higher power in order to further penalize peak values within the optimization problem,

$$PLBL_{cost} = \int_{t_i}^{t_{i+1}} \left\| \bar{\mathbf{u}}^{\mathbf{lumbar}} \right\|_2^4 dt. \tag{6.11}$$

With the aim of finding motions that minimize the PLBL cost, Equation 6.11 raises the integral of the L5/S1 torque to the fourth power.

Finally, a third term is considered, which simply sums Equations 6.10 and 6.11,

$$HYB_{cost} = w_h \int_{t_i}^{t_{i+1}} \left\| \bar{\mathbf{u}}^{\mathbf{lumbar}} \right\|_2^2 dt + w_h \int_{t_i}^{t_{i+1}} \left\| \bar{\mathbf{u}}^{\mathbf{lumbar}} \right\|_2^4 dt \tag{6.12}$$

hypothesizing that this term is able to reduce both factors simultaneously, generating the best trade-off between all three cost functions. The two terms take equal weight coefficients w_h within the cost function.

Within all cost functions, a small regularization term is included that includes all joint torques,

$$REG_{human} = w_{rh} \int_{t_i}^{t_{i+1}} \left\| \bar{\mathbf{u}}^{\mathbf{ALL}} \right\|_2^2 dt \tag{6.13}$$

as to ensure that the result converts to a minima [167]. The weight coefficient w_rh takes the value of $1x10^{-3}$.

All three cost functions are solved both for the case of the human lifting unassisted, and assisted by the model of the SPEXOR exoskeleton. While the exoskeleton actuator's optimization remains the byproduct of the terms minimizing lumbar loads, the small regularization term from Equation 5.3 is still included,

$$w_e \int_{t_i}^{t_{i+1}} (u^{pump})^2 dt \tag{6.14}$$

serving as a regularization term on the actuator's torque, to ensure that the actuator is not used unnecessarily. u^{pump} denotes the normalized control signal of the hydraulic actuator's pump and takes a weight of $w_e = 1x10^{-9}$.

6.2.3 Results of Cost Function Evaluation

Three types of objective functions have been evaluated and compared with each other, as well as the least-squares solution, both for the unassisted, and assisted human lifting scenarios and OCPs. A total of six OCPs were formulated and the results are reported in this subsection. The results are evaluated by comparing the CLBL and PLBL reductions and taking into consideration phase duration times and lumbar flexion angles, actuator and beam contributions for the human-assisted solutions, as well as hip joint torques and rotations. A comparison is made between:

- the unassisted human optimized lifting techniques to the reconstructed reference motion of the unassisted participants (Section 5.2.2),
- the assisted-human optimized lifting techniques to the reconstructed reference motion of the participants with the fitted exoskeleton assistance (Section 5.3),
- all four study blocks: unassisted human with tracking (LSQ); unassisted human with improved lifting technique; assisted-human with tracking (LSQ); and assisted-human with improved lifting technique (Section 6.2).

The post-processing and statistical analysis on the means and standard deviations of the results of the three participants were conducted using MATLAB.

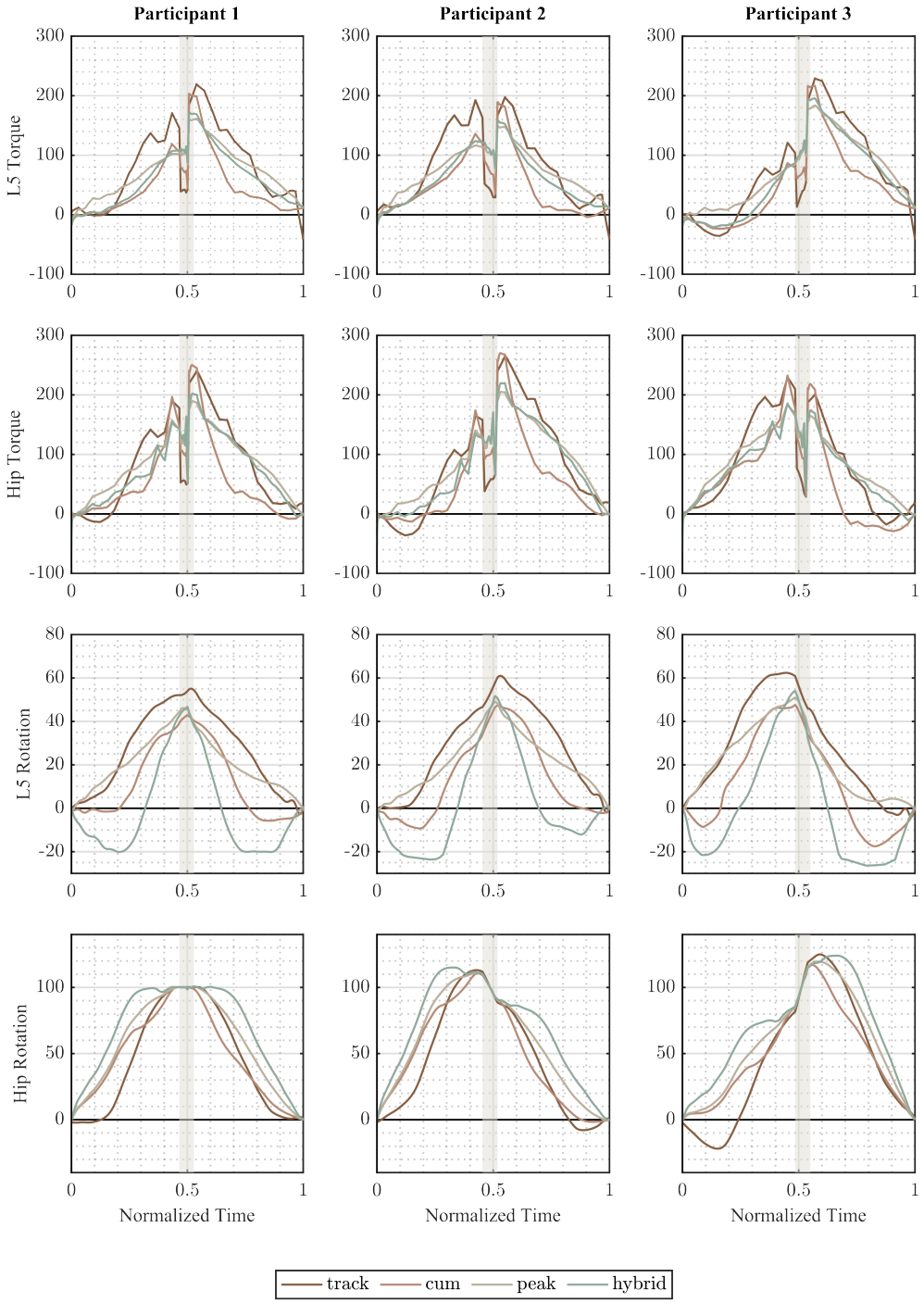

Figure 6.2: A comparison of improved technique performance for CLBL, PLBL and hybrid costs against recorded performance, for all participants (left to right) according to L5 torque, hip torque, L5 flexion angle, and hip angle (top to bottom). The shaded region highlights the duration of the middle phase.

Comparison of Improved Lifting Techniques to LSQ

The simulated improvements to lifting techniques were able to reduce both the CLBL and PLBL risk factors for the unassisted lifts (Table 6.1 and Figure 6.2). The recorded participants performed lifts with an average cumulative torque of $213Nms$ and an average peak torque of $214Nm$ according to the LSQ reconstruction of their lifts, close to the peak torque range reported by Kingma et al. [159] of $199 \pm 12Nm$. The simulation results indicate quite a high average reduction of $35.4 \pm 9.76\%$ of CLBLs for the $CLBL_{cost}$ OCP, with a more moderate reduction of $22.2 \pm 5.22\%$ of PLBLs for the $PLBL_{cost}$ OCP. The HYB_{cost} OCP results in a trade-off between the two values where PLBLs are reduced by $18.2(4.19)\%$ and CLBLs by $20.4(1.33)\%$.

Table 6.1: Reductions in CLBL and PLBL costs based on improved lifting techniques for the unassisted human OCPs, as compared to the LSQ solution of the reconstructed motion for each participant.

Participant	LSQUnassisted		$CLBL_{cost}$		$PLBL_{cost}$		HYB_{cost}	
	CLBL (NmS)	*PLBL (Nm)*	*CLBL (NmS)*	*PLBL (Nm)*	*CLBL (NmS)*	*PLBL (Nm)*	*CLBL (NmS)*	*PLBL (Nm)*
1	243	210	130	195	210	176	190	182
2	172	198	118	189	168	149	139	158
3	223	234	160	216	199	174	178	185
% Reductions Mean (STD)			35.4 (9.76)	6.46 (1.68)	10.8 (2.72)	22.2 (5.22)	20.4 (1.33)	18.2 (4.19)

The lumbar flexion angles of the human reconstruction fall well within the reported values from Kingma et al. [159] ($39 \pm 14°$). In another study [168], 265 participants were trained to perform a lift of a 12 to 13 kg box to improve their lifting technique. The average peak moment was reduced from $225Nm$ to $178Nm$ throughout the training period. It is therefore evident that this reduction is similar to the reduction of the PLBL in the three participants of this study, validating the human-only synthesized motions that reduced the peak moment from an average of $214Nm$ to $166Nm$ in the $PLBL_{cost}$ OCP. For the CLBL metric, the $CLBL_{cost}$ OCP was reduced from an average of $213Nms$ to $136Nms$. These simulation results indicate that training and improved technique, with no further assistance, can indeed produce considerable reductions in cumulative loads, but rather modest reductions in peak loads.

Comparison of Assisted Lifting to LSQ

Larger reductions in both CLBLs and PLBLs are observed in the assisted human-with-exoskeleton OCPs (Table 6.2 and Figure 6.3). While it was not possible to reduce the average PLBL of the three participants more than 22.2% in the human-only simulation, the exoskeleton-assisted simulation was able to achieve a high of $38.4 \pm 2.01\%$ recution in the $PLBL_{cost}$ OCP, and for the $CLBL_{cost}$ OCP the

CLBLs were reduced by an even higher $46.9 \pm 10.8\%$, giving evidence of considerable improvements with external exoskeleton assistance. In addition, the exoskeleton was able to reduce further both CLBL and PLBL in all cases when compared to the human-only reconstructed motions. There appears to be a greater effect in reducing these metrics depending on the cost function used, since even though there are minor reductions in the assisted LSQ lift because of the exoskeleton, the combination of the exoskeleton assistance and the improved technique, considerably increases these reductions. As with the unassisted cost functions, HYB_{cost} offers a balanced trade-off between the two metrics, with reductions of $25.9 \pm 12.9\%$ in cumulative and $32.7 \pm 4.51\%$ in peak loads.

De Looze (2016) et al. reports similar peak moment reductions of 19.5% and 15% when participants use the PLAD [56] and BNDR [69] exoskeletons. In contrast, Koopman et al. [54] reports a 5 to 10% reduction in peak moments when using the Laevo exoskeleton. In the context of active back-support exoskeletons, the XoTrunk exoskeleton [169] achieves a peak moment reduction of 17%. The passive SPEXOR exoskeleton, produced a maximum of 23 ± 3% reduction in the peak L5/S1 extension moment [54] for ten subjects using different lifting techniques, including exoskeleton assistance. Based on the simulation results of the active SPEXOR exoskeleton, a reduction of 20.5% is predicted (according to the CLBL cost function) to 34.8% (according to the PLBL cost function).

Table 6.2: Reductions in CLBL and PLBL costs based on improved lifting techniques for the exoskeleton-assisted OCPs, as compared to the human-only LSQ solution of the reconstructed motion for each participant.

Participant	LSQAssisted		$CLBL_{cost}$		$PLBL_{cost}$		HYB_{cost}	
	CLBL (NmS)	*PLBL (Nm)*	*CLBL (NmS)*	*PLBL (Nm)*	*CLBL (NmS)*	*PLBL (Nm)*	*CLBL (NmS)*	*PLBL (Nm)*
1	217	177	101	165	193	138	148	148
2	164	174	103	154	138	125	149	123
3	206	208	135	192	166	157	167	162
% Reductions Mean (std)	7.66 (3.02)	13.0 (2.42)	46.9 (10.8)	20.5 (2.27)	22.0 (3.14)	34.8 (2.01)	25.9 (12.9)	32.7 (4.51)

The lumbar flexion angle is determined by the cost function as a dominant factor, as seen in Figure 6.3. Over the three participants, the $CLBL_{cost}$ cost function engages slightly smaller angles throughout the lift but reaches the highest peak in the middle phase, and appears to end the downward reach in a faster time than the rest. Consequently, since cumulative torque is a direct function of time this would make sense for reducing it on the overall lifting motion. The $PLBL_{cost}$ function on the other hand seems to engage slightly higher angles throughout the lift while

reaching the lowest peak angle of the four OCPs, hence proving that the magnitude of the lumbar flexion angle is directly proportional to the magnitude of the torque.

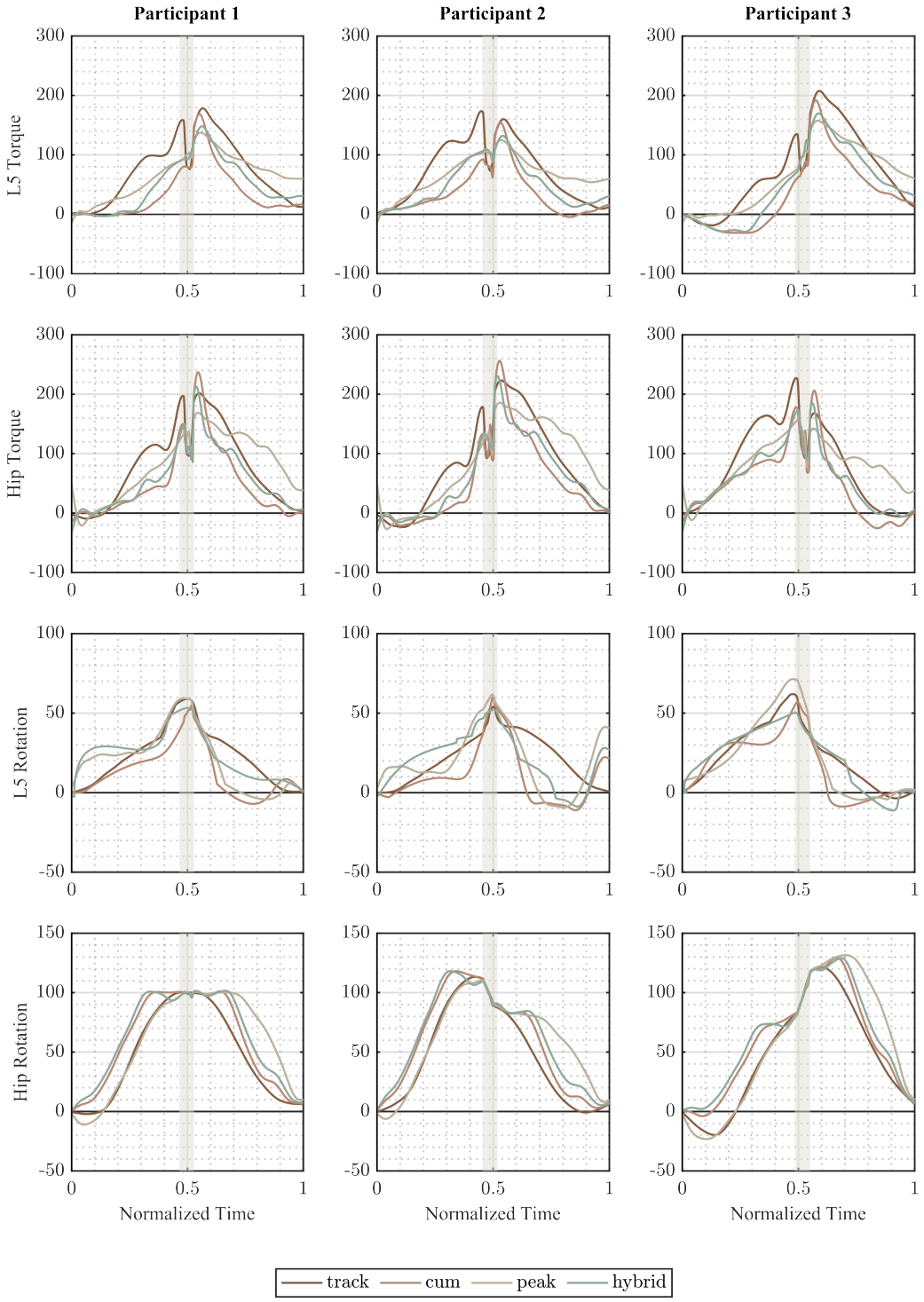

Figure 6.3: A comparison of exoskeleton assistance and improved technique performance for CLBL, PLBL and hybrid costs against recorded performance, for all participants (left to right) according to L5 torque, hip torque, L5 flexion angle, and hip angle (top to bottom). The shaded region highlights the duration of the middle phase.

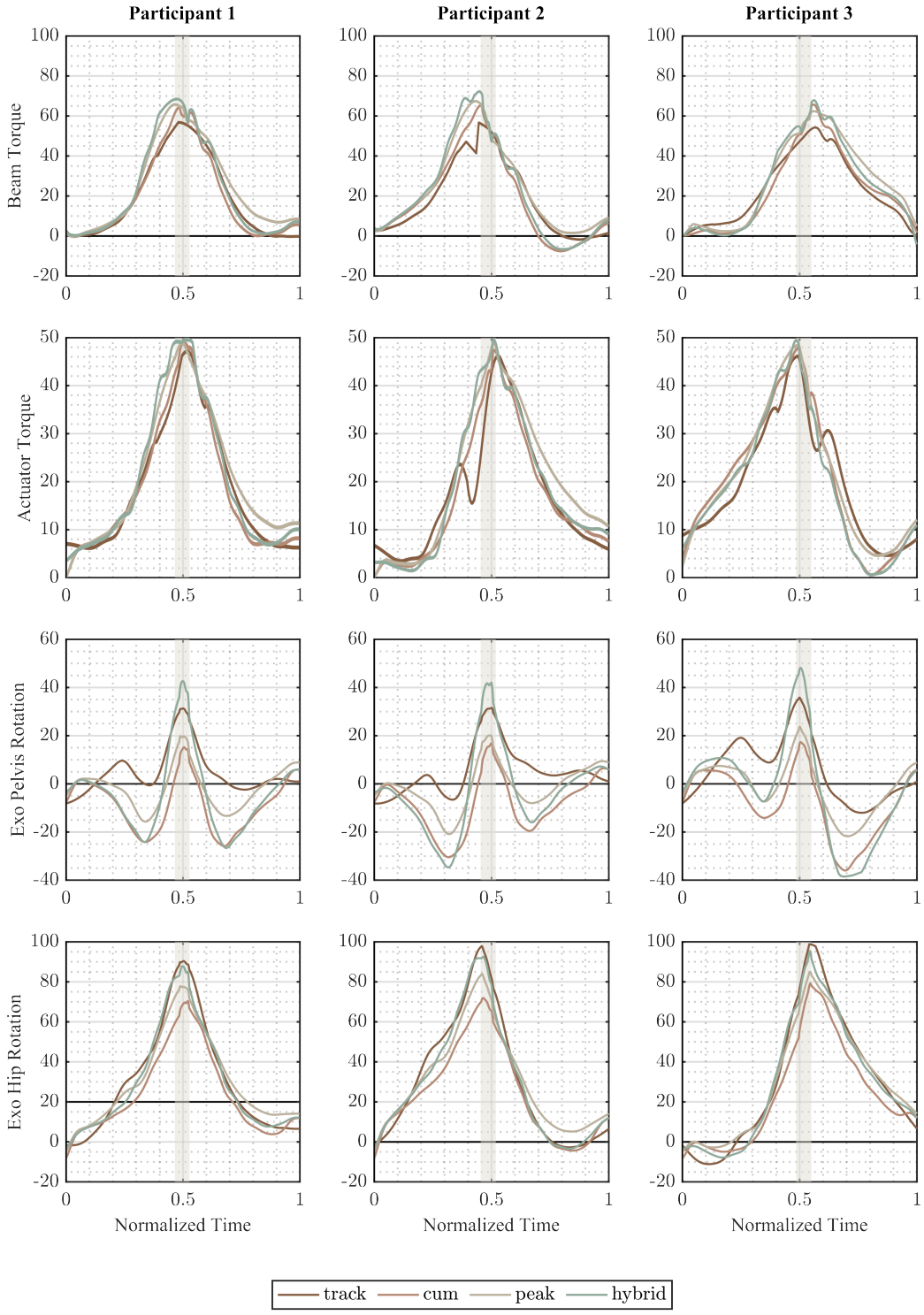

Figure 6.4: Exoskeleton contributions to lumbar load reduction during lifting tasks. Values reported for three participant OCPs (left to right) for beam torque, actuator torque, exoskeleton pelvis interface rotation and exoskeleton hip interface rotation (top to bottom).

The results underscore the effectiveness of the exoskeleton in mitigating lumbar loads during assisted lifts, particularly during the critical middle phase where peak torques typically occur. The pronounced reduction in both cumulative and peak

low-back loads with the exoskeleton's intervention, points to its potential in enhancing ergonomic safety across varied lifting tasks. Additionally, the observed variability in reductions among participants highlights the importance of tailoring exoskeleton settings to individual biomechanics to maximize efficacy. These results not only validate the utility of exoskeletons in reducing biomechanical stress but also emphasize the potential for optimizing lifting techniques through adaptive, personalized assistance settings, enhancing both safety and performance in manual handling tasks.

Exoskeleton Contributions to Lifting Techniques

The exoskeleton support elements' behavior can be observed in Figure 6.4, illustrating the contributions for each cost function for all three participants. The actuator and beam profiles exhibit similar behaviors for all cost functions as they are engaged throughout the motion to provide the optimal support. Particularly for the the $CLBL_{cost}$, the actuator torque occupies a smaller area under its curve compared to the $PLBL_{cost}$ which engages the actuator for a longer period. All three cost functions synthesizing the motion achieve the highest value provided by the two actuators ($50N$), while not saturating it, subject to the constraints applied in the OCP formulation.

Due to the free motion of the pelvis interface, the hydraulic actuator manages to engage a higher torque profile for the beams by applying a counter-torque at the base of the pelvis interface, carried out through the hip joint. This is evident by the higher torque profiles of the three synthesized cost functions, when compared to the reconstructed LSQ exoskeleton-assisted solution. The exoskeleton pelvis interface rotation differs to the human pelvis as a function of the free-rotating nature, and remains within the bounds of the physical limits of rotation.

The exoskeleton's support is most pronounced during the middle phase of the lift, where the lumbar torque peaks. This targeted assistance helps in reducing the peak lumbar torques substantially, as evidenced by the reductions in cumulative and peak low-back loads during these phases. The results also highlight the variability in exoskeleton performance across different participants, suggesting that individual customization of exoskeleton settings could further optimize the reduction in back loads. The specific contributions of the exoskeleton's actuators, particularly in terms of torque and angle adjustments, align with the optimized lifting techniques to enhance overall lifting safety and efficiency.

Comparison of Assisted Lifting to Improved Lifting Techniques

The three cost functions, designed to synthesize optimized motion, have shown promising results in both unassisted and exoskeleton-assisted scenarios across all participants. These findings set the stage for a deeper investigation into whether

improved lifting techniques alone can sufficiently mitigate the risk of low-back injury, or if the incorporation of exoskeleton assistance emerges as a necessary intervention to manage low-back loads. This comparative evaluation not only delves into the effectiveness of each approach but also explores the potential of combining these strategies to optimize lifting safety.

Table 6.3 presents the phase durations derived from both the recorded and optimized motion data of participants, providing insights into the impacts of three cost functions and the use of the SPEXOR exoskeleton on lifting durations. The least-squares (LSQ) solution for assisted motion closely mimics the participants' movements, resulting in consistent lift durations across all phases. In contrast, the remaining three cost functions significantly modify the duration required to complete the lifts, both in assisted and unassisted scenarios. Notably, the $CLBL_{cost}$ OCPs consistently achieve the quickest lifts, aiming to minimize cumulative loading as effectively as possible. Conversely, the $PLBL_{cost}$ OCPs extend the duration of the lifts, reducing peak load intensities by distributing the load over a longer period. Across all participants and cost functions, lifts performed with exoskeleton assistance generally require more time than their unassisted counterparts. This increase can be attributed to several factors, including the dynamics of the exoskeleton and the interactions between the human and the device. Specifically, the torque-angle profile of the actuator, constrained by the maximum velocity of the hydraulic piston, and the interaction forces at the human-exoskeleton interfaces play critical roles in shaping the lift dynamics.

Table 6.3: Lift durations (in seconds) for both the unassisted and assisted motion of all three participants, for the four cost functions.

Participant	Unassisted Motion				Assisted Motion			
	LSQ	$CLBL_{cost}$	$PLBL_{cost}$	HYB_{cost}	LSQ	$CLBL_{cost}$	$PLBL_{cost}$	HYB_{cost}
1	2.88	2.35	2.58	2.55	2.88	2.80	3.04	2.81
2	2.48	2.07	2.31	2.26	2.48	2.38	2.61	2.42
3	2.56	2.15	2.43	2.35	2.56	2.47	2.74	2.51
Mean	2.64	2.19	2.44	2.39	2.64	2.55	2.80	2.58

Figure 6.5 illustrates the collective efforts of both the synthesized motions and the exoskeleton assistance in reducing low back loads of both types, compared to the low back loads experienced by the participants in the unassisted recorded motions. As expected, the results suggest that the greatest reductions in CLBL are achieved by the $CLBL_{cost}$ OCPs, for both unassisted and assisted motions. The exoskeleton-assisted motions manage to reduce the cumulative loads even further than the unassisted

improved technique. The largest exoskeleton contributions however, take place in the $PLBL_{cost}$ OCPs where the exoskeleton manages to reduce the peak load by a greater degree than it does the cumulative load. The results additionally suggest that when improved technique takes place, minimizing cumulative loads via the $CLBL_{cost}$ cost function is more successful in mitigating low back injury risk, where as when the exoskeleton is employed the hybrid reduction of both CLBLs and PLBLs generates the best results in peak load reductions. Conclusively, it is evident that while improved technique can help minimize the risk of cumulative loads in the lower back, for minimizing peak loads external assistance is needed.

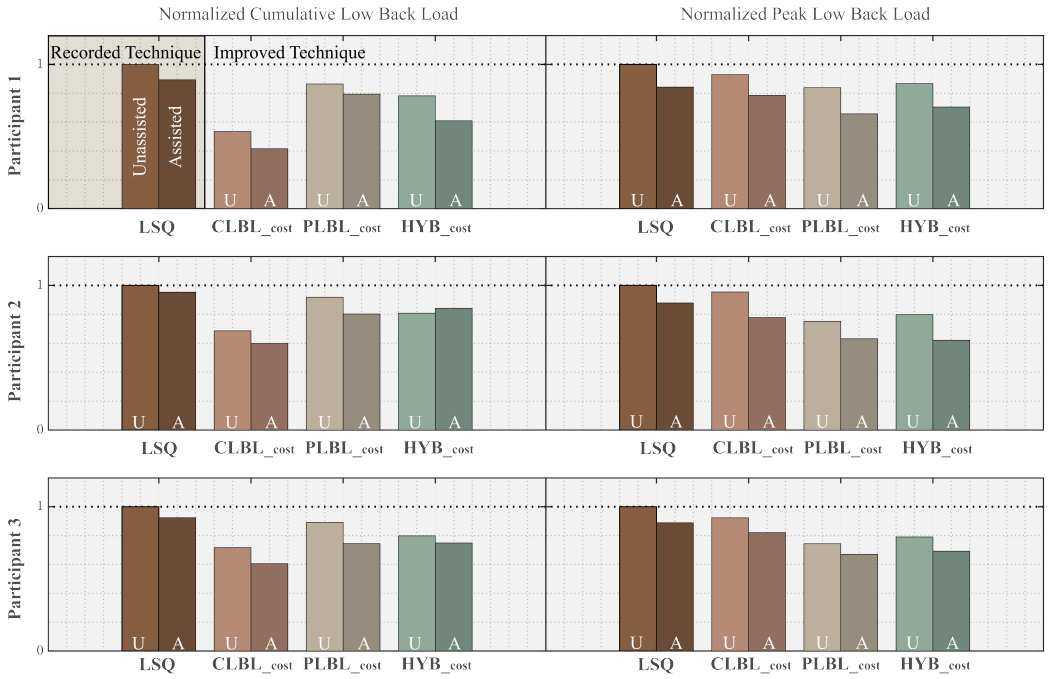

Figure 6.5: Bar plot representing normalized lumbar torques about the L5/S1 joint from simulations of (left) Cumulative low back loads and (right) Peak low back loads. Light-colored bars refer to unassisted motions and dark-colored bars to assisted motions. The torques are normalized according to the L5/S1 joint torque from the result of the unassisted tracking (LSQ) OCP.

6.2.4 Conclusion of Cost Function Evaluation

This section has critically assessed the efficacy of optimized lifting techniques, both unassisted and assisted by an exoskeleton, through three distinct cost functions aimed at minimizing the risks associated with lumbar loads. The evaluations across these scenarios highlighted the potential of both advanced lifting strategies and the integration of exoskeleton technology to mitigate the risks of low-back injuries effectively.

The analysis has demonstrated that each cost function—$CLBL_{cost}$, $PLBL_{cost}$, and HYB_{cost}—significantly influences lifting dynamics and associated injury risks. Specif-

ically, the $CLBL_{cost}$ always facilitated the fastest lifts, reducing CLBLs effectively. This cost function achieved reductions in such cumulative loads by up to 35.4%, showcasing its potential to significantly reduce the duration and intensity of lumbar stress. In contrast, the $PLBL_{cost}$ extended the duration of lifts to spread out the load, effectively mitigating peak lumbar loads by up to 22.2%, thereby reducing the risk of sharp increases in lumbar torque that are critical in acute injury scenarios.

When exoskeleton assistance was incorporated, further reductions in both cumulative and peak lumbar loads were observed. Notably, in the HYB_{cost} scenarios, where a balanced reduction approach was applied, the integration of the exoskeleton led to a reduction of peak loads by up to 38.4% and cumulative loads by approximately 46.9%. This substantial reduction underscores the exoskeleton's capability to adaptively support the wearer by modifying lifting techniques in real-time based on dynamic loading conditions.

The comparative analysis with the least-squares reconstructed motions emphasized that while improved techniques alone can substantially decrease the risk associated with cumulative loads, the management of peak loads—often the more critical factor in preventing acute injuries—was markedly more effective with the aid of the exoskeleton. This finding is pivotal, as it highlights that the greatest reductions in both CLBLs and PLBLs are achieved when the mechanical assistance of an exoskeleton is utilized in conjunction with optimized human motion.

6.3 Intermediate Conclusions

This chapter explored the comparative effectiveness of optimized lifting techniques versus the support provided by exoskeletons. Our analysis demonstrated that while improvements in lifting technique alone can effectively reduce cumulative lumbar loads, they are less efficient at managing peak loads. When integrating a BSE however, both cumulative and peak loads are extensively reduced, with the highest reductions amounting to 46.9% in cumulative and 38.4% in peak low-back loads. These reductions highlight the exoskeleton's ability to provide adaptive and real-time support, while neccessittating its use during physically demanding tasks.

In conclusion, while enhanced lifting techniques may suffice for occasional light lifting, exoskeletons offer a more comprehensive solution in environments where tasks are more demanding and repetitive. They not only improve safety by reducing peak and cumulative loads more effectively but also adapt to varying conditions, making them indispensable for reducing the risk of low back injuries in high-risk manual handling tasks.

Part 2 of this thesis explored the complex intricacies between biomechanical modeling, simulation, and the optimization of exoskeleton-assisted lifting techniques. Building on the foundational biomechanical and control framework established earlier, these chapters focus on enhancing the interaction between human lifting motions and assistive devices. This section also examines methods for quantifying biomechanical risks and assesses strategies to minimize these risks through smarter exoskeleton design and high-level control frameworks.

Through detailed analyses and comparative studies, this part reveals that while improvements in unassisted lifting techniques can decrease the risk of injury, the integration of exoskeletons provides a significantly greater reduction in cumulative and peak lumbar loads. The findings highlight the exoskeleton's role as a pivotal technology in repetitive lifting tasks and demanding environments, offering risk reduction and the potential to transform manual lifting tasks by reducing LBP and enhancing occupational efficiency.

These conclusions reinforce the importance of integrating biomechanical insights with technological innovations to create safer working conditions in industries dependent on manual labor. In the broader field of assistive exoskeletons, the biomechanical evaluation of such devices follows the design and prototyping steps to ensure efficacy, comfort, user acceptance, and safety. Therefore, it is imperative that a standardized biomechanical evaluation is set in place to assess the exoskeleton's performance and the user's adaptation to the device.

Part 3 of this thesis shifts focus and examines the end-user side of exoskeleton development by assessing the very biomechanical parameters that signify an exoskeleton's performance in relation to aiding the user with a predefined task.

Part III

Experimental Evaluation and Optimization of a Lower-Limb Exoskeleton

Defining Familiarization With Lower-Limb Exoskeletons

7

Credit and Publication Statement
Giorgos Marinou designed the concept and methodology of Chapter 7, conducted the investigation and analysis of all experiments, trainings with exoskeleton, and prepared this chapter. Lizeth Sloot aided with the experimental design and guidance of data analysis. Katja Mombaur secured funding for this research study and contributed to its conceptual design and analysis of experiments. This chapter is based on content from published work [170] with Giorgos Marinou as the first author. Partial portions of the text, figures, and analysis have been adapted or reproduced here with acknowledgment of the original publication.

The final part of this research work focuses on the evaluation of the TWIN exoskeleton (Section 2.3.3), investigating the optimization of human-exoskeleton interactions by (1) *optimizing biomechanical evaluation methods to assess and quantify familiarization* and (2) *optimizing user feedback collection and user-exoskeleton transparency for potential control applications*. This research work was carried out as part of the HeiAge project sub-project B2, creating novel work within the project and research field. In the current and following chapters, familiarization is investigated as a mean for improving efficient data collection in the developmental cycles of exoskeleton testing, benchmarking biomechanical evaluation of exoskeletons, and assessing user comfort to these devices.

As discussed in Chapter 1, a great number of exoskeletons and assistive devices are developed to support individuals with limited or zero mobility, successfully restoring partial or full movement and hence enhancing their quality of life. Even so, the transfer of these state-of-the-art technologies to certain population groups such as older adults, who are still mobile, yet frail, still remains difficult. Many of these devices are too bulky or heavy for being operated by frail populations, or they restrict range of motion that was previously achievable, thus failing to complement the user's physical capacity. For example, most LLEs do not accommodate hip adduction and abduction, which necessitates the use of elbow crutches for maintaining static and dynamic balance, two high contributors to risk of falls for older adults [171]. Additionally, challenges in developing intuitive, user-controlled systems further hinder the usability of these devices. Designing motion-intention-detection algorithms that incorporate sensors and control systems tailored to diverse patient

needs and individual preferences remains complex. These problems intensify with the increasing aging population in Western societies, and the diversified nature of mobility problems.

The study of familiarization int he context of technology transfer and evaluation of such devices becomes crucial, as the effectivenes of any assistive technology depends not only on its technical design but also on the user's ability to adapt and integrate it into their natural walking patterns. Studying familiarization helps in identifying the barriers of using exoskeletons such as discomfort, limited motion, unintuitive controls, cognitive difficulties, and provides insights into optimizing training protocols for diverse user groups. By addressing these challenges, we can improve the accessibility and adaptability of exoskeletons, ensuring they meet the specific needs of older adults and other populations.

This Chapter presents the motivation behind studying familiarization to LLEs, while highlighting the need for a more standardized methodology, outlined in Section 7.1. Section 7.2 details the devised methodologies using motion capture systems to quantify familiarization via biomechanical principles, and Section 7.2.1 reports the results and discusses the importance of the study's outcomes within the field of LLEs. Lastly, the main highlights are concluded in Section 7.4, while discussing about the limitations of the study and future work necessary to fortify the claims made regarding familiarization and propel this work even further.

7.1 What is Familiarization?

Familiarization refers to the process through which individuals acquire proficiency in perceiving, understanding, and interacting with a new system, technology or activity. Here, we define familiarization as the foundation that enables initial interactions with a device, forming the basis of adaptation. Adaptation, in turn, is the evolution of these initial interactions into long-term proficient use. In the case of exoskeletons, familiarization involves understanding and learning the operation and functions of a device, whereas adaptation is the process where the operator can consistently achieve smooth movement patterns that minimize energy expenditure. Learning to operate an exoskeleton based on a different controller strategy for example, would require the process of familiarization to that controller, which will contribute to the overall adaptation to the device.

In the context of biomechanics and rehabilitation, familiarization is crucial for ensuring accurate data collection and effective device evaluation and use. For lower-limb exoskeletons, this involves users adjusting their gait and movement strategies to work synergistically with mechanical assistance, which can significantly impact the outcomes of biomechanical evaluations and the subsequent optimization of the

device. If, for example, a user is not yet adequately familiarized to an exoskeleton, the data collected to evaluate the quality of the device is not reliable or meaningful. Hence, in this thesis, familiarization is considered as a dynamic process and a function of time, hypothesizing a directly proportional relationship between the two.

A number of studies highlight the role of familiarization in biomechanical research as a methodological necessity to reduce variability in human performance data. In the field of assistive device interactions, Firouzi et al. [172] review the application of biomechanical gait models in the development of lower-limb exoskeletons, emphasizing the necessity of familiarization in enhancing device functionality and user comfort. Similarly, Cenciarni et al. [173] underscore how familiarization is critical in the initial stages of exoskeleton use, posing it as a biomechanical consideration in exoskeleton design. It is therefore the key to achieving representative walking patterns that reflect both the capabilities and the limitations of exoskeletons, as well as enhancing safety and ease of operation.

The importance of familiarization is also underscored by its impact on the transparency of human-exoskeleton interaction, where greater familiarity can lead to more intuitive control and better integration of user feedback into system adjustments. This aspect is critical for the development of adaptive control systems that enhance the effectiveness of assistive devices in real-world environments. These perspectives make it clear that familiarizing users with lower-limb exoskeletons is not only beneficial but necessary for refining device functionality, improving user satisfaction, and advancing the field of rehabilitative and assistive robotics.

7.1.1 Familiarizing with Exoskeletons

Lower-limb exoskeletons and in general assistive devices go through multiple rounds within their developmental cycles in order to improve upon and optimize their performance and purpose (Figure 7.1), both in mechanical design and software and control implementation. Within the context of parameter optimization and human-in-the-loop control architectures, such as model-predictive control [174] or EMG model-driven controllers [175], several testing iterations over new algorithms or mechanical parameters and adjustments are performed to evaluate their functionality and compare between various prototypes. Almost with every new implementation of software or hardware parameters of these devices, we need to carry out biomechanical tests in order to evaluate the effects and assess their quality. In order to do so, however, we need to know when we can actually start gathering important data. As with every new device, there is a familiarization window in the beginning that we need to account for in order to disregard irrelevant data.

Figure 7.1: (Left) An ideal developmental cycle for a lower-limb exoskeleton, integrating an evaluation process of the biomechanical effects to users, and collecting feedback on both physical and cognitive workload, after the initial familiarization period and informed training. (Right) The TWIN lower-limb exoskeleton from the INAIL group at IIT [47].

To know how long people have to walk with each set of new hardware or software adjustments before we start evaluating them, we need to study and assess familiarization, given specific constant outcomes and metrics. This is particularly important in patient groups that can't walk for a long time before fatigue affects the comparison, such as older adults. In order to increase the efficiency and accuracy of assessing new exoskeleton adjustments, we need to assess the familiarization period needed for such devices. Once we observe patterns of familiarization, we know the participant is ready for assessing the new solutions. In addition, the time that users take to achieve familiarization could be used as a performance indicator across different exoskeletons.

To study familiarization, however, we first need to define it. It is of great interest first, to see how young healthy adults get familiarized with such devices, in order to be able to reference familiarization as a controlled indicator. Unlike the intended user group of such an exoskeleton, able-bodied participants can exhibit stronger signs of resistance to the device, especially within their lower limbs, essentially affecting static and dynamic balance, fluent movement patterns, but also influencing spatiotemporal parameters of exoskeleton gait such as step length, stance width, and direction of travel. The psychological aspect of familiarization can also add to the barriers of adaptation, which can be improved by training and better facilitation procedures [176].

7.2 Quantifying Familiarization

Though familiarization can be as a qualitative measure, in the fields of user-centered and assistive technologies, especially within the healthcare sector, a quantifiable approach is necessary. In this study, biomechanical metrics based on spatiotemporal gait parameters are defined as familiarization indicators for exoskeleton-assisted walking, through a set of biomechanical experiments. The aim of these experiments is to produce a more objective way to quantify and benchmark familiarization when walking with a LLE. The TWIN exoskeleton is employed (Section 2.3.3) and the experimental protocol establishes four biomechanical walking metrics as gait familiarization indicators: *stride duration*, *mediolateral deviation* from a straight path, *polygon of support* area, and *muscle activity* as the propulsive muscle effort in the legs, and the crutch-leaning muscle effort in the arms, where additionally effects of co-contraction are examined. Familiarization is then defined as the reduction in the magnitude of these gait parameters and the hypothesis is formed that it takes place with increasing time of operation. The TWIN exoskeleton is a position-controlled exoskeleton with predefined walking trajectories, hence the joint angles along the walking sequence of these device are constant and are not adjustable (subject to the user's anthropomorphic features).

7.2.1 Biomechanical Evaluation

In this section, the experimental methods and equipment used to perform the biomechanical evaluation for data collection are detailed, including the data analysis and statistical procedures followed to generate the familiarization indicators.

The TWIN Exoskeleton

The TWIN exoskeleton (Figure 7.1) actuates flexion/extension of the hip and knee while offering idle support to the ankle. Further specifications and information on the mechanics, control, and gait pattern generation for the TWIN exoskeleton are outlined in Section 2.3.3. The TWIN features two modes of walking operation, both for which it begins the first stride with the right foot, performing one small-sized step. For the manual mode operation, every successive step has to be triggered through the tablet, by an external person, according to the user's input. The participant is instructed to shift their weight on the leg that will remain in contact with the ground, as for the exoskeleton to be able to more easily transfer the leg that is about to take a step. Throughout the stance and stride phases, the participant is instructed to use the crutches as they see fit, to maintain enough static and dynamic balance and thus not fall over. The manual walking bout ends when the button for initiating the last step is triggered. The feet are then brought together and both the exoskeleton and the participant come to a rest. For the automatic mode, the walking sequence utilizes

an IMU placed on the back of the exoskeleton. The participant is instructed to shift their torso forwards, using the crutches to balance. The IMU senses the change in angle and therefore initiates the first step of the walking sequence. The automatic walking bout ends when the participant stays in the upright position.

Experimental Protocol

The study was spread over two separate sessions. It was conducted on five able-bodied young adults of 29.4 ± 4.9 years, 26 ± 1.4 body mass index (BMI), all males and all dominant on their right side. The protocol was approved by the Institutional Review Board of the medical faculty of Heidelberg University and all participants provided written informed consent. On the first day, the participants had their body dimensions measured, were given safety and exoskeleton operation instructions, and got introduced to the device by practicing two to three steps in each mode of walking operation. A few weeks later, on the second session, the biomechanical evaluation of walking with the exoskeleton was performed. Walking bouts were carried out with the exoskeleton in two different conditions: first using the externally controlled manual walking mode of the exoskeleton followed by the more user-controlled automatic walking mode. For both conditions, participants were instructed to initiate and terminate walking at their own pace, at marked positions, placed on a straight path line, ensuring room for at least five successive strides with each leg.

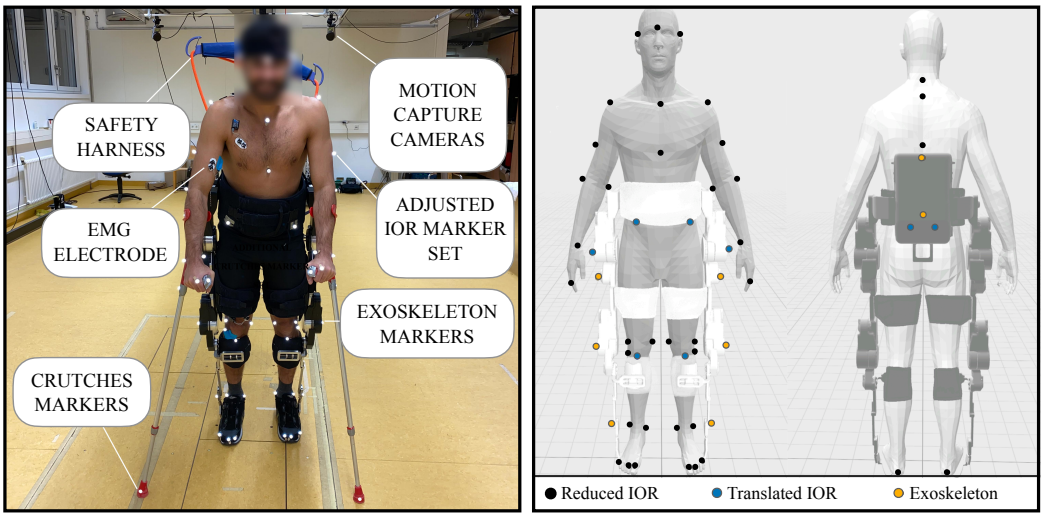

Figure 7.2: (Left) A participant wearing the TWIN exoskeleton in the laboratory setup with motion markers and EMG sensors. (Right) A 3D rendering of a human with the exoskeleton, indicating the reduced IOR marker set, along with the translated markers and additional exoskeleton markers.

Five walking bouts were performed for each walking mode. To aid walking, the participants used crutches that are customary to the use of the exoskeleton. For safety reasons, no randomization took place between the two walking modes, so the manual mode always came first because it allows the user to take steps at their

own pace with greater ease than the automatic mode, which assumes already some experience with the exoskeleton. In addition, the exoskeleton was attached to a suspension harness through its aluminum beams on the back of the pelvis interface. For each mode, the participants walked for two five-minute intervals, with a ten-minute break between the two intervals. This way it was ensured to capture at least five walking bouts at a comfortable level. Between the two walking modes, the participants had a twenty-minute rest time.

Motion and muscle activity data were simultaneously collected using a motion capture system with passive markers at 150 Hz (type 5+ cameras, Qualisys, Gothenburg, Sweden) and a wireless surface EMG system at 1500 Hz (Noraxon, Arizona, USA) with dual wet gel electrodes. Motion capture markers (14 mm) were applied following as closely as possible the full-body IOR marker set [130, 177]. Due to the way the exoskeleton attaches to the body, an adjusted IOR marker set was created, with some markers being translated and also added on the exoskeleton, including 4 additional markers per crutch to capture their location and orientation (Figure 7.2), summing up to 64 markers overall. EMG data were collected on 9 different muscles on the dominant side of the participant. For this study, we focus on four muscles: muscles involved in the crutch leaning (biceps brachii and triceps brachii) and the main lower leg propulsive muscle and its antagonist (gastrocnemius medialis and tibialis anterior). Marker and EMG data were filtered with a bi-directional low-pass fourth- order Butterworth filter, with a cut-off frequency at 6 and 10 Hz respectively. In order to be able to express the EMG during walking to an individual's maximum capacity, MVC trials were conducted prior to the walking bouts according to Konrad [178].

Motion and EMG data were time-normalized to strides based on gait events according to the toe, heel, and sacrum markers. Heel strike was calculated based on local maxima in the time curves of the anteroposterior (in the direction of travel) coordinates – position of the heel relative to the sacrum. Toe-off events were calculated based on local minima in the time curves of the anteroposterior coordinates– the position of the toe relative to the sacrum. The gait events were visually validated.

Familiarization Indicators

The familiarization of gait with a lower-limb position-controlled exoskeleton operating based on predefined walking trajectories, is assessed as a function of four walking characteristics: stride duration (high-level gait parameter), deviation from a straight path and support area (balance), and propulsive and leaning muscle effort in legs and arms respectively (effort), as shown in Figure 7.3. Familiarization is defined as the improvement of the variables that define these metrics, with increasing number of strides taken with the exoskeleton. For the analysis of the data and results, the

dominant side is chosen in each participant. The four quantitative measures are defined as follow:

1. **Stride duration:** the time taken between successive heel strikes of the same foot.
2. **Mediolateral deviation:** the difference in mediolateral distance of the heel marker at a specific stride, from the mediolateral coordinate of a straight-path-line vector, in the overall walking direction.
3. **Polygon of support:** the area enclosed by the convex hull formed by the mediolateral and anteroposterior coordinates of the outermost points of the participant's heels, toes, and crutch markers.
4. **Muscle effort:** the muscle activity of a specific muscle as a percentage of the MVC of that muscle.

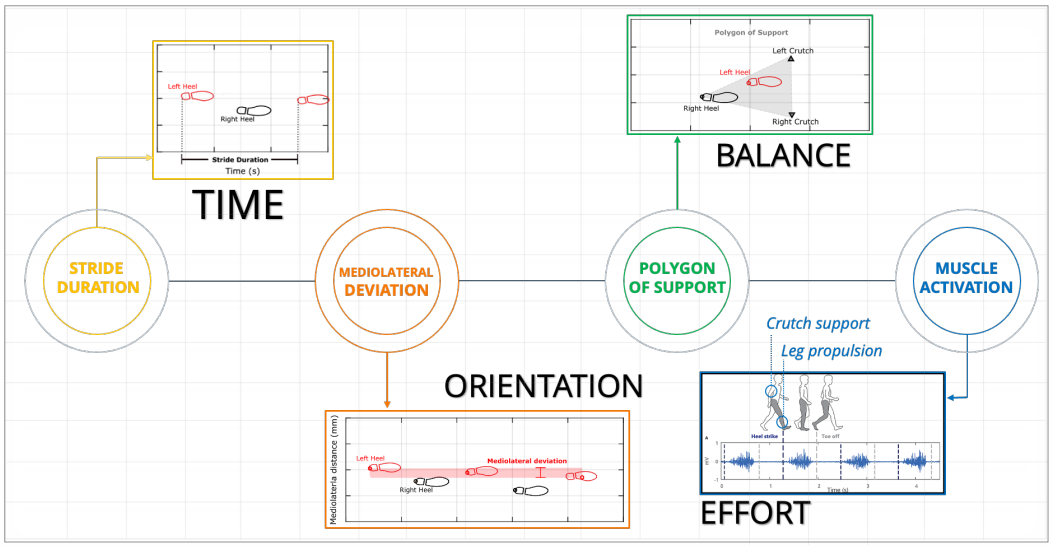

Figure 7.3: The biomechanical metrics used as familiarization indicators: stride duration as a measure of time, mediolateral deviation from a straight path as a measure of orientation, polygon of support as a measure of balance, and muscle activation as a measure of effort.

The straight-path-line vector is created using the coordinates of the heel and toe markers before the walking bout begins. A centerline is formed to calculate how much a participant deviates based on the mediolateral heel coordinate, at every stride. For further analysis, we focus on the average mediolateral stride deviation for each walking bout per participant. It is important to note that the exoskeleton passively supports the ankle and it is restricted in the abduction and adduction of the hip so that the step width remains fixed throughout the motion. Knee and hip joint angles are also fixed throughout the motion based on predefined movement trajectories. The maximum total area covered by the polygon of support is calculated by choosing the outermost points, forming a convex hull. Familiarization, in this

context, is defined as the progressive reduction in one or more measured variables as the time spent walking with the exoskeleton increases.

To quantify muscle effort, the focus is shifted on agonist and antagonist muscle pairs for the upper and the lower body respectively. Hence, we can additionally examine the effects of co-contraction, which is the simultaneous activation of both agonist and antagonist muscles that span over the same joint to make that joint stiffer. For the arms, muscle activity is measured from the biceps and triceps brachii muscles, responsible for handling and leaning on the crutches. For these muscles, co-contraction is necessary in keeping the joints quite rigid, which is required during the loading phase on the crutches. For quantifying muscle effort of the legs, the focus lies on gastrocnemius medialis and tibialis anterior, responsible for propulsion walking. Co-contraction patterns of the lower leg muscles can be rather insightful, since it is a common occurrence that these muscles are contracted simultaneously before a fall, while people try to maintain and assert balance [179].

The stride-normalized EMG curves were normalized to the respective muscle's MVC value, which was measured at the beginning of the experiment. The maximum and Root Mean Square (RMS) values were then calculated, over the whole stride, both for the arm and leg muscles. Based on these two outcomes, the hypothesis is formed that with increasing exoskeleton walking experience, it is expected that (1) muscle activity decreases, and (2) co-contraction decreases in legs and (3) co-contraction increases in arms. Co-contraction was calculated as a ratio between the muscle pairs,

$$c_i = \frac{agonist_{activation}}{antagonist_{activation}} \tag{7.1}$$

using the RMS values of each muscle at each individual stride.

Statistical Analysis

The following variables were taken per participant per bout: the mean stride duration, the mean mediolateral deviation, the mean polygon of the support area, and the mean RMS value of each recorded muscle. To assess an effect over time, Friedman's one-way analysis of variance (ANOVA) test was conducted over the five walking bouts of both the manual and the automatic walking modes [180]. Friedman's test was chosen based on the repetitive measurement nature of the experiment and the non-parametric data collected. When a significant result was found, a post-hoc analysis was performed with a multiple comparisons test on the ten bout pairs. Since the outcome measures were a relatively small sample and not normally distributed, non-parametric tests were performed and the median value for each metric for both walking modes is reported, alongside the interquartile range from the 25th to the 75th percentile. The significance value was set at $p < 0.05$, post-processing and statistical analyses were performed using MATLAB (2020b, Natick, MA, USA).

7.3 Results of the Familiarization Study

This study explored quantifying familiarization of LLE-assisted walking, by assessing three walking metrics describing different aspects of gait: stride duration, mediolateral deviation, polygon of support area and muscle effort. The first three metrics indicated that participants start to show signs of familiarization to the exoskeleton after the first five walking bouts, indicating that familiarization takes place approximately at the same moment in time for all metrics, and suggesting that it is more prone with the automatic mode. Additionally, while there was no evidence supporting familiarization based on muscle effort when looking at individual muscle activity, by examining co-contraction patterns, it was clear that participants got familiarized with the use of crutches for support, from bouts one to five using the manual mode, as well as bouts six to ten with the automatic mode.

7.3.1 Stride Duration

Participants familiarized themselves with the exoskeleton on high-level spatiotemporal gait parameters such as stride duration, supporting our hypothesis. Even so, the process of familiarization started quite later than anticipated; instead of seeing familiarization from the first five walking bouts, it was only observed between bouts six and ten for the stride duration metric. This metric did not particularly change during the first five bouts in the manual mode. There was a decrease of $3.03[3.16]s$ from bout one to five ($p = 0.101$), as shown in Figure 7.4. During the automatic mode bouts, stride duration decreased over time by $2.05[2.61]s$ (average decrease: $16.9\%, p = 0.007$), supporting the familiarization hypothesis.

The results support the familiarization hypothesis, as participants adapted their stride duration over time; however, familiarization occurred later than anticipated, starting only between bouts six and ten. In the manual mode, stride duration did not significantly change during the first five bouts ($p = 0.101$), suggesting that participants required more time to adapt without automated assistance. Contrarily, in the automatic mode, stride duration decreased significantly over time ($16.9\%, p = 0.007$), highlighting the facilitative role of automation in promoting familiarization, but also rising the question if a more fixed-rythm approach promotes familiarization. Stride duration results highlight the importance of adequate training time, validating in part the decision to start every eperiment with the manual mode. Moreover, it can be speculated that adaptive feautures in exoskeleton controllers could result to accelerated learning curves and enahnce user experience.

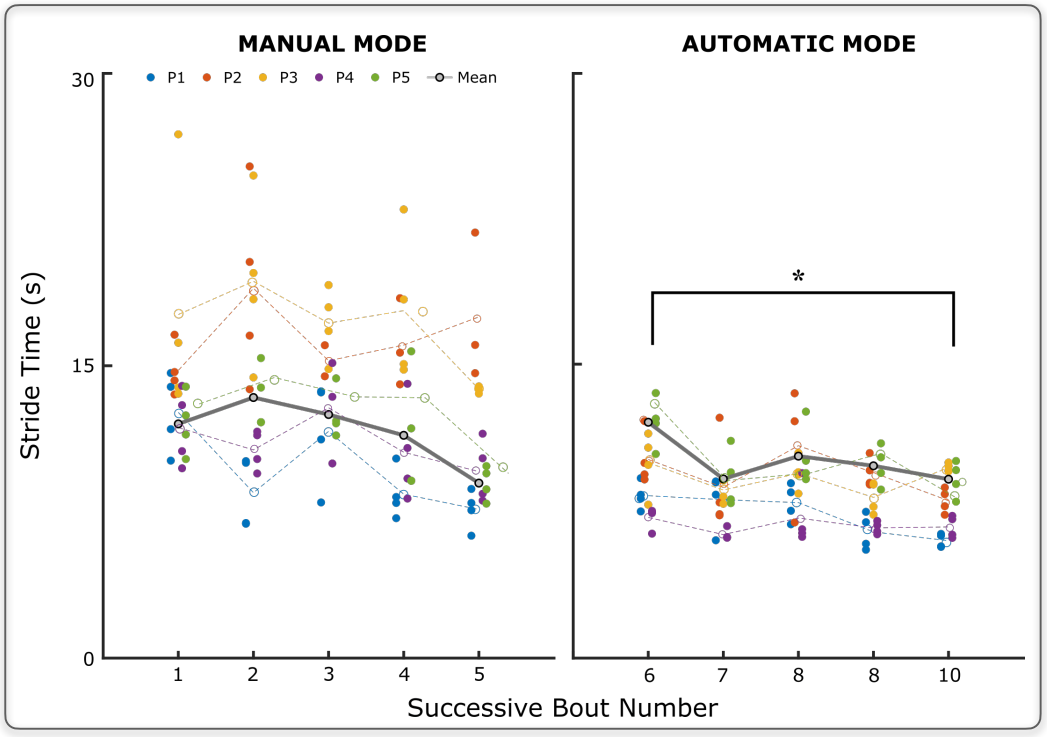

Figure 7.4: Stride duration for the five participants. Circular markers represent values for individual participant strides whereas dashed lines depict the mean line of each participant's stride duration. The grey line represents the mean of all participants. Floating values represented median and IQR per bout across all participants. Legend's P stands for participant. * $p = 0.007$

7.3.2 Mediolateral Deviation

Familiarization was also evident in the balance metrics (mediolateral deviation, and polygon of support area and crutch placement). For the first five bouts with the manual mode, the participants' mediolateral deviation from a straight path varies significantly, and a familiarization trend cannot be established. On the contrary, evidence of familiarization exist when participants are walking with the automatic mode of the exoskeleton. The mediolateral deviation from straight-line walking decreased over time, much similar to the stride duration metric. Hence, the five participants did not change their ability to maintain a straight walking path in the first five bouts while using the manual mode; there was an average decrease of 31.9% in mediolateral deviation from bout one to five ($p = 0.290$). There was however, an improved ability to walk in a straight-line path during the next five bouts in the automatic mode, with a $63.8[32.2]mm$ or $51.7\%(p = 0.014)$ improvement between bout six and ten (Figure 7.5). This indicates that the participants develop the ability to maintain a straight path while walking with the exoskeleton, only between bouts six and ten. It can hence be inferred that the mode of walking impacts the ability of the wearer to walk on a straight path.

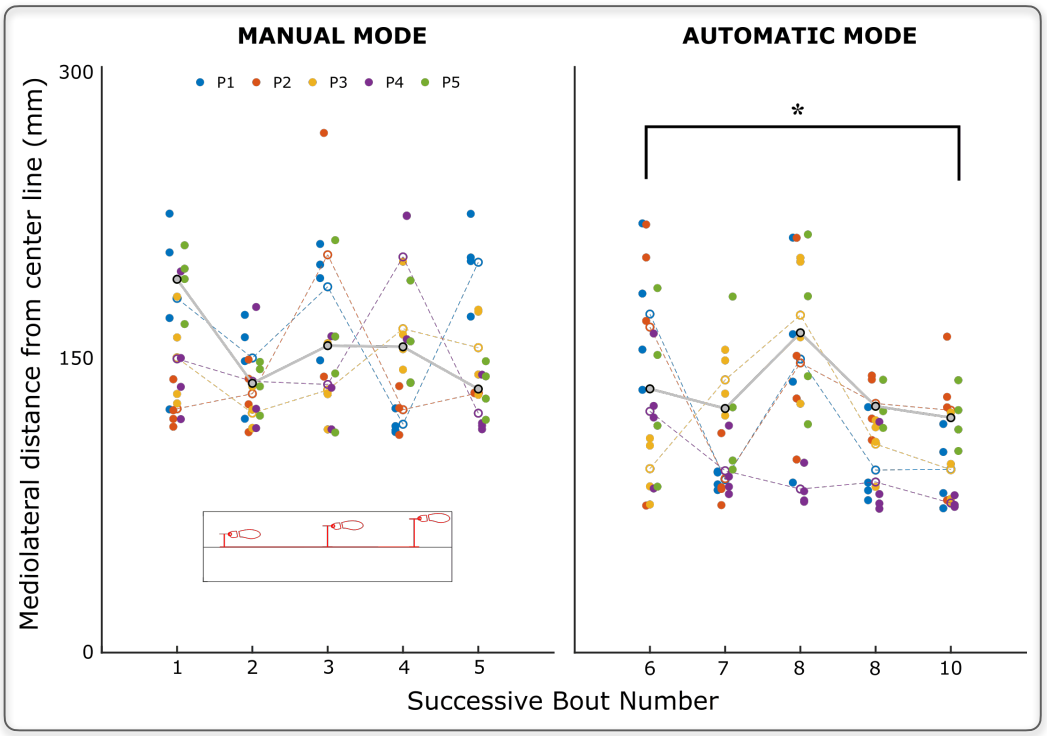

Figure 7.5: Mediolateral deviation distance from a straight path. Circular markers represent values for individual participant strides whereas dashed lines depict the line through each participant's mean stride duration. Legend's P stands for participant. Floating values represented median and IQR per bout across all participants. The insert illustrates how the mediolateral distance from the centerline is measured at each stride. * $p = 0.014$

7.3.3 Polygon of Support

While participants use the manual mode, there seems to be much variability in the polygon of support areas. However, as with the first two metrics, familiarization takes place when the participants use the automatic mode to walk, and especially between bouts seven to ten as shown in Figure 7.6. The average areas for each stride for all participants do not seem to change from walking bouts one to five, therefore there is no evidence of familiarization yet. Participants did not change feet and crutch placement significantly during the first five bouts with the manual mode. There was a 16.5% decrease in the area between bout one to bout five ($p = 0.680$). The support area did decrease over time during the next five bouts with the automatic mode, by $0.0202[0.0505]$ with an average decrease of 30.6% ($p = 0.0316$, Figure 7.6). This change in the size of the area of the polygon of support did not seem to be related to a respective change in shape as shown in Figure 7.7.

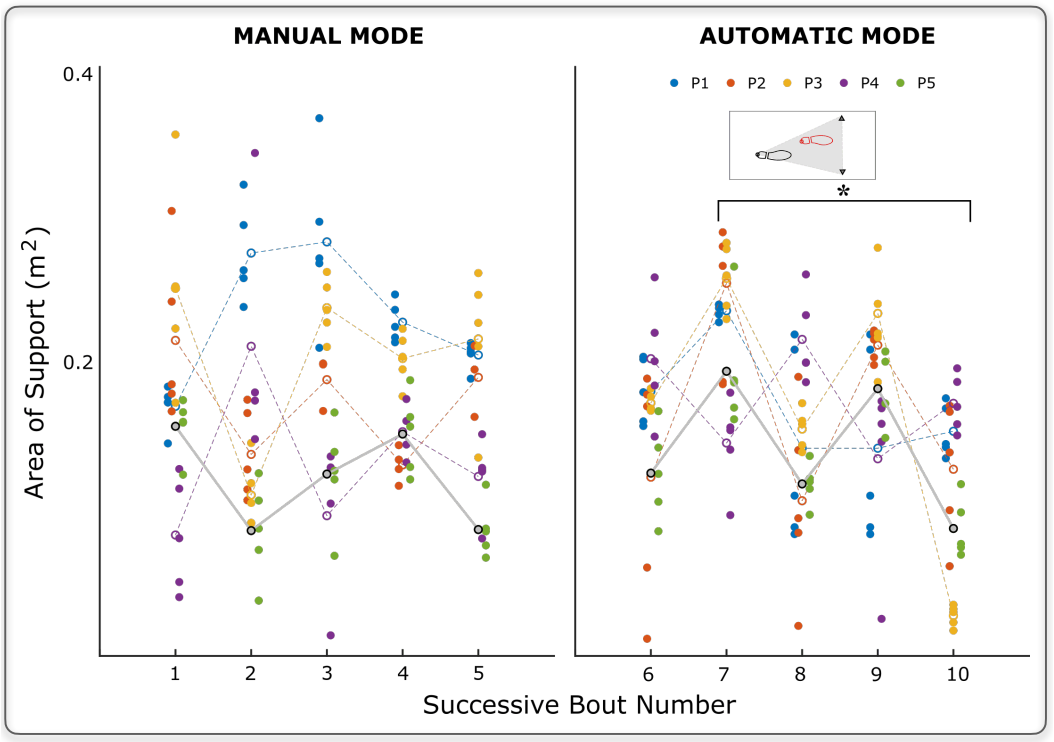

Figure 7.6: The polygon of support area for all participants. circular markers represent values for individual participant strides whereas dashed lines depict the line through each participant's mean polygon area. Floating values represented median and IQR per bout across all participants. Legend's P stands for participant. The insert illustrates the convex hull measured at each stride. * $p = 0.0316$

It is evident in these figures, that the participants demonstrated different patterns when placing their crutches - either at the sides or at the front. For example, participant two between bouts one and five, had placed the crutches to the front at an almost parallel placement, assuming a more tilted position for establishing balance. Bouts six and ten suggest that the same participant changed this pattern by bringing the crutches more to their sides in a diagonal manner. On contrary, participant three had exactly the opposite pattern, where the crutches were placed at the sides at bouts one and five, whereas in bouts six and ten the crutches were placed towards the front. The maximum mediolateral and anteroposterior dimensions of the polygon of support are also reported in Figure 7.7. These results indicate that either the participants need some time before they start getting familiarized, or that the manual mode does not promote familiarization as adequately as the automatic mode. This could be related to the fact that the automatic mode offers a more intuitive exoskeleton-assisted gait, which is a direct mode of communication between the wearer and the robot. Though more testing is needed with a greater number of participants, we can start to speculate on the outcomes of different control methods.

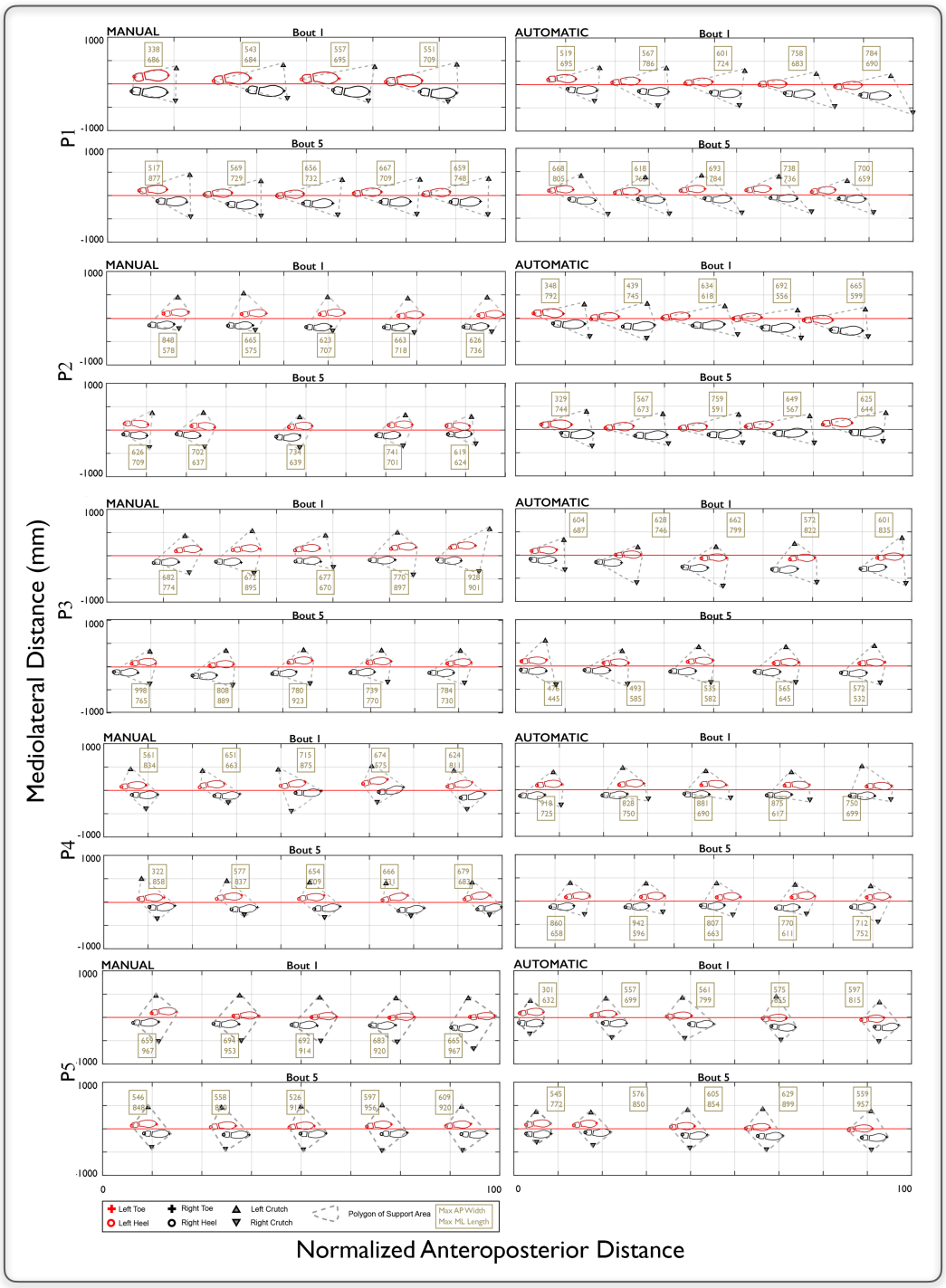

Figure 7.7: Balance metrics: mediolateral deviation and polygon of support for all participants. The heel marker's vertical position is tracked and used to calculate the deviation from the center (red) straight-line path. The convex hull of the polygon of support area is shown with the dashed lines. The maximum width (mediolateral) and length (anteroposterior) distances of the polygon of support are also reported for each stride.

The participants seem to develop various strategies of where to place the crutches to maintain their (perception of) balance and feel safe. They form different polygonal shapes of support (Figure 7.7), during manual mode to increase their base of

support, by having the crutches forward, and far outside the bounds of the polygon formed when walking with the automatic mode later on. No patterns are recognized based on the shape of the polygon, hence, each participant develops their own way of asserting balance with the crutches, hence it can be speculated that it is not influenced by the exoskeleton structure, but instead it is rather a personal preference. During the automatic mode, they seem to start with the same strategies but over time a decrease in the area of the polygon occurs. This is an indication of how people point towards the first establishment of familiarization, based on balance. A further study would be necessary, one perhaps studying the core (adductor) muscles of the body. Additionally, since familiarization was more evident with bout ten, it begs the question of whether more walking bouts and exoskeleton experience are needed for metrics such as the polygon of support to converge to a minimum value and observe a plateau. It is concluded however, from the results of the first three metrics, that motor learning seems to be developing through the manual mode bouts, and being solidified during the automatic mode, hence establishing familiarization.

7.3.4 Muscle Effort

There were no considerable changes in muscle activity over time for any of the examined arm or leg muscles, for neither of the two walking modes' relative values. For both modes, all muscles remain under 20% of their maximum capacity as measured by the MVC trials, as illustrated in Figure 7.8. Though there are some noticeable reductions in specific participants' muscle activity throughout bouts one to ten, no particular trend can be deduced from the data. Lower body muscles are activated accordingly during the stance phase: GM: $6.48[2.00]\%$, ($p = 0.270$), TA : $4.71[1.12]\%$ ($p = 0.360$) and automatic GM : $7.55[4.26]\%$ ($p = 0.49$), TA : $4.52[1.24]\%$ ($p = 0.460$) contributing to propulsive muscular effort. Muscle activity as percentage MVC was reported for the manual mode at $4.51[3.57]\%$ for the biceps muscles ($p = 0.210$) and $8.28[1.38]\%$ for the triceps muscles ($p = 0.210$) and for the automatic mode at $4.44[1.59]\%$ for the biceps ($p = 0.510$) and $7.73[1.02]\%$ for the triceps muscles ($p = 0.530$). Co-contraction was evident and reduced significantly for the upper body muscles in both modes. Maximum values of EMG as a percentage of MVC (Figure 7.8) highlight co-contraction patterns. Co-contraction of biceps and triceps brachii reduced by $18.1\%(0.196[0.316]\%$ of MVC, ($p = 0.0266$) between bouts one and five with the manual mode. During bouts six and ten with the automatic mode, the co-contraction index reduced by 22.6 % $(0.175[0.205]\%$ of MVC, $p = 0.01833$), but it did not change for bouts one to ten for the lower body.

Though muscle activations for the upper-limb did not reduce over time, failing to provide evidence of familiarization, the co-contraction metric upheld our familiarization hypothesis when looking at the synergic contributions of the upper-body muscle pairs during both modes. Co-contraction index decreased from bouts one

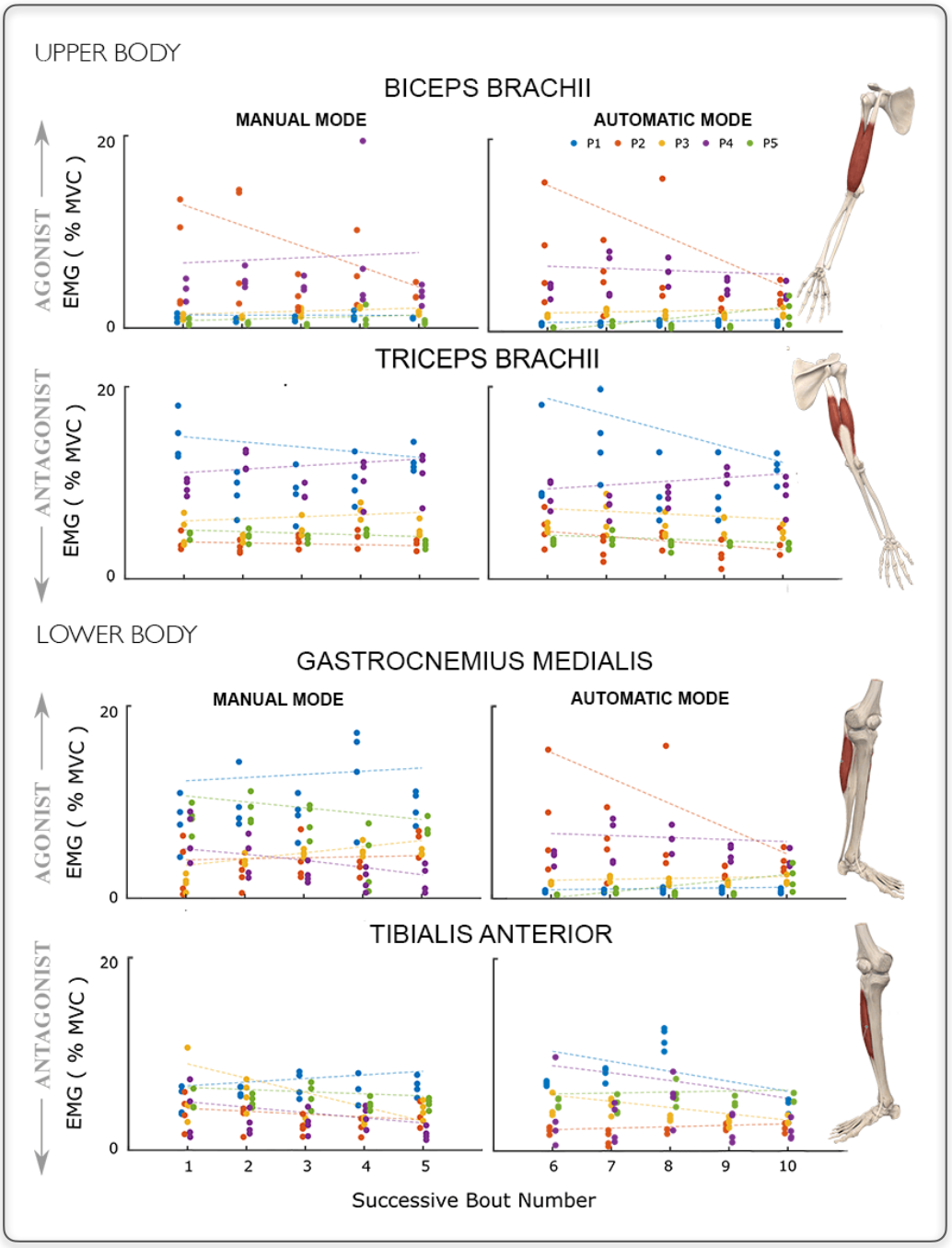

Figure 7.8: RMS of muscle activity as a percentage of MVC for all muscles and all participants per bout iteration for the Manual and Automatic Modes. Circular markers present values for individual participant strides whereas dashed lines depict the line of best fit through each participant's mean muscle RMS. Color coded numbers in squares report maximum EMG signal as percentage of MVC for each participant per bout, rounded to the closest integer. Legend's P stands for participant.

to five, and six to ten for the biceps and triceps muscle pairs. Albeit the reduction, the co-contraction index remained on a relatively average level for the triceps and biceps brachii groups. Though co-contraction reductions show that the participants get familiarized with the exoskeleton, an average level of co-contraction of the arm

muscles when using the crutches is also a good indicator for familiarization. This is due to the fact that co-contraction of muscle pairs aids in making the joints stiffer, which is needed when a person balances on crutches.

There were no clear signs of familiarization based on muscle effort of the lower limb either. In contrast to our expectations, no substantial reductions in muscle activity over time were observed for either mode. This could be due to a number of reasons, mainly that participants need more walking bouts to start familiarizing themselves in terms of muscle effort and use. Secondly, surface EMG is in general a noisy signal and more variable than the rest of the quantities measured. More precise variables could help in deducing familiarization in this metric, for example, we could combine the EMG signal with receiving information from instrumented crutches, that record the ground reaction forces applied when the participant is walking. Additionally, we could compare the propulsion effort of walking with an exoskeleton to the one of walking without an exoskeleton and compare the differences. Lastly, we can analyze more muscles to have a more general idea of how muscle activity relates to exoskeleton-assisted gait.

7.4 Intermediate Conclusion

Biomechanical evaluation of exoskeletons is a fundamental part of testing hardware and software modifications, but it can be quite challenging and inefficient since different users demonstrate different familiarization patterns and time windows. In this study, four biomechanical metrics are defined that serve as gait familiarization indicators for lower-limb exoskeleton assistance, in order to increase the efficiency and accuracy of biomechanical measurements and data collection, for evaluating and optimizing human-exoskeleton interactions. Metrics assessed include stride duration, mediolateral deviation from a straight path, polygon of support area, and muscle effort of the lower and upper body, for five participants performing five walking bouts with a manual and five more with the automatic mode of the TWIN exoskeleton. Familiarization trends are observed only under the automatic mode for the latter five bouts, based on the reduction of the quantities of the first three metrics ($p < 0.05$). Muscle effort showed evidence of familiarization based on reductions of co-contraction for the arms only, while muscle activity did not show any familiarization trends for lower or upper body muscles.

This study demonstrated that the first three biomechanical metrics are promising candidates for establishing familiarization indicators and thus paves the path towards more efficient exoskeleton testing. The presented approach of quantifying a user's familiarization based on two different modes of exoskeleton walking, allows us to distinguish when familiarization begins and when we can start collecting meaningful data to evaluate the device. Future work is however needed, to better evaluate

the patterns of familiarization, in terms of duration, repeatability, and mode of exoskeleton walking to more efficiently adjust and tailor LLE to frail populations with partial mobility.

7.4.1 Limitations of the Study

The main limitation of this study is that able-bodied participants were studied instead of older frail adults. Due to the situation of COVID-19 when the study took place, it was very difficult to admit older adults in this research program, as to quantify familiarization based on the main population of interest of this study. This pushed the project towards a parallel and safer direction, where able-bodied populations are recruited in order to asses familiarization times and based on these findings deduce an appropriate and efficient time window in which frail groups can be tested as to optimize human-exoskeleton interactions. Secondly, a small group size has been measured. Given a larger group of participants, we could detect stronger familiarization patterns during the walking bouts and better assess the contributions of the two different walking modes of the exoskeleton. Additionally, it would be favorable to practice randomization between manual and automatic walking modes during the measurements, however, due to safety reasons the manual mode always came before the automatic one, hence we avoid comparing the two. Another limitation is that in order to be able to better assess the validity of the muscle effort outcomes for the upper body, we would need a method of measuring the ground reaction forces exerted by the crutches. Lastly, due to the small volume of the recording area within the motion-capture lab, uninterrupted long-distance walking with the exoskeleton was not possible. To this end, a more mobile system able to capture biomechanical data would be necessary. The design and development of such a system is outlined in the next Chapter (8), along with its possible applications in not only biomechanical evaluation but also control of exoskeletons.

7.4.2 Extending Familiarization Analysis

By defining these four familiarization metrics, important contributions have been achieved in exoskeleton research. While no studies are found to examine how and for how long a user needs to be familiarized before successfully evaluating the contributions of an exoskeleton, this study has made an important but only a first step in answering several questions. In continuing this research, the aim is to focus on how familiarization can help optimize human-exoskeleton interactions, by facilitating better and more transparent control protocols, that communicate current user states to the device. Additionally, recruiting a larger participant pool can aid in fortifying these initial evidence and indications of familiarization while gaining new and important insights on in-depth and longer familiarization windows.

In order to enable for a more diverse and thorough study of familiarization, it is essential to extend not only the number of participants recruited within the study, but also the distance walked by individual participants with the exoskeleton. For realizing research extensions of this caliper, a new method to evaluate biomechanics more dynamically is needed, to offer the possibility of capturing data beyond the restrictions of traditional laboratory setups. To optimize human-exoskeleton interactions, it is crucial to collect real-time information on the user's state, especially when this data and feedback can be integrated directly into the exoskeleton's control system. In doing so, not only can we enhance device and user transparency but also continuously optimize the user's experience and interaction with the exoskeleton. To this aim, the following chapter details the design and development of a mobile and modular sensory system. This system is intended to serve as a plug-and-play solution for most LLEs, enabling unrestricted data collection across varied environments and facilitating feedback to the high-level controllers of an exoskeleton.

Development of a Custom Sensor System for Exoskeletons

8

Credit and Publication Statement
Giorgos Marinou designed the concept and methodology, developed the hardware and software, conducted and analyzed the validation experiments, and prepared this chapter. Ibrahima Kourouma contributed to the design of the electronics and experiments, and developed the main system software. Katja Mombaur secured funding for this research project and contributed to the conceptual design of the project and analysis of the experiments. This Chapter is based on content from a journal article currently in review [181] with Giorgos Marinou as the first author. Partial portions of the text, figures, and analysis have been reproduced here with acknowledgment of the original publication.

Evaluating the effectiveness and user-acceptance of exoskeleton devices necessitates the simultaneous engagement of multidisciplinary technologies within a data collection framework. Motion capture cameras and various force-sensing systems can be employed to this end, as described in Chapter 3, which details the most common biomechanical evaluation technologies. Even though these systems are highly accurate and set the gold standard in gait analysis, there are still certain challenges that limit their capacity when it comes to evaluating exoskeleton devices and their interactions with humans. These challenges include the high costs associated in purchasing these precise evaluation systems, the closed nature of the proprietary software included, and the complex integration of these technologies in data collection with assistive devices and their use in generating feedback for informing control architectures in real-time [170, 182].

This Chapter explores a need for a more standardized methodology that can be implemented in outdoor scenarios, added to the motivation of improving the efficacy of biomechanical evaluation and control approaches within LLE assessment and control. With the additional aim of reducing costs and promoting collaboration within the field, we present an open-source, modular and mobile sensory system, comprising flexible 3D-printed pressure-sensing insoles, and instrumented force-sensing crutches. Section 8.1 explains the motivation and need leading to the development of this system and Section 8.3 describes the design, development and evaluation of the system against gold standard methodologies. Section 8.5 identifies the transferable biomechanical principles and applications based on the developed

system, as well as proposing possible control frameworks that facilitate a safer and more transparent control architecture, especially regarding the use of LLE with frail and older populations.

8.1 Motion Capture Limitations to Research

Current methodologies, such as marker-based motion analysis and force plate technologies, though accurate, are predominantly confined to laboratory settings due to their prohibitive costs and extensive setup requirements [103, 183]. While they are excellent methodologies for gait analysis research, there are several challenges when using them to evaluate exoskeletons. Recently, marker-less motion capture has begun to address these limitations, offering promising results without the cumbersome setup of traditional systems [184]. However, these technologies still struggle to operate effectively in everyday environments, a critical requirement for practical LLE applications, while still needing camera equipment to cover a certain volume, imposing limitations in freedom of movement.

A number of modular sensor arrays utilizing IMU sensors exist, in the form of suits, enabling for constant monitoring of gait in a more mobile and unrestricted manner (Section 3.1). The integration of IMUs, despite enabling kinematic measurements and gait phase identification outside of lab settings, still faces challenges in calibration and comfort when combined with LLEs [185, 186, 187, 188]. Similarly, surface EMG quantifies muscular effort but is hindered by preparation requirements and sensitivity to environmental conditions [189, 190, 191]. Despite these limitations, both IMU and EMG technologies serve both as valuable biomechanical evaluation and control input when processed correctly, although unreliability issues due to environmental noise have led to exploring alternative sensor-input methods [87, 93, 192, 193, 194, 195].

8.2 Mobile and Integrated Solutions for Exoskeleton Evaluation

Force-measuring crutches and pressure-sensing insoles equipped with strain gauges and piezoelectric sensors within force-sensitive resistors (FSR)s offer another way to analyze movement effectively [196, 197]. Integrating these with IMUs creates a versatile system that enhances user intention assessment via sensor fusion, across various platforms. Although these components are proven to effectively analyze gait in multiple studies [198, 199, 200, 201], there is a notable gap in research combining these technologies into a unified, multi-sensor system. Furthermore, the reproducibility of these methods and hardware is often unclear and complicated,

and the cost is relatively high, while lacking open-sourced protocols, thus hindering further research development. For performing exoskeleton assessments in a real-world setting, new methodologies in biomechanical evaluation are needed.

8.2.1 Instrumented Crutches

Crutch instrumentation, especially for measuring GRFs has been researched in the past with applications ranging in complexity and accuracy. The main purpose of integrating force measuring technologies to crutches is to gain important insights on how upper body contributions influence atypical gait [196], and in the case of this study, exoskeleton-assisted gait. Different sensor technologies are used to this end, varying from simple FSR implementations [202], to load cells [203] and more complex strain gauge instrumentations [204, 205, 206], able to measure the force or pressure applied by the user through the crutch across one or more axis. Instrumented crutches have additionally been used in researching their potential in exoskeleton control [207, 208]. Though these solutions have been applied successfully, the complexity or cost of assembly, or bulkiness added to the crutches still remain quite challenging [209, 208].

8.2.2 Sensorised Insoles

A number of designs exist in commercial and research applications that explore the use of sensorized insoles in the context of measuring plantar pressure for gait monitoring (Section 3.1). Depending on the desired application, mainly varying between CoP measurement and gait phase detection, the number of sensors-specifically FSRs-varies. Designs aiming to accurately measure the CoP use a higher number of sensors spread across the plane of the sole [210, 211]. Insoles primarily focused on gait phase detection contain a minimal set of sensors, as low as three, placed strategically under specific bony landmarks of the foot [212]. In rigid LLEs, the solid plate in the shoe minimizes plantar pressure variability, aiding weight transfer but reducing foot flexibility. This allows for simplifications in sensor arrays for CoP calculation. The same sensors can be used to detect subsequent gait phases, though gait phase is not as straight forward as calculating the CoP.

8.2.3 Fuzzy Logic for Gait Phase Estimation

Fuzzy logic employs a mathematical approach to model reasoning unlike program-based approaches, by allowing for degrees of truth as opposed to strict binary decisions or choices, thus reflecting the approximate nature of human reasoning [213, 214]. This approach is particularly effective for systems where human judgment or involvement plays a pivotal role, such as in control systems and decision-making, with applications like human-machine interactions, or exoskeletons. Fuzzy sets are able to store imprecise information and reflect the uncertainty or certainty of

an object belonging to a specific set, resulting from human input, within variables called membership grades. The membership grade is the output of the membership function which in essence maps the object to be classified between a full membership value (one) and a non-membership value (zero). In this fuzzy context, each value can also be represented as a linguistic variable, which can take various linguistic values representing the zero and one grades.

Previous works in literature have used sensorized insoles in combination with a fuzzy logic algorithm in order to deduce the gait phase of a person via plantar pressure distribution [215, 212]. While offering distinctive implementations and applications, the majority of the presented works share a common approach, of using monotonic membership functions; these functions employ membership grades that either gradually rise or fall to a value of one or zero. Consequently, these studies make use of linguistic variables '*large*' and '*small*', in order to denote the value of the membership function.

In several applications, the output of the fuzzy logic needs to be discretized again through the defuzzification process. Throughout previous works, no account exists that uses this process to aid the gait phase estimation logic, in the context of obtaining a percentage of the gait cycle a person is in. Additionally, all approaches use a fuzzy logic algorithm based on the individual feet, which can be problematic when analyzing atypical gait or gait events that reach outside of the typical gait cycle. In the case of exoskeleton gait, and especially on informing the control of such device, the user's safety requires a highly accurate and thorough gait phase estimator.

The recent upsurge in machine learning approaches have given rise to a number of studies employing it in the case of estimating gait phases [199]. In order to train the models used, not only a large data set is required, but also the quality and relevance of such data sets are highly critical in order for the algorithm to perform accurate predictions [216]. Due to the privacy conditions of attaining medical data, these data sets might often suffer quality and representation, especially when it comes to applications like exoskeleton assisted and atypical gait, and thus yielding unpredictable outcomes. Unlike machine learning, fuzzy logic is computationally inexpensive and follows a rule-based approach, eliminating the need for large datasets that may not exist and avoiding the generation of incorrect data or control inputs for the exoskeleton. This decision-making framework, built on predefined rules, effectively handles the inherent variability in human gait, thus optimizing the exoskeleton's response to user movements [215, 214].

8.2.4 Thinking Outside the Lab

The biomechanical validity of exoskeletons in real-worlds scenarios that take place outside of laboratory bounds is an understudied area within the field. A number of reasons exist in exploring this path, ranging from providing larger distances for uninterrupted walking, testing on various terrains and introducing levels of environmental variability that would be a consequence of using these devices in normal everyday applications. Furthermore, longer assessments of short-term familiarization patterns could be studied, with increased data sets, subject to environmental conditions and interactions. Additionally, technical equipment testing both for exoskeletons and sensory systems should be conducted in various environments to ensure the safety of use of such devices.

To bridge this gap, the research conducted in this study introduces a cost-effective, easy-to-reproduce, and universally compatible sensor system designed explicitly for LLEs. Unlike conventional high-cost systems whose precision exceeds practical necessities and often lacks integration capabilities for direct exoskeleton control, our solution prioritizes functional accuracy and ease of integration [217, 218]. This approach harnesses the power of IMUs and force sensing technologies, combined in a modular framework that supports real-world application across various terrains [185, 189].

We have developed a standalone and modular two-part system consisting of crutches equipped with force sensors and insoles that incorporate pressure sensors, both integrated with IMUs. This multi-sensor assembly not only captures detailed biomechanical data but also interprets user intent with high reliability, establishing intuitive control of the exoskeletons. To underscore our commitment to accessibility and community-driven improvement, we provide this technology as an open-source platform, ensuring that other researchers can adapt and enhance our system without duplicate development efforts. Further, the system can be used independently and fitted to any lower-limb exoskeleton or exosuit. In this study, we continue our work with the same exoskeleton device and test our system using the TWIN LLE [47].

Moreover, we employ fuzzy logic to process sensor inputs, offering a robust alternative to traditional machine learning methods that require extensive data and often yield unpredictable outcomes. Unlike machine learning, fuzzy logic is computationally inexpensive and follows a rule-based approach, eliminating the need for large datasets that may not exist and avoiding the generation of incorrect data or control inputs for the exoskeleton. This decision-making framework, built on predefined rules, effectively handles the inherent variability in human gait, thus optimizing the exoskeleton's response to user movements [215, 214].

Building upon this premise, this study delivers a modular, mobile, and cost-effective sensor-based system for biomechanical evaluation and control of lower-limb exoskeletons. Our standalone system is designed for easy integration with any exoskeleton, enhancing real-world applicability by enabling evaluations outside laboratory settings. We also provide full access to our software and hardware designs to promote collaboration and innovation in the field.

The following section details the design and methods used in this system, alongside validation experiments that benchmark our technology against current standards. Possible applications in biomechanical interpretation of the collected data and control strategies are then elaborated and proposed in Sections 8.5.

8.3 System Design and Development

The modular system consists of two individual sensor systems that can either work together or separately in order to collect biomechanical data from the human and exoskeleton. The first part consists of two instrumented crutches able to measure GRFs using load cells, as well as their acceleration and orientation via IMU units. The second part is a pair of flexible 3D-printed insoles which are sensorized with three FSRs each, in order to primarily measure the anteroposterior CoP of the foot, as well as acceleration and orientation of the foot via an IMU unit. Both of these peripheral modules stream sensor data via a Bluetooth Low Energy (BLE) protocol to a central unit, where they are being stored. The central unit can be fitted onboard the exoskeleton, thus making for a short wireless communication distance. Figure 8.1 shows a basic overview of how the system attaches to the user and exoskeleton, as well as the main components of each of the two units and the hierarchical structure of system operations.

The two flexible insoles can be fitted inside the shoes of the exoskeleton, with the box housing the hardware components attached on the back of the shoe. The two load cells can be screwed on the end tips of the crutches, and the boxes housing the electronics are clipped on the main shaft of each crutch, slightly below the hand unit as to not shift the crutch inertia. A semi-flexible hemispherical unit is attached on the bottom tip of each crutch to ensure that the GRFs run along the central axis of the crutch, thus minimizing bending moments about the mechanical linkage of the load cell. The central unit is attached on the back interface of the onboard computational unit of the exoskeleton, along with a battery power source. The four sensors, or peripherals, connect to the central unit via BLE. The FSR sensors on the insoles collect pressure values while the load cells collect force values. IMUs on all sensors record orientation, velocity and angular acceleration. All four sensors then transmit the data to the central unit as a JSON package, where the data from all sensors is parsed together into a CSV file. A fuzzy logic algorithm computes the gait

phases. Lastly, an Android application manages the communication between the central unit and the peripherals, overseeing data flow and system operations. The following Subsections provide the technical details on both hardware and software design of the system components.

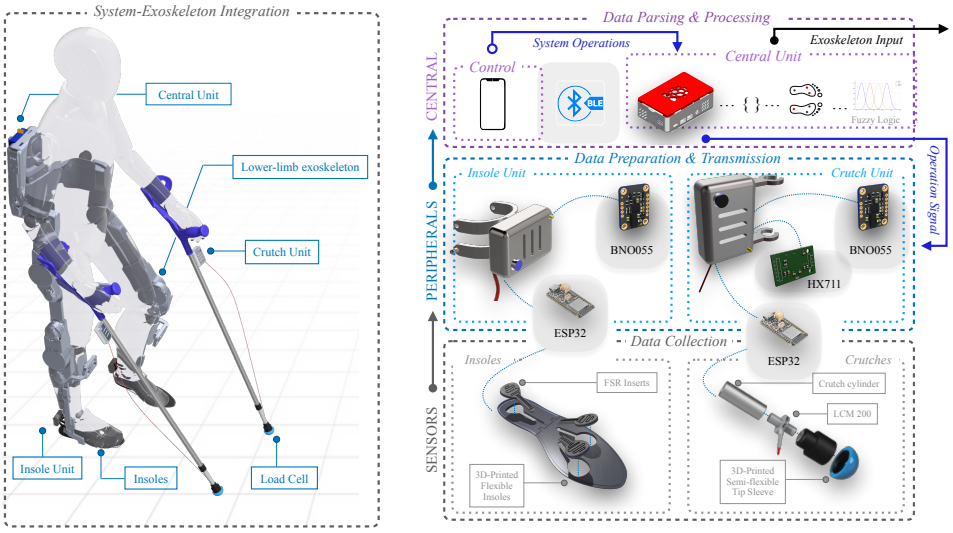

(a) (b)

Figure 8.1: Overview of System Integration and Design. a) The system components integrated onto a lower limb exoskeleton include: (1) two flexible 3D-printed insoles, (2) insole data collection units, (3) forearm crutches with load cells, (4) crutch data collection units, and (5) a central data and control unit mounted on the exoskeleton's back. b) Simultaneous data collection is achieved through a sensor framework. Modular insoles with removable FSR inserts measure pressure at critical points: the heel, first, and fifth metatarsals. Forces are captured by load cells at the crutch tips, encased in semi-flexible sleeves. A BNO055 IMU records orientation, velocity and acceleration on all sensors. Data from the sensors, processed via ESP32-S3 Feather boards, are transmitted to a central unit using BLE. This unit, powered by a Raspberry Pi 4, parses data into a CSV file, while a fuzzy logic algorithm computes gait phases. An Android application manages communication between the central unit and peripherals, overseeing data flow and system operations.

8.3.1 Hardware Design

The system design follows a simple and practical pipeline for assembling the various components for both units, that was implemented with the goal of allowing for easy and low-cost replication. For this reason, the bill of materials consists of off-the-shelf components that can be procured from common electronics resellers and online platforms. The electronics of both units are installed on projects boards, ready to be soldered. Both units components and boards are housed in 3D-printed cases designed for each unit specifically. A replication guide with instructions for the assembly and operation of the system can be downloaded online [219], where more information on the hardware design of the system can be found, along with an online repository of the software code and 3D models (STL format).

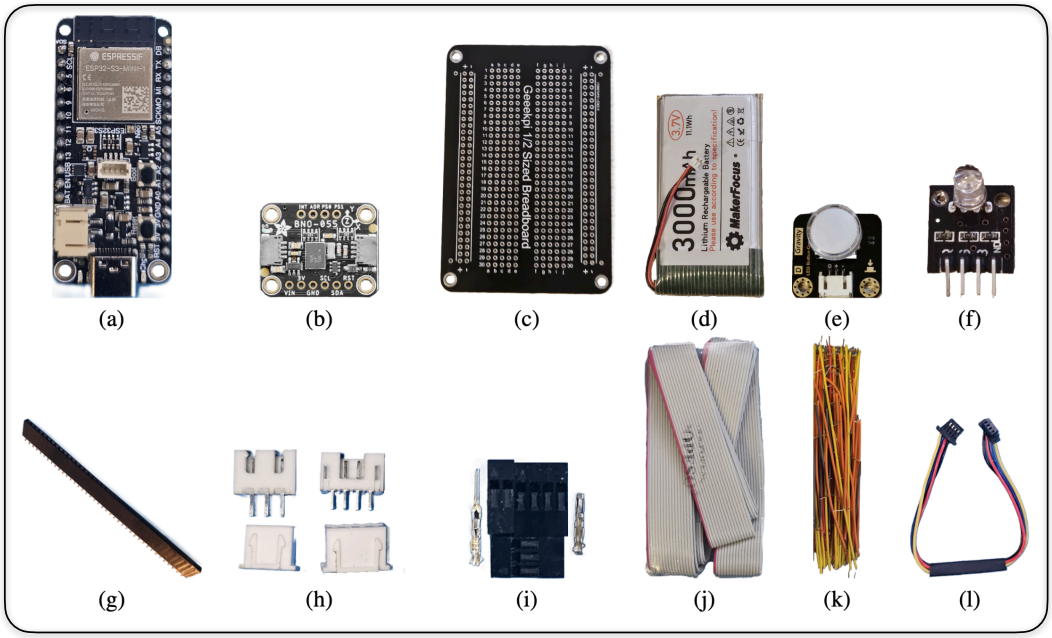

Figure 8.2: Common components of the insole and crutch Units. a) Adafruit ESP32-S3 Feather board featuring a STEMMA QT port, enabling easy integration with various sensor boards designed by Adafruit Industries (USA), as well as a JST 2-PH port for the power source. b) Adafruit BNO055 IMU providing a STEMMA QT port. c) Solderable breadboard with 2.54mm hole-to-hole spacing for housing the necessary components. d) Rechargeable 3000 mAh Lithium polymer (LiPo) battery. e) AZ-Delivery KY-016 FZ0455 3-colors RGB LED module for visual signaling. f) DFRobot Gravity LED Button, which goes with a JST to Dupont (female) cable, for turning unit on and off. g) Female pin headers allowing for plug-and-play connections for more expensive components, such as the ESP32, to avoid direct soldering to the board. h) JST-XH 2.54mm connectors for interfacing various components with the breadboard. i) Dupont connectors for interfacing specifically the button cables with the breadboard. j) Ribbon cables, allowing for removable connections between different electrical interfaces. k) Wire bridges for establishing electrical connections between different points on the breadboard. l) STEMMA QT cable for connecting ESP32 and BNO055 IMU.

The insole and crutch units feature a modular design within their individual setups, allowing for easy replacement of components. The two units share a number of components in their hardware makeup, shown in Figure 8.2. A main soldering board holds their individual components and facilitates the soldered connections between them. For all four sensor units (two for the insoles and crutches each), an Adafruit ESP32-S3 Feather Micro Controller Unit (MCU) (Adafruit, New York, USA) is used for collecting and streamlining the data to the central unit, a Raspberry-Pi 4 (Raspberry Pi Foundation, UK) where the data is saved and the fuzzy logic algorithm estimates the user's gait phase. Both types of sensor units feature a rechargeable $3000mAh$ Lithium-Polymer (LiPo) battery, LEDs for signaling system information such as BLE connection and power status, and a main interface button responsible for powering the device and calibrating sensors. The sensor batteries can be charged by connecting a micro-USB cable to the ESP32 units, which connect to the LiPo batteries via JST connections. For all sensors, a BNO055 IMU (Bosch, Reutlingen, Germany) is connected to the MCU via a STEMMA QT connection.

Crutches Design

For the integration of the load cell sensors within the crutches, a pair of standard forearm crutches were cut just above the bottom tip and reinforced with aluminum inner cylinders on both sides, spanning 5 centimeters long, and featuring threaded inputs. The sensor unit is housed in a 3D-printed case and attached with printed clamps on the shaft of the crutch, just under the handle, which minimally shifts the inertia properties of the crutch. Additionally, a flexible elastic 3D-printed hemispherical sleeve was attached at the bottom tips of the crutches to minimize bending moments about the center of the load cell (Figure 8.1) and help maintain its integrity.

A load cell LCM200 (Miniature threaded in-line, $250lb$, FUTEK, California, USA) was fitted between the two parts in the crutch shaft, forming a strong connection through the central axis of the crutch (Figure 8.3). To avoid high energy requirements and bulky components, an HX711 amplifier (Avia Semiconductor, Xiamen, China) was used to read the load cell's output and relay the data via its 24-bit analog-to-digital converter to the ESP32 unit. The BNO055 IMU was fitted to collect acceleration and orientation data, while the Adafruit ESP32-S3 Feather MCU was employed for collecting sensor data, featuring a BNO055 IMU, an RGB-LED for visually signaling the state of the peripherals and battery level, and a button for direct physical interaction. A rechargeable $3000mAh$ lithium polymer battery powers each board.

To maintain the simplicity, low weight and volume, and cost-effectiveness of the crutches assembly, unlike previous studies where strain gauges were integrated along with bulky braces on the sides of the crutch tip [209, 208], a uni-axial load cell was chosen based on preliminary experiments within this study. In these tests, the crutch GRFs contributions in the three axes were examined during exoskeleton-assisted gait for three participants, comparing the force vector components from a force plate by translating them into the crutches' reference systems. The transverse components were deemed negligible when compared to the central axis of the crutch, ranging from $12.6 \pm 3.74N$ for mediolateral forces to $24.2 \pm 6.78N$ for anteroposterior forces, averaging less than 7% of the vertical forces, as shown in Figure 8.4a, matching values previously reported in literature [220], for crutch-assisted four-point gait.

Hence, the assumption is made that the value recorded from the load cell, of the force running along the central axis of the crutch, is the resultant ground reaction force. To fortify this assumption, the integration of the flexible hemispherical sleeve at the bottom of the crutch tip aids with correctly orienting the crutch. Thus, by exploiting the orientation values from the crutches' IMUs, we can decompose the resultant GRFs into their components and further investigate the anteroposterior and mediolateral contributions, shedding light on propulsive/braking and balancing forces, respectively. IMU data, including orientation and angular accelerations, and load cell data are serialized to a JSON format. These sensor units conclude the

crutches' peripherals, integrated into the wireless protocol along with the insoles peripherals, described in Subsection "*Central Unit and Data Handling*".

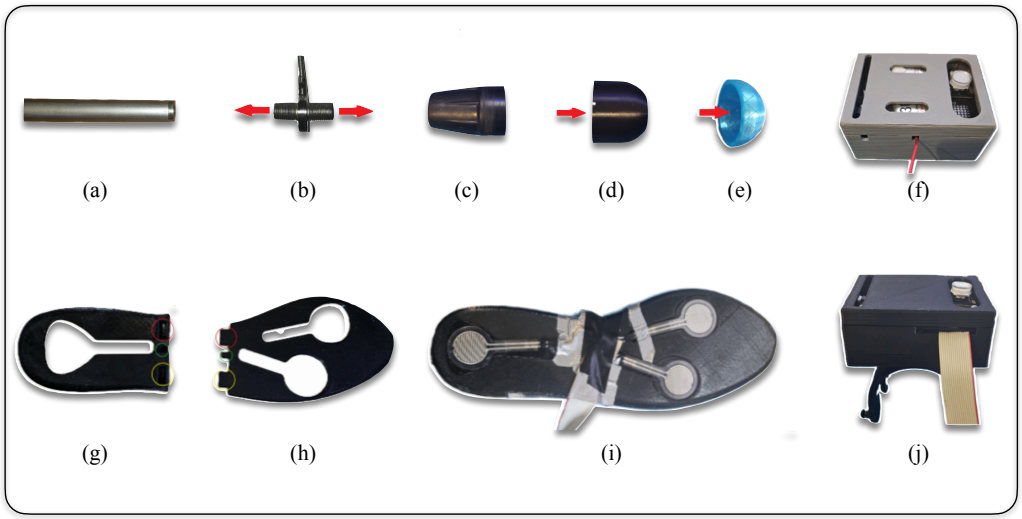

Figure 8.3: Components of the crutch and insole units: (a) the female-threaded drilled shaft of the crutch, (b) the male-to-male threaded load cell with signal cable leading to the peripheral unit, (c) the female-threaded aluminum shaft inserted in the rubber tip of the crutch, (d) a 3D-printed rigid hemispherical sleeve, (e) a 3D-printed flexible hemispherical cover, (f) the complete crutch peripheral unit including all components, (g) the bottom half of the 3D-printed flexible insole, (h) the top half of the 3D-printed flexible insole, (i) the connected insole including the FSR sensor inserts and ribbon cable leading to the peripheral unit, and (j) the complete insole peripheral unit.

Insoles Design

The design of the 3D-printed insoles is primarily driven by considerations of cost-effectiveness, comfort, and ease of application, such as facilitating sensor interchangeability among different insole sizes—small, medium, and large, including different sized top and bottom modules. Our main objective is to investigate the anteroposterior CoP, thus designs utilizing over 20 sensors to cover the entire foot [197, 200, 221, 122] were deemed excessive. Instead, our design adopts a minimalist approach, strategically placing a reduced number of sensors at critical foot locations. As already shown in previous works [215], gait phases can be detected and categorized with using as low as four FSR sensors, but based on preliminary tests we carried out using the Moticon Insoles (Munich, Germany), we concluded that three sensors would satisfy the requirements of our applications.

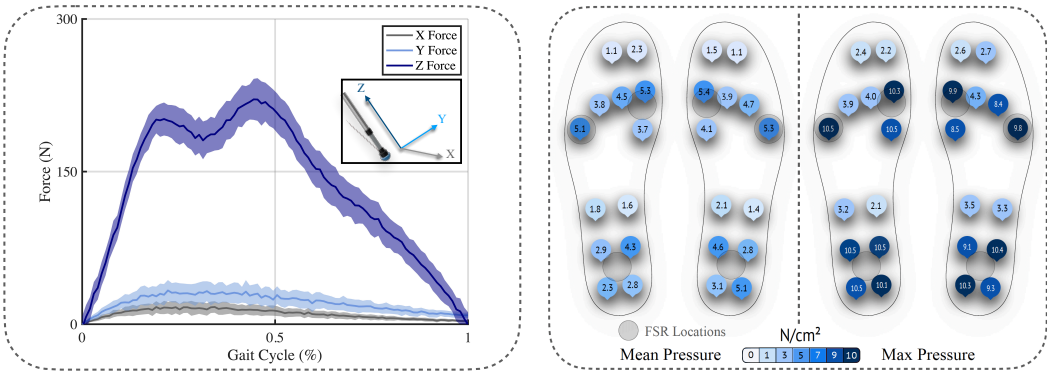

(a) (b)

Figure 8.4: Preliminary tests for informing system design. a) Comparison of GRF components for exoskeleton assisted walking. Multiple crutch strike force data were collected by the force plate and averaged over normalized gait cycles. The mean of each component is plotted along with the standard deviation is illustrated in the shaded region. The insert represents the orientation of forces relative to the crutch. b) Pressure distribution during exoskeleton-assisted walking. Plantar pressures for 30 gait cycles were recorded using Moticon insoles featuring 14 sensors distributed across the foot. The average mean (left) and maximum (right) pressures for each sensor are denoted.

A participant used the insoles while walking with the exoskeleton, completing a total of 30 gait cycles. The results were analyzed, showing the highest centers of plantar pressure in the middle of the heel, first, and fifth metatarsals (Figure 8.4b). In pursuit of simplicity, we positioned one sensor at each of these key locations for both insoles. This placement aligns with the physical design constraints of LLEs, which typically feature a robust plate at the bottom of the footwear, effectively transforming the foot into a single rigid body driven by passive ankle flexion. This design assumption supports the division of the foot into two primary contact areas—the heel and the metatarsals—and facilitates a simplified formulation of gait phase estimation outcomes.

The flexible insoles were 3D-printed in small, medium, and large sizes using TPU-90 flexible filament (NinjaTek NinjaFlex, Airwolf 3D, Florida, USA) to ensure a solid yet comfortable surface. The insoles feature three gaps each, where key-shaped inserts containing the FSR sensors can be fitted. The bottoms of the insoles have guided ribbon cables that connect to the inserted sensors. This modular design allows for low-cost and efficient sensor interchangeability between different insole sizes. Additionally, if any sensor failure occurs, replacing the sensors is highly efficient.

A 3D-printed clamp mechanism allows for the attachment of the sensor cases to the shoe of the exoskeleton. The analog FSR data are converted by the 12-bit ADC onboard the ESP32-S3 Feather, which also takes in IMU data from the BNO055 included in the sensor unit. Angular accelerations and orientations from IMUs, along with FSR readings, are serialized to a JSON format. These sensor units complete the

insole peripherals, integrated into the wireless protocol described in the following subsection.

While maintaining a low design complexity and cost than previously developed solutions, our devices offer significant advantages in comfort, modularity, and ease of reproduction. The insoles are not only more comfortable but also modular, allowing for easy sensor interchangeability. The crutches are designed to be lightweight and less bulky, enhancing user convenience. We propose a unified sensor system that can operate together or independently, delivering high-quality results in a more streamlined and cost-effective manner.

Central Unit and Data Handling

The central unit comprises of a Raspberry PI-4 Model-B as to ensure seamless communication and computations between the four sensors. It is powered by a battery pack which is attached on a 3D-printed mounting interface, able to fit on the back of most common LLEs. Wireless communication is established via a BLE interface facilitated by Bluetooth 4.0, enabling high-speed energy-efficient data transmission. The system allows for both BLE and Bluetooth classic protocols, for higher throughput in data transmission. This enables the peripherals to transmit packets of serialized JSON data to the central, which are then deserialized and written in a tabular CSV file, as well as being fed into a fuzzy logic algorithm. The central system can work we both sensors at the same time, or either one of them independently of the other, based on the desired application. One RGB LED is connected to the Raspberry Pi in order to signal key events such as sensor connection, start and end of recordings, and power status among others.

The raw data collected and stored in the CSV file include the three-dimensional angular accelerations and orientations of the four IMUs, the two amplified load cell values from the crutches, and the six FSR readings from the two insoles, at each timestamp. The frequency and sampling rate of data collection can be easily adjusted as to enable for higher throughput and speed or a bigger transmission distance when the central unit is not on-board the exoskeleton or person. Data transmission can be maintained for up to 30 meters with no interruption, at a maximum frequency of 130 Hz. An Android App facilitates the control of the system via the Bluetooth network. By choosing through a number of inputs, the user can select to calibrate the system, start and end recordings, browse through previous recordings, select which sensors to include in the recording and additionally send triggers to external devices such as camera systems, which can be easily integrated by an accessory module we have created. For more information on handling additional devices please see the Instruction Manual [219].

External Trigger

As it's many times the case, there's the requirement of combining several measurement systems together, primarily motion capture technologies and force sensing equipment. In order to accurately map the data collected at different frequencies from different systems together for each timestamp, the data must be synchronized. In order to enable for this application in our system, we designed an external trigger box, featuring an ESP32 Firebeetle with an audio jack 3.5 mm breakout board, able to connect to most motion capture systems such as Noraxon, Vicon and Qualisys. The trigger unit was integrated within the wireless BLE framework and for every start, pause and end of recordings a trigger signal of respective lengths is sent to the host system or computer, by setting the output pin of the Firebeetle to high for a specific amount of time [219].

8.3.2 Software Design

The software design of this system includes the wireless communication between the central and the peripherals, as well as the control of the central via an Android application, the sensor-specific software on each of the peripherals, and the fuzzy logic algorithm installed on the central unit. This Subsection provides a description on the application and software design of each of these units. The software implementation, much like the hardware design, follows a simple and easy to reproduce pipeline in order to facilitate simpler research interactions.

Central Unit

The software for the Central Unit is primarily responsible for initiating the connection with the peripherals once they advertise their service over BLE and collecting their data. Once the system is powered on, the central starts searching for the peripherals until it can establish a connection with all of them. The onboard LED signals the state of this process.

After a successful connection, a new calibration procedure or recording can be initiated via the Android application. When the recording starts and ends, if an external trigger exists in the wireless framework, a sync signal is sent. The LED communicates the start and end of the calibration and recording procedures, as well as possible issues with connection to the peripherals. During the recording, the data is continuously written to a CSV file in the central system.

The central unit software can be installed on any Linux-based operating system, with two provided Docker files: one for cross compiling for Advanced RISC Machines architecture and one for building a docker image so that the software can be contained and run in a Docker container. While it is possible to run a Docker container on other operating systems, such as macOS and Windows, containers

do not have access to the Bluetooth service on the former and for the latter, some adjustments could be possibly made so that they do have the necessary access.

Peripheral Software

The software of the peripherals allows for the device to advertise a BLE service and transmit data once connected. Crutch Units send IMU and load cell data, while Insole Units send FSR data instead of load cell data. An LED on each peripheral signals the calibration and connection status of each unit via advertising a service over BLE. After successful calibration, the advertisement switches from calibration state to sensor readings.

Any errors during sensor initialization or communication with the ESP32 leads to an immediate restart, a few seconds after a red steady light is shown. Furthermore, peripherals can be brought to sleep mode with a button press of 5 seconds. For the Crutch Units, a button press of one second leads to the tearing of the load cell, which is also teared during startup.

The software on each peripheral is targeted specifically for the ESP32 MCU family, and are programmed using the ESP-IDF environment (Espressif, Shanghai, China). The software can be flushed on each MCU using serial communication.

Android Application

While at the time of the experiments the Android application was still under development, a publicly available 'BLE Scanner' application was used as to communicate with out system. The application recognized the services and characteristics advertised by the central and peripherals and could connect directly to the peripherals in case of any issues in calibration, or simply directly to the central where the commands could be send to. The commands varied between starting calibration, starting and ending recordings, sending a 'manual' trigger signal, restarting or shutting down the system, and inputting file names for each recording. Visual feedback was shown through the central's LED to indicate whether false commands have been sent.

8.3.3 Fuzzy Logic

Fuzzy logic was employed to process gait values collected from the insoles, aiming to effectively estimate the gait phase. Commonly found works [222, 122], utilize membership functions expressed as sigmoid functions that evaluate the absolute values of FSR readings,

$$\mu(F_i) = \frac{1}{1 + e^{-s*(F_i - F_0)}} \tag{8.1}$$

with F_i being the FSR readings and $\mu(F_i)$ representing the membership grade as result of an FSR reading being evaluated by the membership function. The parameter s determines the slope of the sigmoid curve and F_0 defines the threshold in terms of

the absolute value, meaning the point at which F_1 yields a membership grade of 0.5. An option is to utilize half of the maximum possible FSR reading for F_0. The greater s, the greater the change in $\mu(F_i)$ with small changes in F_i.

During testing with the fuzzy logic algorithm, it was observed that the FSR readings often did not achieve their theoretical maximum values, even under loads exceeding their specified ratings. Consequently, this approach of formulating membership functions may lead to less accurate results, that hinder the accuracy of phase estimation. To mitigate the effects of saturation in FSRs, the readings should be normalized. Other works introduced the normalization of FSR readings for primarily taking into account different walking styles and weight distributions [222, 122], by scaling down each FSR reading with the sum of all readings.

$$F_i^* = \frac{F_i}{\Sigma_{i=1}^{n} Fi} \tag{8.2}$$

Given these circumstances, following membership function is used

$$\mu(F_i) = \frac{1}{1 + e^{-0.15*(F_i - 0.45)}} \tag{8.3}$$

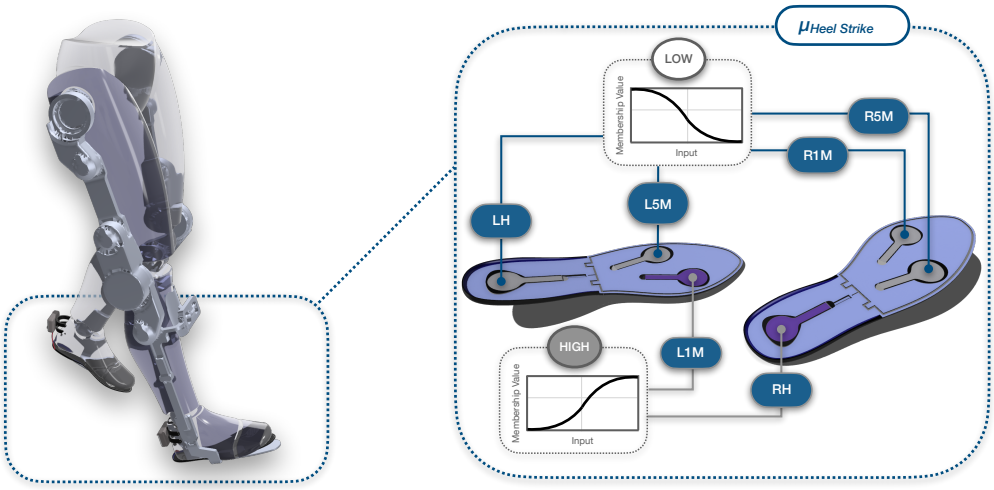

Figure 8.5: Example of heel strike through fuzzy logic rule-based approach. During exoskeleton gait, the gait phase is decided through a set of rules based on the membership grades assigned to the FSRs of both insoles using membership functions. Linguistic variables and logical expressions are used in order to decide the outcome, or gait phase.

Following the work of Kong and Tomizuka [215], the linguistic variables 'High' and 'Low', expressed through the aforementioned membership function, are utilized for the fuzzy representation of FSR readings.

$$\begin{aligned} \text{High} &= \mu(F_i) \\ \text{Low} &= 1 - \mu(F_i) \end{aligned} \tag{8.4}$$

These linguistic variables are used to construct the fuzzy rules that are based on fundamental logical expressions in the form of

$$\begin{aligned}&\text{IF } F^*_{\text{LH}} \text{ IS LOW AND IF } F^*_{\text{L5M}} \text{ IS HIGH AND}\\&\text{IF } F^*_{\text{L1M}} \text{ IS HIGH AND IF } F^*_{\text{RH}} \text{ IS HIGH AND}\\&\text{IF } F^*_{\text{R5M}} \text{ IS LOW AND IF } F^*_{\text{R1M}} \text{ IS LOW}\\&\text{THEN } G \text{ IS HEELSTRIKE}\end{aligned} \tag{8.5}$$

where F^* designated with the respective subscript represents the scaled-down FSR reading of each sensor placement, while G represents the gait phase. The abbreviations $LH, L1M, L5M, RH, R1M, R5M$ stand for the heel, first metatarsal and fifth metatarsal of the left and right foot respectively. Conditional statements, such as IF $F^*_{\text{LEFT HEEL}}$ IS HIGH determine the membership grade of F^* to a particular fuzzy set or linguistic variable, which, in this instance, is HIGH.

Chaining several of these expressions with the AND operator yields the minimum membership grade, representing the membership grade of G to a particular gait phase. This is expressed by conclusive statements like THEN G IS HEELSTRIKE , illustrated in Figure 8.5 where the two 'high' sensors are in a darker colour and the rest 'low' sensors in a lighter shade, during a heel strike phase.

Table 8.1: Fuzzy logic rules and gait phase outcomes based on FSR insole membership grades. Outcomes based on right insole.

	FSR Grades ($F*$)						**Outcome**
	LH	**L5M**	**L1M**	**RH**	**R5M**	**R1M**	
	Low	High	High	High	Low	High	Heel Strike
V	Low	Low	High	High	High	Low	Loading Response
A	Low	Low	Low	High	High	High	Mid-Stance
L	High	Low	Low	Low	High	High	Terminal Stance
U	High	Low	Low	Low	Low	High	Pre-Swing
E	High	High	High	Low	High	Low	Initial Swing
	High	High	High	Low	Low	Low	Mid-Swing
	Low	High	High	Low	Low	Low	Terminal Swing

Table 8.1 presents all rules for gait phase estimation in respect to the right foot. To obtain the rules for the left side, the conditional statements in each rule need to be inversed. 'High' signifies the condition F^* IS HIGH and 'Low' signifies the condition F^* IS LOW for a FSR placement. Once all rules are evaluated, each of the eight gait phases is assigned a membership grade.

8.4 System Evaluation

Three different experiments took place in order to validate the hardware and software capabilities of the system, against gold standard marker motion capture (Qualisys, Gothenburg, Sweden) and force plate (Kistler Group, Winterhur, Switzerland) technologies. The first two experiments comprised of standalone equipment testing, while for the third experiment three able-boded participants (1 female and 2 males, age 36 ± 7 years, weight 68.7 ± 12.1 kg, height 1.67 ± 0.08 m) were recruited. Figure 8.6 shows the equipment setup for the gait experiments with the three participants. The participants performed a set of six walking bouts each, with the TWIN lower-limb exoskeleton [47]. All participants signed informed consent forms prior to the experiments, the procedures of which were in accordance with the Declaration of Helsinki and approved by the Ethical Committee of Heidelberg University (resolution S-313/2020).

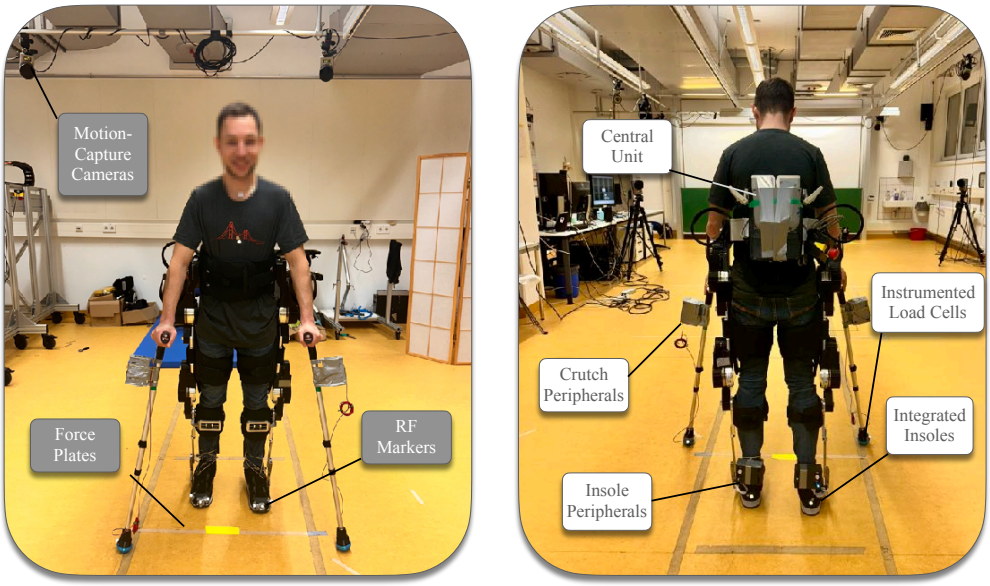

Figure 8.6: The experimental setup and equipment used for the validation experiments, indicating by one participant wearing the TWIN exoskeleton and the developed system comprising pressure-sensing insoles and force-sensing crutches. (Left:) front view of the participant wearing the TWIN exoskeleton with indications of the gold standard methodologies: motion capture cameras and force plates. (Right:) rear view of the participant wearing the TWIN exoskeleton with indications for the developed system.

All post-processing computations, data and statistical analyses were conducted using MATLAB (MathWorks Inc., Natick, Massachusetts, USA). For synchronization of data recordings, the trigger sub-system was used described in the previous section, by connecting the ESP32 Firebeetle trigger unit to the Qualisys system, incorporating the force plates, for sending a trigger signal through at the start and end of every recording. The three biomechanical metrics used to validate the system's capabilities against gold standard equipment are outlined in the next three subsections.

8.4.1 Anteroposterior Center of Pressure

The center of pressure is a critical metric for assessing balance and understanding the intentions—whether propulsive, braking, or stationary—of an exoskeleton user. For estimating gait phases and detecting user motion-intention, the anteroposterior direction (the direction of travel) plays the most critical role. Consequently, the anteroposterior CoP, measured along the length of the foot, was prioritized in our analysis of the system's capabilities. To capture the entire area of the feet, a person placed one foot on a force plate and performed circular clockwise motions, shifting their center of mass to record comprehensive CoP data. This circular motion was performed 18 times across three separate experiments. The CoP was then calculated from the FSR data of the insoles by computing the weighted averages for mediolateral and anteroposterior coordinates using the locations of the FSRs,

$$y_{\text{CoP}} = \frac{(y_H \cdot F_H) + (y_M 1 \cdot F_M 1) + (y_M 5 \cdot F_M 5)}{F_{\text{total}}} \tag{8.6}$$

where $y_H, y_M 1, y_M 5$ are the anteroposterior coordinates of the heel, first metatarsal, and fifth metatarsal sensors, respectively; $F_H, F_M 1, F_M 5$ are the FSR values measured at these points; and F_{total} is the sum of these values. Subsequently, the force plate CoP was transformed using the markers on the shoe from the global laboratory reference system to the insole reference system, as to enable comparison between the two values.

8.4.2 Crutches Ground Reaction Forces

A crucial yet often overlooked metric in the assessment of exoskeleton-assisted gait is the contribution of the upper body. To address this gap, our instrumented crutches are designed to provide detailed insights into how users utilize forearm crutches to support their gait. In one of the experiments, a person repeated a total of 18 circular movements over three experiments while applying forces to the crutch and maintaining it in contact with a force plate. The resulting force vector, captured by the force plate, was then translated into the crutch's reference system using markers placed on the crutch. The data from the load cells were subsequently compared to

the translated vertical component of the force plate, which aligned with the crutch's central axis.

8.4.3 Heel Strike Gait Detection

To assess the capability of our sensors to accurately estimate gait phases, we focused on a fundamental variable: the heel strike. Three participants, each equipped with the system and markers, performed 18 bouts across the laboratory using the exoskeleton. By analyzing the data from the heel FSRs, we identified the time frames of local maxima, which were then compared to those captured by motion capture cameras. Heel strikes from markers were defined by calculating the maximum and minimum distances between toe and sternum, and heel and sternum markers, as outlined in our prior research [170]. Toe-off events were also analyzed to provide further comparative data and enhance the evaluation of our system's robustness.

8.4.4 Data and Statistical Analysis

Data were collected from our custom sensor system (CSS), motion capture cameras, and force plates at sampling rates of 130 Hz, 150 Hz, and 1500 Hz, respectively. To ensure clarity and remove noise, a Butterworth filter with respective orders and cut-off frequencies was applied to each data stream separately. For comparative analysis, the data from higher sampling rates were down-sampled to match the lowest frequency data, thus normalizing the datasets. This approach to data treatment preserved the integrity and essential features of the raw data, ensuring an accurate representation for further analysis.

For our statistical analysis, a Shapiro-Wilk test at a significance level of $\alpha = 0.05$ revealed a non-normally distributed nature for our data sets. This led to all of our comparisons between paired data sets of biomechanical metrics collected using two different systems, to be made using the non-parametric Wilcoxon Signed-Rank test, where $p < 0.05$. Hence, our data is reported as median and Inter-Quartile Range (IQR) and based on the significance of the results, we report the median and IQR values for the differences between different collection methods, and the minimum, maximum, mean and standard deviations of Root Mean Square Error (RMSE) and the Pearson correlation coefficients between the data sets. Results are reported for the left side insole and crutch, as the Wilcoxon Signed-Rank test between the two sides did not show a significant difference.

8.4.5 Results of the Validation Experiments

Lower-limb exoskeletons have advanced wearable technology by significantly restoring mobility and rehabilitating impaired gait for individuals with movement disorders [223]. However, their efficient integration into daily life requires thorough biome-

chanical assessment, typically reliant on costly lab-based equipment that fails to capture critical biomechanical parameters in practical settings. Moreover, achieving transparent control remains challenging, with current solutions often depending on expensive sensors or complex machine learning techniques that may lack adequate user feedback and comfort.

To address these challenges in a cost-effective and user-centered manner, we developed a modular sensor-based system for typical LLEs, capable of recording key biomechanical metrics for assessment and motion intention-based control. The system includes forearm crutches with load cells and flexible 3D-printed insoles with pressure sensors, both integrated with IMUs. Data is processed through a fuzzy logic algorithm for efficient and accurate gait phase estimation. Additionally, we provide full open-source access to our hardware and software designs, along with instruction manuals. This approach advances real-life applications of LLEs, and to the authors' knowledge, these technologies have not been combined before, particularly in such a low-cost, simple, and effective manner.

To validate our system and the accuracy of the data recorded from the sensors, we performed a set of validation experiments against force plate and motion capture systems, based on three different metrics. Figures 8.7 to 8.9 visualize the comparative performance of our system against these gold-standard approaches, and Table 8.2 summarizes key statistical outcomes extracted from these three metrics.

Table 8.2: Pearson correlation coefficients and RMSE for all three metrics across all bouts and participants (where applicable).

	Anteroposterior Center of Pressure		**Crutch Ground Reaction Forces**		**Heel Strike Detection**	
	Pearson Corr.	**RMSE (mm)**	**Pearson Corr.**	**RMSE (N)**	**Pearson Corr.**	**RMSE (s)**
Min	0.873	14.4	0.921	10.5	0.997	0.0195
Max	0.948	19.2	0.967	17.9	0.999	0.0362
Mean	0.907 ± 0.038	17.2 ± 2.49	0.945 ± 0.023	15.3 ± 4.21	0.998 ± 0.001	0.0291 ± 0.0084

Anteroposterior Center of Pressure

The plantar CoP is a crucial metric for both assessing balance and informing the control of LLEs, with the anteroposterior component indicating whether the user intends to move forward or remain stationary. The anteroposterior coordinates of the CoP as recorded from the force plate and the insoles are shown in Figure 8.7, parts A to C, for each of the three bouts separately, as well as the actual difference values in part D, for each trial separately. Table 8.2 shows that the mean RMSE of the difference between the left insole and the force plate measurements over all three bouts is $17.2 \pm 2.50mm$. This indicates a high degree of accuracy, suggesting that the insole measurements closely match those of the force plate.The p-values for the

first, second, and third bouts are 0.178, 0.165, and 0.141, respectively, indicating no statistically significant difference between the insole and force plate measurements. A high Pearson coefficient of 0.907 ± 0.038 indicates a close correlation between the two measurement technologies.

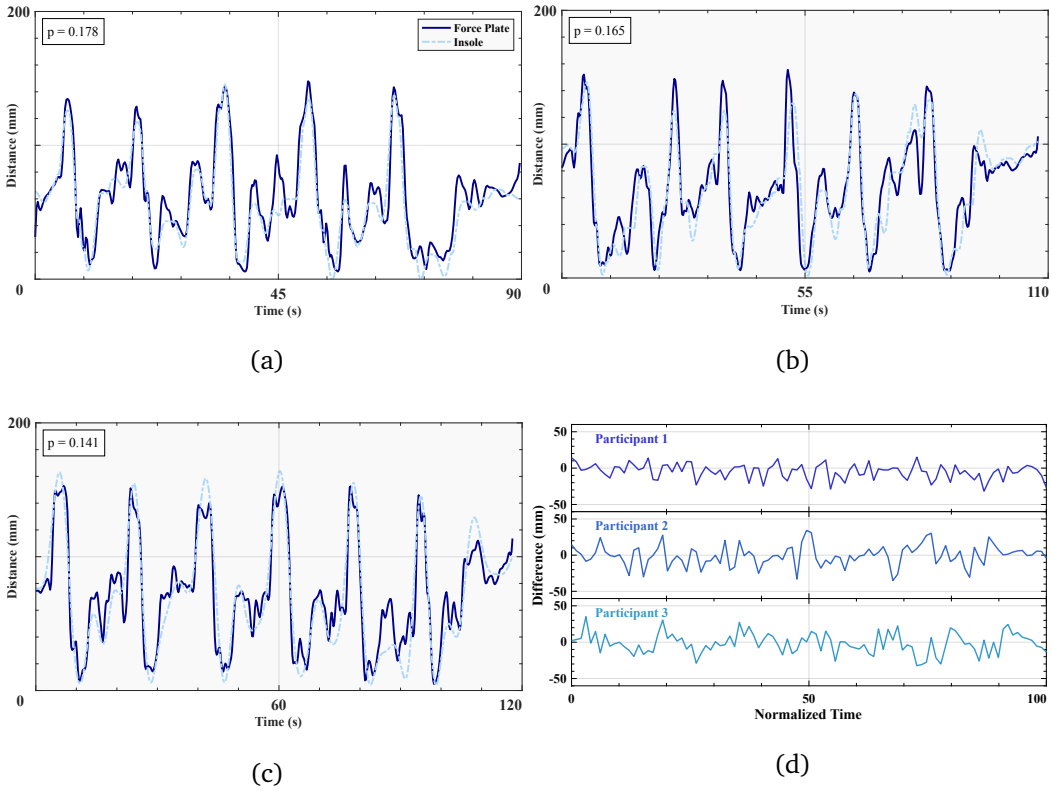

Figure 8.7: Anteroposterior center of pressure comparison between insole and force plate. (a) - (c) Three time series of the anteroposterior CoP as recorded by force plate and insole, from each participant in order, performing circular motions about their foot. p values are provided for each trial. (d) Actual values of the anteroposterior CoP differences between the force plate and the insole, for all three bouts separately.

Based on these results, the anteroposterior CoP measured by our insoles demonstrates a high degree of accuracy when compared to force plate data, comparable to previous research [224] (Pearson correlation coefficients $0.84 - 0.90$). For analyzing gait intentions and determining whether specific sensor membership grades vary from high to low, our system is more than adequate, as shown by the close matches of high and low peaks in Figure 8.7. Additionally, the high level of accuracy provided by the insoles offers a reliable biomechanical metric for assessing balance in assisted gait, achieved through a minimal array of three sensors.

Crutches Ground Reaction Forces

Upper body contributions in exoskeleton-assisted gait are often overlooked, thus the effort exerted by the user cannot truly be quantified as a whole. For long-term use of assistive exoskeletons, upper body efforts need to be evaluated and minimized to achieve an energy-efficient integration of exoskeletons into daily life [225]. Forearm

crutches GRFs provide important insight into how much upper body effort users exert when using LLEs. Figure 8.8 reports the GRFs recorded from the left crutch for each of the three bouts separately (A - B) and also for the median and IQR of the differences between the two collection systems over the three bouts. Values for the Pearson coefficients (0.945 ± 0.023) and RMSEs (15.3 ± 4.21) are reported in Table 8.2. The mean RMSE between the force plate and crutch is 15.3 ± 4.21 N over the three bouts, and the p values for each trial are 0.244, 0.103, and 0.599.

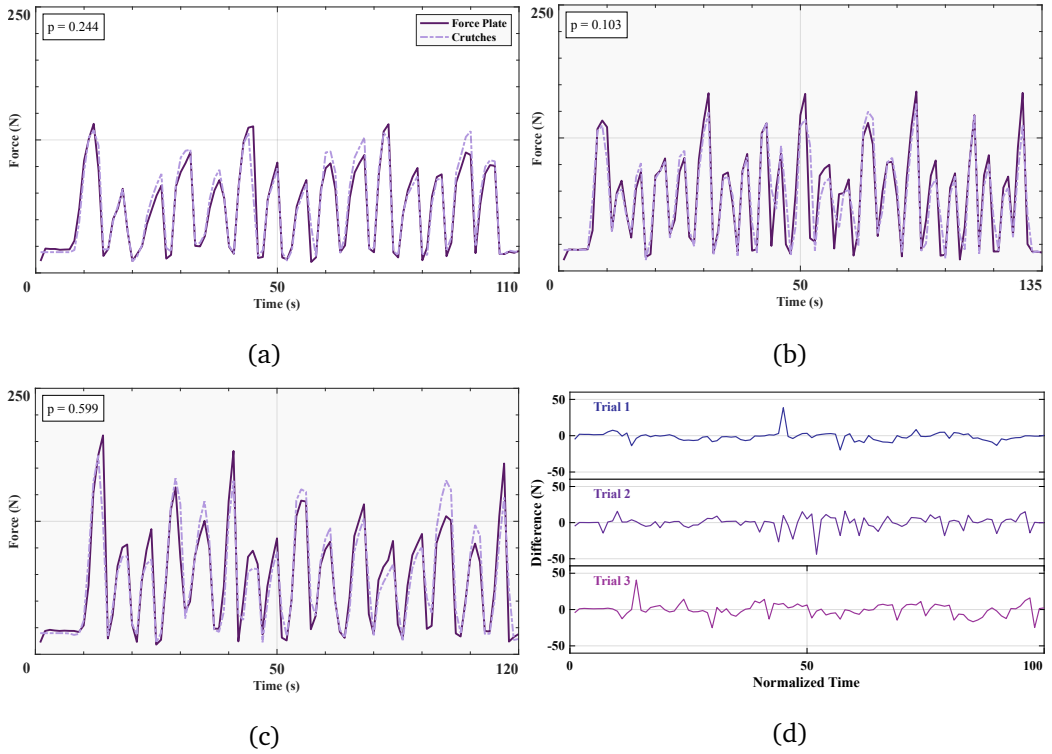

Figure 8.8: Ground reaction forces comparison between crutch and force plate. (a) - (c) Three time series of the GRFs as recorded by force plate and insole, from each participant in order, performing circular motions about their foot. p values are provided for each trial. (d) Median and IQR values of the GRFs differences between the force plate and the insole, over all three bouts.

The GRFs recorded from the instrumented crutches achieved a very high level of accuracy when compared to values obtained from force plates, as shown both in Figure 8.8 and Table 8.2. The deviation of the crutches was minimal, and the percentage mean RMSE of the ground-truth GRF (4.84%) is comparable to similar instrumented crutches studies using more comprehensive sensor arrays [220, 209] ($2\% - 5.4\%$ mean RMSE of total crutch GRF). In conclusion, our instrumented crutches offer a cost-effective and reliable method for accurately investigating upper body contributions via GRFs in LLE-assisted gait.

Heel Strike Gait Detection

Whether assessing key biomechanical metrics such as gait speed and stride duration, or accurately segmenting gait cycles from beginning to end, the heel strike is arguably the most important phase indicator [226]. The heel strike timestamps detected from markers on the left shoe and the FSRs of the left insole are compared in Figure 8.9. Part A reports the median and IQR values for each participant and each of the six bouts separately, whereas part B visualizes the errors for each individual heel strike over the three participants, as compared to the heel strikes calculated from marker data.

The mean RMSE between the markers and the insole over the six bouts for all three participants is $0.0291 \pm 0.0084s$, as reported in Table 8.2, highlighting the insole's high precision and robustness. This corresponds to an mean absolute error of 28.1 milliseconds which indicates high precision and performance of the system, especially in the context of exoskeleton gait. When compared to marker-derived timestamps of heel strikes, our method demonstrated a mean error of $0.844\% \pm 0.317\%$ relative to the respective step durations, where the mean step duration with the exoskeleton was 3.33 ± 1.16 seconds.

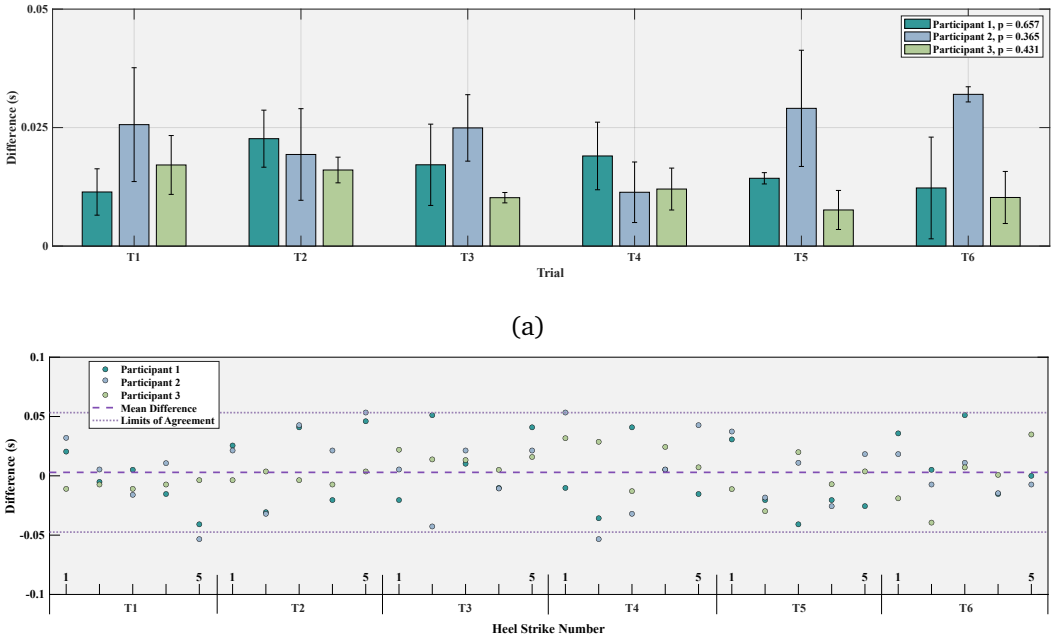

Figure 8.9: Heel strike comparison between insoles and markers. (a) Bar plots for six bouts reporting the median and interquartile ranges of the differences in heel strikes for each of the three participants. p values reported in the legend for each participant. (b) Difference of markers and insole heel strikes plotted against, for each participant heel strike over six bouts, along with the median difference and limits of agreement.

Figure 8.9b shows close agreement between marker-calculated heel strikes and insole, supported by a very strong Pearson correlation of 0.998 ± 0.001 across all participants. The limits of agreement present on the figure correspond to $\pm 1.96SD$ (95% confidence), and the equal spread of data below and above the mean highlight that the errors were symmetrically distributed around the true values, indicating no systematic bias in the method. Comparable to previous studies using insoles to identify heel strikes and segment gait, with a mean absolute error of $0.0168s$ [227, 228] mean absolute errors 0.01 to $0.03s$), our insoles demonstrate high precision, which validates the calculation of gait phase duration, as well as the use of FSR sensors within the fuzzy logic context for a rule-based approach to gait phase estimation.

8.4.6 Interim Conclusion of Validation Experiments

The experimental validation of our low-cost, modular sensory system showed that it can achieve a high level of accuracy in recording key biomechanical metrics, when compared to gold standard motion capture and force plate technologies. Hence, the reliability of the system is validated and confirmed in its ability to assess balance, ground reaction forces, and gait metrics, highlighting its potential for real-life applications in combination with LLEs. It is evident however that a larger participant sample would help yield higher accuracy results, therefore an extension of this study with a larger and more diverse population, investigating gait in a less controlled and perhaps outdoor environment that would allow for long continuous recordings would aid in fortifying the outcomes of this work. Additionally, implementing and validating a real-time control strategy for LLEs based on this system and the biomechanical metrics collected, as a way of assessing the user's motion intention, could significantly enhance the system's usability and practical applications, and help increase system transparency and safety, especially when it comes to older adults.

8.5 System Applications

Our modular sensor system offers a versatile platform for advancing the functionality and assessment of LLE. This section explores the two primary applications of our system: biomechanical evaluation and high-level control. By leveraging an array of biomechanical metrics and advanced control algorithms, our system does not only offer the potential to enhance the understanding of exoskeleton-user interactions but also significantly contributes to the development of responsive and adaptive assistive technologies.

8.5.1 Biomechanical evaluation

Integrated load cells and IMUs on crutches capture upper body dynamics during gait, offering data on propulsive, braking, and balancing GRFs, essential for exoskeleton assessment and improvement. Similarly, insoles equipped with force-sensitive resistors measure the CoP trajectories, crucial for analyzing balance and stability in real-time across various gait scenarios. Key metrics such as stride duration and gait speed are also derived, enabling comprehensive gait analysis. Orientation and acceleration data from IMUs provide detailed insights into limb positions and movements throughout the gait cycle.

Our system uniquely combines crutches' IMUs and insole sensors to accurately determine distinct gait phases, offering the capability of aligning exoskeleton mechanics with the user's natural movements and enhancing device responsiveness. A significant advantage of our system is its capability to perform evaluations in non-laboratory environments, broadening the scope for real-world exoskeleton testing and adaptation. This feature is invaluable for the iterative design and refinement of exoskeletons tailored for daily use. Its open and adaptable design ensures it can be customized to meet specific research or clinical demands, fostering innovation and continuous improvement.

In the context of user familiarization and the assessment of human-exoskeleton interactions, a set of transferrable metrics can be derived from this system that aid in evaluating LLEs in unrestricted environments, a clearly identified need proposed in our previous study, outlined in Chapter 7. Time-dependent metrics such as stride duration or gait velocity can be directly quantified through the fuzzy logic output, reinstating our validated familiarization metrics. In addition, gait metrics such as double and single support time, gait phase durations and crutch placement timings can be investigated. In terms of balance, the polygon of support metric can be translated into the anteroposterior CoP, and four-point gait contributions can be assessed in terms of applied pressure and forces. The GRFs from the crutches can serve as a valuable metric in upper-body involvement within exoskeleton-assisted gait, including their orientation components, exhibiting user preference when assessing balance and utilizing the propulsive and braking attributes of forearm crutches.

Distance-related metrics could potentially be derived via the relative position of the IMUs, by an adequate corrective algorithm for the accelerometer drift. Through a sensor-fusion approach, the heel strike moments detected via the insole FSR sensors can serve as zero-acceleration reference points. Considering the exponential nature of drift accumulation, the corrective algorithm should dynamically account for this proportional behavior to ensure accurate distance estimation, possibly via discretizing gait on a stride-to-stride basis and applying an exponential correction factor through a moving average approach. This kind of methodology could enable

the investigation of metrics such as polygon of support, crutch placement, distance walked and mediolateral deviations along a planned straight path.

Due to the possibility of longer uninterrupted walking bouts, cognitive functions can be assessed and serve as familiarization indicators, both in a qualitative and quantitative manner, by assessing the participant's perceived efforts, and comparing effects of different cognitive conditions such as single and dual tasking. It is evident therefore, that the mobile solution offered by the developed system offers a wide range of new approached in evaluating the biomechanics of human-exoskeleton interactions.

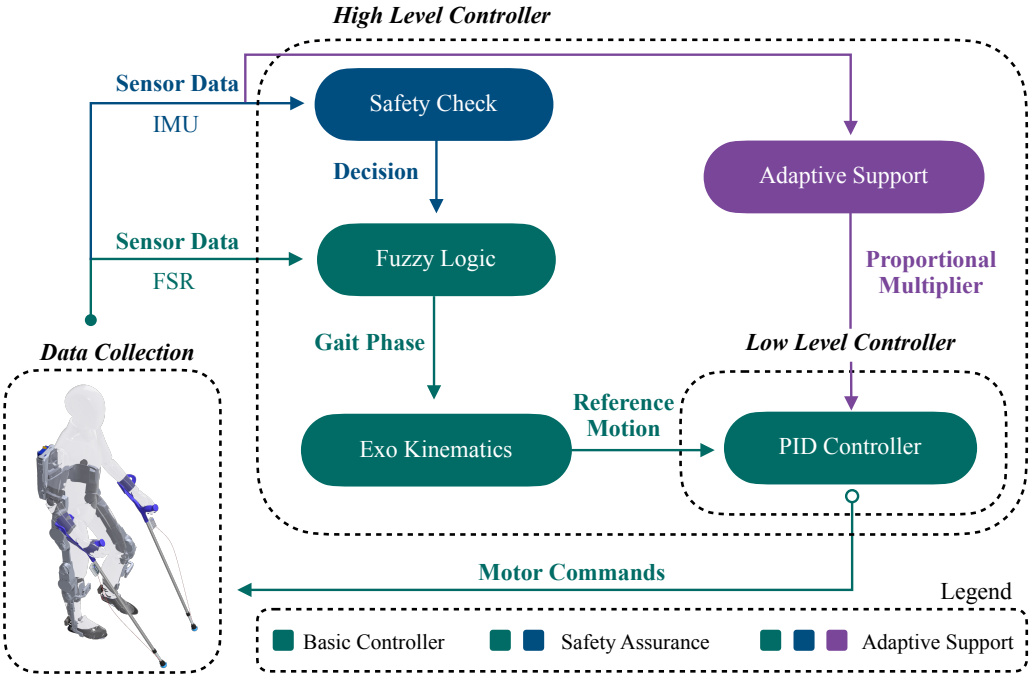

Figure 8.10: Proposed controllers example. The green schematic describe the normal processes of the basic controllers, whereas the additional blue controls outline the extra functions incorporated by the safety assurance controller, within the higher level controller of the system. If the decision made from the safety check proves true (or safe) then the basic controller processes take place. Finally, the purple schematics introduce the proportional multiplier directly applied onto the PID controller of the lower level control of the exoskeleton.

8.5.2 High-level controller

Real-time control of exoskeletons can be achieved by using the variables collected from our modular sensor system and based on fuzzy logic as a gait phase estimator, in order to achieve precise motion intention detection and provide adequate assistance to the user. Various control strategies can be employed using different subsystem configurations. In this section we provide proposals for three simple feedback-based control schemes that can be created from the collected data. Figure 8.10 displays three proposed control architectures, building on top of a more basic and

straightforward control, to a safety-inclined controller and a more adaptive-support architecture.

Basic Gait Phase Detection Controller

A basic control loop utilizes a simple fuzzy logic approach based on FSR voltages to identify distinct gait phases. The controller processes the sensor data to construct membership functions that determine the current phase of the gait cycle. Once a specific gait phase is recognized, the controller sends a signal to the exoskeleton to initiate or adjust movement, ensuring that the device is synchronized with the user's natural walking pattern. This basic control loop is crucial for smooth operation and enhances the natural feel of the exoskeleton during use. The transparency of the system is distinctively increased, especially from the current autonomous status of the exoskeleton. By managing to increase and shift the feeling of control to the user, LLEs can be adapted to older adults or other frail populations in an easier and more confident way.

Safety Assurance Controller

Building on the basic gait phase detection, a safety assurance controller incorporates additional safety checks using sensor data to verify the orientation and stability of both crutches and insoles. Before executing any movement commands, the system checks that both crutches are in contact with the ground confirming stable support, both feet have executed forward movements as indicated from IMU accelerations, and the orientation of the crutches and insoles is within predefined safe ranges to prevent falls or improper loading. This safety controller ensures that all conditions are met before allowing the exoskeleton to proceed with movement, significantly reducing the risk of accidents and enhancing user confidence. In cases where the gait cycle strives away from a typical assisted gait cycle, the check runs again to assess the current state of the person while the exoskeleton remains in a balanced position.

Adaptive Support Controller

The most advanced control loop is the adaptive support controller, which not only recognizes gait phases and ensures safety but also adjusts the level of support provided by the exoskeleton in real-time. This controller uses GRFs data from crutches to modulate the support intensity; higher forces detected via the load cells lead to increased assistance, adapting to the user's exertion level. IMU data is used to gauge the inclination of the crutches, which correlates with walking speed intentions. A lower inclination angle could indicate a desire to walk faster, prompting the controller to decrease the response time of support mechanisms. This proportional control strategy ensures that the exoskeleton's assistance is both responsive and

attuned to the user's immediate needs, providing a tailored support experience that adjusts dynamically to changes in walking dynamics or user fatigue.

8.6 Intermediate Conclusion

This study addressed the challenges of cost-effective and user-centered integration of LLEs into daily life, by means of advancing biomechanical evaluation and tackling limitations of current methodologies, as well as exploring various pathways in the enhancement of control transparency. We develop and validate a modular sensor-based system capable of recording key biomechanical metrics for both assessment and motion intention-based control. The proposed system, comprising force-sensing crutches and 3D-printed flexible insoles with integrated lod cells, IMUs and pressure sensors, employs fuzzy logic for accurate and efficient phase estimation. The validation experiments against gold standard methodologies indicated high accuracy in measuring anteroposterior CoP of the foot, GRFs from the crutches and detection of heel strikes. The results demonstrate strong correlations and low RMSE values, thus confirming the effectiveness of the system in capturing critical biomechanical parameters. In addition, we not only address limitations in terms of space restrictions of current technologies, but we promote collaborations and foster further developments in the scientific community by offering open-source guides and materials for the ease of reproducing the proposed system. By bridging the gap between laboratory-based assessments and real-world applications, this work sets a foundation for advancing both biomechanical evaluation and control strategies for LLEs.

8.6.1 Limitations of the Study

While the results reported in this study validate the robustness and accuracy of the system, certain limitations still prevail. Most importantly, the validation experiments were conducted in controlled laboratory settings with a limited participant pool, lacking assessment of larger and more diverse populations. Due to the limited space, the experiments were restricted to short-duration recordings, lacking environmental variability.m Testing in outdoor settings over extended durations is needed to evaluate the system's performance under more variable and realistic conditions, such as uneven terrain and environmental noise.

One prominent limitation of this custom sensor system is the lack of accurate detection of the mediolateral coordinate of the CoP (perpendicular to the direction of travel of the foot). The determination of this quantity was not required for the application we intended the system for, however, the necessary provisions are set in place and are described in our replication guide, as to enable for more FSR sensors integration and thus capture more information on the mediolateral plane. In

addition, the full utilization of IMU sensors holds significant potential for determining relative position details. Developing an algorithm to mitigate accelerometer drift could enhance accuracy, potentially leveraging FSR data to identify ground contact and zero-acceleration points. This approach could enable a continuous correction of drift through a discretized non-linear relationship, improving the reliability of position estimates.

Extending the system's capabilities in testing the proposed control strategies and their implementation and validation was not possible within the time frame of this study. However, the open-source nature of the system allows researchers to exploit the available hardware and software for real-time control experiments in the field, fostering broader applications and innovations in exoskeleton-assisted gait research.

8.6.2 Advancing the Applications of Biomechanical Evaluation

Next steps in extending research in biomechanical evaluation of exoskeletons should expand to larger and more diverse population groups, longer testings and more diverse environmental conditions, as to ensure the applicability of the system through a number of different usage scenarios. In addition, outdoor studies should be conducted to examine the system's reliability and usability in real-world environments, as well as investigating familiarization patterns with LLEs in extended, real-world scenarios. This type of assessment could provide valuable insights into user behavior and device interaction over time, bringing the interface of human and exoskeletons a step closer to adaptation to frail older populations or population groups with mobility disorders.

Finally, an important pathway for future investigation involves employing this system for the real-time control of LLEs. A robust starting point would be the control methodologies proposed in this study, particularly those focusing on user safety and adaptive support. This work is pivotal in ensuring safe and efficient integration of LLEs into everyday activities, particularly for frail or older populations. The next Chapter details a large outdoor study employing this newly developed system to track biomechanical metrics for exoskeleton-assisted gait, with a main application in quantifying familiarization.

Quantifying Familiarization via an Outdoor Dual-Task Study

9

Credit and Publication Statement
Giorgos Marinou co-designed the concept and methodology, conducted the experiments and investigation, carried out initial fittings and trainings with the exoskeleton, implemented the custom sensor system from Heidelberg University, and performed the analysis of biomechanical metrics. Norman Riedel of the Karlsruhe Institute of Technology co-designed the concept and methodology, conducted the experiments and investigation, acquired ethics approval, implemented the cognitive tasks in the experiments, and performed the analysis on cognitive performance and comparison between assisted and unassisted gait of biomechanical metrics collected with the Noraxon IMU suit. Katja Mombaur and Barbara Deml secured funding for this research study and contributed to its conceptual design and analysis of the experiments. This Chapter is based on content from a journal article currently in submission with Giorgos Marinou as the first author, and contains a short summary of a journal paper in review [229] with Norman Riedel as first author and Giorgos Marinou as second author.

This Chapter introduces novel experimental work, aiming to take a significant step forward in the biomechanical evaluation of LLEs, by conducting a study in a real-world, outdoor environment. Existing literature on biomechanical evaluation of exoskeletons takes place primarily within controlled laboratory settings [230]. Studies that aim at evaluating long distances of assisted exoskeleton walking, utilize treadmills within motion capture facilities [231, 51]. However, these studies mainly involve exoskeletons that target a single joint-such as the ankle-or soft exosuits, that do not require external assistance from crutches, or do not restrict or cause balance implications. In addition, these evaluation procedures fail to investigate effects of environmental variability and how human-exoskeleton interaction would be affected in a more real-world setting.

This study embraces the complexity and variability of the real world, in order to better understand how users familiarize themselves with these devices and what role the environment plays in this process. In addition, studying how users adapt to exoskeletons can improve understanding of safety procedures, especially when transferring this technology to frail populations. The motivation for conducting a large-scale outdoor study lies in its potential to bridge the gap between experimental

findings and practical applications, ensuring that exoskeleton designs align more closely with the demands of everyday mobility. Within this framework, we aim towards a more human-centric design while keeping the user part of the evaluation and optimization process of exoskeleton development.

Building on the foundation of familiarization research presented in Chapter 7, as well as previous research works in literature [170, 232, 233], this study offers insights into how users adapt biomechanically and cognitively when interacting with exoskeletons. Familiarization is explored through biomechanical principles, in tandem with the investigation of cognitive performance such as dual-tasking, and motor learning. The addition of such concepts is specifically impactful when considering the ultimate goal of the HeiAge project, which is translating exoskeleton technology to older adults and frail populations. By investigating how young, able-bodied participants adapt and learn to use exoskeletons with and without secondary cognitive tasks, this study lays the groundwork for understanding adult motor learning processes. Such insights can directly inform the design of personalized training protocols, promoting both technology acceptance and effective use in populations requiring mobility support. The final goal of this research is to contribute to the optimization of exoskeletons, potentially offering an accessible platform for human-in-the-loop optimization, starting from developmental cycles and up to the user-specific integration of the device.

This Chapter comprises the culmination of the research work presented in Chapters 7 and 8. It details a large, outdoor biomechanical study with a multifold purpose; first, quantifying short-term familiarization to the LLE TWIN, over long distances, examined as a function of a set of biomechanical parameters that are collected using the sensory system described in Chapter 8. Secondly, the cognitive performance of participants walking with the exoskeleton is investigated through a comparative study between assisted and unassisted gait, as well as single and dual tasking conditions. Moreover, familiarization is examined as an early marker for motor learning, in the context of LLE. The findings of this study related to familiarization, cognitive performance and motor learning patterns are examined as means of easing technology transfer to frail population groups such as older adults.

9.1 Biomechanical Evaluation of Exoskeletons

Exoskeleton performance can be assessed via a number of different methodologies and technologies, producing a set of biomechanical properties that quantify the differences in performance between assisted and unassisted conditions. Metrics such as joint kinematics and muscle activity [234, 235], metabolic cost [236], and gait dynamics [183] serve as relative performance indicators and help benchmark these devices across the field [51]. Most of these biomechanical evaluation protocols

are conducted within the limits of a laboratory space, restricting the uninterrupted distances participants walk, maintaining a very controlled environment without external influences, and taking long times in preparing, calibrating, and adjusting the measurement equipment on the users. While different exoskeletons exhibit different functions and target different demographics, an overall more efficient and standardized evaluation procedure could bring about a number of added benefits: more participants could be tested, frail participants could be tested without reaching their limits of fatigue, more meaningful comparisons could be made between exoskeletons targeting overlapping demographics, and exoskeleton features needed to be individualized to the wearer would become clearer, possibly promoting human-in-the-loop optimization procedures. Finally, familiarization of biomechanical and cognitive processes could be studied as means of expediting user adaptation and facilitating a more efficient integration of new technologies.

9.1.1 Lower-Limb Exoskeleton Familiarization

Chapter 7 defined familiarization as the reduction of a set of biomechanical parameters that describe the spatiotemporal and balance states of the human and the exoskeleton. Even though the study of physical human-exoskeleton interactions in literature is quite limited [237], a few studies attempt to investigate various aspects of user adaptation. Research works like Shushtari et al. [238] define the level of human-exoskeleton interactions on short-term user familiarization by analyzing muscle activity and interaction torques. Poggensee et al. [239] study the reduction of energy cost based on metabolic consumption as an indicator for familiarization, and relate reduction patterns of experienced users to their joint kinematics. The type of exoskeleton controller used is an additional variable influencing the familiarization process, as predefined motion trajectories (such as the TWIN exoskeleton) are less variable than force-based controllers or more user-intuitive types.

The field of studying human-exoskeleton interaction with the means of expediting and making the process of adaptation more efficient is relatively quite new and requires a more standardized methodology. While expensive equipment such as camera systems and respiratory monitors can capture accurate biomechanical metrics, it's not always easy to employ them in versatile environments, and they tend to need lengthy setup protocols. To counter this problem, a study from Lancini et al. [240] aimed to familiarize and train able-bodied users to attain atypical gait patterns, with the use of audio-feedback instrumented crutches, in order to increase the reliability and transferability of results from experiments using able-bodied participants. However, this approach still does not help expedite familiarization procedures with a wide variety of target groups. In addition, these studies fail to include environmental variability of the everyday scenarios these exoskeletons are meant to be used within.

Familiarization plays a critical role in optimizing the interaction between humans and exoskeletons, influencing the effectiveness of training protocols and the usability of these devices. By identifying strategies that expedite familiarization and minimize barriers to adaptation, researchers and developers can create more effective and inclusive training protocols, ultimately enabling exoskeleton technology to better support diverse user populations, including frail individuals and those with specific rehabilitation needs.

9.1.2 Cognitive-Motor Interference and Familiarization

Little is the number of studies that examine the cognitive human-exoskeleton interactions through the familiarization window or even after. As much as physical effects, cognitive effects of exoskeleton use are equally important and play a pivotal role in assessing the level of interaction between the device and the human. Upasani et al. [241] explored the mental demands of operating whole-body powered exoskeletons via eye-tracking, finding that novices experienced higher workload with increased pupil dilation, while experts exhibited distinct visuomotor strategies with more downward-directed path fixations, suggesting the potential of eye-tracking measures to assess mental workload. Similarly, Bequette et al. [242] investigated the effects of such an exoskeleton, both on physical and cognitive performance, highlighting variability in individual responses, slower reaction times, and increased perceived workload, underscoring the importance of considering a cognitive fit in exoskeleton design. In this way, dual-task conditions, involving simultaneous cognitive and motor tasks, are often introduced to examine cognitive interference by analyzing performance outcomes and variability across conditions.

In dual-task studies, gait parameters reveal the relationship between motor performance and cognitive demands. In a study by Al-Yahya et al. [243], dual-tasking was investigated on its effect on gait variability, a marker of motor control. Low variability reflects automated processes, while high variability indicates attentional engagement. High variability has been linked to negative health outcomes, such as falls in older adults [244]. While simple secondary tasks can reduce variability by promoting automated walking, complex tasks increase variability by competing for attention. This aligns with Huxhold et al.'s [245] 'Dual-Process Model', which explains a U-shaped relationship: variability decreases with simple tasks but rises again with complex ones, reflecting a balance between attentional focus and task difficulty. It is therefore important to understand how mentally demanding conditions affect gait variability and cognitive performance, especially when using exoskeletons with elderly or frail populations, where both physical and mental exhaustion need to be carefully addressed.

In the context of familiarization, the level of interference of mental tasks on motor performance could be a key factor in understanding how users generally adapt to

exoskeletons. Cognitive resources could be allocated differently from the start to the later stages of the familiarization period, leading to higher variability in physical and cognitive metrics and lower adaptation rates. On the contrary, as users become more proficient with the use of exoskeletons, cognitive demands could decrease, therefore promoting less variable motor patterns. This dynamic trade-off between cognitive and motor demands underscores the need for further research into optimizing the familiarization process. A more integrated approach to studying cognitive and motor interactions during familiarization can set the groundwork for exoskeleton designs and protocols that better support user needs.

9.1.3 Motor Learning, Transferrable Skills and Familiarization

Within the framework of human-exoskeleton interaction systems, motor learning can aid in understanding the underlying mechanisms of skill retention and transfer. Understanding how users adapt to exoskeletons can inform the development of training protocols that enhance both physical and cognitive familiarization. This is particularly important for older adults, as effective motor learning can facilitate technology transfer and improve their mobility. To this end, motor control and adaptation are critical through the design phase, to the implementation and control of exoskeletons and assistive devices.

Agarwal et al. [246] not only highlight the importance of motor learning within adaptation of a robotic exoskeleton, but the adaptation of training strategies, through dynamic allocation of task difficulty, assistance level and feedback, based on individual performances. This underscores the need to not only focus on adaptable training strategies but also incorporate a deep understanding of musculoskeletal and neuromuscular dynamics, as these are fundamental to designing effective exoskeleton systems and ensuring accurate predictions of user needs. As reported by Stollenmaier et al. [247], musculoskeletal dynamics, including neuromuscular characteristics are critical for accurately predicting the torque and power needed to be provided by assistive devices, as simpler models underestimate these requirements. On a higher level, we could potentially identify common motor learning markers that could facilitate an easier familiarization process to assistive technologies for new users. The work of Van Dijsseldonk et al. [248], highlights the potential to predict motor learning patterns in exoskeleton users based on individual characteristics, offering valuable insights for understanding and optimizing adaptation processes. Early training outcomes were influenced by factors such as lesion level and active lifestyle, while predictors like BMI, age, and an active lifestyle became more relevant in later stages of training. These findings suggest that individual traits can serve as indicators of skill acquisition and progression, providing a foundation for tailoring training protocols.

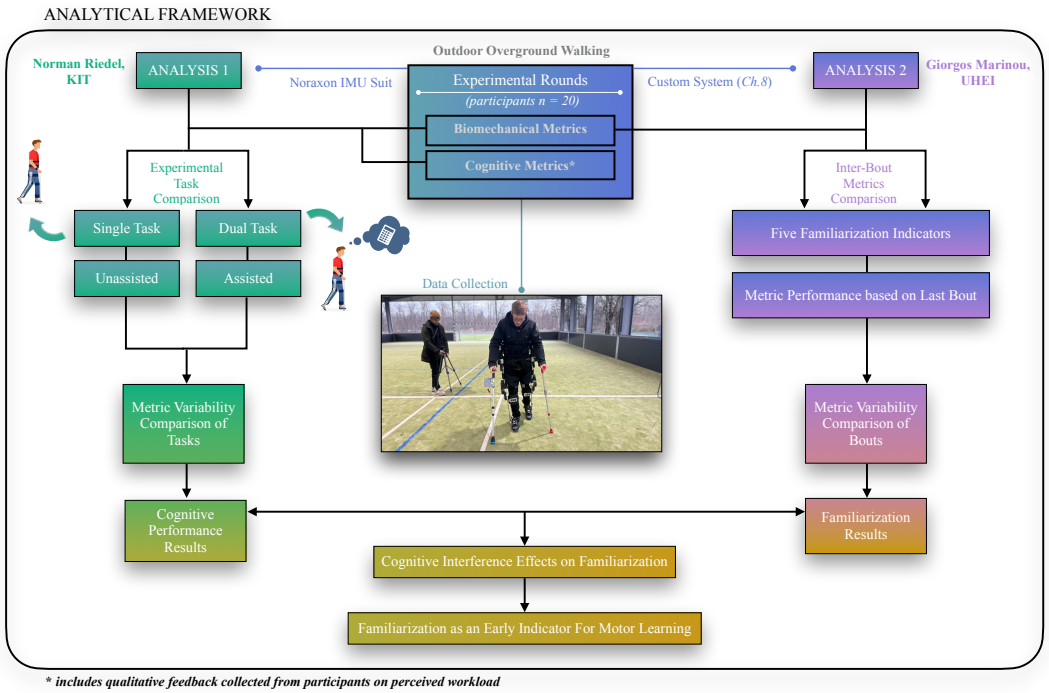

Figure 9.1: Framework for biomechanical and cognitive analysis in outdoor exoskeleton-assisted walking study. Biomechanical and cognitive metrics were collected during single-task and dual-task conditions using a Noraxon IMU suit and a CSS (see Chapter 8). The analysis focuses on reductions in task variability and changes in metrics within and across walking bouts, providing insights into user adaptation during outdoor, overground walking. Using the results from the two distinct analysis methodologies, initial indicators for motor learning and familiarization can be produced.

While there has been made progress in understanding motor learning and musculoskeletal dynamics, there's still a lack of studies connecting biomechanical adaptation with cognitive and motor learning outcomes. Hence, focus should be shifted on exploring motor learning at different levels—skill attainment, retention, and transfer—especially when it comes to assistive technologies. These aspects are closely tied to familiarization, as both are part of the broader process of adapting to exoskeletons. By studying the physical and cognitive factors involved in familiarization and motor learning, we can better understand how users adapt in the short term and how that sets the stage for long-term success. Analyzing behaviors during the early stages of familiarization could reveal key indicators of motor learning potential, helping us predict how users will respond over time. This insight could guide the development of training protocols that improve exoskeleton adaptation and meet the needs of a diverse range of users. In the study presented in this chapter, user adaptation is defined both by motor learning and familiarization indications. The analytical framework followed and the work split between the two parties (Giorgos Marinou and Norman Riedel of KIT) in order to detect indicators for familiarization, and examine cognitive interference effects on exoskeleton-assisted walking, as well as inferring early markers for motor learning is detailed in Figure 9.1, and outlined further, as part of the experimental protocol and data analysis, in Section 9.2

9.2 Study Contributions

Current exoskeleton technologies face limitations due to an incomplete understanding of how exoskeleton adaption influences biomechanical outcomes, through its disciplines of familiarization and motor learning. Initial training protocols, as well as technology transfer through a diverse spectrum of end-user population groups, could be positively impacted by understanding these basic concepts of adaptation. Additionally, there is insufficient evidence on how cognitive interference conditions impact assisted gait in terms of mental and physical performances, especially in real-world settings. These gaps hinder the optimization of exoskeleton training protocols and limit their potential to support users effectively, particularly in frail populations. Finally, typical methodologies in exoskeleton validation tend to take place in controlled environments and more than often within laboratory bounds, therefore limiting environmental variability conditions, that would better reflect the intended use for these devices.

The study presented in this chapter addresses these challenges by uniquely focusing on outdoor overground walking with a LLE, while introducing dual-task conditions. We simultaneously collect biomechanical gait parameters, as well as cognitive performance metrics and qualitative user feedback. The outdoor nature of the experiment enables simulation of real-world conditions in order to test applicability of exoskeletons. The study of familiarization becomes possible via investigating both physical and cognitive metrics, and their evolution through the experiment as to comprehensively study adaptation. Familiarization is then examined as an early indicator for motor learning, which in turn enables the deeper understanding of exoskeleton training and evaluation through a user centric approach.

The findings from this study aim to inform the design of training protocols that cater to the specific needs of frail populations, enabling them to benefit from exoskeleton technologies. By providing insights into how exoskeletons can better complement human movement and cognitive demands, this research contributes to advancing human-exoskeleton interactions, ensuring these devices are not only functional but also intuitive and adaptable to diverse user groups.

This study seeks to answer several key questions aimed at addressing the challenges of human-exoskeleton interaction. First, how can familiarization be leveraged to improve the biomechanical and cognitive aspects of these interactions? Second, can we use familiarization to detect early markers for motor learning, and use this in helping users to adapt more efficiently? Finally, how can the insights gained from this research support the design and integration of exoskeletons for frail populations? By focusing on these questions, this study aims to ensure that exoskeletons are both accessible and effective to a wider population.

Research Objectives

Hence, to answer these questions we set out to complete the following objectives:

1. Quantification of familiarization via biomechanical and cognitive metrics, by outdoor exoskeleton-assisted walking.
2. Evaluation of the impact of cognitive interference on the physical and cognitive performance, as well as the adaptation to LLE.
3. Investigation of motor learning and its implication for transferrable skills
4. Examine familiarization as an early indicator for motor learning

Research Hypotheses

The defined objectives for this study and experimental round, give rise to the following hypotheses and expectations:

- **H0:** Stride duration reduces from the first to the last bout,
- **H1:** Gait velocity increases from the first to the last bout,
- **H2:** Double support time reduces from the first to the last bout,
- **H3:** Anteroposterior center of pressure increases from the first to the last bout,
- **H4:** Crutch ground reaction forces reduce from the first to the last bout,
- **H5:** Cognitive-motor interference increases during exoskeleton-assisted walking compared to unassisted walking, resulting in decreased cognitive performance, motor performance, or both,
- **H6:** Familiarization can be used as an early motor learning indicator, defined through biomechanical and cognitive metrics,

where H0 to H4 are the biomechanical metrics (see Subsection 9.4.1), that serve as familiarization indicators, showing that familiarization occurs with increased usage of the exoskeleton.

We therefore aim to set a standard to biomechanical evaluation of exoskeletons, while simultaneously better define the concept of user adaptation through quantifying familiarization, as well as inferring motor learning from initial outcomes. In the following two sections, the experimental protocol and analysis methodologies, aiming in answering the research questions posed are described. The results are presented in Section 9.6 and discussed extensively in relation to the initial hypotheses and claims of this chapter in Section 9.7. Finally, Section 9.8 offers the main conclusions and outcomes of the study, the implications to research, and mentions the limitations and future improvements to our study.

9.3 Quantifying Familiarization via an Outdoor Dual-Task Study

This project was realized through a collaboration between Heidelberg University and Karlsruhe Institute of Technology via the HeiKa cooperation agreement. The two main responsible parties included Norman Riedel of the iFAB group from the Karlsruhe Institute of Technology and Giorgos Marinou from the ORB group of Heidelberg University and the author of this chapter and thesis. The research was equally shared between the two parties and conducted in accordance with the American Psychological Association Code of Ethics and received approval from the KIT-Ethics Committee. Participants provided written informed consent.

9.3.1 Participant and Equipment Information

Twenty able-bodied young adults (age 25.3 ± 4.1 years, height $1.73 \pm 0.10m$, weight $69 \pm 12.1kg$, 10 female, 11 male) participated in the study. The participants recruited were students at the Karlsruhe Institute of Technology. The experimental rounds and data collection took place on an outdoor soccer facility, on a 25 meter long track, with a covered roof to prevent issues with rainfall (Figure 9.2A). In order to facilitate assisted walking, the TWIN exoskeleton [47] (described in Chapters 7 and 8 was used. Two measurement systems were employed, offering a combination of pressure, force and inertial measurements.

The Noraxon Ultium Motion IMU system (Noraxon, U.S.A. Inc., Scottsdale, AZ) in combination with the MyoResearch 3.20.40 software was used to collect and process kinematic data for the lower limb, by utilizing seven IMUs at the feet, shanks, thighs and pelvis. These sensors were attached to the participants based on the detailed instructions from Noraxon using velcro-type straps. For recording participant spoken word during cognitive task experiments, a recording device (Sony) with a clip-on microphone (Phillips) were used. Noraxon data was recorded at 200 Hz and Norman Riedel of KIT was responsible for recording these data and analyzing it.

The CSS described in Chapter 8, comprising instrumented insoles and crutches, was used as to collect spatiotemporal parameters from the exoskeleton and user. For further details on the system, please see the relevant chapter. Data with this system, was recorded at 130 Hz, and the implementation and analysis was carried out by Giorgos Marinou. An electronic box housing a microcontroller responsible for sending a 'trigger' signal to the Noraxon software was installed on the Noraxon receiver, as a means of synchronizing the two systems. Figure 9.2B details the placement of the main components of each of these systems.

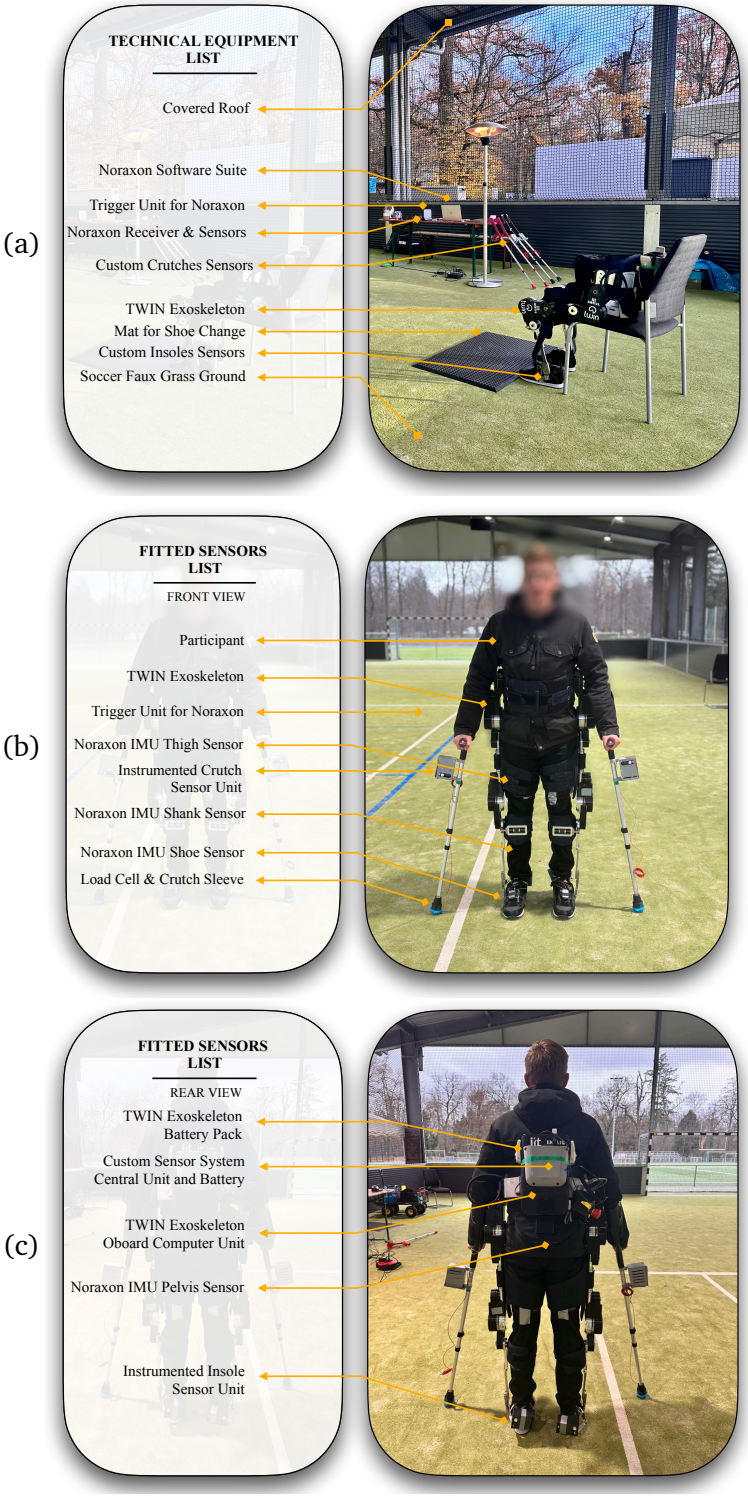

Figure 9.2: Experimental setup of the outdoor experiment. (a) Equipment setup and initial placement of exoskeleton prior to the experiment. Preparation station of Noraxon and custom measurement systems. (b) - (c) A participant during the outdoor walking experiment, wearing the TWIN exoskeleton, equipped with the CSS sensors as well as the Noraxon suit.

9.3.2 Experimental Protocol

For each participant, the experiment comprised of two separate appointments. First, an initial preparation appointment took place, where the participants signed informed consent forms, and were fitted to the exoskeleton according to their anthropometric measurements. A short instruction tutorial on the use of the exoskeleton and crutches took place right after, where each participant performed a maximum of five steps with the exoskeleton, thus forming a foundation but avoiding any familiarization effects with the exoskeleton.

Following the first appointment, the data collection day took place at least two weeks later. The exoskeleton sizes and crutches' height were prepared prior to the participant's arrival based on the measurements of day one. The experimental protocol is outlined in Figure 9.3. The experiment started with an initial cognitive task, where the participant performed a serial subtraction task while seated. The participants were given a random number between 301 and 999 and were asked to subtract 7 in a serial order, maintaining speed and accuracy as possible. Participant repeated this round twice, 60 seconds each, and rated perceived mental and physical workload based on the NASA-TLX scale.

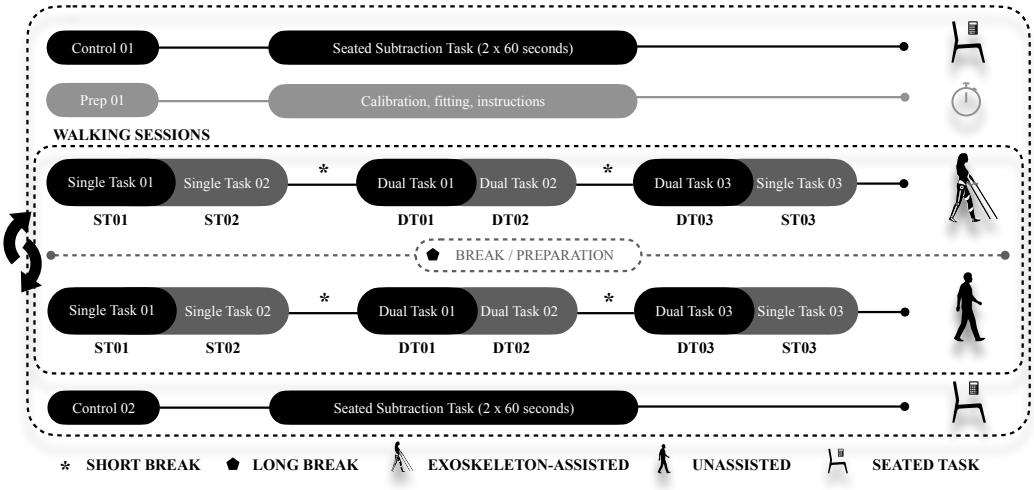

Figure 9.3: Experimental protocol for the data collection day on the second participant appointment. The experiment is initiated with a seated cognitive task, followed by preparation and equipment calibration, before executing the two randomized and counterbalanced walking sessions; one exoskeleton-assisted and one unassisted. The experiment is then concluded with a final seated cognitive task.

After the initial task, participants were fitted with the Noraxon IMU suit and the calibration procedure, including a static and dynamic sequence, took place. Following a standalone calibration of the CSS, the two randomized walking sessions took place; one unassisted (without the exoskeleton) walking session and one assisted (with the exoskeleton) walking session. Each walking session comprised of three

experimental blocks, each including two 25 meter walking bouts. At the end of each bout a short break of approximately two minutes was enforced, while at the end of each block a longer five minute break took place. The first block consisted of two walking bouts without a secondary task, namely single-task bouts (ST01 and ST02). The second block, consisted of two dual-task bouts where the serial subtraction cognitive task was incorporated during walking (DT01 and DT02). The third and final block required participants to first perform one last dual-task bout and end the session with a final single-task bout (DT03 and ST03). During the breaks (short and long) at the end of each walking bout, the participants rated their perceived mental and physical workload.

While the participants walked without the exoskeleton, only the Noraxon IMU suit was used to measure kinematics and the audio recorder to record participant dual-task answers. Participants then walked at their preferred walking speed. During the exoskeleton-assisted walking session, the participants donned the TWIN exoskeleton, carefully transferring the shoe IMU of the Noraxon suit to the exoskeleton. The instrumented insoles were incorporated within the shoes of the exoskeleton and the instrumented crutches were given to the participants. A brief repetition of usage instructions was given to the participants. Once the walking sessions were finished, every participant repeated the serial subtraction task twice, while seated, much like the beginning of the experiment. The total duration of the second experiment reached a maximum of three hours.

9.4 Data Analysis Pipeline

Data Declaration: Data for this experiment were analyzed based on the combine measurement systems recordings, as well as the audio recorder data. The analysis was split between the two responsible parties - iFAB and ORB groups of Karlsruhe Institute of Technology, and Heidelberg University respectively. Norman Riedel from the iFAB group processed the Noraxon IMU Suit and audio recordings data, while Giorgos Marinou from the ORB group processed the CSS data. All biomechanical metrics were cross checked between both measurement systems, and were found in excellent agreement. This data validation is not included in this chapter as a validation of the CSS is offered in Chapter 8, and would be outside the scope of this study. The data presented hereafter, are a product of both systems. A definition on the derivation of each metric is provided in this Subsection. The software platform Matlab R2023a (The MathWorks, Natick, MA, United States) was used to perform all relevant data and statistical analysis procedures.

9.4.1 Metrics Derivation

Motor Performance

For the *primary analysis* of this study, a set of biomechanical metrics was calculated based on the data collected from the CSS. As familiarization is the main question of this study, the biomechanical metrics from Chapter 7 were adjusted according to the system capabilities discussed in Chapter 8, to yield results for stride duration, gait velocity, double support time (DST), anteroposterior center of pressure (APCoP), and GRFs from the instrumented crutches. These biomechanical metrics served both as motor performance, as well as familiarization indicators. The five metrics were defined as follows:

1. Stride Duration: The time for one complete gait cycle, or the time from a heel strike to the subsequent heel strike of the same foot.

2. Gait Velocity: The distance traveled over the time duration to travel that distance, for one walking bout. The time was calculated from the first valid heel strike of one walking bout, to the last one, and the distance of those bouts was determined by multiplying the number of strides with the fixed stride length of the exoskeleton. The stride length differed for each participant according to their height and segment dimensions.

3. Double Support Time: For each stride, the DST was calculated as the time duration between the heel strike of one foot to that of the contralateral foot.

4. Anteroposterior Center of Pressure: The average of the CoP in the direction of travel-along the central axis of the foot-for one stride. The APCoP was normalized according to the scale shown in Figure 9.8, where 0 is the location of the heel sensor and 1 that of the fifth metatarsal sensor.

5. Crutches Ground Reaction Forces: The average of the GRFs of one crutch over a complete stride, divided by the participant's weight in kilograms.

Gait segmentation and event detection was carried out by the fuzzy logic algorithm included in the central unit of the CSS, utilizing the insole FSR sensors, and validated against heel strike events detected using the Noraxon IMU suit and the dual minima method, which relies on the angular velocity measured from the shank [249]. For each bout of the walking sessions, the first two and last two strides were excluded from the data analysis as to mitigate irregularities. Each bout included on average 23 strides for the exoskeleton-assisted condition and 15 for the unassisted condition.

Cognitive Performance

The dual-task condition facilitated a framework for quantifying cognitive performance both through walking and seated tasks, via measuring the **correct response rates (CRR)** of the participants during the serial subtraction task [250]. The CRR is calculated by multiplying the response rate, in this case subtractions per second,

with the accuracy of the responses (percentage of correct subtractions). For both exoskeleton-assisted and unassisted sessions, a 60-second interval was sampled. Analysis of these data was carried out by Norman Riedel.

Perceived Workload

Two metrics were defined for **mental and physical perceived workload** for each participant. Participants answered the NASA-TLX scale for the perceived workload for both metrics at the end of each walking bout, within the range of 0 and 100. Analysis of these data was carried out by Norman Riedel.

9.4.2 Statistical Analysis

For the statistical analysis, the biomechanical data comprised the calculated metrics for each participant per walking bout. A normality test was conducted to guide the selection of appropriate statistical analyses and post-hoc tests.

Normality Assessment

- **(A)** A Shapiro-Wilk test was conducted in order to assess the normality of the distribution of data for each bout and participant. Outliers were removed prior to the assessment as to prevent skewing of data, based on the range $[Q1 - 1.5 * IQR, Q3 + 1.5 * IQR]$, where Q1 and Q3 represent the first and third quartiles respectively, and IQR the interquartile range. Following the assessment, the data of all participants were pooled together per bout, and a set of 5000 randomly selected data points (as to ensure reliability of the Shapiro-Wilk test) were tested.
- **(B)** Normal distribution plots (histograms) and Q-Q plots for each metric separately were plotted as to visually inspect and cross-validate results of the normality test (please see Appendix B).
- **(C)** On both accounts (A and B), the distribution of the data was deemed not normal, which is expected for repetitive biomechanical measurements, yielding non-parametric data. Consequently, for all subsequent statistical operations, values of median and IQR were calculated and used.
- **(D)** A post-hoc analysis on the results included non-parametric Friedman tests to test the significance of each bout data, followed by a Wilcoxon signed-rank test for post-hoc pairwise bout-to-bout comparisons. All statistical tests were assessed with a significance level of $\alpha = 0.05$, with Bonferroni corrections applied to post-hoc pairwise comparisons.

For the cognitive-related data, including the CRR and the perceived workload, parametric tests took place based on the normality of the data, which was processed separately (statistical and data analyses can be found in Riedel et al. [229]), using

repeated measures analysis of variance and respective post-hoc testing. The results of this data therefore, are reported in mean and standard deviation (STD) terms. To address the research hypotheses, further analyses were performed on the calculated metrics to identify patterns, relationships, and significant changes that support or refute the proposed hypotheses.

9.4.3 Quantifying Familiarization

Primary Analysis: To test the first hypothesis, the results of each bout for each metric were compared, where the data of all participants for the given metric were pooled together. Statistical values for the description of results included the median and IQR of each bout, as well as the p-values for inter-bout comparisons. A relative decrease (or increase) in median and IQR from the first to the latter bouts would validate the hypothesis and prove familiarization on a first level.

Secondary Analysis: A further step in the motor performance analysis involved defining a "within-target step" for each metric individually. This was based on the results of the initial analysis for each metric. A "within-target step" was defined as one whose value fell within the IQR of the last bout (ST03), which, according to the first hypothesis, was considered the most 'familiarized' bout. An increase of within-target steps from the first to the last bout for each metric would reinforce the claim of familiarization, on a second level.

Tertiary Analysis: A variability analysis was conducted where the coefficient of variation (CV) was calculated for each bout of each metric. A decrease in variability with the progressive increase of bouts, would signify an increase in familiarization according to the first hypothesis.

9.4.4 Cognitive Interference Effects on Familiarization

To assess the second hypothesis, 2x2-rmANOVAs were conducted for perceived mental and physical workload, stride time variability, DST variability and gait velocity with within-factors Walking Condition (Unassisted walking, Exoskeleton-assisted walking) and Task Condition (Single-task, Dual-task). Since CRR were only assessed for the dual-task conditions, t-tests were conducted accordingly. The data from the third walking bout of both walking sessions (DT03, ST03) were used for the analysis.

9.4.5 Familiarization as a Motor Learning Indicator

In order to assess the above metrics in their ability to indicate early signs of motor learning, the three fundamental levels of motor learning [251, 246] were defined based on the current data, as follows. **Skill Acquisition:** Initial evidence of learning

from bout one (ST01) to bout two (ST02), consistent with rapid improvements often see in early practice phases.
Skill Retainment: Maintaining (and/or improving) learning from bout two (ST02) to bout six (ST03), serving as the hallmark of motor learning.
Skill Transfer: A classic assessment to the generalization of learned skills, by applying the skills in a more complex environment. In this study, this skill is defined by comparing a single-task bout (ST02) and a dual-task bout (DT02).

9.5 Cognitive Performance Results of the Outdoor Dual-Task Study

The work in this Section provides a summary of the results of the combined analysis, performed largely by Norman Riedel of KIT, in order to complement the results and findings of this thesis based on the common experiments. This analysis focuses mainly on the effects of cognitive interference and compares single and dual task conditions, within the conditions of assisted and unassisted gait.

In order to assess the cognitive performance of participants, motor performance, CRR and perceived workload metrics were examined and compared between the walking task conditions (unassisted walking vs. exoskeleton assisted walking), time and familiarization conditions (first walking bout vs. last walking bout), and cognitive task conditions (single- vs. dual- task). The results are reported in this subsection and important metrics on the walking task and cognitive task conditions are displayed in Figure 9.4.

Motor Performance

The three time-dependent biomechanical variables were used as to describe the participants' motor performance in relation to the walking and cognitive task conditions. Simple main effects tests revealed that stride time variability was higher during exoskeleton-assisted walking compared to unassisted walking in the single-task condition ($p < .001$), but not in the dual-task condition ($p = .062$). Stride time variability increased significantly from single-task to dual-task during unassisted walking ($p < .001$) but decreased non-significantly during exoskeleton-assisted walking ($p = .165$). For gait velocity, participants significantly reduced speed from single-task to dual-task during unassisted walking ($p < .001$), while speed increased during exoskeleton-assisted walking ($p = .018$). Gait velocity was significantly greater during unassisted walking compared to exoskeleton-assisted walking under both single-task ($p < .001$) and dual-task conditions ($p < .001$). Double support time variability showed no significant interaction effects ($p = .065$), with trends resembling stride time variability.

Correct Response Rate

A t-test comparison between walking conditions revealed that the CRR was noticeably lower during overall exoskeleton-assisted walking ($p = 0.003$). This indicates that fewer correct subtraction tasks were carried out during this condition, in comparison to unassisted walking. In contrast, when examining the effects of time and familiarization, there was an evident increase of the CRR from bout three (DT01) to bout five (DT03) during the exoskeleton-assisted walking condition ($p = 0.005$). No similar significant differences were detected between comparisons of bouts three and four (DT02) ($p = 0.066$), and four and five ($p = 1.00$).

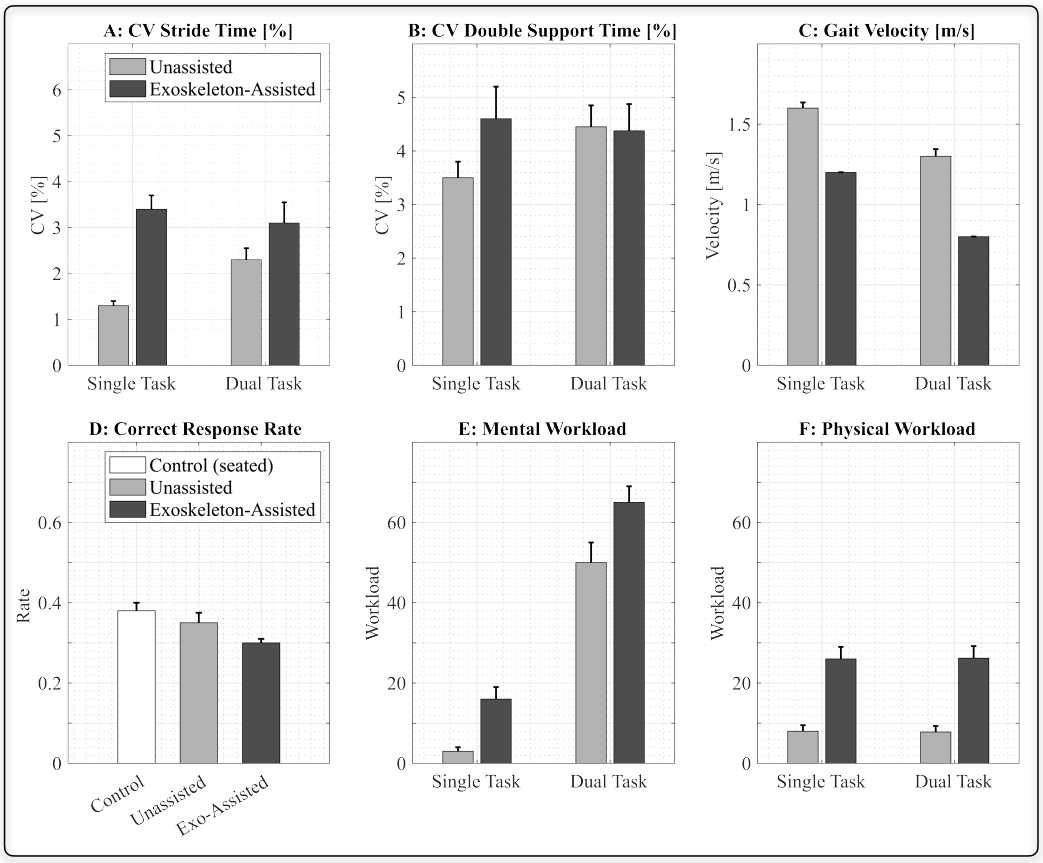

Figure 9.4: (A) CV of stride duration, (B) CV of double support time, (C) mean gait velocity, (D) correct response rate, (E) mental workload and (F) physical workload for unassisted and exoskeleton-assisted walking under single-task and dual-task conditions. Bars indicate standard errors. The first row presents time-dependent motor performance metrics, while the second row reports cognitive performance and perceived workload metrics.

Perceived Workload

For both mental and physical workload comparisons between walking conditions as well as task conditions, the interactions between the groups were not significant ($p = 0.337$ and $p = 0.285$ respectively). Significant main effects of the walking condition (assisted vs. unassisted) were found on mental workload ($p < 0.001$) and

physical workload ($p < 0.001$). The task condition (single- vs dual- task) significantly affected mental workload ($p < 0.001$) but not physical workload ($p = 0.914$). A Friedman test showed significant effects on perceived mental workload ($p < 0.001$) and physical workload ($p = 0.011$), from the first to the last walking bouts. Post-hoc tests revealed significant decreases in mental ($p < 0.001$) and physical workload ($p = 0.027$) from the first to the third trial, with no significant differences between the first and second trial (mental workload: $p = 0.342$; physical workload: $p = 0.707$) or between the second and third trial (mental workload: $p = 0.066$; physical workload: $p = 0.464$).

9.6 Familiarization Results of the Outdoor Dual-Task Study

The work in this Section provides a detail review of the results of the familiarization study and analysis based on the biomechanical metrics collected with the CSS of Giorgos Marinou. This analysis focuses mainly on the inter-bout comparison of these metrics and the changes over time that can be observed and confirmed statistically.

In this study, the biomechanical and cognitive processes that characterize early-stage familiarization and motor learning during exoskeleton-assisted walking are examined through real-world environmental conditions. A dual-task paradigm was employed in an outdoor experiment, collecting biomechanical and cognitive task data across six walking bouts of 25 meters each. Unlike previous laboratory-confined studies, this work uniquely incorporated both single and dual-task conditions with a LLE, allowing for an exploration of user adaptation in dynamic and complex scenarios. The main findings reveal that familiarization takes place concurrently across various metrics throughout 150 meters of assisted walking (H0-H4), cognitive interference improves exoskeleton walking (H5), and that familiarization based on these metrics shows early markers for motor learning within just a few hours of exoskeleton use (H6).

9.6.1 Biomechanical Performance Metrics

The results presented in this section are reported according to the four analyses described in Subsection 9.4.3. The three hypotheses are then answered by inferring these distinct outcomes. As a summary of main indications, Table 9.1 offers an overview of all metrics results and CVs for all bouts of the exoskeleton-assisted walking session, according to the primary and tertiary analysis of metrics.

Table 9.1: Median and IQR values for biomechanical metrics and coefficients of variation (CV) across all bouts with exoskeleton assistance, as well as mean and standard deviations of CRR over both assisted and unassisted bouts, and perceived participant workload.

Motor Performance	**ST01**	**ST02**	**DT01**	**DT02**	**DT03**	**ST03**
Stride Duration (s)	7.67 [0.76]	7.43 [0.50]	7.28 [0.52]	7.24 [0.39]	7.12 [0.42]	6.85 [0.53]
Stride Duration CV (%)	5.36 [2.44]	4.87 [2.38]	4.88 [1.85]	4.01 [1.85]	4.19 [1.73]	3.80 [1.66]
Gait Velocity (m/s)	0.0938 [0.0211]	0.101 [0.0176]	0.103 [0.0183]	0.0988 [0.0130]	0.126 [0.0101]	0.109 [0.0103]
Gait Velocity CV (%)	9.28 [5.15]	8.67 [4.37]	8.70 [4.10]	7.23 [3.78]	6.68 [3.51]	6.33 [3.00]
Double Support Time (s)	9.29 [1.29]	9.39 [1.09]	8.68 [1.06]	8.60 [1.12]	8.53 [1.10]	8.36 [1.05]
Double Support Time CV (%)	5.78 [2.24]	4.51 [2.78]	4.78 [2.40]	4.67 [2.33]	4.13 [2.08]	4.09 [2.25]
Anteroposterior Center of Pressure (Normalized)	0.56 [0.09]	0.60 [0.10]	0.64 [0.09]	0.65 [0.07]	0.65 [0.08]	0.65 [0.07]
Anteposterior Centre of Pressure CV (%)	7.18 [4.93]	7.07 [4.50]	6.96 [3.71]	5.89 [3.67]	4.91 [3.65]	4.32 [3.87]
Crutches Ground Reaction Forces (N/kg)	7.42 [0.40]	7.20 [0.31]	7.28 [0.40]	7.17 [0.47]	6.83 [0.34]	6.80 [0.32]
Crutches Ground Reaction Forces CV (%)	2.33 [1.97]	1.91 [1.65]	1.94 [1.27]	2.01 [1.66]	1.63 [1.34]	1.37 [0.80]
Cognitive Performance						
	Unassisted Walking					
Correct Response Rate			0.34 (0.06)	0.35 (0.08)	0.37 (0.04)	
	Assisted Walking					
Correct Response Rate	–	–	0.26 (0.08)	0.30 (0.08)	0.30 (0.10)	–
Perceived Workload						
Mental Workload	28.3 (12.2)	24.9 (12.1)	68.8 (18.8)	63.4 (20.5)	59.9 (21.2)	17.0 (12.0)
Physical Workload	31.9 (14.7)	28.0 (11.4)	27.8 (12.5)	26.6 (14.4)	25.9 (15.7)	25.3 (15.8)

Stride Duration

The first five hypotheses of this research, H0 - H4, are drawn from previous work in familiarization presented in Chapter 7 and in Marinou et al. [170]. Here, we speculate that the longer the interaction with the exoskeleton, the greater the familiarization effects, measured through significant reductions, of biomechanical metrics. Participants performed their first walking bout (ST01) with the exoskeleton with a stride duration of $7.67[0.76]s$, and their last bout (ST03) $6.85[0.53]s$ (Figure 9.5, Table 9.1), a significant reduction in time taken for each stride of 10.7% ($p < 0.001$). From the first (ST01) to the second bout (ST02), a reduction of 3.12% took place ($p < 0.05$) in the median of the stride duration of all participants, whereas from the fifth (DT03) to the last bout (ST03), the highest successive inter-bout reduction reported a decrease in stride duration of 4.03% ($p < 0.001$). The pairwise comparisons indicate that the first two dual-task bouts (DT01 and DT02) did not show any significant differences between them, nor the second single-task bout.

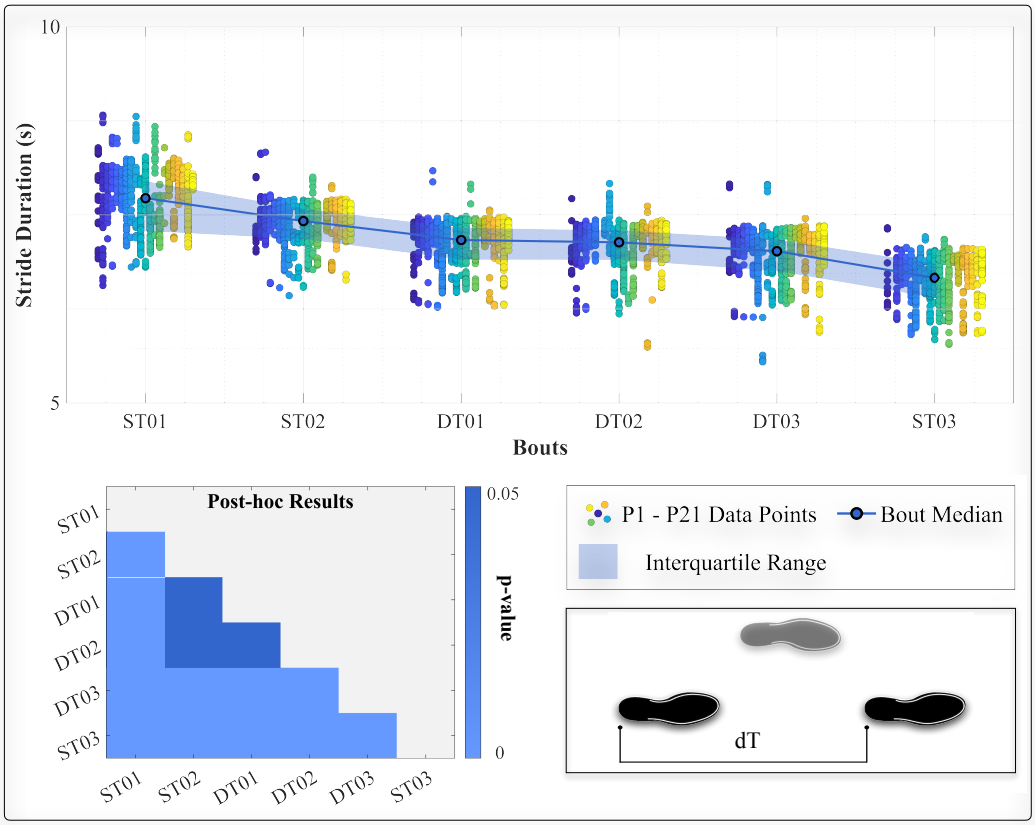

Figure 9.5: Stride duration values for all six exoskeleton-assisted walking bouts. Scattered multicolored markers correspond to individual participant values for each walking bout, for both feet. Larger outlined markers connected by a line represent the median of each bout across all participants. Legend's 'P' stands for participant. The inset under the figure on the left reports the pairwise comparison of bouts results, based on the p-value color map on the right; a low p-value corresponds to a statistically significant difference between the bout pair ($p < 0.05$); a high p-value corresponds to a statistically insignificant difference ($p \geq 0.05$). The inset under the legend provides an illustrative description of the metric.

Gait Velocity

Gait velocity exhibited a similar trend to stride duration, given its direct dependence on it (Figure 9.6). Even though gait velocity is calculated based on the total distance and time taken for the whole bout for each participant, the scattered markers represent the individual participant stride velocity values, for a more comprehensive visual representation of stride-to-stride variations. From bout one (ST01) to bout six (ST03), the median gait velocity increased by 16.2%, from $0.0938m/s$ to $0.109m/s$ ($p < 0.001$). Participants picked up their pace noticeably between bout one and two (ST02), reaching a median velocity of $0.101m/s$. Bouts two to four increased slightly in velocity, but the pairwise comparisons indicated no significantly different results between them. Results for bout five (DT03) report a big increase in velocity of participants from $0.0988m/s$ in bout four to $0.121m/s$, an overall increase of 34.3% ($p < 0.001$) from bout 1. This was followed by a decrease in median velocity in the final bout (ST03) by 13.4% ($p < 0.05$).

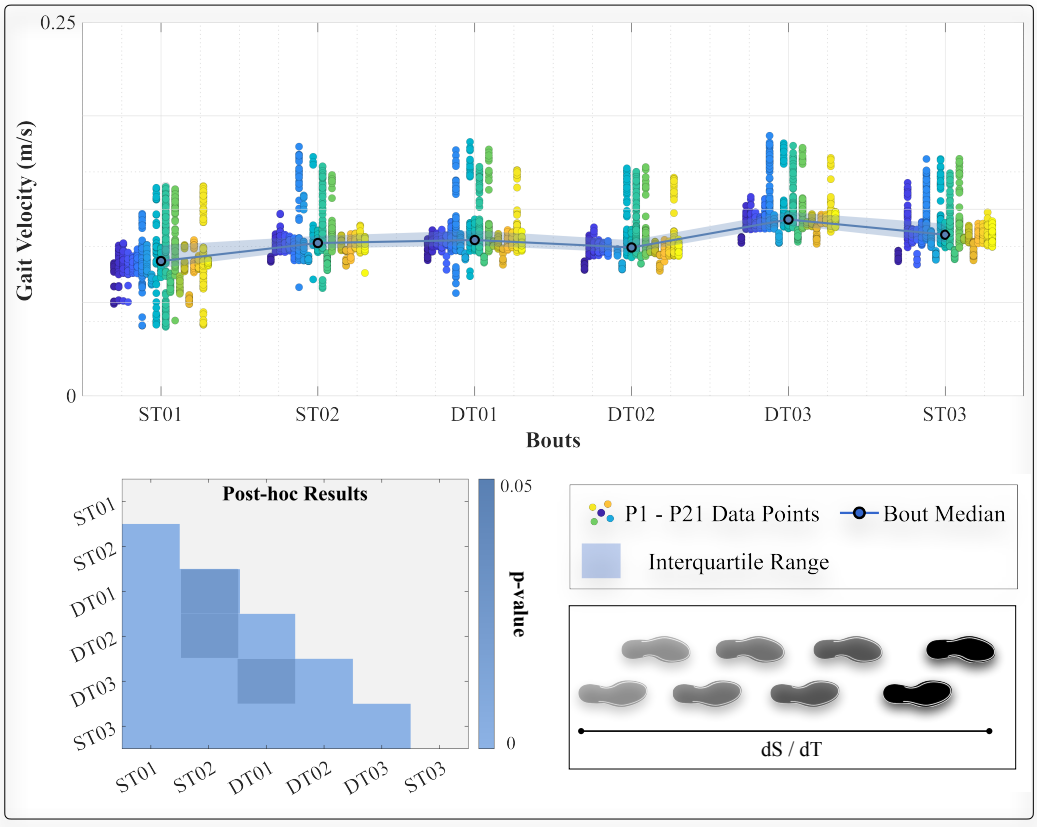

Figure 9.6: Gait velocity values for all six exoskeleton-assisted walking bouts. Scattered multicolored markers correspond to individual participant values for each walking bout, for both feet. Larger outlined markers connected by a line represent the median of of each bout across all participants. Legend's 'P' stands for participant. The inset under the figure on the left reports the pairwise comparison of bouts results, based on the p-value color map on the right; a low p-value corresponds to a statistically significant difference between the bout pair ($p < 0.05$); a high p-value corresponds to a statistically insignificant difference ($p \geq 0.05$). The inset under the legend provides an illustrative description of the metric.

Double Support Time

DST results report the time spent in the contact phase for both feet and crutches during each gait cycle (Figure 9.7). There was a 12% ($p < 0.001$) overall decrease in the time participants spent in double support from bout one (ST01) to bout six (ST03). Initially, the DST increased slightly from the first to the second bout (ST02), from $9.29[1.29]s$ to $9.39[1.09]$. With the introduction of the first dual-task bout (DT01), the DST decreased $8.68[1.06]s$, the most significant reduction between successive bouts. There was a gradual decrease between bouts three and five, and the pairwise comparisons report no significant changes between these bouts ($p > 0.05$). For the last single-task bout (ST03), participants decreased time spent in double support, with the median value dropping from $8.53[1.10]s$ in bout five (DT03) to $8.36[1.05]s$.

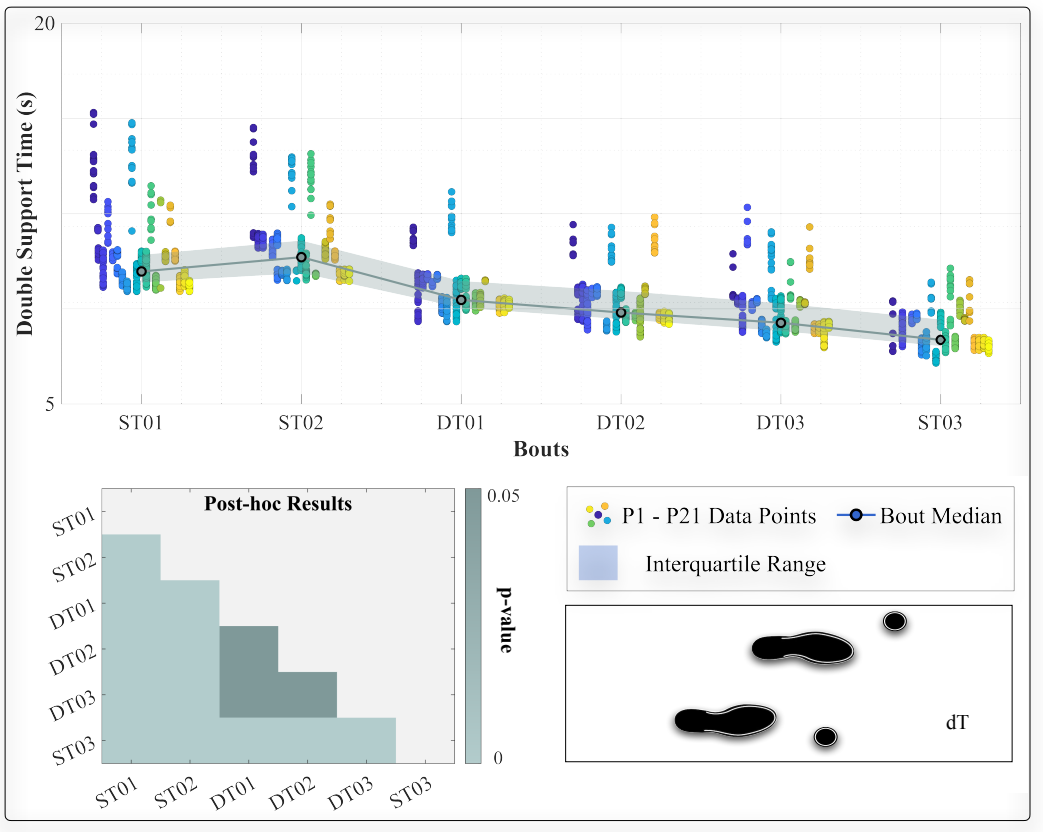

Figure 9.7: Double support time values for all six exoskeleton-assisted walking bouts. Scattered multicolored markers correspond to individual participant values for each walking bout. Larger outlined markers connected by a line represent the median of each bout across all participants. Legend's 'P' stands for participant. The inset under the figure on the left reports the pairwise comparison of bouts results, based on the p-value color map on the right; a low p-value corresponds to a statistically significant difference between the bout pair ($p < 0.05$); a high p-value corresponds to a statistically insignificant difference ($p \geq 0.05$). The inset under the legend provides an illustrative description of the metric.

Anteroposterior Center of Pressure

The normalized APCoP describes the location of the CoP in the direction of travel, in relation to the farthest sensor, as shown in Figure 9.8. The exoskeleton generally requires a center of mass, or pressure, projected forward, in order to correctly support users while walking. Numerically, this value should be larger than 0.5, which represents the middle of the insole, or foot. According to the results, participants familiarized themselves to this requirement along the six walking bouts, with an increase of normalized CoP from $0.56[0.09]$ to $0.65[0.07]$ from bout one (ST01) to six (ST03). Significant changes took place from successive bouts one to two ($0.60[0.10]$) and three ($0.64[0.09]$). Bouts four to six did not show any significant changes in CoP as the median value remained at 0.65, a pattern observed by the pairwise comparisons of these bouts as well.

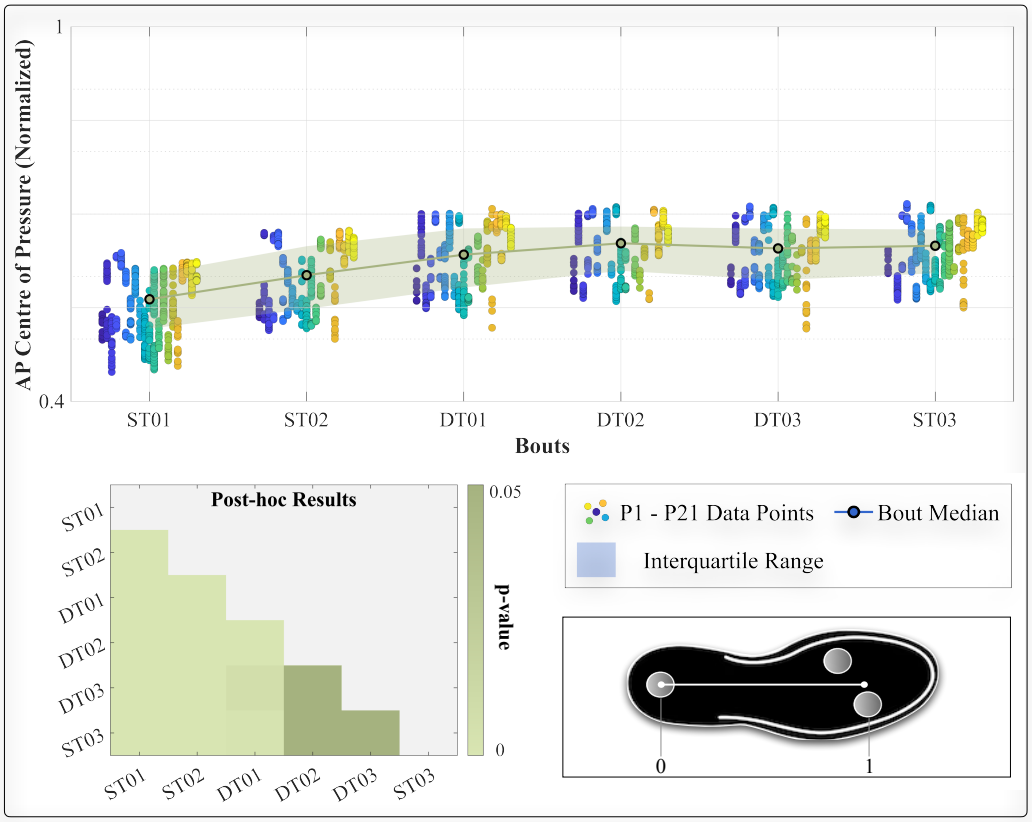

Figure 9.8: Anteroposterior center of pressure values for all six exoskeleton-assisted walking bouts. Scattered multicolored markers correspond to individual participant values for each walking bout. Larger outlined markers connected by a line represent the median of each bout across all participants. Legend's 'P' stands for participant. The inset under the figure on the left reports the pairwise comparison of bouts results, based on the p-value color map on the right; a low p-value corresponds to a statistically significant difference between the bout pair ($p < 0.05$); a high p-value corresponds to a statistically insignificant difference ($p \geq 0.05$). The inset under the legend provides an illustrative description of the metric.

Crutches Ground Reaction Forces

GRFs for each participant are expressed as a ratio of their weight in kilograms. The individual participant values plotted in Figure 9.9 represent each crutch separately and are pooled together for both sides. Participants familiarized themselves in similar patterns reported by the previous metrics. There was an overall reduction of 8.36% ($p < 0.001$) in GRFs from bout one (ST01) to six (ST03). Initially, participants exerted less force on the crutches in bout two ($7.20[0.31]N/kg$) compared to bout one ($7.42[0.40]N/kg$). Between bouts two and four, there was generally no important differences in the median GRFs for the two crutches, and according to the post-hoc results no significant differences in successive bouts. On the contrary, bout five (DT03) reports a decrease from $7.17[0.47]N/kg$ to $6.83[0.34]N/kg$, which was maintained at $6.80[0.32]N/kg$ during the last bout (ST03).

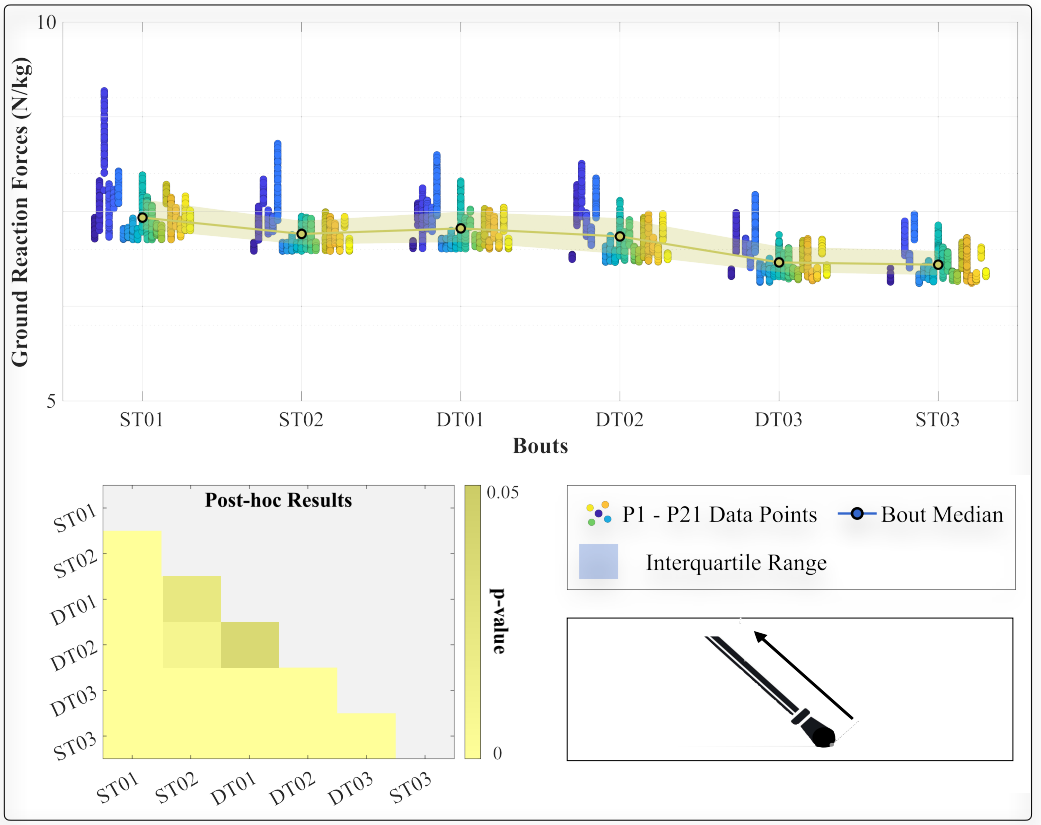

Figure 9.9: Ground reaction forces for each crutch for all six exoskeleton-assisted walking bouts. Scattered multicolored markers correspond to individual participant values for each walking bout, for both crutches. Larger outlined markers connected by a line represent the median of each bout across all participants. Legend's 'P' stands for participant. The inset under the figure on the left reports the pairwise comparison of bouts results, based on the p-value color map on the right; a low p-value corresponds to a statistically significant difference between the bout pair ($p < 0.05$); a high p-value corresponds to a statistically insignificant difference ($p \geq 0.05$). The inset under the legend provides an illustrative description of the metric.

9.6.2 Within-Target Participant Steps

Based on the familiarization results derived from the five biomechanical metrics, within-target steps lie within the IQR of the last bout (ST03) for each metric. These results serve as a secondary analysis to the familiarization hypotheses (H0 - H4), offering a validation for each metric, as they present a convergence towards the final familiarized state of this walking session (Figure 9.10).

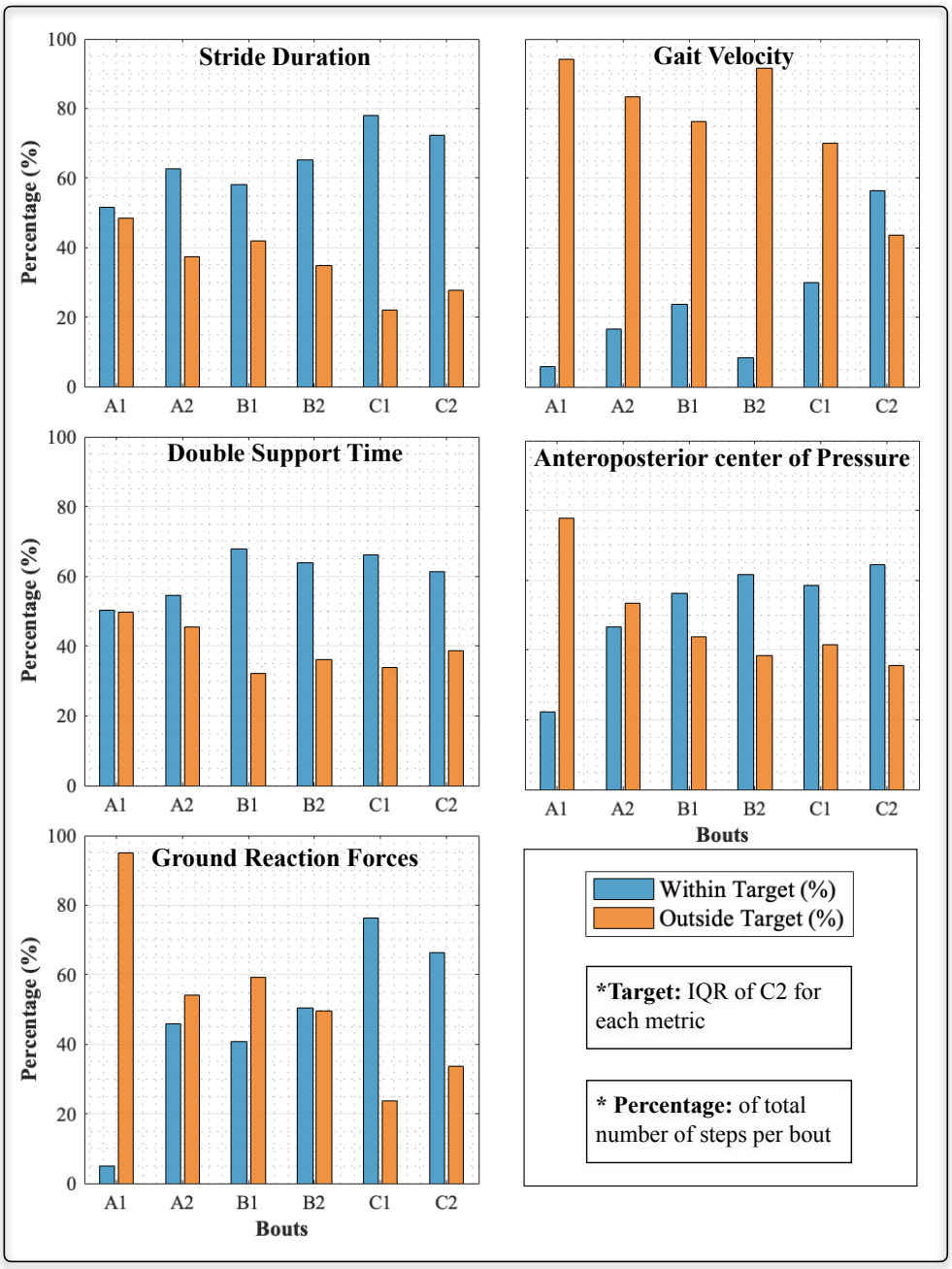

Figure 9.10: Within-target steps of all participants per bout, for each metric. A target step for a specific metric lies within the IQR of the last bout of the given metric. The percentage value on the y axis represents the percentage of the total number of steps for a given bout.

The results for within-target participant steps, presented in Figure 9.10, demonstrate a clear progression toward the familiarized state across all biomechanical metrics. Stride duration showed an increase in within-target steps from 22.4% in bout one (ST01) to 64.5% in bout six (ST03), with a notable rise between bouts two (ST02) and three (DT01). Similarly, gait velocity exhibited a consistent upward trend, starting at 18.7% in ST01 and reaching 62.1% in ST03, with smaller gains observed between bouts three (DT01) and five (DT03). DST showed a steady progression from

28.9% in ST01 to 68.3% in ST03, with a pronounced increase between ST02 and DT01. The normalized APCoP mainly demonstrated an increase from 30.5% in ST01 to 72.4% in ST03. Lastly, GRFs followed a similar pattern, increasing from 24.1% in ST01 to 69.7% in ST03, with the most significant growth occurring between ST02 and DT01. These results collectively highlight a progressive convergence of steps toward the familiarized state across all metrics as the walking session advanced.

9.7 Interpretation of Results and Main Outcomes

9.7.1 Familiarization Takes Place Concurrently Through All Metrics

This study aimed to investigate the process of familiarization during exoskeleton-assisted walking by defining biomechanical metrics as familiarization indicators as to understand how biomechanical and cognitive adaptations evolve over successive walking bouts. Our initial hypothesis on familiarization speculated that increased time with the exoskeleton would lead to improvements in familiarization, quantifiable through key metrics, reductions in inter-bout variability and adaptation to cognitive interferences. The findings collectively demonstrate that familiarization with the exoskeleton occurs concurrently across all biomechanical metrics, with reductions in variability (CV) and improvements in median values underscoring this process. These findings align with established motor learning theories, which suggest that reductions in variability are indicative of improved motor performance [252]. The hypothesis therefore that familiarization systematically increases and can be quantified via simple spatiotemporal and cognitive parameters is validated.

Evidence of Early Familiarization

The early signs of familiarization between bouts one and two reflect the participants' initial phase of adaptation to the exoskeleton. Stride duration and gait velocity showed significant improvements, suggesting that participants quickly began to adapt their gait mechanics. The simultaneous reductions in DST and GRFs indicate that participants gained more confidence in their balance and relied less on external support from the crutches. This shift represents a period in which participants improved on the requirements of their motor performance, imposed by the TWIN exoskeleton, thus adapting more efficient movement strategies. This rapid adaptation is consistent with previous studies demonstrating early improvements in gait mechanics during robotic assistance [253].

This 'exoskeleton-imposed' strategy is reflected in the results for the normalized APCoP where participants had to truly align their movement with the exoskeleton's requirements, since a forward-projected center of pressure is needed for the successful operation of the device. Though the metrics vary in nature, it can be speculated that these results represent the initial familiarization period reported in Marinou et al. [170], which took place similarly after 25 to 30 meters of assisted walking.

Plateau Phase in the Mid-Bouts

The plateau observed in the middle bouts (DT01 to DT03) suggests that participants entered a stabilization phase where motor performance improvements leveled off. Metrics such as gait velocity, DST, and GRFs maintained consistent median values, signaling that participants had consolidated their initial adaptations but were not making further significant gains during this period.

This period of stable values in the five metrics, coincided with the introduction of dual-task conditions, hence introducing cognitive interference. Balancing cognitive and motor demands, especially when operating an exoskeleton, likely diverted the participants' focus from fine-tuning their gait mechanics, resulting in a temporary halt of the familiarization process. This observation aligns with findings by McPhee et al. [254], who reported that cognitive interference can impede motor performance during dual-task scenarios. However, the lack of familiarization evidence does not immediately indicate a lack of motor performance improvement. The interplay between cognitive tasks and motor performance during this phase is exploitative of the adaptation processes of exoskeletons but highlights the necessity of strategies accounting for both physical and cognitive challenges in training protocols.

Although this phase represents a temporary limit in familiarization, it also reflects a critical period where participants maintained their adapted strategies under increased task complexity. This consistency indicates that participants were able to retain their earlier improvements, even when faced with additional cognitive demands.

Renewed Familiarization Toward the Final Bout

The renewed phase of familiarization observed from bout five (DT03) to the final bout (ST03) demonstrates the participants' continued familiarization as they neared the end of the experiment. Simultaneous reductions in stride duration, double support time, GRFs and improvements in APCoP and gait velocity suggest that participants became increasingly familiar with the exoskeleton's mechanics, achieving more efficient and automated movement strategies. Similar findings by Fang et al. [255] showed that individuals increased their walking speed after four training bouts with an ankle exoskeleton, with lower stride variability.

The notable drop in variability across all metrics during this phase, validates the speculation of a later-stage familiarization within this short-term adaptation framework. Based on the biomechanical metrics quantified, the reduction in variability gives evidence for improved motor performance and control, concluding that familiarization does not only depend on improving average performance, but also maintaining it.

Role of Variability in Familiarization

The CVs provide critical insights into the familiarization process and complement the results on the above absolute metric improvements. Across all metrics, the CV decreased steadily from bout one to six, reinforcing the hypothesis that reduced variability correlates with increased familiarization. In the case of stride duration, the CV decreased from 5.36% in the first bout, to 3.80% in the last bout, signifying a higher level of consistency between individual participant strides. Similarly, the CV of gait velocity dropped by 2.95% over the first six bouts. A similar trend is observed across metrics. The results on variability, not only confirm the process of familiarization across this walking session, but also confirm the improvement of motor performance, pointing to initial markers for motor learning as a function of long-term adaptation. This reduction in variability is a hallmark of motor learning, as noted by Newell [256].

The interdependence of metrics such as stride duration and gait velocity is evident, as changes in one metric often mirrored trends in another. This interconnectedness highlights familiarization as a global process, where adjustments in one aspect of gait mechanics influence overall motor performance. Additionally, differences in the progression rates of metrics, such as the earlier stabilization of APCoP compared to the gradual reductions in DST, suggest that distinct facets of familiarization follow unique trajectories. The concurrent improvements and reductions in variability across metrics underscore the utility of these measures as reliable indicators of familiarization.

These findings emphasize the importance of tailoring exoskeleton training protocols to leverage early gains in familiarization while addressing potential plateaus during cognitive or dual-task conditions. A phased approach to training, beginning with simpler tasks and progressing to more complex scenarios, could facilitate both physical and cognitive adaptation. Moreover, the decrease in variability highlights the potential for these metrics to serve as benchmarks for assessing the stability of user adaptation.

9.7.2 Familiarization Increases Progressively With Time

The progression of within-target participant steps across all metrics highlights a consistent trajectory toward familiarization, complementing the findings reported in

the primary analysis of the five biomechanical metrics. The increasing proportion of within-target steps in later bouts reflects participants' growing ability to align their gait patterns with the requirements of the exoskeleton, as evidenced by the earlier reductions in stride duration, double support time, and ground reaction forces. The steady rise in within-target steps from the first to the last bout, suggests that familiarization is detected within the whole distribution of steps of each metric, with more steps converging toward a consisted, adapted result.

Interestingly, the rapid increase in within-target steps for double support time and ground reaction forces during the transition from single-task (ST02) to dual-task (DT01) conditions aligns with the observed stabilization phases in those metrics. This indicates that the dual-task condition may have acted as a catalyst for refining motor strategies, as suggested by [257], aiding participants to achieve a more stable and efficient gait. Similarly, the normalized APCoP's higher percentage of within-target steps in later bouts corroborates its early stabilization, suggesting that this metric may represent one of the faster-adapting components of exoskeleton familiarization.

Consequently, the bout-to-bout progression of within-target steps across all metrics, reinforces the hypothesis of being able to quantify familiarization based on a multi-metric and time-progressive approach. It further underscores the utility of this secondary analysis as a validation approach to the familiarization process. These findings further support the idea that familiarization not only improves average motor performance but also reduces variability, leading to more consistent and reliable gait patterns over time.

9.7.3 Cognitive Interference Shows Evidence of Expedited Familiarization

Cognitive interference during both unassisted and exoskeleton-assisted walking sessions was introduced via the dual-task paradigm. Valuable insights into the mental demands of using the TWIN exoskeleton were gathered by a subtraction task performed by participants, along with the simultaneous operation of the exoskeleton. This approach not only assessed the interaction between cognitive and motor tasks but also offered a unique perspective on how cognitive resource allocation impacts gait mechanics. It could be thus speculated, that diverting cognitive focus from exoskeleton operation in such a way, could partially simulate the challenges faced by older adults or frail populations, who may experience similar cognitive-motor constraints in real-worlds scenarios.

Initial findings from the assessment of familiarization based on the five biomechanical metrics suggest a motor interference due to the introduction of the subtraction task during the dual-task walking bouts. A plateau in familiarization was inspected

in all five metrics for the duration of these bouts. This indicates that the cognitive load imposed by the secondary task momentarily limits further physical familiarization. Such findings align with the dual-task interference framework, which posits that cognitive and motor tasks compete for shared resources, potentially slowing biomechanical adaptation during dual-task conditions [258].

For the unassisted walking condition, the results indicate a decrease in gait velocity during the dual-task condition vs. the single task-condition, in line with a number of studies, indicating that higher-order cognitive processes are involved [243]. Interestingly, gait velocity increased during the dual-task walking bouts with the exoskeleton, which defies the previous findings with unassisted walking. This could indicate that participants exhibit the tendency to converge towards a preferred walking velocity, similar to the findings of Gupta et al. [259] therefore exploiting less cognitive resources for motor tasks, which are held up by the subtraction task.

Stride duration variability during the unassisted walking condition increased from single- to dual- task walking bouts. Following a similar contradictory fashion to gait velocity however, stride duration variability decreased for the exoskeleton-assisted walking condition from single- to dual- task walking bouts. The improved motor performance during the subtraction task fell in line with qualitative feedback collected from the participants, describing how the additional task diverted their attention from operating the exoskeleton, indicating a reduction in exploratory behavior.

Treadmill studies show that externalizing attention can reduce gait variability during simple tasks by automating gait execution [260, 229], but this has not been replicated in overground walking [261]. Similar to treadmills, the TWIN exoskeleton provides rhythmic regulation through predefined trajectories and auditory signals before each step. Similar findings from studies with LLEs highlight that external cues enhance motor performance [262, 263]. These findings suggest that external feedback may improve exoskeleton user performance, particularly during real-world tasks requiring external focus, which begs the question on how familiarization outcomes change with additional auditory and possibly even visual cues.

9.7.4 Short-Term Familiarization as an Early Marker for Motor Learning

Motor learning in human-exoskeleton interaction systems is critical to understanding skill acquisition, retention, and transfer. Familiarization, as highlighted in this study, serves as an early marker for motor learning. The ability to quantify short-term biomechanical familiarization provides insights into the progression of motor skills and the transfer to new conditions. This kind of methodology is essential for designing effective training protocols that support older adults and frail populations.

Here, three key motor learning processes are assessed: skill attainment, skill transfer, and skill retainment, described according to the metrics analyzed in this study.

Skill Attainment: Initial Adaptations

The rapid improvements in stride duration, gait velocity, double support time, and ground reaction forces from the first (ST01) to the second bout (ST02) highlight early-stage skill attainment. Median stride duration decreased by 3.12% ($p < 0.05$), while gait velocity increased by 7.7% ($p < 0.05$). Simultaneously, reductions in DST and GRFs indicate participants' increased confidence in balance and decreased reliance on crutches.

This rapid adaptation aligns with motor learning theories, which describe a steep initial learning curve as individuals refine movement strategies in response to new task demands [252]. Similar trends have been observed in studies where users adapt to robotic assistance in the early practice phases [253, 233]. These findings suggest that familiarization metrics can serve as reliable indicators of initial motor learning.

Skill Transfer: Adapting to Cognitive Interference

Skill transfer was evaluated by comparing single-task (ST02) and dual-task (DT02) conditions. The introduction of cognitive interference in the dual-task condition caused a temporary plateau in gait velocity and DST, but the participants maintained consistent CV levels for stride duration and normalized anterior-posterior center of pressure (APCOP). This suggests that participants were able to transfer their learned motor skills to the cognitively demanding dual-task condition.

Interestingly, gait velocity increased by 1.98% during exoskeleton-assisted dual-task walking ($p = .018$), a finding that contrasts with the decrease observed in unassisted dual-task conditions ($p < .001$). This aligns with studies showing that exoskeletons can offload cognitive resources by stabilizing gait mechanics, allowing users to allocate attention to secondary tasks [264, 243].

Skill Retainment: Sustaining Adaptations

Skill retainment is observed through the steady improvements and reduced variability indicated across bouts two to six. Stride duration variability (CV) decreased from 4.87% in ST02 to 3.80% in ST03, while gait velocity variability decreased by 2.34%. This consistency underscores participants' ability to retain motor improvements over successive walking bouts.

The reduction in CV aligns with motor learning markers, as reduced variability indicates greater automatization and stability of movement patterns [256]. Similarly, the notable improvements in normalized APCoP further highlight that participants

adapted their posture in accordance with the exoskeleton's requirements, maintaining forward-projected stability.

These results highlight the importance and value of familiarization as an early marker for motor learning, in turn inspiring a practical framework for designing phased training protocols. The findings align with recommendations by Schmidt and Lee [252], who emphasize the importance of structured progression in motor skill acquisition.

9.8 Intermediate Conclusion

This study explored the process of familiarization during exoskeleton-assisted walking, focusing on how biomechanical and cognitive adaptations evolve over time. Our findings show that familiarization happens simultaneously across various metrics, as seen in reductions in variability (CVs) and consistent improvements in stride duration, gait velocity, and anterior-posterior center of pressure (APCOP).

Three key phases of short-term familiarization were identified in this study. The early phase (bouts one to two) showed participants quickly adapting their gait mechanics and improving motor performance as to match the TWIN exoskeleton. The middle phase (bouts three to four) indicated a stabilization period, where improvement and familiarization levelled off with the introduction of a secondary congnitive task. In the latter phase (bouts five to six), participant skills appear to improve once again and solidify, leaning towards smoother and more efficient movement patterns. These results highlight the link between familiarization and motor learning, particularly in terms of skill attainment, transfer, and retention. The environmental variability introduced by the outdoor nature of the experiment offers an additional level of robustness to the results, especially for cases of exoskeleton-assisted walking, reflecting real-life scenarios.

9.8.1 Limitations of the Study

While this study offers valuable insights, there are a few limitations to note. First, the research focused on short-term familiarization during a single session, so it does not capture the long-term effects of repeated training or prolonged adaptation. Future studies could examine changes over multiple sessions or better yet weeks, to better understand how motor learning progresses and stabilizes over time.

Second, our participants were young, healthy adults, which limits how broadly these results can be applied to other populations, such as older adults or individuals with mobility challenges. Since these groups often face different physical and cognitive demands, it's crucial to study how their familiarization process might differ.

9.8.2 Future Work and Technology Transfer

Building on these findings, future studies should focus on exploring long-term adaptation to exoskeleton use. Tracking participants over time and across multiple sessions could reveal how familiarization transitions into lasting motor learning. Furthermore, introducing older or frail participants would provide important insights into the individual challenges of more diverse population groups and therefore do not rely on generalized claims on adaptation.

From a practical perspective, this research offers valuable guidance for designing training protocols and improving exoskeleton usability. The metrics identified in this study can help tailor training programs to user needs, focusing first on simple tasks to encourage skill attainment and gradually increasing complexity to support skill transfer.

These findings also hold promise for clinical and rehabilitation applications. By monitoring familiarization through the identified metrics, therapists and device manufacturers can create more effective strategies to support users as they integrate exoskeletons into their daily lives. Ultimately, this approach can help bridge the gap between initial familiarization and the long-term adoption of these technologies by frail and mobility-impaired populations.

Conclusion and Outlook

This thesis explored the optimization of human-exoskeleton interactions, addressing challenges in biomechanical validation, design, and performance enhancement of assistive devices. This thesis, through a two-fold pursue of injury risk reduction and mobility enhancement, offered important contributions in the advancement of the fields of occupational back-support exoskeletons and lower-limb assistive devices by offering revolutionary solutions to improve user-centric design along with functionality.

The first research avenue focused on optimizing back-support exoskeletons under the SPEXOR project, targeting the reduction of low back loads during repetitive lifting tasks. Through detailed modeling of the human-exoskeleton system, the research demonstrated how tailored torque profiles, grounded in biomechanical principles, significantly reduced cumulative and peak lumbar loads. A comparative evaluation analysis highlighted that while improved lifting techniques offered notable benefits, the integration of exoskeleton assistance provided superior protection against both cumulative and acute injuries, hence underlying the indispensible potential of back-support exoskeletons in enhancing ergonomic environments in labor-intensive industries.

Optimizing Exoskeleton Support through Modeling and Simulation

Lower-back pain is a widespread occupational health issue, often exacerbated by repetitive lifting tasks. Active back-support exoskeletons can mitigate these risks, but optimizing their design requires a deeper understanding of human-exoskeleton interactions and their biomechanical impact. This study developed detailed biomechanical models of the human spine and the SPEXOR back-support exoskeleton, targeting the minimization of cumulative and peak low-back load through simulations of lifting motions. An optimization framework was set in place to evaluate multiple cost functions to identify torque profiles that minimize spinal loads while maintaining feasible interaction forces.

We developed a computational framework to simulate human-exoskeleton interactions, impose comfort limits on users, and yield critical lumbar moment insights during lifting motions. Hence, we identified optimal exoskeleton torque strategies to assist these lifting motions, successfully reducing low back loads via employing the SPEXOR exoskeleton model to the human lifts. The study demonstrated how tailored torque profiles can reduce both ergonomic risks and user effort, advancing the understanding of exoskeleton efficacy.

This work established a foundational method for optimizing exoskeleton control strategies based on biomechanical models, enhancing their effectiveness in occupa-

tional settings. The findings inform both device design and future simulation-based studies for optimal support torque generation.

Evaluating Lifting Strategies and Exoskeleton Assistance

While back-support exoskeletons aim to reduce low-back loads, their efficacy in repetitive lifting tasks compared to optimized human lifting techniques remains underexplored. This study compared the biomechanical benefits of optimized lifting strategies with active exoskeleton assistance. Using the previously developed models, cumulative and peak low-back loads were analyzed under various motion strategies, incorporating an evaluation of trade-offs between human effort and device support.

We demonstrated that optimized human lifting techniques alone can significantly reduce cumulative low-back loads, although not to the extent external support from an active exoskeleton can. In addition, we deduced that improved technique suffers when it comes to minimizing peak low-back loads. Hence, by quantifying the trade-offs between technique improvements and device support via a broad cost-function evaluation study, we produced a framework that can design user-specific strategies for lumbar moment minimization. Lastly, we lay the foundation for establishing the necessary criteria for when exoskeleton assistance becomes indispensable, particularly in repetitive lifting scenarios within industrial settings and not only.

This study underscores the complementary role of exoskeletons alongside human lifting optimization. By delineating the conditions under which exoskeletons are most beneficial, the findings guide their practical application in reducing occupational risks.

Developing a Modular Sensory System for Biomechanical Evaluation

Robust biomechanical evaluation of exoskeletons in outdoor environments requires portable, adaptable, and reliable measurement systems. Existing systems often lack modularity and usability for non-experts, as well as being offered at a rather high cost. A modular, cost-effective, open-source wireless sensor system was designed to record motion and force data seamlessly in laboratory and outdoor settings. The system integrates force-sensitive resistors, inertial measurement units, and custom crutch-mounted load-cell sensors, offering plug-and-play functionality.

We designed and validated the custom sensor system against gold-standard methodologies in the motion capture research field. Through the development of this system, we managed to enable the synchronized collection of biomechanical data across diverse environments, demonstrating its reliability and adaptability. The system delivered validated metrics for gait parameters, such as stride duration, centre of pressure and ground reaction forces. A proposal was made with software

developed for facilitating high-level control of exoskeletons via sensor feedback, enabling an easy integration for lower-limb exoskeletons, in the hopes of promoting an open-source collaborative work.

This system provides a versatile platform for biomechanical research and exoskeleton evaluation, bridging laboratory precision and field practicality. The open-source nature ensures widespread accessibility for researchers and developers.

Benchmarking User Familiarization with Exoskeletons

User adaptation to lower-limb exoskeletons, particularly in real-world settings, remains poorly understood. Familiarization processes are critical for optimizing both device design and training protocols. This study developed a benchmarking framework for quantifying familiarization using biomechanical metrics, such as gait velocity, stride duration, and ground reaction forces. An outdoor dual-task walking study was conducted to assess user adaptation over long distances.

By empirically establishing biomechanical metrics as familiarization indicators over two significant studies, we witnessed evidence of familiarization and exoskeleton adaptation through the improvement of these metrics progressively over time. Through employing a dual-task paradigm, we identified cognitive interference effects on familiarization, providing important 3insights into the interplay between cognitive and physical demands of exoskeleton operation, relating to more frail and older populations. The potential of familiarization as an early marker for motor learning was established across physical and cognitive metrics, promoting its effectiveness in guiding training and efficient protocols for diverse, frail populations.

This work sets a standard for evaluating user-exoskeleton adaptation in real-world conditions, offering a robust methodology for future studies. The findings have direct implications for designing exoskeleton training protocols that prioritize user comfort and efficiency.

Outlook

While this thesis has made substantial contributions to optimizing human-exoskeleton interactions, some limitations could be better addressed, forming the foundation for future research work.

In the SPEXOR project, the sagittal-plane modeling approach, while effective, limits the generalizability of findings to three-dimensional motion scenarios. Investigating force-based interactions between humans and exoskeletons could improve the accuracy of torque profiles and better account for dynamic variabilities in lifting tasks. Additionally, extending cost-function evaluations to include fatigue modeling and endurance-related factors would enhance the applicability of these models for real-world conditions.

For the HeiAge project, the modular sensor system developed offers significant potential for biomechanical and user-integration refinement. Enhancements such as real-time feedback loops for adaptive control and improvements in sensor integration could further optimize the system's usability and accuracy. Though the outdoor familiarization study was extensive and large scale, able-bodied participants do not represent the diverse population groups these devices are meant for. Potential work in the future should use the findings from this study as to design a safe protocol where frail population groups could be used to evaluate lower-limb exoskeletons. Repeated experiments with the same participants should take place over a length of time as to assess motor learning in its entirety through principles of skill retention and transfer. The benchmarks established in this thesis could also be used to develop personalized training protocols that accelerate familiarization and ensure sustained motor learning.

In conclusion, this thesis underscores the vast potential of evaluating and optimizing human-exoskeleton interactions within both industrial and assistive settings. It provides a robust foundation for enhancing safety, usability and accessibility of exoskeleton technologies, facilitating a more efficient introduction into the real world. The work presented here contributes to a future where exoskeletons integrate seamlessly into diverse aspects of human life, whether to empower individuals to achieve greater mobility, restore function, induce productivity or regain independence.

Appendix

A Minimizing Lumbar Loads of Recorded Lifting Motions with Exoskeleton Support

This section outlines the procedure of adjusting the optimal control framework explained in Section 5.3 as to incorporate an extra minimization term on the lumbar torques of the human model. The goal of this minimization is to fully engage the passive and active elements of the exoskeleton as to successfully minimize lumbar loads, while not fundamentally altering the kinematics of the recorded motion of the participants.

The LSQ problem remains unchanged, incorporating the addition to the cost function Equations 5.1, 5.2 and 5.3, of a new minimization term,

$$w_3 \int_{t_i}^{t_{i+1}} \left\| \bar{\mathbf{u}}^{\mathbf{lumbar}} \right\|_2^2 dt \tag{.1}$$

which minimizes the controls of the lumbar torques of the human model for the custom spine model joints $\bar{\mathbf{u}}^{\mathbf{lumbar}}$ T12/L1, L1/L2, L2/L3, L3/L4, and L5/S1, according to the dynamic chain described in Subsection 4.1.1. The entries of $\bar{\mathbf{u}}^{\mathbf{lumbar}}$ are normalized according to the maximum possible torque values of the respective lumbar joints. The weight w_3 was adjusted according to the methodology of the next Subsection, which tested a number of different weights in order to deduce the most appropriate value. The main aim of the variability study of the value chosen for w_3 examined the trade-off between minimizing lumbar loads while minimally altering the recorded movement of the participants.

A.1 Solution Dependency Study on the Lumbar Load Minimization Weight

Three different weight values were tested for minimizing lumbar loads in the exoskeleton-assisted LSQ problem. These weights, denoted as w_{3L}, w_{3M}, and w_{3S}, correspond to large, medium, and small magnitudes, with values of $w_{3L} = 1 \times 10^{-1}$, $w_{3M} = 1 \times 10^{-3}$, and $w_{3S} = 1 \times 10^{-6}$, respectively. The reformulated OCP, now consisting of terms in Equations 5.1 - .1, was solved with all three values for w_3. The criteria of the comparison consisted of higher reductions in lumbar loads about the L5/S1 joint and minimal alteration of the recorded kinematics. Hence, the optimization problem explored in this section aims to optimally complement the participant's motion by ultimately reducing lumbar loads. Following the introduction of this weighted term, it is subsequent that the fitting accuracy of the solution will

be compromised, proportional to the magnitude of $w3$. The results of this study are reported and discussed in the next Subsection.

A.2 Results of the Solution Dependency Study

This section presents the results of the weight variability study for the lumbar torque minimization term in the exoskeleton-assisted optimization problem. The outcomes highlight the effects of varying the weight (w_3) on lumbar torque reduction and kinematic preservation. The results compare lumbar load reductions at the L5/S1 joint and the corresponding deviations in participant kinematics for three tested weight values (w_{3L}, w_{3M}, w_{3S}). Figure 11 illustrates the performance of the three different minimization terms, compared to the values calculated from the original LSQ problem, whereas Table 2 summarizes the contributions in reducing lumbar loads and Table 3 reports the effect the weights have on the accuracy of kinematic tracking, related to the LSQ solution. The main outcomes of this study are reported and discussed following the reported results. The post-processing and statistical analysis on the means and standard deviations of the results of the three participants were conducted using MATLAB (2020b, Natick, MA, USA).

Table 2: Reduction of CLBLs and PLBLs for each weight value.

Torque Reductions (Nm)												
	L5 CLBL Reduction (%)				**L5 PLBL Reduction (%)**				**Mean Hip Reduction (%)**			
	P1	**P2**	**P3**	**Mean**	**P1**	**P2**	**P3**	**Mean**	**P1**	**P2**	**P3**	**Mean**
$\mathbf{W_{3S}}$	26.8	19.2	25.7	23.9	18.3	16.4	17.3	17.3	-1.62	17.9	13.7	9.99
$\mathbf{W_{3M}}$	31.3	24.3	22.1	25.9	20.2	18.6	15.4	18.1	11.4	28.4	24.8	21.5
$\mathbf{W_{3L}}$	32.3	28.9	28.2	29.8	23.5	21	19.4	21.3	26.2	40.5	37.4	34.7

Table 3: Kinematic alterations for lumbar and hip angles, for each weight value.

Kinematics Alterations (RMSE)								
	Mean RMSE L5 (°)				**Mean RMSE Hip (°)**			
	P1	**P2**	**P3**	**Mean**	**P1**	**P2**	**P3**	**Mean**
$\mathbf{W_{3S}}$	1.1	1.05	1.59	1.25	6.36	8.1	13.5	9.33
$\mathbf{W_{3M}}$	2.13	1.98	2.45	2.19	12.7	12.4	18.6	14.6
$\mathbf{W_{3L}}$	3.24	3.12	3.54	3.30	22.6	20.6	27.1	23.5

$\mathbf{W_{3M}}$ as the Best Trade-Off

The results indicate that $\mathbf{W_{3M}}$ offers the most balanced solution between reducing lumbar torques and maintaining movement kinematics close to those of the recorded motion. For the CLBL, Wm produces a 25.9% reduction, which is higher than Ws (23.9%) but lower than Wl (29.8%). Similarly, for the PLBL, Wm reduces torques by 18.1%, slightly better than Ws but lower than Wl. Additionally, the mean hip torque reduction for Wm is significantly higher than Ws at 21.5%.

The kinematic deviations, however, indicate that $\mathbf{W_{3M}}$ does a relatively good job in preserving lumbar and hip movement patterns, compared to the higher Wl. The RMSE for L5 in Wm is 2.19°, while the RMSE for hip amounts to 14.6°, which is a moderate increase compared to Ws but still significantly lower than Wl. Therefore, Wm presents the best trade-off in torque reduction while not deviating too much from natural kinematic patterns.

Wl and Movement Freedom

The results for Wl show that it achieves the greatest reduction in both CLBL (29.8%) and PLBL (21.3%) compared to the other weights. The significant torque reductions may be linked to the altered movement dynamics facilitated by the exoskeleton, as seen in the high hip torque reductions of 34.7%. However, the larger deviations in kinematic patterns, with an L5 RMSE of 3.30°and a hip RMSE of 23.5°, indicate that Wl may allow for a different movement strategy, which might explain the reduction in lumbar loads.

It is unclear if this improvement stems from the exoskeleton's mechanical advantages, such as better leverage or engagement angles, or if the human models present modified techniques to reduce lumbar stress. Further investigation is needed to clarify whether the reduction is due to **biomechanical factors** of the exoskeleton or **human adaptation**.

Minimizing Squared Torques of CLBL vs. PLBL

The strategy of minimizing the squared torques seems to effectively target reductions in CLBL. Both Ws and Wm show respectable reductions in cumulative loads (23.9% and 25.9%, respectively), indicating success in addressing this factor. However, PLBL reductions (17.3% for Ws and 18.1% for Wm) are less pronounced, suggesting that minimizing the square of torques may not be as effective in reducing peak loads. The discrepancy between the cumulative and peak load reductions highlights a need to adjust the optimization approach to better address PLBLs, which are critical in high-intensity repetitive tasks such as lifting.

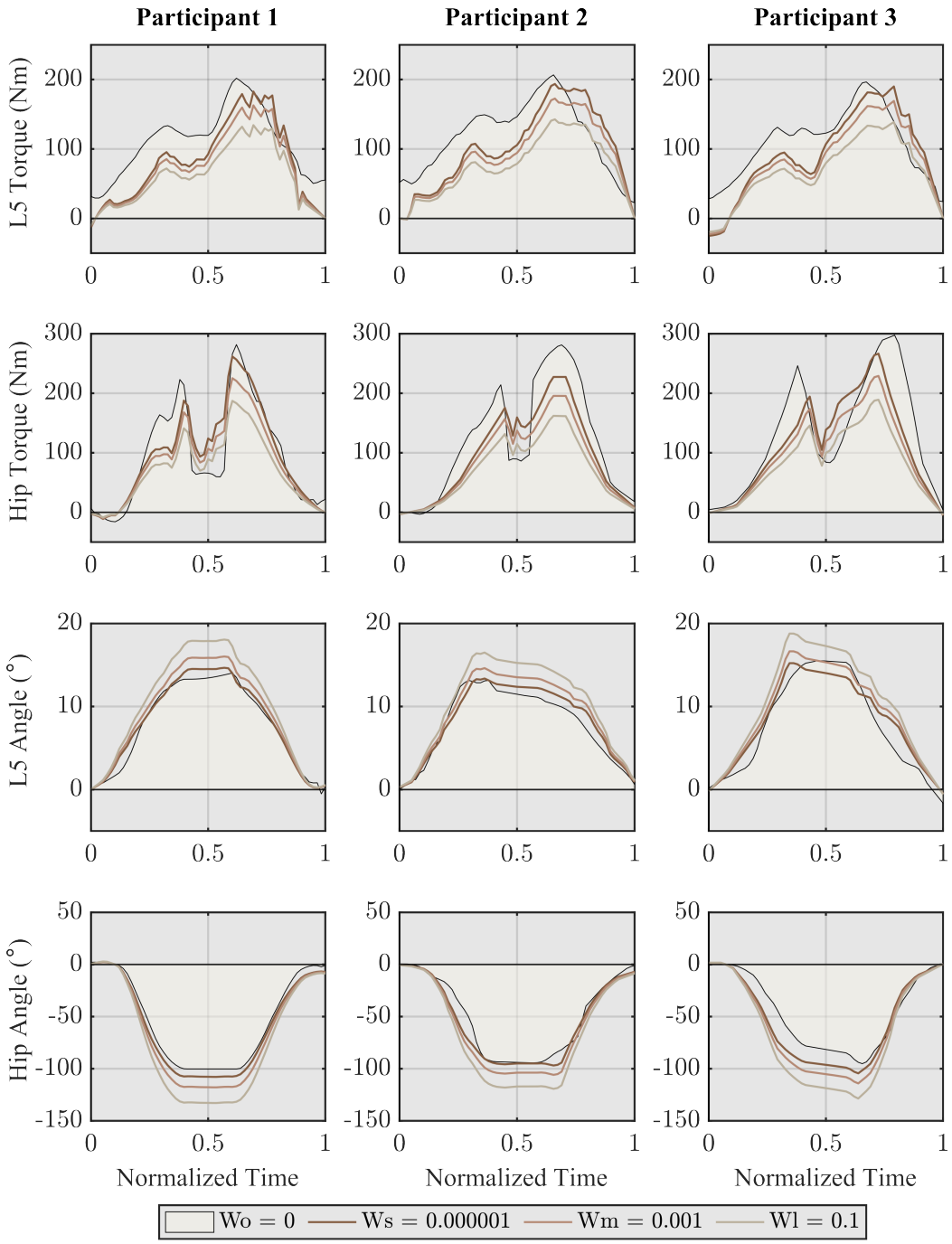

Figure 11: Comparison of the three weights (w_{3L}, w_{3M}, w_{3S}) of the solution dependency study, for the reduction of lumbar torques (row 1) and hip torques (row 2), and the alteration of the kinematics of the lumbar (row 3) and hip (row 4) joints. Results for the three weights are plotted against the original LSQ solution where $w_o = 0$.

A.3 Conclusions of the Weight Variability Study of the Lumbar Load Minimization Term

The results of the weight variability study shine light to a number of conclusions on the optimization problem for the lifting motions. First, the medium weight on the term minimizing the lumbar torques, Wm, provides the best trade-off between minimizing lumbar torques and maintaining recorded motion kinematics. It achieves a 25.9% reduction in cumulative low back loads (CLBL) and an 18.1% reduction in peak low back loads (PLBL), with relatively moderate alterations to kinematic patterns, showing an RMSE of 2.19° for the L5 joint and 14.6° for the hip. In contrast, Wl delivers the highest reductions in both CLBL (29.8%) and PLBL (21.3%), but at the expense of significant deviations in kinematic accuracy, with an RMSE of 3.30° for L5 and 23.5° for hip. This suggests that Wl facilitates a different movement strategy, though it remains unclear whether the improvement is due to the exoskeleton's mechanical advantages or the participant's adaptation to minimize lumbar stress, necessitating further investigation. Meanwhile, Ws provides smaller torque reductions, particularly in terms of hip torque, while maintaining kinematic patterns closest to the recorded motion (RMSE of 1.25° for L5 and 9.33° for hip), making it less effective for significant lumbar load reduction. Finally, the optimization strategy of minimizing squared torques is effective in reducing CLBL, but is less successful at addressing PLBL. This discrepancy highlights the need to refine the optimization approach to better address peak lumbar loads during high-intensity tasks, such as lifting, promoting the idea for synthesizing movements that offer a safer and more task-efficient technique.

B Normality Assessment on Outdoor Study Data

This section of the appendix contains results figures on the normality assessment of the data collected from the large-scale outdoor experiment. These results support the decision on using non-parametric statistical assessment tests due to the lack of normally distributed data for all five deduced metrics as shown in the following figures.

The normality assessment plots for the five variables—crutches ground reaction forces (GRFs), anteroposterior center of pressure (CoP), double support time (DST), stride duration (SD), and gait velocity (GV)—reveal clear deviations from normal distribution. In the probability density plots, the distributions often exhibit skewness, where the curves are asymmetrical, and tails extend disproportionately, particularly in GRFs and CoP metrics. Logarithmic scaling mitigates but does not eliminate these patterns, indicating inherent non-normal characteristics. The Q-Q plots further confirm this deviation, with observed quantiles diverging significantly from the theoretical normal quantile line, particularly in the tails of the distributions. These divergences are most pronounced in the DST and SD metrics, where data points cluster away from the diagonal line, suggesting variability in temporal gait parameters. Collectively, these visual markers across the plots underscore the non-normality of the assessed variables, likely reflecting the biomechanical and cognitive challenges of assisted walking conditions.

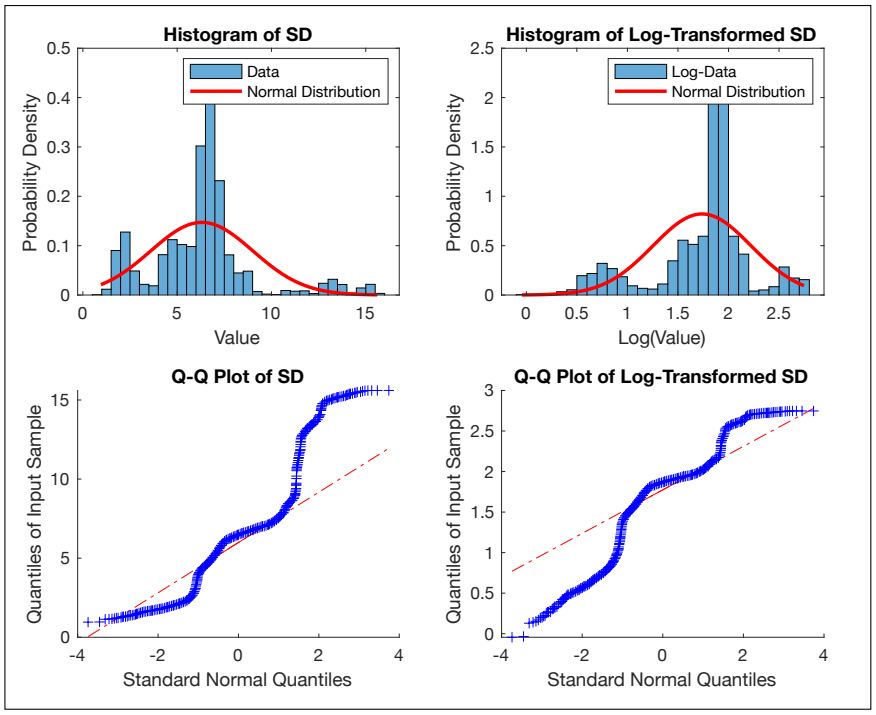

Figure 12: Normality results for the stride duration metric. Top row reports probability density of group values. (Left) Normal scale, (Right) Logarithmic scale. Bottom row plots the QQ quantile values for input samples and normal quantiles.

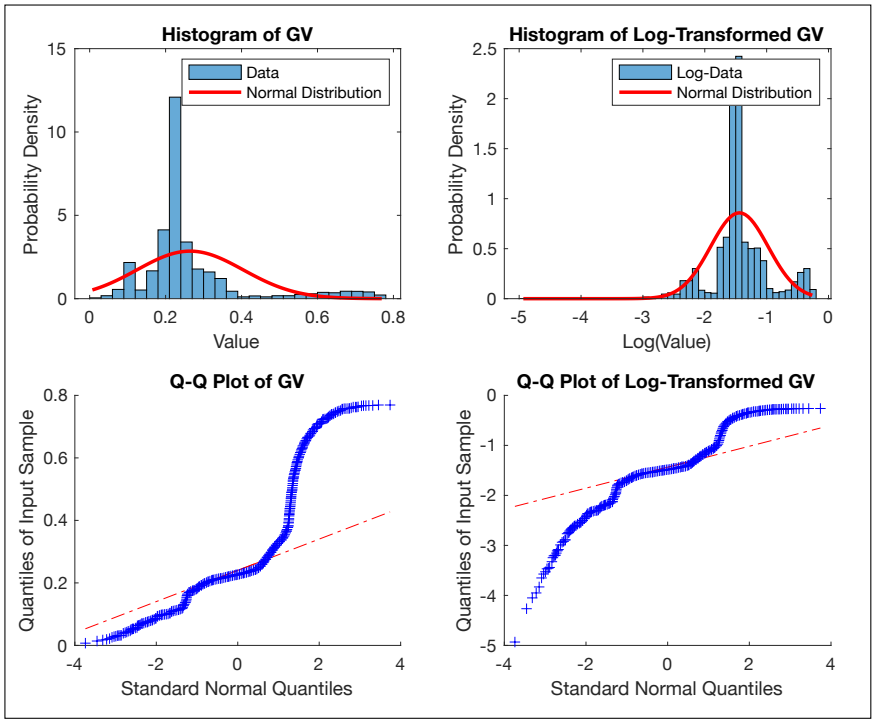

Figure 13: Normality results for the gait velocity metric. Top row reports probability density of group values. (Left) Normal scale, (Right) Logarithmic scale. Bottom row plots the QQ quantile values for input samples and normal quantiles.

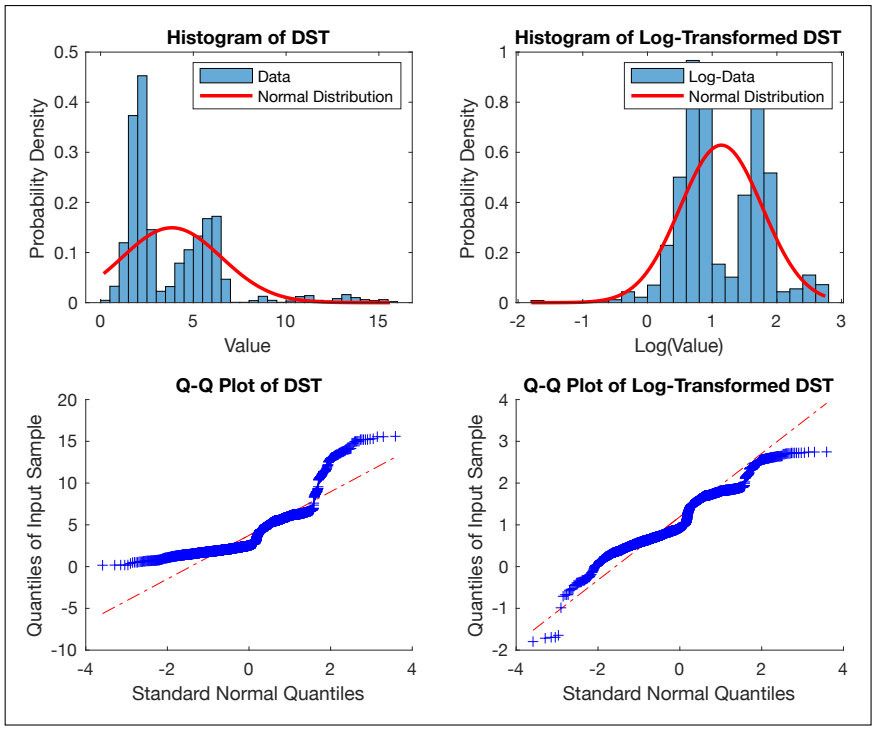

Figure 14: Normality results for the double support time metric. Top row reports probability density of group values. (Left) Normal scale, (Right) Logarithmic scale. Bottom row plots the QQ quantile values for input samples and normal quantiles.

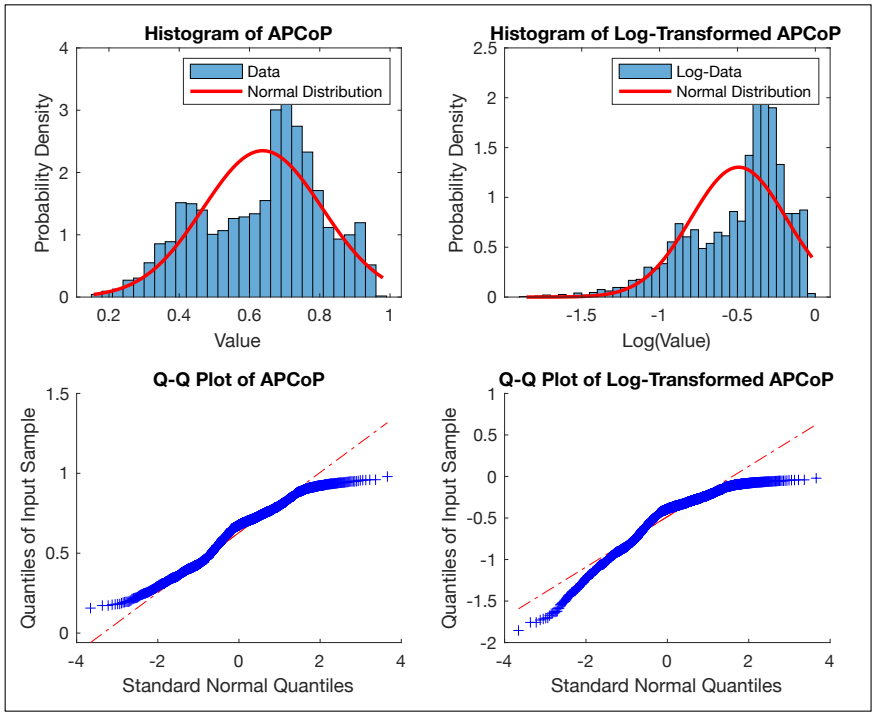

Figure 15: Normality results for the anteroposterior centre of pressure metric. Top row reports probability density of group values. (Left) Normal scale, (Right) Logarithmic scale. Bottom row plots the QQ quantile values for input samples and normal quantiles.

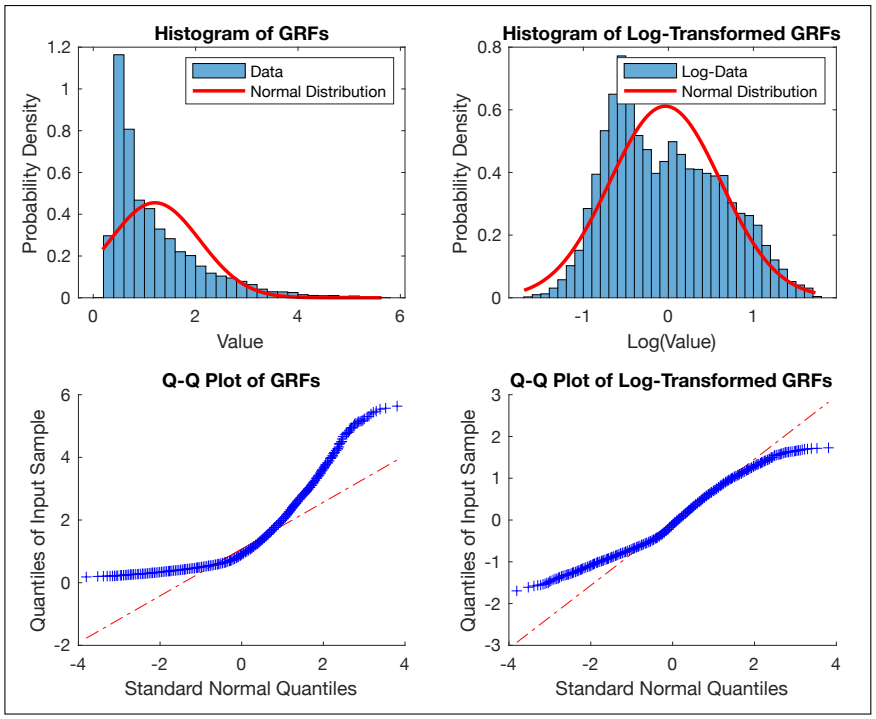

Figure 16: Normality results for the crutches ground reaction forces metric. Top row reports probability density of group values. (Left) Normal scale, (Right) Logarithmic scale. Bottom row plots the QQ quantile values for input samples and normal quantiles.

Acronyms and Abbreviations

]

ABA	Articulated Body Algorithm	88
ALS	Amyotrophic Lateral Sclerosis	1
ANOVA	One-Way Analysis of Variance	153
APCoP	Anteroposterior Center of Pressure	207
BLE	Bluetooth Low Energy	170
BLEEX	Berkeley Lower Extremity Exoskeleton	59
BMI	Body Mass Index	150
BNDR	Bending Non-Demand Return	41
BSE	Back-Support Exoskeleton	24
CLBL	Cumulative Low-Back Load	20, 248
CoM	Centre of Mass	74
CoP	Centre of Pressure	55
CRBA	Composite Rigid Body Algorithm	88
CRR	Correct Response Rates	207, 249
CSS	Custom Sensor System	183
CV	Coefficient of Variation	209
DoF	Degree of Freedom	51, 246
DST	Double Support Time	207
EMG	Electromyography	39
FSR	Force-Sensitive Resistors	166
GRFs	Ground Reaction Forces	27
GUI	Graphical User Interface	64
H-WEX	Hyundai Waist Exoskeleton	43
HAL	Hybrid Assistive Exoskeleton	55
HWAD	Honda Walking Assist Device	57

IIT Italian Institute of Technology 64

IK Inverse Kinematics 73, 248

IMU Inertial Measurement Unit 47

IQR Inter-Quartile Range 183

JRFs Joint Reaction Forces 28

KKT Karush-Kuhn-Tucker 82

LBP Low Back Pain 1

LCF Lumbar Compression Forces 37

LES Lumbar Erector Spinae 37

LLE Lower-Limb Exoskeleton 10, 246

LSQ Least-Squares Quadratic 79, 246

MCU Micro Controller Unit 172

MPC Model-Predictive Control 58

MSDs Musculoskeletal Disorders 1

MTGs Muscle Torque Generators 91

MVC Maximum Voluntary Contraction 72

NLP Nonlinear Program 81

OCP Optimal Control Problem 78, 246

ODE Ordinary Differential Equation 80

ORB Optimization, Robotics And Biomechanics 45

PDEs Partial Differential Equations 51

PEA Parallel-Elastic Actuator 43

PLAD Personal Lift Augmentation Device 39

PLBL Peak Low-Back Load 20, 248

RBDL Rigid Body Dynamics Library 87

RMS Root Mean Square 153

RMSE Root Mean Square Error 183

RNEA Recursive Newton Euler Algorithm 87

ROM	Range of Motion	17
SCI	Spinal Cord Injury	1
SEA	Series Elastic Actuator	56
SPEXOR	SPinal EXOskeletal Robot	8
SQP	Sequential Quadratic Programming	81
SSL	Smart Suit Lite	39
STD	Standard Deviation	209
TSA	Twisted String Actuators	42
UCD	User-Centered Design	64
WAD	Wearable Assistive Device	39
WMRD	Wearable Restoring Moment Device	41
WSAD	Wearable Stooping-Assist Device	42
YLDs	Years Lived With Disability	15

List of Figures

List of Tables

Bibliography

[1] World Health Organization. *Musculoskeletal Health*. July 2022 (cit. on p. 1).

[2] M. Ferreira and J. Steinmetz. *The Lancet: New study shows low back pain is the leading cause of disability around the world | Institute for Health Metrics and Evaluation* (cit. on p. 1).

[3] Davide Cattaneo, Elisa Gervasoni, Elisabetta Pupillo, et al. „Mobility disorders in Stroke, Parkinson disease, and multiple sclerosis: A multicenter cross-sectional study". In: *American Journal of Physical Medicine and Rehabilitation* 99.1 (Jan. 2020), pp. 41–47 (cit. on p. 1).

[4] Jan Babič, Matteo Laffranchi, Federico Tessari, et al. „Challenges and solutions for application and wider adoption of wearable robots". In: 2 (2021), p. 14 (cit. on p. 1).

[5] N Yagn. *Apparatus for facilitating walking*. Jan. 1890 (cit. on p. 1).

[6] B. J. Makinson. „Research and Development Prototype for Machine Augmentation of Human Strength and Endurance. Hardiman I Project". In: *Defence Technical Information Center (DTIC)* (1971) (cit. on p. 1).

[7] *Apogee | Aktives Exoskelett mit Hebe- und Laufunterstützung · German Bionic* (cit. on p. 1).

[8] Jacques Kerdraon, Jean Gabriel Previnaire, Maegan Tucker, et al. „Evaluation of safety and performance of the self balancing walking system Atalante in patients with complete motor spinal cord injury". In: *Spinal Cord Series and Cases 2021 7:1* 7.1 (Aug. 2021), pp. 1–8 (cit. on pp. 1, 58).

[9] Jean Jacques Hublin, Abdelouahed Ben-Ncer, Shara E. Bailey, et al. „New fossils from Jebel Irhoud, Morocco and the pan-African origin of Homo sapiens". In: *Nature* 546.7657 (June 2017), pp. 289–292 (cit. on p. 15).

[10] Michel Brunet, Franck Guy, David Pilbeam, et al. „A new hominid from the upper Miocene of Chad, Central Africa". In: *Nature* 418.6894 (July 2002), pp. 145–151 (cit. on p. 15).

[11] Dennis M. Bramble and Daniel E. Lieberman. „Endurance running and the evolution of Homo". In: *Nature* 432.7015 (Nov. 2004), pp. 345–352 (cit. on p. 15).

[12] European Risk Observatory. „Eurostat (Labour Force Survey ad hoc module". In: *European Statistics on Accidents at Work*. European Health, 2013 (cit. on p. 15).

[13] Manuela L Ferreira, Katie de Luca, Lydia M Haile, et al. „Global, regional, and national burden of low back pain, 1990Ã¢â‚¬â€œ2020, its attributable risk factors, and projections to 2050: a systematic analysis of the Global Burden of Disease Study 2021". In: *The Lancet Rheumatology* 5 (2023), e316–e329 (cit. on p. 15).

[14] EU-OSHA. *Musculoskeletal disorders | Safety and health at work EU-OSHA*. 2020 (cit. on p. 15).

[15] Jeffrey M.. Spivak and Patrick J.. Connolly. *Orthopaedic Knowledge Update: Spine 3*. American Academy of Orthopaedic Surgeons, 2006, p. 526 (cit. on p. 19).

[16] Michele C. Battié and Tapio Videman. „Lumbar disc degeneration: Epidemiology and genetics". In: *Journal of Bone and Joint Surgery* 88.SUPPL. 2 (2006), pp. 3–9 (cit. on p. 19).

[17] Kyoung Sim Jung, Jin Hwa Jung, Tae Sung In, and Hwi Young Cho. „Effects of Prolonged Sitting with Slumped Posture on Trunk Muscular Fatigue in Adolescents with and without Chronic Lower Back Pain“. In: *Medicina 2021, Vol. 57, Page 3* 57.1 (Dec. 2020), p. 3 (cit. on p. 19).

[18] Nic Saraceni, Amity Campbell, Peter Kent, et al. „Exploring lumbar and lower limb kinematics and kinetics for evidence that lifting technique is associated with LBP“. In: *PLOS ONE* 16.7 (July 2021), e0254241 (cit. on p. 19).

[19] Angela Maria Lis, Katia M. Black, Hayley Korn, and Margareta Nordin. „Association between sitting and occupational LBP“. In: *European Spine Journal* 16.2 (Feb. 2007), p. 283 (cit. on p. 19).

[20] Nicholas B. Washmuth, Abby D. McAfee, and C. Scott Bickel. „Lifting Techniques: Why Are We Not Using Evidence To Optimize Movement?“ In: *International Journal of Sports Physical Therapy* 17.1 (2022), p. 104 (cit. on p. 19).

[21] Alf L. Nachemson. „Disc pressure measurements“. In: *Spine* 6.1 (1981), pp. 93–97 (cit. on p. 19).

[22] Hans Joachim Wilke, Peter Neef, Marco Caimi, Thomas Hoogland, and Lutz E. Claes. „New in vivo measurements of pressures in the intervertebral disc in daily life“. In: *Spine* 24.8 (Apr. 1999), pp. 755–762 (cit. on p. 19).

[23] Katsuhiko Sato, Shinichi Kikuchi, and Takumi Yonezawa. „In vivo intradiscal pressure measurement in healthy individuals and in patients with ongoing back problems“. In: *Spine* 24.23 (Dec. 1999), pp. 2468–2474 (cit. on p. 19).

[24] Hans Joachim Wilke, Peter Neef, Barbara Hinz, Helmut Seidel, and Lutz Claes. „Intradiscal pressure together with anthropometric data - A data set for the validation of models“. In: *Clinical Biomechanics* 16.SUPPL. 1 (2001) (cit. on p. 19).

[25] A Rohlmann, D Pohl, A Bender, F Graichen, and J Dymke. „Activities of Everyday Life with High Spinal Loads“. In: *PLoS ONE* 9.5 (2014), p. 98510 (cit. on p. 19).

[26] Robin Schäfer, Katharina Trompeter, Daniela Fett, et al. „The mechanical loading of the spine in physical activities“. In: *European Spine Journal* 32 (2023), pp. 2991–3001 (cit. on p. 19).

[27] Danuta Roman-Liu, Joanna Kamińska, and Tomasz Tokarski. „Differences in lumbar spine intradiscal pressure between standing and sitting postures: a comprehensive literature review“. In: *PeerJ* 11 (Oct. 2023), e16176 (cit. on p. 20).

[28] P. Dolan and M. A. Adams. „Repetitive lifting tasks fatigue the back muscles and increase the bending moment acting on the lumbar spine“. In: *Journal of Biomechanics* 31.8 (Aug. 1998), pp. 713–721 (cit. on p. 20).

[29] M. F. Antwi-Afari, H. Li, D. J. Edwards, et al. „Biomechanical analysis of risk factors for work-related musculoskeletal disorders during repetitive lifting task in construction workers“. In: *Automation in Construction* 83 (Nov. 2017), pp. 41–47 (cit. on p. 20).

[30] Lisa C. Brereton and Stuart M. McGill. „Frequency response of spine extensors during rapid isometric contractions: effects of muscle length and tension“. In: *Journal of electromyography and kinesiology : official journal of the International Society of Electrophysiological Kinesiology* 8.4 (Aug. 1998), pp. 227–232 (cit. on pp. 20, 130).

[31] Pieter Coenen, Idsart Kingma, Cécile R.L. Boot, Paulien M. Bongers, and Jaap H. Van Dieën. „Cumulative mechanical low-back load at work is a determinant of low-back pain“. In: *Occupational and Environmental Medicine* 71.5 (May 2014), pp. 332–337 (cit. on pp. 20, 130).

[32] van Dieën JH and Kingma I. „Effects of antagonistic co-contraction on differences between electromyography based and optimization based estimates of spinal forces“. In: *Ergonomics* 48.4 (Mar. 2005), pp. 411–426 (cit. on pp. 20, 130).

[33] M. P. de Looze, H. M. Toussaint, J. H. van Dieën, and H. C.G. Kemper. „Joint moments and muscle activity in the lower extremities and lower back in lifting and lowering tasks“. In: *Journal of Biomechanics* 26.9 (Sept. 1993), pp. 1067–1076 (cit. on p. 22).

[34] Jaap H. Van Dieën, Marco J.M. Hoozemans, and Huub M. Toussaint. „Stoop or squat: a review of biomechanical studies on lifting technique“. In: *Clinical Biomechanics* 14.10 (Dec. 1999), pp. 685–696 (cit. on p. 23).

[35] David Nolan, Kieran O'Sullivan, Chris Newton, Gurpreet Singh, and Benjamin E. Smith. „Are there differences in lifting technique between those with and without low back pain? A systematic review“. In: *Scandinavian Journal of Pain* 20.2 (Apr. 2020), pp. 215–227 (cit. on p. 24).

[36] Kari Pekka Martimo, Jos Verbeek, Jaro Karppinen, et al. „Effect of training and lifting equipment for preventing back pain in lifting and handling: systematic review“. In: *BMJ* 336.7641 (Feb. 2008), pp. 429–431 (cit. on p. 24).

[37] Christine Hsieh, Stephanie Fleegle, and Christine A. Arenson. „Mobility, Gait, Balance, and Falls“. In: *Geriatric Urology* 9781461490470 (Dec. 2014), pp. 89–102 (cit. on p. 25).

[38] Walter Pirker and Regina Katzenschlager. „Gait disorders in adults and the elderly: A clinical guide“. In: *Wiener Klinische Wochenschrift* 129.3-4 (Feb. 2017), pp. 81–95 (cit. on p. 25).

[39] Qian Mao, Wei Zheng, Menghan Shi, and Fan Yang. „Scientometric Research and Critical Analysis of Gait and Balance in Older Adults“. In: *Sensors* 24.10 (May 2024), p. 3199 (cit. on p. 25).

[40] Y. P. Ivanenko, R. E. Poppele, and F. Lacquaniti. „Five basic muscle activation patterns account for muscle activity during human locomotion“. In: *Journal of Physiology* 556.1 (Apr. 2004), pp. 267–282 (cit. on p. 28).

[41] Michael W. Whittle. „An introduction to gait analysis“. In: *An Introduction to Gait Analysis* (Feb. 2007), pp. 1–255 (cit. on p. 29).

[42] David A. Winter. „Biomechanics and Motor Control of Human Movement: Fourth Edition“. In: *Biomechanics and Motor Control of Human Movement: Fourth Edition* (Sept. 2009), pp. 1–370 (cit. on p. 29).

[43] L. P. Fried, C. M. Tangen, J. Walston, et al. „Frailty in older adults: evidence for a phenotype“. In: *The journals of gerontology. Series A, Biological sciences and medical sciences* 56.3 (2001) (cit. on p. 29).

[44] Kenneth Rockwood, Xiaowei Song, Chris MacKnight, et al. „A global clinical measure of fitness and frailty in elderly people“. In: *CMAJ : Canadian Medical Association journal = journal de l'Association medicale canadienne* 173.5 (Aug. 2005), pp. 489–495 (cit. on pp. 29, 63).

[45] Janice J. Eng and Pei Fang Tang. „Gait training strategies to optimize walking ability in people with stroke: A synthesis of the evidence“. In: *Expert review of neurotherapeutics* 7.10 (Oct. 2007), p. 1417 (cit. on p. 30).

[46] Baltej Singh Rupal, Sajid Rafique, Ashish Singla, et al. „Lower-limb exoskeletons: Research trends and regulatory guidelines in medical and non-medical applications“. In: *International Journal of Advanced Robotic Systems* 14.6 (Dec. 2017) (cit. on p. 30).

[47] Matteo Laffranchi, Stefano D'Angella, Christian Vassallo, et al. „User-Centered Design and Development of the Modular TWIN Lower Limb Exoskeleton". In: *Frontiers in Neurorobotics* 15 (Oct. 2021) (cit. on pp. 31, 57, 64, 148, 169, 181, 203).

[48] Linda Shore, Valerie Power, Adam de Eyto, and Leonard W. O'Sullivan. „Technology Acceptance and User-Centred Design of Assistive Exoskeletons for Older Adults: A Commentary". In: *Robotics 2018, Vol. 7, Page 3* 7.1 (Jan. 2018), p. 3 (cit. on p. 33).

[49] Stefano Toxiri, Matthias B. Näf, Maria Lazzaroni, et al. „Back-Support Exoskeletons for Occupational Use: An Overview of Technological Advances and Trends". In: *IISE Transactions on Occupational Ergonomics and Human Factors* 7.3-4 (2019), pp. 237–249 (cit. on pp. 33, 130).

[50] Muhammad Ahsan Gull, Shaoping Bai, and Thomas Bak. „A Review on Design of Upper Limb Exoskeletons". In: *Robotics 2020, Vol. 9, Page 16* 9.1 (Mar. 2020), p. 16 (cit. on p. 34).

[51] David Pinto-Fernandez, Diego Torricelli, Maria Del Carmen Sanchez-Villamanan, et al. „Performance Evaluation of Lower Limb Exoskeletons: A Systematic Review". In: *IEEE Transactions on Neural Systems and Rehabilitation Engineering* 28.7 (July 2020), pp. 1573–1583 (cit. on pp. 34, 48, 195, 196).

[52] Michiel P. de Looze, Tim Bosch, Frank Krause, Konrad S. Stadler, and Leonard W. O'Sullivan. „Exoskeletons for industrial application and their potential effects on physical work load". In: *Ergonomics* 59.5 (May 2016), pp. 671–681 (cit. on pp. 36, 37).

[53] Dina B. Eisinger, Rajeswari Kumar, and Randi Woodrow. „Effect of lumbar orthotics on trunk muscle strength". In: *American journal of physical medicine & rehabilitation* 75.3 (May 1996), pp. 194–197 (cit. on p. 37).

[54] Axel S. Koopman, Idsart Kingma, Gert S. Faber, Michiel P. de Looze, and Jaap H. van Dieën. „Effects of a passive exoskeleton on the mechanical loading of the low back in static holding tasks". In: *Journal of Biomechanics* 83 (Jan. 2019), pp. 97–103 (cit. on pp. 37, 135).

[55] Hyun K. Kim, Muhammad Hussain, Jaehyun Park, Jongwon Lee, and Jin Won Lee. „Analysis of Active Back-Support Exoskeleton During Manual Load-Lifting Tasks". In: *Journal of Medical and Biological Engineering* 41.5 (Oct. 2021), pp. 704–714 (cit. on p. 37).

[56] Mohammad Abdoli-E, Michael J. Agnew, and Joan M. Stevenson. „An on-body personal lift augmentation device (PLAD) reduces EMG amplitude of erector spinae during lifting tasks". In: *Clinical Biomechanics* 21.5 (June 2006), pp. 456–465 (cit. on pp. 39, 135).

[57] Brett H. Whitfield, Patrick A. Costigan, Joan M. Stevenson, and Catherine L. Smallman. „Effect of an on-body ergonomic aid on oxygen consumption during a repetitive lifting task". In: *International Journal of Industrial Ergonomics* 44.1 (Jan. 2014), pp. 39–44 (cit. on p. 39).

[58] Yumeko Imamura, Takayuki Tanaka, Yoshihito Suzuki, Kazuki Takizawa, and Masanori Yamanaka. „Analysis of Trunk Stabilization Effect by Passive Power-Assist Device". In: () (cit. on p. 39).

[59] Hadi Heydari, Maryam Hoviattalab, Mahmood Reza Azghani, Masoud Ramezanzadehkoldeh, and Mohamad Parnianpour. „Investigation on a developed wearable assistive device (WAD) in reduction lumbar muscles activity". In: *https://doi.org/10.4015/S101623721* 25.3 (May 2013) (cit. on p. 40).

[60] Rehacare. *New back-support exoskeleton from Ottobock*. 2023 (cit. on p. 40).

[61] Orthexo. *IX BACK AIR Back Exoskeleton From SuitX*. 2023 (cit. on p. 40).

[62] SuitX. *IX BACK AIR exoskeleton | SUITX*. 2023 (cit. on p. 40).

[63] A Barrett and F Fathallah. „Evaluation of Four Weight Transfer Devices for Reducing Loads on the Lower Back during Agricultural Stoop Labor". In: *Annual International Meeting of the American Society of Agricultural Engineers*. 2001 (cit. on p. 40).

[64] Lowe's Innovation Labs. *Associate Exosuits — Lowe's Innovation Labs - Building the Future of Home Improvement.* (Cit. on p. 40).

[65] Athulya A. Simon, Mohammad Mehdi Alemi, and Alan T. Asbeck. „Kinematic effects of a passive lift assistive exoskeleton". In: *Journal of Biomechanics* 120 (May 2021), p. 110317 (cit. on p. 40).

[66] Mohammad Mehdi Alemi, Athulya A. Simon, Jack Geissinger, and Alan T. Asbeck. „Modeling the metabolic reductions of a passive back-support exoskeleton". In: *Journal of Applied Physiology* 132.3 (Mar. 2022), pp. 737–760 (cit. on p. 40).

[67] Tim Bosch, Jennifer van Eck, Karlijn Knitel, and Michiel de Looze. „The effects of a passive exoskeleton on muscle activity, discomfort and endurance time in forward bending work". In: *Applied Ergonomics* 54 (May 2016), pp. 212–217 (cit. on p. 41).

[68] Brent L. Ulrey and Fadi A. Fathallah. „Effect of a personal weight transfer device on muscle activities and joint flexions in the stooped posture". In: *Journal of Electromyography and Kinesiology* 23.1 (Feb. 2013), pp. 195–205 (cit. on p. 41).

[69] Michael Wehner, David Rempel, and Homayoon Kazerooni. „Lower Extremity Exoskeleton Reduces Back Forces in Lifting". In: *Proceedings of the ASME Dynamic Systems and Control Conference 2009, DSCC2009* PART B (Sept. 2010), pp. 49–56 (cit. on pp. 41, 135).

[70] HeroWear. *Home | HeroWear* (cit. on p. 41).

[71] Erik P. Lamers, Aaron J. Yang, and Karl E. Zelik. „Feasibility of a biomechanically-assistive garment to reduce low back loading during leaning and lifting". In: *IEEE Transactions on Biomedical Engineering* 65.8 (Aug. 2018), pp. 1674–1680 (cit. on p. 41).

[72] Haohan Zhang, Abhijit Kadrolkar, and Frank C. Sup. „Design and preliminary evaluation of a passive spine exoskeleton". In: *Journal of Medical Devices, Transactions of the ASME* 10.1 (Mar. 2016) (cit. on p. 42).

[73] H. Kazerooni, Wayne Tung, and Minerva Pillai. „Evaluation of Trunk-Supporting Exoskeleton". In: *https://doi.org/10.1177/1071181319631261* 63.1 (Nov. 2019), pp. 1080–1083 (cit. on p. 42).

[74] Ziguo Luo and Yong Yu. „Wearable stooping-assist device in reducing risk of low back disorders during stooped work". In: *2013 IEEE International Conference on Mechatronics and Automation, IEEE ICMA 2013* (2013), pp. 230–236 (cit. on p. 42).

[75] Zhejun Yao, Christine Linnenberg, Robert Weidner, and Jens Wulfsberg. „Development of a soft power suit for lower back assistance". In: *Proceedings - IEEE International Conference on Robotics and Automation* 2019-May (May 2019), pp. 5103–5109 (cit. on p. 42).

[76] Yoshiki Muramatsu, Hiroyuki Kobayashi, Yutaka Sato, et al. „Quantitative Performance Analysis of Exoskeleton Augmenting Devices-Muscle Suit-for Manual Worker". In: () (cit. on p. 42).

[77] German Bionic. *German Bionic | Smart Wearable Tools for Workplace Safety · German Bionic* (cit. on p. 43).

[78] Cyberdyne. *Labor Support | Cyberdyne USA Inc.* (Cit. on p. 43).

[79] Hun Keon Ko, Seok Won Lee, Dong Han Koo, Inju Lee, and Dong Jin Hyun. „Waist-assistive exoskeleton powered by a singular actuation mechanism for prevention of back-injury". In: *Robotics and Autonomous Systems* 107 (Sept. 2018), pp. 1–9 (cit. on p. 43).

[80] Robo-Mate. *Robo-Mate - Home* (cit. on p. 43).

[81] Stefano Toxiri, Andrea Calanca, Jesús Ortiz, Paolo Fiorini, and Darwin G. Caldwell. „A Parallel-Elastic Actuator for a Torque-Controlled Back-Support Exoskeleton". In: *IEEE Robotics and Automation Letters* 3.1 (Jan. 2018), pp. 492–499 (cit. on p. 43).

[82] SPEXOR. *SPEXOR – Spinal Exoskeletal Robot for Low Back Pain Prevention and Vocational Reintegration* (cit. on pp. 44, 46).

[83] Matthias B. Näf, Axel S. Koopman, Saskia Baltrusch, et al. „Passive back support exoskeleton improves range of motion using flexible beams". In: *Frontiers Robotics AI* 5.JUN (2018) (cit. on pp. 46, 95).

[84] Bram Vanderborght, Nikos G. Tsagarakis, Claudio Semini, Ronald Van Ham, and Darwin G. Caldwell. „MACCEPA 2.0: Adjustable compliant actuator with stiffening characteristic for energy efficient hopping". In: *Proceedings - IEEE International Conference on Robotics and Automation* (2009), pp. 544–549 (cit. on pp. 46, 96).

[85] Jan Babič, Tadej Petrič, Katja Mombaur, et al. „SPEXOR: Design and development of passive spinal exoskeletal robot for low back pain prevention and vocational reintegration". In: *SN Applied Sciences* 1.3 (Mar. 2019), pp. 1–5 (cit. on p. 47).

[86] G. S. Faber, I. Kingma, C. C. Chang, J. T. Dennerlein, and J. H. van Dieën. „Validation of a wearable system for 3D ambulatory L5/S1 moment assessment during manual lifting using instrumented shoes and an inertial sensor suit". In: *Journal of Biomechanics* 102 (Mar. 2020), p. 109671 (cit. on p. 48).

[87] Yuanxi Sun, Yuntao Tang, Jia Zheng, et al. „From sensing to control of lower limb exoskeleton: a systematic review". In: *Annual Reviews in Control* 53 (Jan. 2022), pp. 83–96 (cit. on pp. 49, 166).

[88] Martin Andreas Koch and Josep M. Font-Llagunes. „Lower-Limb Exosuits for Rehabilitation or Assistance of Human Movement: A Systematic Review". In: *Applied Sciences 2021, Vol. 11, Page 8743* 11.18 (Sept. 2021), p. 8743 (cit. on p. 49).

[89] EksoBionics. *EksoNR - Eksobionics* (cit. on pp. 49, 53).

[90] ReWalk. *Lifeward Personal 6.0 Exoskeleton For Spinal Cord Injury* (cit. on p. 49).

[91] Yoshiyuki Sankai. „HAL: Hybrid Assistive Limb Based on Cybernics". In: *Springer Tracts in Advanced Robotics* 66.STAR (2010), pp. 25–34 (cit. on pp. 50, 59).

[92] Skip. *Skip - Move More with Powered Movewear Technology* (cit. on pp. 50, 60).

[93] Slávka Neťuková, Martin Bejtic, Christiane Malá, et al. „Lower Limb Exoskeleton Sensors: State-of-the-Art". In: *Sensors 2022, Vol. 22, Page 9091* 22.23 (Nov. 2022), p. 9091 (cit. on pp. 50, 166).

[94] Agnieszka Wisniowska-Szurle, Natalia Woloszyn, Justyna Brozonowicz, et al. „Enhanced Rehabilitation Outcomes of Robotic-Assisted Gait Training with EksoNR Lower Extremity Exoskeleton in 19 Stroke Patients". In: *Medical Science Monitor : International Medical Journal of Experimental and Clinical Research* 29 (2023), pp. 940511–1 (cit. on p. 53).

[95] Stephen Clive Hayes, Matthew White, Christopher Richard James Wilcox, Hollie Samantha Forbes White, and Natalie Vanicek. „Biomechanical differences between able-bodied and spinal cord injured individuals walking in an overground robotic exoskeleton“. In: *PLOS ONE* 17.1 (Jan. 2022), e0262915 (cit. on p. 55).

[96] Candy Tefertiller, Kaitlin Hays, Janell Jones, et al. „Initial Outcomes from a Multicenter Study Utilizing the Indego Powered Exoskeleton in Spinal Cord Injury“. In: *Topics in Spinal Cord Injury Rehabilitation* 24.1 (Jan. 2018), pp. 78–85 (cit. on p. 55).

[97] Mirko Aach, Thomas Armin Schildhauer, Amrei Zieriacks, et al. „Feasibility, safety, and functional outcomes using the neurological controlled Hybrid Assistive Limb exoskeleton (HAL®) following acute incomplete and complete spinal cord injury – Results of 50 patients“. In: *The Journal of Spinal Cord Medicine* 46.4 (2023), p. 574 (cit. on p. 55).

[98] Jos Meuleman, Edwin Van Asseldonk, Gijs Van Oort, Hans Rietman, and Herman Van Der Kooij. „LOPES II - Design and Evaluation of an Admittance Controlled Gait Training Robot with Shadow-Leg Approach“. In: *IEEE Transactions on Neural Systems and Rehabilitation Engineering* 24.3 (Mar. 2016), pp. 352–363 (cit. on p. 56).

[99] Je Hyung Jung and Jan F. Veneman. „Real time computation of Centroidal Momentum while human walking in the lower limbs rehabilitation exoskeleton: Preliminary trials“. In: *IEEE International Conference on Rehabilitation Robotics* 2019-June (June 2019), pp. 721–726 (cit. on p. 56).

[100] Xiruo Cheng, Justin Fong, Ying Tan, and Denny Oetomo. „Investigating User Volitional Influence on Step Length in Powered Exoskeleton Designed for Users with SCI“. In: *IEEE International Conference on Rehabilitation Robotics* 2022-July (2022) (cit. on p. 56).

[101] Yongtian He, Kevin Nathan, Anusha Venkatakrishnan, et al. „An integrated neuro-robotic interface for stroke rehabilitation using the NASA X1 powered lower limb exoskeleton“. In: *2014 36th Annual International Conference of the IEEE Engineering in Medicine and Biology Society, EMBC 2014* (Nov. 2014), pp. 3985–3988 (cit. on p. 57).

[102] Yoshinao Satoh, Takumi Yamada, Yasuhisa Arai, et al. „The immediate effect of the Honda Walking Assist Device on foot and ankle function in hemiplegic stroke patients“. In: () (cit. on p. 57).

[103] Giulia Barbareschi, Rosie Richards, Matt Thornton, Tom Carlson, and Catherine Holloway. „Statically vs dynamically balanced gait: Analysis of a robotic exoskeleton compared with a human“. In: *Proceedings of the Annual International Conference of the IEEE Engineering in Medicine and Biology Society, EMBS* 2015-November (Nov. 2015), pp. 6728–6731 (cit. on pp. 58, 166).

[104] Paul Aarne Koljonen, Anna Sternin Virk, Yoon Jeong, et al. „Outcomes of a Multicenter Safety and Efficacy Study of the SuitX Phoenix Powered Exoskeleton for Ambulation by Patients With Spinal Cord Injury“. In: *Frontiers in Neurology* 12 (July 2021), p. 689751 (cit. on p. 58).

[105] Ahmadreza Shahrokhshahi, Majid Khadiv, Ali Taherifar, et al. „Sample-Efficient Policy Adaptation for Exoskeletons under Variations in the Users and the Environment“. In: *IEEE Robotics and Automation Letters* 7.4 (Oct. 2022), pp. 9020–9027 (cit. on p. 59).

[106] Chris A. McGibbon, Andrew Sexton, Arun Jayaraman, et al. „Evaluation of the Keeogo exoskeleton for assisting ambulatory activities in people with multiple sclerosis: An open-label, randomized, cross-over trial“. In: *Journal of NeuroEngineering and Rehabilitation* 15.1 (Dec. 2018), pp. 1–14 (cit. on p. 59).

[107] Adam B. Zoss, H. Kazerooni, and Andrew Chu. „Biomechanical design of the Berkeley Lower Extremity Exoskeleton (BLEEX)“. In: *IEEE/ASME Transactions on Mechatronics* 11.2 (Apr. 2006), pp. 128–138 (cit. on p. 60).

[108] B. T. Quinlivan, S. Lee, P. Malcolm Lee, et al. „Assistance magnitude versus metabolic cost reductions for a tethered multiarticular soft exosuit“. In: *Science Robotics* 2.2 (Jan. 2017) (cit. on p. 60).

[109] Roam Robotics. *Wearable Robotic Technology for Military & First Responders — Roam* (cit. on p. 61).

[110] HeiAge. *HeiAge | Assistenzsysteme und digitale Technologien zur Verbesserung der Mobilität im Alter (Universität Heidelberg)* (cit. on pp. 62, 63).

[111] INAIL. *Home - Rehab Technologies - INAIL - IIT Lab - IIT* (cit. on p. 64).

[112] Lazzaro Di Biase, Alessandro Di Santo, Maria Letizia Caminiti, et al. „Gait Analysis in Parkinson's Disease: An Overview of the Most Accurate Markers for Diagnosis and Symptoms Monitoring“. In: *Sensors 2020, Vol. 20, Page 3529* 20.12 (June 2020), p. 3529 (cit. on p. 67).

[113] Steffi L. Colyer, Murray Evans, Darren P. Cosker, and Aki I.T. Salo. „A Review of the Evolution of Vision-Based Motion Analysis and the Integration of Advanced Computer Vision Methods Towards Developing a Markerless System“. In: *Sports Medicine - Open* 4.1 (Dec. 2018), pp. 1–15 (cit. on p. 68).

[114] Vicon. *Award Winning Motion Capture Systems | Vicon* (cit. on p. 68).

[115] Qualisys. *Motion Capture Technology and Systems | Qualisys | Qualisys* (cit. on p. 68).

[116] NDI. *NDI - Electromagnetic Tracking & Optical Navigation Solutions* (cit. on p. 68).

[117] Theia. *Theia Markerless - Markerless Motion Capture Redefined* (cit. on p. 68).

[118] CMU. *GitHub - CMU-Perceptual-Computing-Lab/openpose: OpenPose: Real-time multi-person keypoint detection library for body, face, hands, and foot estimation* (cit. on p. 68).

[119] Kishor Das, Thiago de Paula Oliveira, and John Newell. „Comparison of markerless and marker-based motion capture systems using 95% functional limits of agreement in a linear mixed-effects modelling framework“. In: *Scientific Reports* 13.1 (Dec. 2023) (cit. on p. 68).

[120] Lauren C. Benson, Anu M. Räisänen, Christian A. Clermont, and Reed Ferber. „Is This the Real Life, or Is This Just Laboratory? A Scoping Review of IMU-Based Running Gait Analysis“. In: *Sensors 2022, Vol. 22, Page 1722* 22.5 (Feb. 2022), p. 1722 (cit. on p. 70).

[121] Kistler. *Measurement systems and sensors | Kistler* (cit. on p. 70).

[122] Shuo Ding, Xiaoping Ouyang, Zhihao Li, and Huayong Yang. „Proportion-based fuzzy gait phase detection using the smart insole“. In: *Sensors and Actuators A: Physical* 284 (2018), pp. 96–102 (cit. on pp. 71, 174, 178, 179).

[123] Tiancheng Cheng and Mojtaba Sharifi. „Development of an Assistive Ankle-Foot Exoskeleton With Sensorized Silicone-Based Insole“. In: *Journal of Engineering and Science in Medical Diagnostics and Therapy* 7.2 (May 2024) (cit. on p. 71).

[124] Moticon. *Sensor insoles for clinical grade mobile gait & motion analysis* (cit. on p. 71).

[125] Novel. *Accurate pressure and force sensors | novel.de* (cit. on p. 71).

[126] Bertec. *Bertec* (cit. on p. 72).

[127] Noraxon. *Surface EMG Systems | Noraxon Electromyography Solutions* (cit. on p. 72).

[128] Peter Konrad. „The ABC of EMG A Practical Introduction to Kinesiological Electromyography". In: (2005) (cit. on p. 72).

[129] Paolo De Leva. „Joint center longitudinal positions computed from a selected subset of Chandler's data". In: *Journal of Biomechanics* 29.9 (Sept. 1996), pp. 1231–1233 (cit. on pp. 74, 88).

[130] A. Cappozzo, F. Catani, U. Della Croce, and A. Leardini. „Position and orientation in space of bones during movement: anatomical frame definition and determination". In: *Clinical Biomechanics* 10.4 (June 1995), pp. 171–178 (cit. on pp. 74, 151).

[131] Luciano Luporini Menegaldo, Agenor De Toledo Fleury, and Hans Ingo Weber. „Biomechanical modeling and optimal control of human posture". In: *Journal of Biomechanics* 36.11 (Nov. 2003), pp. 1701–1712 (cit. on p. 78).

[132] Michael Roller, Staffan Björkenstam, Joachim Linn, and Sigrid Leyendecker. „Optimal control of a biomechanical multibody model for the dynamic simulation of working tasks". In: () (cit. on p. 78).

[133] Sina Porsa, Yi Chung Lin, and Marcus G. Pandy. „Direct Methods for Predicting Movement Biomechanics Based Upon Optimal Control Theory with Implementation in OpenSim". In: *Annals of Biomedical Engineering* 44.8 (Aug. 2016), pp. 2542–2557 (cit. on p. 78).

[134] Manish Sreenivasa, Matthew Millard, Martin Felis, Katja Mombaur, and Sebastian I. Wolf. „Optimal control based stiffness identification of an ankle-foot orthosis using a predictive walking model". In: *Frontiers in Computational Neuroscience* 11 (Apr. 2017), p. 237717 (cit. on p. 78).

[135] Martin L. Felis, Katja Mombaur, and Alain Berthoz. „An optimal control approach to reconstruct human gait dynamics from kinematic data". In: *IEEE-RAS International Conference on Humanoid Robots* 2015-December (Dec. 2015), pp. 1044–1051 (cit. on pp. 79, 115).

[136] Katja Mombaur, Anne Hélène Olivier, and Armel Crétual. „Forward and inverse optimal control of bipedal running". In: *Cognitive Systems Monographs* 18 (2013), pp. 165–179 (cit. on p. 80).

[137] H. G. Bock and K. J. Plitt. „A Multiple Shooting Algorithm for Direct Solution of Optimal Control Problems". In: *IFAC Proceedings Volumes* 17.2 (July 1984), pp. 1603–1608 (cit. on p. 81).

[138] Daniel B. Leineweber, Irene Bauer, Hans Georg Bock, and Johannes P. Schlöder. „An efficient multiple shooting based reduced SQP strategy for large-scale dynamic process optimization. Part 1: theoretical aspects". In: *Computers & Chemical Engineering* 27.2 (Feb. 2003), pp. 157–166 (cit. on p. 81).

[139] Giorgos Marinou, Matthew Millard, Nejc Šarabon, and Katja Mombaur. „Comparing the risk of low-back injury using model-based optimization: Improved technique versus exoskeleton assistance". In: *Wearable Technologies* 2 (2021), e13 (cit. on pp. 87, 127).

[140] Roberto. Ierusalimschy, Luiz Henrique de. Figueiredo, and Waldemar. Celes. „Lua 5.1 reference manual". In: (2006), p. 103 (cit. on p. 87).

[141] Martin L. Felis. „RBDL: an efficient rigid-body dynamics library using recursive algorithms“. In: *Autonomous Robots* 41.2 (Feb. 2017), pp. 495–511 (cit. on pp. 87, 115).

[142] Matthew Millard, Anna Lena Emonds, Monika Harant, and Katja Mombaur. „A reduced muscle model and planar musculoskeletal model fit for the simulation of whole-body movements“. In: *Journal of biomechanics* 89 (May 2019), pp. 11–20 (cit. on pp. 88, 91, 92).

[143] Miguel Christophy, Nur Adila Faruk Senan, Jeffrey C. Lotz, and Oliver M. O'Reilly. „A Musculoskeletal model for the lumbar spine“. In: *Biomechanics and Modeling in Mechanobiology* 11.1-2 (2012), pp. 19–34 (cit. on pp. 89, 90, 130).

[144] N Bogduk M J Pearcy. „Instantaneous axes of rotation of the lumbar intervertebral joints“. In: *Medicine, Geology Spine* (1988) (cit. on p. 89).

[145] Nobutaka Mitsuhashi, Kaori Fujieda, Takuro Tamura, et al. „BodyParts3D: 3D structure database for anatomical concepts“. In: *Nucleic Acids Research* 37.SUPPL. 1 (2009), pp. 782–785 (cit. on pp. 89, 90).

[146] Kris W.N. Wong, Keith D.K. Luk, John C.Y. Leong, S. F. Wong, and Kenneth K.Y. Wong. „Continuous dynamic spinal motion analysis“. In: *Spine* 31.4 (2006), pp. 414–419 (cit. on pp. 89, 90).

[147] J. Baumgarte. „Stabilization of constraints and integrals of motion in dynamical systems“. In: *Computer Methods in Applied Mechanics and Engineering* 1.1 (1972), pp. 1–16 (cit. on pp. 90, 101).

[148] F. Zajac. „Muscle and tendon: properties, models, scaling, and application to biomechanics and motor control.“ In: *Critical reviews in biomedical engineering* (1989) (cit. on pp. 90, 92).

[149] Christian Kleinbach, Oleksandr Martynenko, Janik Promies, et al. „Implementation and validation of the extended Hill-type muscle model with robust routing capabilities in LS-DYNA for active human body models“. In: *BioMedical Engineering Online* 16.1 (Sept. 2017), pp. 1–28 (cit. on p. 91).

[150] Matthew Millard, Thomas Uchida, Ajay Seth, and Scott L. Delp. „Flexing computational muscle: Modeling and simulation of musculotendon dynamics“. In: *Journal of Biomechanical Engineering* 135.2 (Feb. 2013) (cit. on p. 91).

[151] Hartmut Geyer and Hugh Herr. „A Muscle-reflex model that encodes principles of legged mechanics produces human walking dynamics and muscle activities“. In: *IEEE Transactions on Neural Systems and Rehabilitation Engineering* 18.3 (June 2010), pp. 263–273 (cit. on p. 91).

[152] Daniel F.B. Haeufle, Isabell Wochner, David Holzmüller, et al. „Muscles Reduce Neuronal Information Load: Quantification of Control Effort in Biological vs. Robotic Pointing and Walking“. In: *Frontiers in Robotics and AI* 7 (June 2020) (cit. on p. 91).

[153] Matthew Millard, Manish Sreenivasa, and Katja Mombaur. „Predicting the motions and forces of wearable robotic systems using optimal control“. In: *Frontiers Robotics AI* 4.AUG (2017), pp. 1–12 (cit. on pp. 91, 130).

[154] M. Lamas, F. Mouzo, F. Michaud, U. Lugris, and J. Cuadrado. „Comparison of several muscle modeling alternatives for computationally intensive algorithms in human motion dynamics“. In: *Multibody System Dynamics* 54.4 (Apr. 2022), pp. 415–442 (cit. on p. 92).

[155] Marko Ackermann and Antonie J. van den Bogert. „Optimality principles for model-based prediction of human gait“. In: *Journal of Biomechanics* 43.6 (Apr. 2010), pp. 1055–1060 (cit. on p. 92).

[156] John C. Holladay. „A Smoothest Curve Approximation“. In: *American Mathematical Society: Mathematical Tables and Other Aids to Computation* 11.60 (1957), pp. 233–243 (cit. on p. 94).

[157] Monika Harant. „Optimization-Based Design and Control of a Spinal Exoskeleton and Feedback System“. PhD thesis. Heidelberg: Heidelberg University, 2023 (cit. on pp. 95, 96, 115).

[158] Žiga Kozinc, Jan Babič, and Nejc Šarabon. „Human pressure tolerance and effects of different padding materials with implications for development of exoskeletons and similar devices“. In: *Applied Ergonomics* 93 (May 2021), p. 103379 (cit. on pp. 103, 124).

[159] I ; Kingma, T ; Bosch, L ; Bruins, et al. „Foot positioning instruction, initial vertical load position and lifting technique: effects on low back loading“. In: *Ergonomics* 47.13 (Oct. 2004), pp. 1365–1385 (cit. on pp. 121, 123, 134).

[160] Pieter Coenen, Idsart Kingma, Cécile R.L. Boot, Paulien M. Bongers, and Jaap H. Van Dieën. „Inter-rater reliability of a video-analysis method measuring low-back load in a field situation“. In: *Applied Ergonomics* 44.5 (Sept. 2013), pp. 828–834 (cit. on pp. 128, 130).

[161] Stuart M. McGill and Robert W. Norman. „Effects of an anatomically detailed erector spinae model on L4L5 disc compression and shear“. In: *Journal of Biomechanics* 20.6 (Jan. 1987), pp. 591–600 (cit. on p. 130).

[162] Mark de Zee, Lone Hansen, Christian Wong, John Rasmussen, and Erik B. Simonsen. „A generic detailed rigid-body lumbar spine model“. In: *Journal of biomechanics* 40.6 (2007), pp. 1219–1227 (cit. on p. 130).

[163] Yujiang Xiang and Asif Arefeen. „Two-dimensional team lifting prediction with floating-base box dynamics and grasping force coupling“. In: *Multibody System Dynamics* 50.2 (Oct. 2020), pp. 211–231 (cit. on p. 130).

[164] Monika Harant, Matthew Millard, Nejc Sarabon, and Katja Mombaur. „Cost function evaluation for optimizing design and actuation of an active exoskeleton to ergonomically assist lifting motions“. In: *IEEE-RAS International Conference on Humanoid Robots* 2019-October (Oct. 2019), pp. 186–193 (cit. on p. 130).

[165] Pieter Coenen, Idsart Kingma, Cécile R.L. Boot, Paulien M. Bongers, and Jaap H. Van Dieën. „The contribution of load magnitude and number of load cycles to cumulative low-back load estimations: A study based on in-vitro compression data“. In: *Clinical Biomechanics* 27.10 (Dec. 2012), pp. 1083–1086 (cit. on p. 131).

[166] Matthias Jäger, Claus Jordan, Andreas Theilmeier, et al. „Lumbar-load analysis of manual patient-handling activities for biomechanical overload prevention among healthcare workers“. In: *The Annals of occupational hygiene* 57.4 (May 2013), pp. 528–544 (cit. on p. 131).

[167] Vaishnavh Nagarajan and J Zico Kolter. „Gradient descent GAN optimization is locally stable“. In: () (cit. on p. 132).

[168] Eric P. Lorenz, Steven A. Lavender, and Gunnar B.J. Andersson. „Determining what should be taught during lift-training instruction“. In: *Physiotherapy Theory and Practice* 18.4 (2002), pp. 175–191 (cit. on p. 134).

[169] Maria Lazzaroni, Ali Tabasi, Stefano Toxiri, et al. „Evaluation of an acceleration-based assistive strategy to control a back-support exoskeleton for manual material handling“. In: *Wearable Technologies* 1 (Jan. 2020), e9 (cit. on p. 135).

[170] Giorgos Marinou, Lizeth Sloot, and Katja Mombaur. „Towards efficient lower-limb exoskeleton evaluation: Defining biomechanical metrics to quantify assisted gait familiarization“. In: *Proceedings of the IEEE RAS and EMBS International Conference on Biomedical Robotics and Biomechatronics* 2022-August (2022) (cit. on pp. 145, 165, 183, 196, 213, 221).

[171] Jaqueline Mello Porto, Renato Campos Freire Júnior, Larissa Bocarde, et al. „Contribution of hip abductor-adductor muscles on static and dynamic balance of community-dwelling older adults“. In: *Aging clinical and experimental research* 31.5 (May 2019), pp. 621–627 (cit. on p. 145).

[172] Vahid Firouzi, Andre Seyfarth, Seungmoon Song, oskar von stryk oskar von, and maziar ahmad sharbafi maziar ahmad. „Biomechanical models in the lower-limb exoskeletons development: A review“. In: *Authorea Preprints* (Oct. 2023) (cit. on p. 147).

[173] Massimo Cenciarini and Aaron M. Dollar. „Biomechanical considerations in the design of lower limb exoskeletons“. In: *IEEE International Conference on Rehabilitation Robotics* (2011) (cit. on p. 147).

[174] Letian Wang, Edwin H.F. Van Asseldonk, and Herman Van Der Kooij. „Model Predictive Control-based gait pattern generation for wearable exoskeletons“. In: *IEEE ... International Conference on Rehabilitation Robotics : [proceedings]* 2011 (2011) (cit. on p. 147).

[175] Guillaume Durandau, Massimo Sartori, Magdo Bortole, et al. „EMG-driven models of human-machine interaction in individuals wearing the H2 exoskeleton“. In: *IFAC-PapersOnLine* 49.32 (Jan. 2016), pp. 200–203 (cit. on p. 147).

[176] Jan C.L. Lau and Katja Mombaur. „Preliminary Study on a Novel Protocol for Improving Familiarity with a Lower-Limb Robotic Exoskeleton in Able-Bodied, First-Time Users“. In: *Frontiers in robotics and AI* 8 (Jan. 2022) (cit. on p. 148).

[177] Alberto Leardini, Fabio Biagi, Andrea Merlo, Claudio Belvedere, and Maria Grazia Benedetti. „Multi-segment trunk kinematics during locomotion and elementary exercises“. In: *Clinical biomechanics (Bristol, Avon)* 26.6 (July 2011), pp. 562–571 (cit. on p. 151).

[178] Peter Konrad. *The ABC of EMG A Practical Introduction to Kinesiological Electromyography*. Tech. rep. 2005 (cit. on p. 151).

[179] Maria Rubega, Roberto Di Marco, Marianna Zampini, et al. „Muscular and cortical activation during dynamic and static balance in the elderly: A scoping review“. In: *Aging brain* 1 (2021), p. 100013 (cit. on p. 153).

[180] Rudolf J. Freund and William J. Wilson. *Statistical Methods*. Ed. by Barbara Holland. Elsevier, 2003 (cit. on p. 153).

[181] Giorgos Marinou, Ibrahima Kourouma, and Katja Mombaur. „Development and Validation of a Modular Sensor-Based System for Gait Analysis and Control in Lower-Limb Exoskeletons“. In: *IEEE TMRB (in review - preprint avail. on arxiv)* (Jan. 2024) (cit. on p. 165).

[182] Wen Zhou Li, Guang Zhong Cao, and Ai Bin Zhu. „Review on Control Strategies for Lower Limb Rehabilitation Exoskeletons“. In: *IEEE Access* 9 (2021), pp. 123040–123060 (cit. on p. 165).

[183] Drew B. Fineberg, Pierre Asselin, Noam Y. Harel, et al. „Vertical ground reaction force-based analysis of powered exoskeleton-assisted walking in persons with motor-complete paraplegia“. In: *The journal of spinal cord medicine* 36.4 (July 2013), pp. 313–321 (cit. on pp. 166, 196).

[184] Robert M. Kanko, Elise K. Laende, Elysia M. Davis, W. Scott Selbie, and Kevin J. Deluzio. „Concurrent assessment of gait kinematics using marker-based and markerless motion capture“. In: *Journal of biomechanics* 127 (Oct. 2021) (cit. on p. 166).

[185] Nuno Ferrete Ribeiro and Cristina P. Santos. „Inertial measurement units: A brief state of the art on gait analysis“. In: *ENBENG 2017 - 5th Portuguese Meeting on Bioengineering, Proceedings* (Mar. 2017) (cit. on pp. 166, 169).

[186] Sangheon Park and Sukhoon Yoon. „Validity Evaluation of an Inertial Measurement Unit (IMU) in Gait Analysis Using Statistical Parametric Mapping (SPM)“. In: *Sensors 2021, Vol. 21, Page 3667* 21.11 (May 2021), p. 3667 (cit. on p. 166).

[187] Thomas Seel, Jörg Raisch, and Thomas Schauer. „IMU-Based Joint Angle Measurement for Gait Analysis“. In: *Sensors 2014, Vol. 14, Pages 6891-6909* 14.4 (Apr. 2014), pp. 6891–6909 (cit. on p. 166).

[188] Jesús De Miguel-Fernández, Miguel Salazar-Del Rio, Marta Rey-Prieto, et al. „Inertial sensors for gait monitoring and design of adaptive controllers for exoskeletons after stroke: a feasibility study“. In: *Frontiers in Bioengineering and Biotechnology* 11 (Aug. 2023), p. 1208561 (cit. on p. 166).

[189] Junghoon Park, Hyunkyu Park, and Jung Kim. „Performance estimation of the lower limb exoskeleton for plantarflexion using surface electromyography (sEMG) signals“. In: *Journal of Biomechanical Science and Engineering* 12.2 (2017) (cit. on pp. 166, 169).

[190] Yong Ku Kong, Kyeong Hee Choi, Min Uk Cho, et al. „Ergonomic Assessment of a Lower-Limb Exoskeleton through Electromyography and Anybody Modeling System“. In: *International Journal of Environmental Research and Public Health* 19.13 (July 2022) (cit. on p. 166).

[191] Mohammad Abdoli-Eramaki, Caroline Damecour, John Christenson, and Joan Stevenson. „The effect of perspiration on the sEMG amplitude and power spectrum“. In: *Journal of Electromyography and Kinesiology* 22.6 (2012), pp. 908–913 (cit. on p. 166).

[192] Dae Hoon Moon, Donghan Kim, and Young Dae Hong. „Intention Detection Using Physical Sensors and Electromyogram for a Single Leg Knee Exoskeleton“. In: *Sensors (Basel, Switzerland)* 19.20 (Oct. 2019) (cit. on p. 166).

[193] H Kawamoto, Suwoong Lee, S Kanbe, and Y Sankai. „Power assist method for HAL-3 using EMG-based feedback controller“. In: *SMC'03 Conference Proceedings. 2003 IEEE International Conference on Systems, Man and Cybernetics. Conference Theme - System Security and Assurance (Cat. No.03CH37483)*. Vol. 2. 2003, pp. 1648–1653 (cit. on p. 166).

[194] E Guizzo and H Goldstein. „The rise of the body bots [robotic exoskeletons]“. In: *IEEE Spectrum* 42.10 (2005), pp. 50–56 (cit. on p. 166).

[195] Nadeem Iqbal, Tufail Khan, Mukhtaj Khan, et al. „Neuromechanical Signal-Based Parallel and Scalable Model for Lower Limb Movement Recognition“. In: *IEEE Sensors Journal* 21.14 (2021), pp. 16213–16221 (cit. on p. 166).

[196] Inigo Cesar Gil. „Development of an Instrumented Crutch for Quantitative Gait Monitoring and Diagnosis of Patients with Multiple Sclerosis“. PhD thesis. University of the Basque Country, 2021 (cit. on pp. 166, 167).

[197] Amith Khandakar, Sakib Mahmud, Muhammad E H Chowdhury, et al. „Design and Implementation of a Smart Insole System to Measure Plantar Pressure and Temperature“. In: *Sensors* 22.19 (2022) (cit. on pp. 166, 174).

[198] Udomporn Manupibul, Warakorn Charoensuk, and Panya Kaimuk. „Design and development of SMART insole system for plantar pressure measurement in imbalance human body and heavy activities“. In: *The 7th 2014 Biomedical Engineering International Conference*. 2014, pp. 1–5 (cit. on p. 166).

[199] Diego Henrique Antunes Nascimento, Fabrício Anicio Magalhães, George Schayer Sabino, et al. „Development of a Human Motion Analysis System Based on Sensorized Insoles and Machine Learning Algorithms for Gait Evaluation“. In: *Inventions* 7.4 (2022) (cit. on pp. 166, 168).

[200] Iván González, Jesús Fontecha, Ramón Hervás, and José Bravo. „An Ambulatory System for Gait Monitoring Based on Wireless Sensorized Insoles“. In: *Sensors (Basel)* 15.7 (July 2015), pp. 16589–16613 (cit. on pp. 166, 174).

[201] Patrcia M M Silva, Ledycnarf J Holanda, Edith E Granados, and Edgard Morya. „Building Pressure-Sensitive Foot Insoles for Public Health Evaluation in Smart Cities“. In: *2017 IEEE First Summer School on Smart Cities (S3C)*. 2017, pp. 153–156 (cit. on p. 166).

[202] Rajesh Kannan Megalingam, M. G. Greeshma, and Soumya S. Pillai. „Design and implementation of intelligent crutches for medical applications“. In: *Proceedings of the 2019 IEEE International Conference on Communication and Signal Processing, ICCSP 2019* (Apr. 2019), pp. 926–929 (cit. on p. 167).

[203] Iñigo Sesar, Asier Zubizarreta, Itziar Cabanes, et al. „Instrumented Crutch Tip for Monitoring Force and Crutch Pitch Angle“. In: *Sensors 2019, Vol. 19, Page 2944* 19.13 (July 2019), p. 2944 (cit. on p. 167).

[204] Matteo Lancini, Mauro Serpelloni, Simone Pasinetti, et al. „Upper limb loads during robotic assisted gait: A measuring system to guide training“. In: *Human-Centric Robotics- Proceedings of the 20th International Conference on Climbing and Walking Robots and the Support Technologies for Mobile Machines, CLAWAR 2017* (2018), pp. 613–620 (cit. on p. 167).

[205] Matteo Lancini, Mauro Serpelloni, Simone Pasinetti, and Eleonora Guanziroli. „Healthcare Sensor System Exploiting Instrumented Crutches for Force Measurement during Assisted Gait of Exoskeleton Users“. In: *IEEE Sensors Journal* 16.23 (Dec. 2016), pp. 8228–8237 (cit. on p. 167).

[206] Matteo Lancini, Mauro Serpelloni, and Simone Pasinetti. „Instrumented crutches to measure the internal forces acting on upper limbs in powered exoskeleton users“. In: *Proceedings - 2015 6th IEEE International Workshop on Advances in Sensors and Interfaces, IWASI 2015* (Aug. 2015), pp. 175–180 (cit. on p. 167).

[207] Modar Hassan, Hideki Kadone, Kenji Suzuki, and Yoshiyuki Sankai. „Wearable Gait Measurement System with an Instrumented Cane for Exoskeleton Control“. In: *Sensors 2014, Vol. 14, Pages 1705-1722* 14.1 (Jan. 2014), pp. 1705–1722 (cit. on p. 167).

[208] Yongqi Felix Chen, Danielle Napoli, Sunil K. Agrawal, and Damiano Zanotto. „Smart Crutches: Towards Instrumented Crutches for Rehabilitation and Exoskeletons-Assisted Walking“. In: *Proceedings of the IEEE RAS and EMBS International Conference on Biomedical Robotics and Biomechatronics* 2018-August (Oct. 2018), pp. 193–198 (cit. on pp. 167, 173).

[209] Emilio Sardini, Mauro Serpelloni, and Matteo Lancini. „Wireless Instrumented Crutches for Force and Movement Measurements for Gait Monitoring“. In: *IEEE Transactions on Instrumentation and Measurement* 64.12 (Dec. 2015), pp. 3369–3379 (cit. on pp. 167, 173, 186).

[210] Jong Gab Ho, Young Kim, and Se Dong Min. „Customized Textile Capacitive Insole Sensor for Center of Pressure Analysis“. In: *Sensors 2022, Vol. 22, Page 9390* 22.23 (Dec. 2022), p. 9390 (cit. on p. 167).

[211] Jessica DeBerardinis, Conner Neilsen, Daniel E Lidstone, Janet S Dufek, and Mohamed B Trabia. „A comparison of two techniques for center of pressure measurements“. In: *Journal of Rehabilitation and Assistive Technologies Engineering* 7 (Jan. 2020), p. 2055668320921063 (cit. on p. 167).

[212] Z. Dong, H. H. Chu, C. Hansen, and Jiann Shing Shieh. „Design a Center of Pressure Measurement Device into the Insole“. In: *IFMBE Proceedings* 47 (2015), pp. 100–103 (cit. on pp. 167, 168).

[213] Anup Kumar Mallick and Achintya Das. „An Analytical Survey of Defuzzification Techniques“. In: *2021 IEEE 4th International Conference on Computing, Power and Communication Technologies, GUCON 2021* (Sept. 2021) (cit. on p. 167).

[214] Lotfi A Zadeh. „Fuzzy sets“. In: *Information and Control* 8.3 (1965), pp. 338–353 (cit. on pp. 167–169).

[215] Kyoungchul Kong and Masayoshi Tomizuka. „Smooth and continuous human gait phase detection based on foot pressure patterns“. In: *2008 IEEE International Conference on Robotics and Automation*. 2008, pp. 3678–3683 (cit. on pp. 168, 169, 174, 179).

[216] Alhanoof Althnian, Duaa AlSaeed, Heyam Al-Baity, et al. „Impact of Dataset Size on Classification Performance: An Empirical Evaluation in the Medical Domain“. In: *Applied Sciences 2021, Vol. 11, Page 796* 11.2 (Jan. 2021), p. 796 (cit. on p. 168).

[217] Kaiyang Yin, Kui Xiang, Muye Pang, et al. „Personalised Control of Robotic Ankle Exoskeleton Through Experience-Based Adaptive Fuzzy Inference“. In: *IEEE Access* 7 (2019), pp. 72221–72233 (cit. on p. 169).

[218] Anna L. Ármannsdóttir, Philipp Beckerle, Juan C. Moreno, et al. „Assessing the Involvement of Users During Development of Lower Limb Wearable Robotic Exoskeletons: A Survey Study“. In: *Human Factors* 62.3 (May 2020), pp. 351–364 (cit. on p. 169).

[219] Giorgos Marinou and Ibrahima Kourouma. *CMSS: Custom Modular Sensor System - for biomechanical evaluation of lower-limb exoskeletons, with the possibility of informing feedback control architectures.* 2024 (cit. on pp. 171, 176, 177).

[220] Çağlar Seylan and Uluc Saranli. „Estimation of ground reaction forces using low-cost instrumented forearm crutches“. In: *IEEE Transactions on Instrumentation and Measurement* 67.6 (June 2018), pp. 1308–1316 (cit. on pp. 173, 186).

[221] Chathuri M. Senanayake and S. M.N.Arosha Senanayake. „Computational intelligent gait-phase detection system to identify pathological gait“. In: *IEEE transactions on information technology in biomedicine : a publication of the IEEE Engineering in Medicine and Biology Society* 14.5 (Sept. 2010), pp. 1173–1179 (cit. on p. 174).

[222] Bing Chen, Chun Hao Zhong, Xuan Zhao, et al. „Reference Joint Trajectories Generation of CUHK-EXO Exoskeleton for System Balance in Walking Assistance“. In: *IEEE Access* 7 (2019), pp. 33809–33821 (cit. on pp. 178, 179).

[223] Dana Terrazas-Rodas, Lisbeth Rocca-Huaman, Cesar Ramirez-Amaya, et al. „Control Systems in Lower-limb Exoskeletons for Rehabilitation and/or Assistance: A Brief Review“. In: *2022 International Conference on Smart Systems and Power Management (IC2SPM)* (2022), pp. 117–123 (cit. on p. 183).

[224] Maria Jönsson, Tobias Munkhammar, Lena Norrbrand, and Hans E. Berg. „Foot centre of pressure and ground reaction force during quadriceps resistance exercises; a comparison between force plates and a pressure insole system“. In: *Journal of biomechanics* 87 (Apr. 2019), pp. 206–210 (cit. on p. 185).

[225] Barkan Ugurlu, Hironori Oshima, and Tatsuo Narikiyo. „Lower body exoskeleton-supported compliant bipedal walking for paraplegics: How to reduce upper body effort?“ In: *Proceedings - IEEE International Conference on Robotics and Automation* (Sept. 2014), pp. 1354–1360 (cit. on p. 185).

[226] Mary Roberts, David Mongeon, and Francois Prince. „Biomechanical parameters for gait analysis: a systematic review of healthy human gait“. In: *Physical Therapy and Rehabilitation* 4.1 (2017), p. 6 (cit. on p. 187).

[227] Jeong Kyun Kim, Myung Nam Bae, Kang Bok Lee, and Sang Gi Hong. „Gait event detection algorithm based on smart insoles“. In: *ETRI Journal* 42.1 (Feb. 2020), pp. 46–53 (cit. on p. 188).

[228] Simona Crea, Marco Donati, Stefano Marco Maria De Rossi, Calogero Maria Oddo, and Nicola Vitiello. „A Wireless Flexible Sensorized Insole for Gait Analysis“. In: *Sensors (Basel, Switzerland)* 14.1 (Jan. 2014), p. 1073 (cit. on p. 188).

[229] Norman Riedel, Giorgos Marinou, Katja Mombaur, and Barbara Deml. „An Outdoor Dual-Task Study on Cognitive-Motor Interference during Exoskeleton-Assisted Walking“. In: *Applied Ergonomics* (in review) (2024) (cit. on pp. 195, 208, 224).

[230] Patrick Slade, Mykel J. Kochenderfer, Scott L. Delp, and Steven H. Collins. „Personalizing exoskeleton assistance while walking in the real world“. In: *Nature 2022 610:7931* 610.7931 (Oct. 2022), pp. 277–282 (cit. on p. 195).

[231] Duojin Wang, Xiaoping Gu, Wenzhuo Li, et al. „Evaluation of safety-related performance of wearable lower limb exoskeleton robot (WLLER): A systematic review“. In: *Robotics and Autonomous Systems* 160 (Feb. 2023), p. 104308 (cit. on p. 195).

[232] G. Diamond-Ouellette, A. Telonio, T. Karakolis, et al. „Exploring the Change in Metabolic Cost of Walking before and after Familiarization with a Passive Load-Bearing Exoskeleton: A Case Series“. In: *IISE Transactions on Occupational Ergonomics and Human Factors* 10.3 (Oct. 2022), pp. 161–172 (cit. on p. 196).

[233] Katherine L. Poggensee and Steven H. Collins. „How adaptation, training, and customization contribute to benefits from exoskeleton assistance“. In: *Science Robotics* 6.58 (Sept. 2021) (cit. on pp. 196, 225).

[234] Kristel Knaepen, Pieter Beyl, Saartje Duerinck, et al. „Human-robot interaction: Kinematics and muscle activity inside a powered compliant knee exoskeleton“. In: *IEEE Transactions on Neural Systems and Rehabilitation Engineering* 22.6 (Nov. 2014), pp. 1128–1137 (cit. on p. 196).

[235] Yi Zheng, Peisi Zhong, Kunhua Liu, Kaige Yang, and Qingchao Yue. „Human Motion Capture System Based 3D Reconstruction on Rehabilitation Assistance Stability of Lower Limb Exoskeleton Robot Climbing Upstairs Posture“. In: *IEEE Sensors Journal* 20.20 (Oct. 2020), pp. 11778–11786 (cit. on p. 196).

[236] Michael Shepertycky, Sarah Burton, Andrew Dickson, Yan Fei Liu, and Qingguo Li. „Removing energy with an exoskeleton reduces the metabolic cost of walking“. In: *Science* 372.6545 (May 2021) (cit. on p. 196).

[237] Stefano Massardi, David Rodriguez-Cianca, David Pinto-Fernandez, et al. „Characterization and Evaluation of Human–Exoskeleton Interaction Dynamics: A Review“. In: *Sensors 2022, Vol. 22, Page 3993* 22.11 (May 2022), p. 3993 (cit. on p. 197).

[238] Mohammad Shushtari, Julia Foellmer, and Arash Arami. „Human–exoskeleton interaction portrait“. In: *Journal of NeuroEngineering and Rehabilitation* 21.1 (Dec. 2024), pp. 1–20 (cit. on p. 197).

[239] Katherine L. Poggensee and Steven H. Collins. „Lower limb biomechanics of fully trained exoskeleton users reveal complex mechanisms behind the reductions in energy cost with human-in-the-loop optimization“. In: *Frontiers in Robotics and AI* 11 (Jan. 2024), p. 1283080 (cit. on p. 197).

[240] Matteo Lancini, Simone Pasinetti, Marco Ghidelli, et al. „A Workaround for Recruitment Issues in Preliminary WR Studies: Audio Feedback and Instrumented Crutches to Train Test Subjects“. In: *Biosystems and Biorobotics* 27 (2022), pp. 627–631 (cit. on p. 197).

[241] Satyajit Upasani and Divya Srinivasan. „Gaze Behavior and Mental Workload While Using a Whole-Body Powered Exoskeleton: A Pilot Study“. In: *https://doi.org/10.1177/21695067231192201* 67.1 (Oct. 2023), pp. 980–981 (cit. on p. 198).

[242] Blake Bequette, Adam Norton, Eric Jones, and Leia Stirling. „Physical and Cognitive Load Effects Due to a Powered Lower-Body Exoskeleton“. In: *Human factors* 62.3 (May 2020), pp. 411–423 (cit. on p. 198).

[243] Emad Al-Yahya, Helen Dawes, Lesley Smith, et al. „Cognitive motor interference while walking: a systematic review and meta-analysis“. In: *Neuroscience and biobehavioral reviews* 35.3 (Jan. 2011), pp. 715–728 (cit. on pp. 198, 224, 225).

[244] Frederico Pieruccini-Faria, Sandra E. Black, Mario Masellis, et al. „Gait variability across neurodegenerative and cognitive disorders: Results from the Canadian Consortium of Neurodegeneration in Aging (CCNA) and the Gait and Brain Study“. In: *Alzheimer's & dementia : the journal of the Alzheimer's Association* 17.8 (Aug. 2021), pp. 1317–1328 (cit. on p. 198).

[245] Oliver Huxhold, Shu Chen Li, Florian Schmiedek, and Ulman Lindenberger. „Dual-tasking postural control: aging and the effects of cognitive demand in conjunction with focus of attention“. In: *Brain research bulletin* 69.3 (Apr. 2006), pp. 294–305 (cit. on p. 198).

[246] Priyanshu Agarwal and Ashish D. Deshpande. „A Framework for Adaptation of Training Task, Assistance and Feedback for Optimizing Motor (Re)-Learning With a Robotic Exoskeleton“. In: *IEEE Robotics and Automation Letters* 4.2 (Apr. 2019), pp. 808–815 (cit. on pp. 199, 209).

[247] Katrin Stollenmaier, Ilka S. Rist, Fabio Izzi, and Daniel F.B. Haeufle. „Simulating the response of a neuro-musculoskeletal model to assistive forces: Implications for the design of wearables compensating for motor control deficits“. In: *Proceedings of the IEEE RAS and EMBS International Conference on Biomedical Robotics and Biomechatronics* 2020-November (Nov. 2020), pp. 779–784 (cit. on p. 199).

[248] Rosanne B. van Dijsseldonk, Hennie Rijken, Ilse J.W. van Nes, Henk van de Meent, and Noël L.W. Keijsers. „Predictors of exoskeleton motor learning in spinal cord injured patients“. In: *Disability and Rehabilitation* 43.14 (2021), pp. 1982–1988 (cit. on p. 199).

[249] Kai Bötzel, Fernando Martinez Marti, Miguel Ángel Carvajal Rodríguez, Annika Plate, and Alberto Olivares Vicente. „Gait recording with inertial sensors – How to determine initial and terminal contact“. In: *Journal of Biomechanics* 49.3 (Feb. 2016), pp. 332–337 (cit. on p. 207).

[250] Robyn Galletly and Sandra G. Brauer. „Does the type of concurrent task affect preferred and cued gait in people with Parkinson's disease?“ In: *The Australian journal of physiotherapy* 51.3 (2005), pp. 175–180 (cit. on p. 207).

[251] Mark G. Fischman, Robert W. Christina, and Max J. Vercruyssen. „Retention and Transfer of Motor Skills: A Review for the Practitioner“. In: *Quest* 33.2 (July 1981), pp. 181–194 (cit. on p. 209).

[252] Richard Schmidt and Timothee D. Lee. *Motor Learning and Performance 6th Edition with Web Study Guide-Loose-Leaf Edition: From Principles to Application*. 6th. Human Kinetics, 2019 (cit. on pp. 220, 225, 226).

[253] Chao Zhang, Yanhe Zhu, Jizhuang Fan, Jie Zhao, and Hongying Yu. „Design of a quasi-passive 3 DOFs ankle-foot wearable rehabilitation orthosis“. In: *Bio-Medical Materials and Engineering* 26 (2015), S647–S654 (cit. on pp. 220, 225).

[254] Anna Michelle McPhee, Theodore C.K. Cheung, and Mark A. Schmuckler. „Dual-task interference as a function of varying motor and cognitive demands“. In: *Frontiers in Psychology* 13 (Sept. 2022), p. 952245 (cit. on p. 221).

[255] Ying Fang, Greg Orekhov, and Zachary F. Lerner. „Adaptive ankle exoskeleton gait training demonstrates acute neuromuscular and spatiotemporal benefits for individuals with cerebral palsy: A pilot study“. In: *Gait & Posture* 95 (June 2022), pp. 256–263 (cit. on p. 221).

[256] Karl M. Newell. *Variability and motor control*. Ed. by Karl M Newell and Danial M Corcos. Vol. 168. 4. Champagne, IL: Human Kinetics Publishers, Aug. 1993, pp. 317–358 (cit. on pp. 222, 225).

[257] Hui Ting Goh, Katherine J. Sullivan, James Gordon, Gabriele Wulf, and Carolee J. Winstein. „Dual-task practice enhances motor learning: A preliminary investigation“. In: *Experimental Brain Research* 222.3 (Oct. 2012), pp. 201–210 (cit. on p. 223).

[258] Johan Engström, Gustav Markkula, Trent Victor, and Natasha Merat. „Effects of Cognitive Load on Driving Performance: The Cognitive Control Hypothesis“. In: *Human factors* 59.5 (Aug. 2017), pp. 734–764 (cit. on p. 224).

[259] Aditi Gupta, Damian G. Kelty-Stephen, Madhur Mangalam, Ryan J. McKindles, and Leia Stirling. „Walking speed and dual task input modality impact performance on a self-paced treadmill“. In: *Applied Ergonomics* 109 (May 2023), p. 103986 (cit. on p. 224).

[260] Leslie M. Decker, Fabien Cignetti, Nathaniel Hunt, et al. „Effects of aging on the relationship between cognitive demand and step variability during dual-task walking“. In: *Age (Dordrecht, Netherlands)* 38.4 (Aug. 2016), pp. 363–375 (cit. on p. 224).

[261] Rachel Hybart and Daniel Ferris. „Gait variability of outdoor vs treadmill walking with bilateral robotic ankle exoskeletons under proportional myoelectric control“. In: *PloS one* 18.11 (Nov. 2023) (cit. on p. 224).

[262] Lei Wang, Jin Lin Peng, Wu Xiang, Yi Jie Huang, and Ai Lian Chen. „Effects of rhythmic auditory stimulation on motor function and balance ability in stroke: A systematic review and meta-analysis of clinical randomized controlled studies“. In: *Frontiers in neuroscience* 16 (Nov. 2022) (cit. on p. 224).

[263] Myunghee Kim, Hyeongkeun Jeong, Prakyath Kantharaju, et al. „Visual guidance can help with the use of a robotic exoskeleton during human walking“. In: *Scientific Reports 2022 12:1* 12.1 (Mar. 2022), pp. 1–10 (cit. on p. 224).

[264] Rainer Beurskens, Fabian Steinberg, Franziska Antoniewicz, Wanja Wolff, and Urs Granacher. „Neural Correlates of Dual-Task Walking: Effects of Cognitive versus Motor Interference in Young Adults“. In: *Neural plasticity* 2016 (2016) (cit. on p. 225).